TOTAL SYNTHESIS AND BIOLOGICAL EVALUATION OF ALKALOID NATURAL PRODUCTS (+)-7-BROMOTRYPARGINE AND PHIDIANIDINES A & B AND THE DEVELOPMENT OF A NOVEL CLASS OF POSITIVE ALLOSTERIC MODULATORS FOR THE METABOTROPIC GLUTAMATE RECEPTOR SUBTYPE 1

BY

John T. Brogan

Dissertation
Submitted to the Faculty of the
Graduate School of Vanderbilt University
in partial fulfillment of the requirements
for the degree of
DOCTOR OF PHILOSOPHY
in
Chemical and Physical Biology
August, 2013
Nashville, Tennessee
Approved:
Professor Craig W. Lindsley
Professor Brian O. Bachmann
Professor J. Scott Daniels
Professor Lawrence J. Marnett
Professor Gary A. Sulikowski

DEDICATION

To my family:

Kevin and Nena,

Chase, Larkin, and Abbey,

and my wife Pooja

ACKNOWLEDGEMENTS

Many individuals and organizations have provided me with indispensable help and support and I wish to specifically name and thank a number of them. First and foremost, I would like to acknowledge my advisor, Dr. Craig Lindsley. In January of 2007, Craig gave me the opportunity to begin learning organic chemistry in a research setting. Ever since then, he has provided an ideal balance of professional support and intellectual freedom in all aspects of my scientific career. Craig is one of the most brilliant, hardworking, and productive scientists I have ever known and I will forever be indebted to him for taking me on as an undergraduate research assistant and as a graduate student in his laboratory. I attribute any and all of my research success - projects, publications, conferences and beyond - to Craig's aid and leadership during my undergraduate and graduate careers.

I would like to acknowledge my committee: Brian Bachmann, Scott Daniels, Larry Marnett, and Gary Sulikowski. I asked each to join my committee because I respected their work and enjoyed the graduate courses they taught. Their instruction and advice has been greatly appreciated over the past four years. Lindsay Meyers in the BRET Office has been an ever present source of information and assistance in all things Vanderbilt. The CPB program would not be the same without Lindsay. Amanda Renick in the CBI Office has always offered a friendly ear and has made scheduling committee meetings a far simpler process than it could have been.

The Lindsley laboratory and the entire VCNDD have provided an unparalleled graduate research environment and I would like to thank a number of individuals for their contribution to my personal growth and research accomplishments. Phil Kennedy took me on as an

undergraduate student and taught me a great deal about organic synthesis technique. Tom Bridges has served as a great role model and paved the way for a number of chemical biology students in the laboratory. Leslie Aldrich and Niyi Fadeyi led by example during their time in the lab. They demonstrated what it means to be motivated and hardworking graduate students. Mike Schulte, Matt O'Reilly, and Uyen Le made studying for coursework first and second years an enjoyable process. They were each excellent classmates and I wish them all the best. Patrick Gentry has provided years of friendship, intellectual support, and error correction. I'm excited to see where his scientific career takes him. Bruce Melancon, Darren Engers, and Kyle Emmitte all gave their time on numerous occasions, providing synthetic discussion and support for a range of different projects. I appreciate their constant willingness to troubleshoot reactions and manuscripts. Matt Mulder and Nathan Kett provided indispensable SFC and HRMS analytical chemistry support. Hyekyung Plumley in the Conn laboratory deserves special thanks for her instruction in cell culture and calcium assay technique. She is a talented researcher and a great friend.

Lastly, I would like to thank my family and friends for all the love and support that they have offered over the course of my graduate career. My parents Kevin and Nena listened and offered advice and encouragement whenever possible. My brother Chase and my sister Abbey stood by me as I became even more of a science geek. My late sister Larkin set a wonderful example of hard work and dedication. I wish she could be here today but I know she will always be with me. Finally, I would like to thank my loving wife Pooja for sharing every challenge and success of graduate school with me. We did this together.

TABLE OF CONTENTS

LIST OF FIGURES

Figure Page

LIST OF TABLES

Table Page

LIST OF SCHEMES

Scheme Page

LIST OF ABBREVIATIONS

Ac	acetyl
AcOH	acetic acid
BINOL	1,1'-bi-2-napthol
Bn	benzyl
BnBr	benzyl bromide
Boc	t-Butyloxycarbonyl
BzOH	benzoic acid
^{o}C	degrees Celsius
Cat.	catalytic
CBz	carboxy benzyl
$CDCl_3$	deuterated chloroform
CD_3OD	deuterated methanol
CH_2Cl_2	dichloromethane
CH_3CN	acetonitrile
$CHCl_3$	chloroform
CNS	central nervous system
$(COCl)_2$	oxalyl chloride
Conc	concentration
CRC	concentration response curve
Cs_2CO_3	cesium carbonate
CYP450	cytochrome P450

δ	chemical shift in ppm
δOR	delta opioid receptor
d	doublet
DAT	dopamine transporter
DBU	1, 8-diazabicyclo[5.4.0]undec-7-ene
dd	doublet of doublet
ddd	doublet of doublet of doublet
DIEA	N,N diisopropylethylamine
DMAP	4-dimethylaminopyridine
DMF	N, N-dimethylformamide
DMPK	Drug Metabolism/Pharmacokinetics
DMSO	dimethyl sulfoxide
d_6-DMSO	deuterated dimethyl sulfoxide
dt	doublet of triplet
Eq.	equivalent(s)
EC_{50}	half maximal effective concentration
Et	ethyl
Et3N	triethylamine
Et_2O	diethyl ether
EtOAc	ethyl acetate
EtOH	ethanol
GPCR	G-protein coupled receptor

h	hour
HCl	hydrogen chloride
H_3	histamine 3 receptor
HPLC	high pressure liquid chromatography
HOBT	hydroxybenzotriazole
HTS	high-throughput screening
Hz	hertz, coupling constant
IC_{50}	half maximal inhibitory concentration
IP	inositol monophosphate
IP_2	inositol bisphosphate
IP_3	inositol trisphosphate
iPr$_2$Net	diisopropylethylamine
K_2CO_3	potassium carbonate
κOR	kappa opioid receptor
L	liter(s)
LCMS	liquid chromatography mass spectrometry
$LiAlH_4$	lithium aluminum hydride
Me	methyl
$mGlu_{1\text{-}8}$	metabotropic glutamate receptor subtypes 1-8
MHz	megahertz
min	minute(s)
mol	mole(s)

MeI	iodomethane
MeOH	methanol
MS	molecular sieves
μOR	mu opioid receptor
NaOH	sodium hydroxide
NET	norepinephrine transporter
NMO	N-methylmorpholine N-oxide
NMR	nuclear magnetic resonance
PAM	positive allosteric modulator
Ph	phenyl
Pd/C	palladium on carbon
Ph	phenyl
ppm	parts per million
py	pyridine
SAR	structure-activity relationship(s)
SERT	serotonin transporter
Tf	trifluoromethanesulfonyl
TEA	triethylamine
TFA	trifluoroacetic acid
THF	tetrahydrofuran
TLC	thin layer chromatography
Tos	tosylate, 4-toluenesulfonyl

TREx-293	cell lines stably expressing the tetracycline repressor protein
UV	ultraviolet
VCNDD	Vanderbilt Center for Neuroscience Drug Discovery
WT	wild-type

CHAPTER I

TOTAL SYNTHESIS AND BIOLOGICAL EVALUATION OF (+)-7-BROMOTRYPARGINE

1.1 Introduction

Drug discovery based on natural products, and marine natural products in particular, has been a highly successful approach toward novel lead series and marketed therapeutics for both peripheral and central nervous system (CNS) disorders[1,2]. With the recent decline in natural products research by the pharmaceutical industry[3], academic labs such as our own have undertaken the task of synthesizing and evaluating small molecule natural products for therapeutic potential. To that end, a number of marine natural products, such as aplysamine **1.1**,[4] verogamine **1.2**,[5] conessine **1.3**[6] and dispyrin **1.4**,[7,8] have been shown to display both affinity for, and inhibition of the histamine subtype 3 (H_3) receptor (Figure 1.1.1)[9,10,11]. The H_3 receptor is a presynaptic autoreceptor within the Class A GPCR family, which also functions as a heteroreceptor modulating levels of neurotransmitters such as dopamine, acetylcholine, norepinephrine, serotonin, GABA and glutamate[9,10,11]. As a result, the H_3 receptor has garnered a great deal of interest from the pharmaceutical industry for the possible treatment of obesity, epilepsy, circadian arrhythmia, schizophrenia, Alzheimer's disease, neuropathic pain and ADHD[9,10,11].

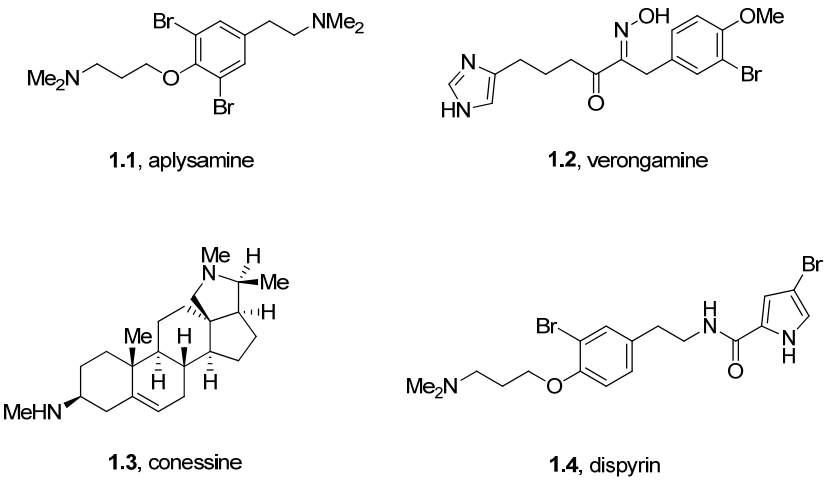

1.1, aplysamine

1.2, verongamine

1.3, conessine

1.4, dispyrin

Figure 1.1.1: Marine natural products **1.1 - 1.4** with significant affinity for, and inhibition of the H_3 receptor.

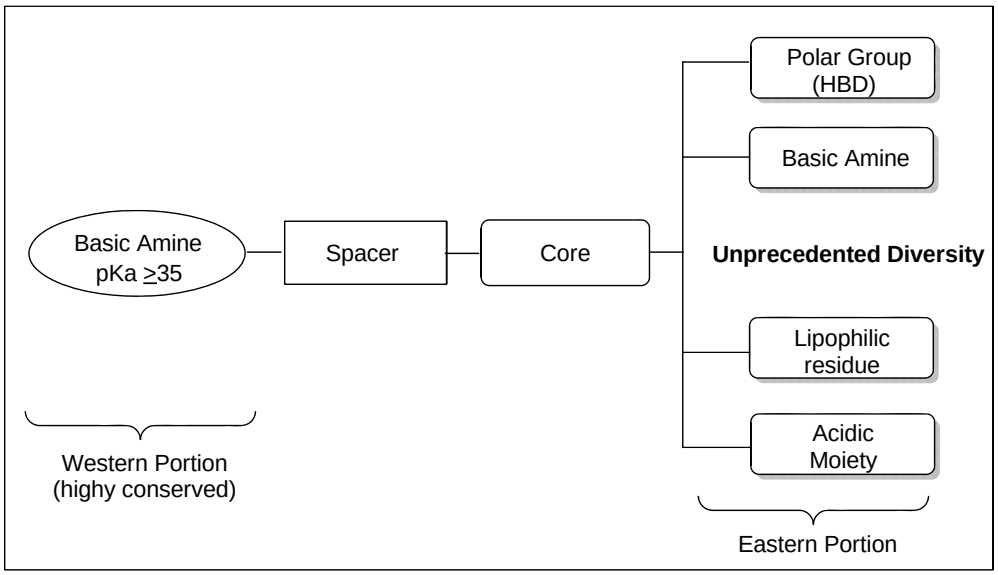

Figure 1.1.2: The refined H_3 pharmacophore model, to which synthetic small molecule and natural product H_3 antagonists conform.

Importantly, conserved elements have been identified within small molecule H_3 ligand scaffolds that have resulted in a highly predictive pharmacophore model, and many marine natural products conform to this model[9,10,11]. This pharmacophore is best represented by generally linear structures featuring a basic amine situated on the western-most section of the

molecule. An aliphatic spacer region connects the western amine to the core, which can feature a range of different functionalities including hydrogen bond donor groups, additional basic amines, lipophilic aromatic or saturated ring systems, and acidic moieties.

β-Carboline alkaloids are a prevalent class of biologically active natural products from marine organisms. They exhibit diverse structural features and distinct neuropharmacological profiles[12,13]. Our lab has worked extensively in this arena[14,15], and we were attracted to a class of β-carboline alkaloids represented by the trypargines **1.5-1.7** (Figure 1.1.3), as these alkaloids mapped well onto the H_3 pharmacophore model and offered a synthetic challenge[16,17]. Both trypargine **1.5**[16] and 6-hydroxytrypargine **1.6**[17] are highly toxic alkaloids. (+)-7-Bromotrypargine **1.7**, was only recently isolated by Quinn and coworkers from the Australian marine sponge *Ancornia sp.*, and found to possess antimalarial activity[18]. 6-Bromotyramine **1.8** was isolated along with **1.7** in similar quantities, and is believed to be a key biosynthetic precursor[18]. Based on the neuropharmacological profiles of β-carboline alkaloids, and the electron-deficient nature of **1.7**, relative to the electron-rich congeners **1.5** and **1.6**, which might diminish the cytotoxicity, the total synthesis of **1.7** and biological evaluation seemed warranted.

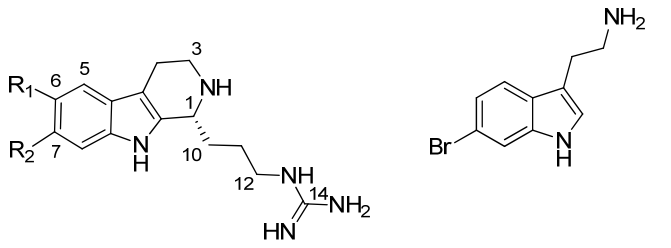

1.5, R_1 = H, R_2 = H, (+)-trypargine
1.6, R_1= OH, R_2 = H, (+)-6-OH-trypargine
1.7, R_1= H, R_2 = Br, (+)-7-Br-trypargine

1.8, 6-bromotryptamine

Figure 1.1.3: Structures of the (+)-trypargines **1.5 - 1.7** and 6-bromotryptamine **1.8**.

1.2 Retrosynthetic Analysis of (+)-7-bromotrypargine

Our retrosynthesis of **1.7** (Figure 1.2.1) began by disconnecting the guanidine moiety, as it could easily be incorporated late in the synthesis. We envisioned two approaches to cyclize the β-carboline C ring: either utilize the recently reported Brønsted-acid catalyzed, enantioselective Protio-Pictet-Spengler reaction[19,20], or a Bischler-Napieralski reaction[14], followed by an asymmetric Noyori transfer hydrogenation protocol[21].

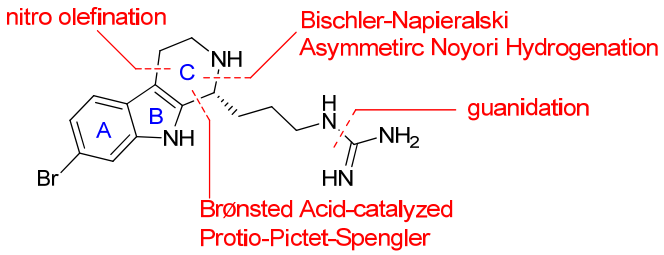

Figure 1.2.1: Retrosynthetic Analysis of (+)-7-bromotrypargine

1.3 Enantioselective Protio-Pictet-Spengler Route

We viewed the enantioselective protio-Pictet-Spengler reaction as a more favorable route, as it would utilize newly developed chemistry to form the C ring and set the C-1 stereocenter in a single reaction, whereas the Bischler-Napieralski reaction/Noyori transfer hydrogenation route involved a two-step procedure and has been previously featured in other well established protocols[15,21].

1.3.1 Synthesis of 6-bromotryptamine

As both envisioned routes toward **1.7** required the synthesis of 6-bromotyramine **1.8,** our forward synthesis began with 6-bromoindole. As shown in Scheme 1.3.1.1, acid-mediated nitro olefination of 6-bromo-1*H*-indole **1.9**, as prescribed by Büchi[12], proceeded smoothly affording nitro olefin **1.10** in 98% yield. Exhaustive reduction with $LiAlH_4$ then provided natural 6-bromotyramine **1.8** in 76% yield.

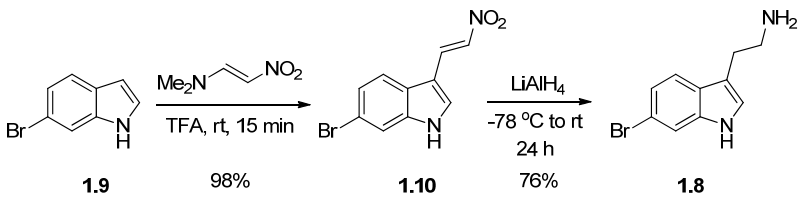

Scheme 1.3.1.1: Synthesis of 6-bromotryptamine **1.8**.

1.3.2 Synthesis of Key Aldehyde 1.13

Key aldehyde **1.13** was synthesized in two steps starting from commercially available 4-aminobutanol (Scheme 1.3.2.1). Phthalamide protection under microwave conditions proceeded smoothly, followed by Swern oxidation to yield the desired aldehyde **1.13**.

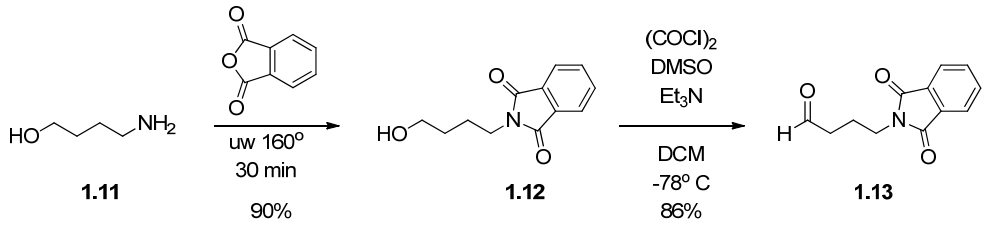

Scheme 1.3.2.1: Synthesis of key aldehyde **1.13**.

1.3.3 Synthesis of Asymmetric Pictet-Spengler Catalyst

The Jacobsen thiourea asymmetric Pictet-Spengler catalyst was synthesized in two steps starting from *N*-methylanaline and *N*-Boc protected L-valine. Standard EDC coupling conditions were employed, followed by acid mediated Boc group cleavage to render the free amine **1.16**. Base induced thiourea formation from the corresponding thiocyanate **1.17** yielded the complete catalyst **1.18** in good yield (Scheme 1.3.3.1). Optical rotation analysis confirmed that we had synthesized the correct enantiomer of the catalyst[19].

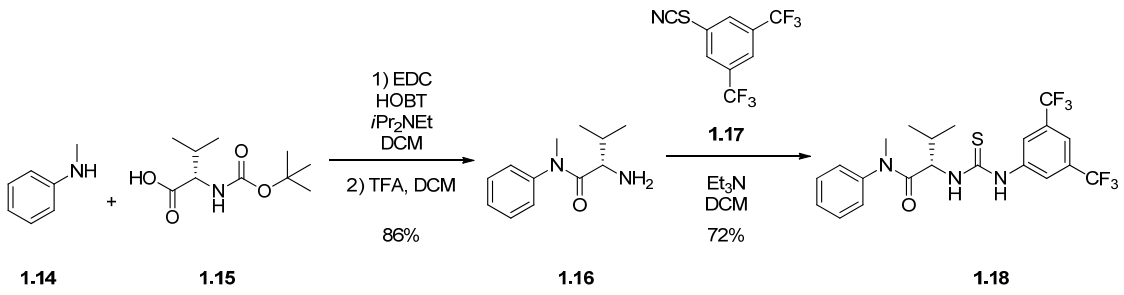

Scheme 1.3.3.1: Synthesis of the Jacobsen thiourea asymmetric Pictet-Spengler catalyst

1.3.4 Protio-Pictet-Spengler Route

With gram quantities of **1.8** and **1.13** in hand, we evaluated both the Jacobsen thiourea Brønsted-acid catalyzed, enantioselective Protio-Pictet-Spengler reaction[19] as well as the Dixon chiral BINOL-derived phosphoric acid variation[20] to produce the key, chiral β-carboline core **1.19** (Scheme 1.3.4.1).

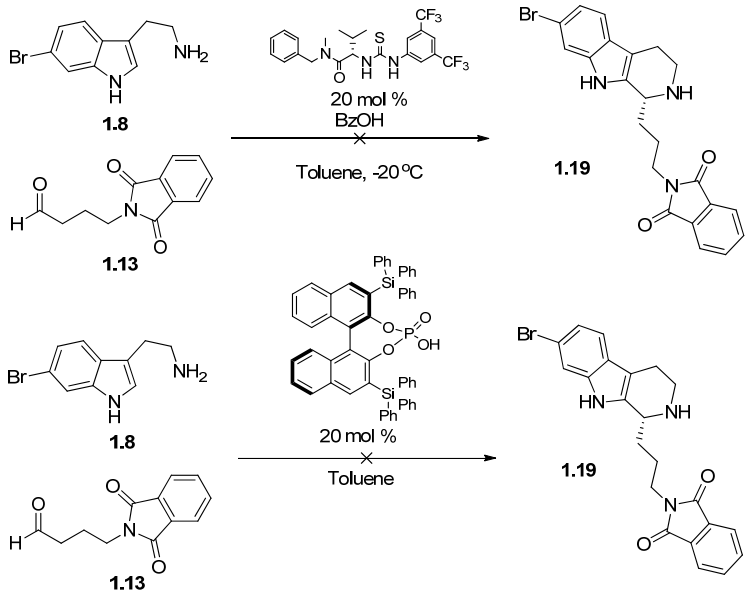

Scheme 1.3.4.1: Brønsted-acid catalyzed, enantioselective Protio-Pictet-Spengler approach.

Interestingly, neither protocol afforded **1.19**. A range of different conditions were employed, including modifications to stoichiometric equivalents of starting materials and

catalysts, solvents, and reaction temperatures. We found that conversion to **1.19** could be forced under both protocols (~80% yield) at temperatures above 50° C, however enantioselectivity eroded, with both catalyst systems yielding racemic mixtures. We hypothesized that the electron-withdrawing character of the bromine atom could be removing sufficient electron density from the indole system to prohibit nucleophilic attack onto the corresponding imine formed from the condensation reaction between **1.8** and **1.13**.

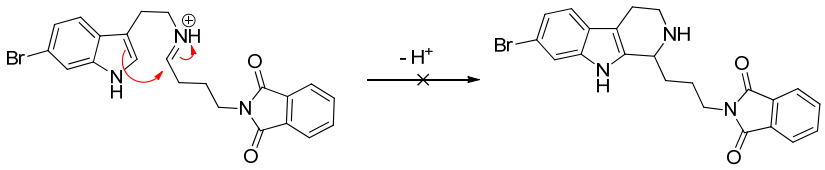

Scheme 1.3.4.2: Key nucleophilic attack by indole C-2 position.

In order to test this hypothesis, an electron rich congener of **1.8**, in the form of 6-methoxytryptamine **1.20** was employed. When **1.13** and **1.20** were combined under the optimized conditions reported by Jacobsen and coworkers, the reaction proceeded smoothly, providing **1.21** in good enatiomeric excess and conversion.

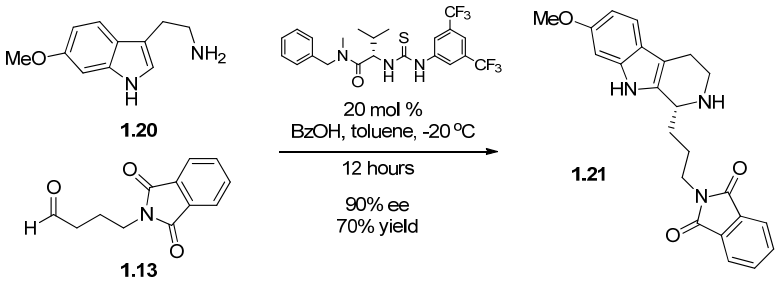

Scheme 1.3.4.3: Electron-rich congener Protio-Pictet-Spengler reaction.

With these data in hand, we concluded that the Brønsted-acid catalyzed, enantioselective Protio-Pictet-Spengler approach with the more electron deficient **1.8**, was an intractable route toward the natural product. Indeed, the original reports by Jacobsen and Dixon utilized only

electron rich substrates[19,20]. Thus, our focus shifted towards a Bischler-Napieralski/Noyori asymmetric transfer hydrogenation approach[15,21].

1.4 Bischler-Napieraslki/Noyori Transfer Hydrogenation Route

In order to proceed with the Bischler-Napieralski reaction, key acid **1.23** was prepared in 98% yield by treating 4-aminobutanoic acid **1.22** with phthalic anhyride under microwave conditions (Scheme 1.4.1). Standard EDC/HOBT amide coupling conditions were then employed with **1.8** and **1.23,** providing amide **1.24** as the cyclization precursor.

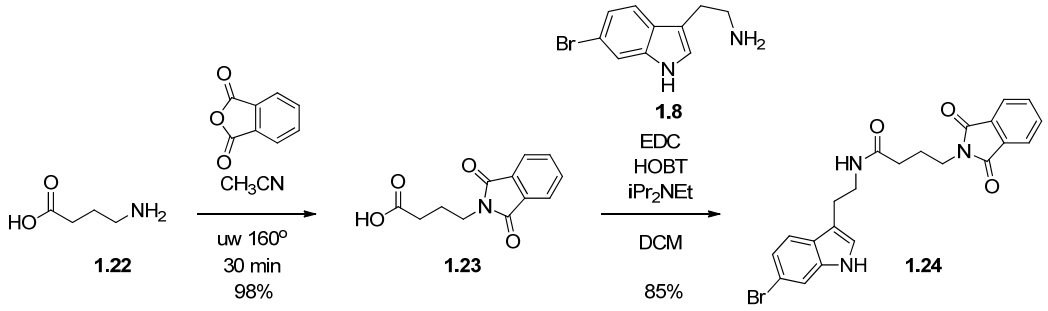

Scheme 1.4.1: Phthalamide protection and amide coupling.

1.4.1 Synthesis of Noyori Transfer Hydrogenation Catalyst

The Noyori transfer hydrogenation catalyst was synthesized by heating (p-Cymene)ruthenium dichloride dimer in isopropyl alcohol with *N*-((1R,2R)-2-amino-1,2-diphenylethyl)-4-tosylate (Scheme 1.4.1.1)[22].

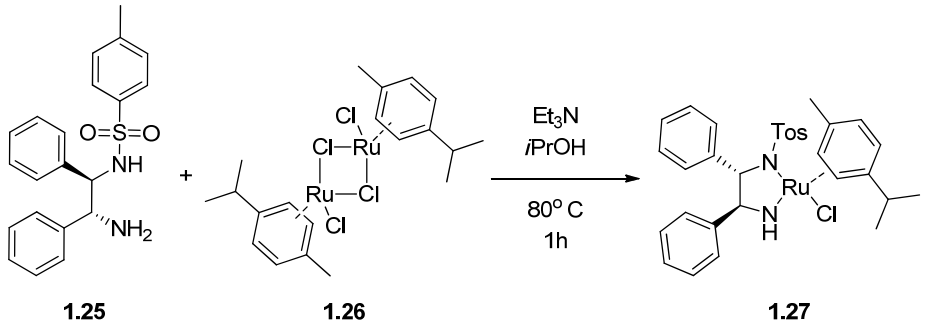

Scheme 1.4.1.1: Synthesis of transfer hydrogenation catalyst **1.27**.

1.4.2 Bischler-Napieralski Reaction and Noyori Transfer Hydrogenation

The Bischler-Napieralski reaction[15,21] was facilitated by treatment of amide **1.19** with $POCl_3$ in refluxing acetonitrile, yielding imine **1.20** in 88% yield. Noyori asymmetric transfer hydrogenation with formic acid, triethylamine, and (*S,S*)-ruthenium catalyst **1.27** delivered the β-carboline core **1.19** in 80% yield and 90% ee, which we confirmed utilizing chiral SFC chromatography.

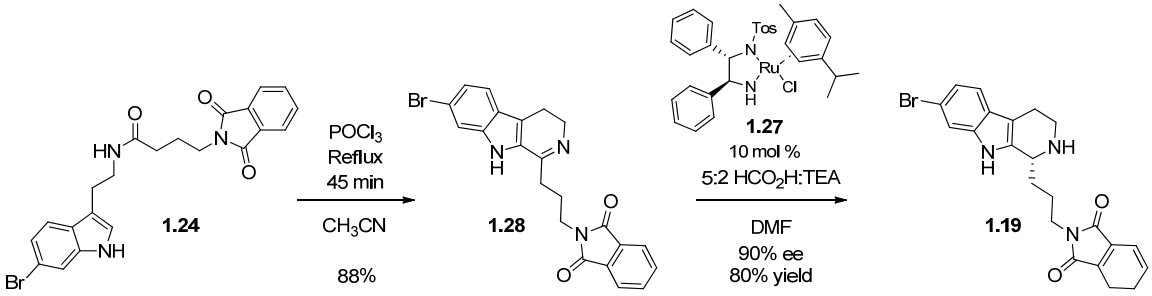

Scheme 1.4.2.1: Bischler-Napieralski reaction / Noyori asymmetric transfer hydrogenation.

1.5 Final Steps Toward 1.7

After setting the stereocenter, we then removed the phthalimide protecting group with hydrazine to afford amine **1.29**. Guanidation and removal of the *bis*-Boc protecting groups proceeded in 84% yield over the three steps delivering, for the first time, (+)-7-bromotrypargine

1.7. Synthetic **1.7** exhibited physical and spectroscopic data identical to that of natural **1.7**[18], confirming the structure and absolute stereochemistry. Overall, the synthesis proceeds in 9 steps, 8 steps longest linear sequence, in 40% overall yield which provided significant material to enable detailed biological evaluation.

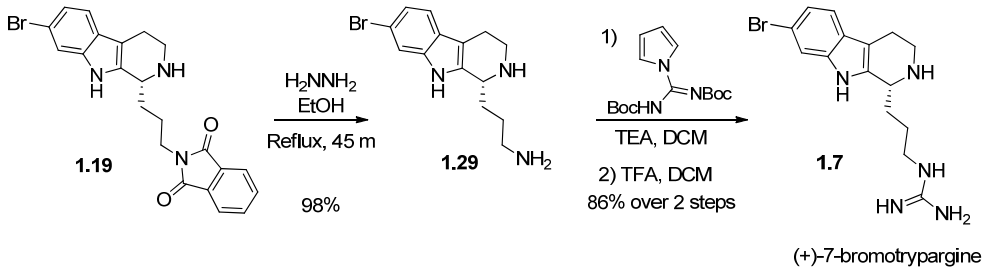

Scheme 1.5.1: Final steps to complete **1.7**.

1.6 Biological Evaluation of (+)-7-bromotrypargine

In order to examine the effects of **1.7** and unnatural analogs at various therapeutic targets, we first addressed questions of general cytotoxicity.

1.6.1 Cytotoxicity Screening

As **1.5** and **1.6** are highly toxic alkaloids, we first evaluated **1.7** in a standard cytotoxicity assay and found **1.7** to be non-toxic up to concentrations of 20 μM, suggesting that the pharmacological profile of **1.7** might diverge from **1.5** and **1.6**[23]. This surprising result led us to study **1.7** in our standard HCT116 colon carcinoma cell viability assay[24,25]. Here as well, **1.7** had no effect on HCT116 cell viability after 48 hours. In contrast, advanced intermediate **1.29**, an unnatural analog of **1.7**, displayed an IC_{50} value of 3 μM in this assay, completely killing the cells after 48 hours.

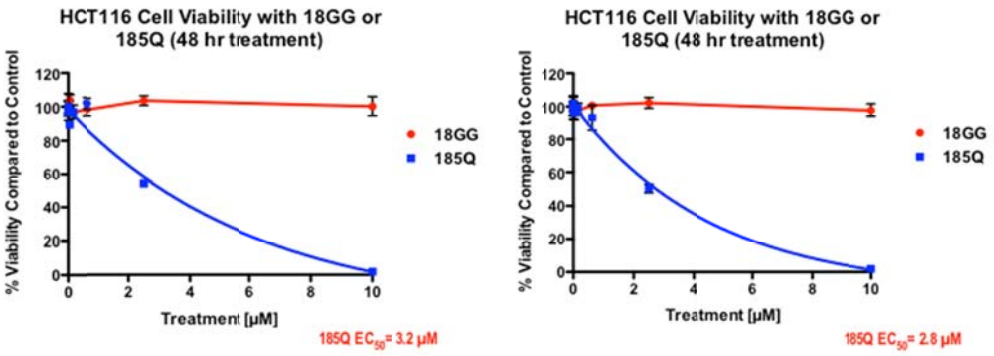

Figure 1.6.1.1: HCT116 Cell Viability Assays with **1.7** (18GG) and **1.29** (185Q). IC_{50} Values of 3.2 µM and 2.8 µM were calculated for **1.29**.

These data prompted examination of unnatural analog **1.29** in additional colon carcinoma (SW620 and H520) cell lines[25]. Interestingly, **1.29** dramatically inhibited cell viability as well as cell proliferation in BrdU assays[23]. In contrast, **1.7** was devoid of activity in all of these assays.

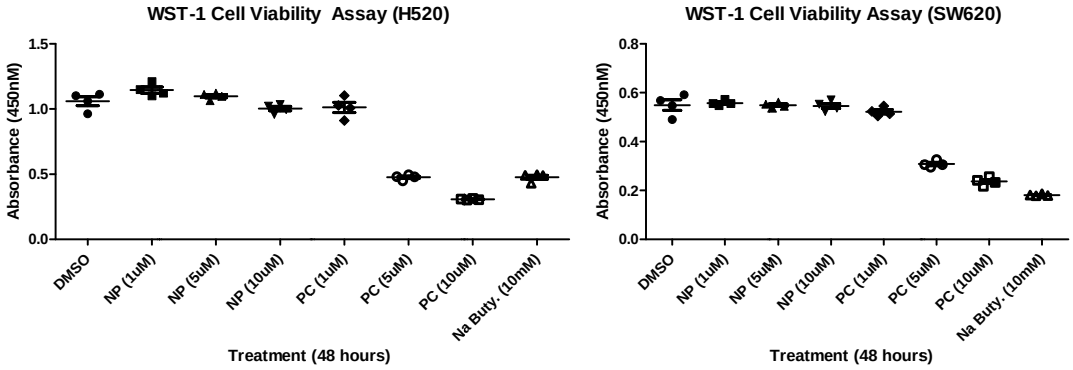

Figure 1.6.1.2: WST-1 Cell Viability Assay results with **1.7** (NP) and **1.29** (PC). Na Butyrate is a positive control for inhibition of cell proliferation.

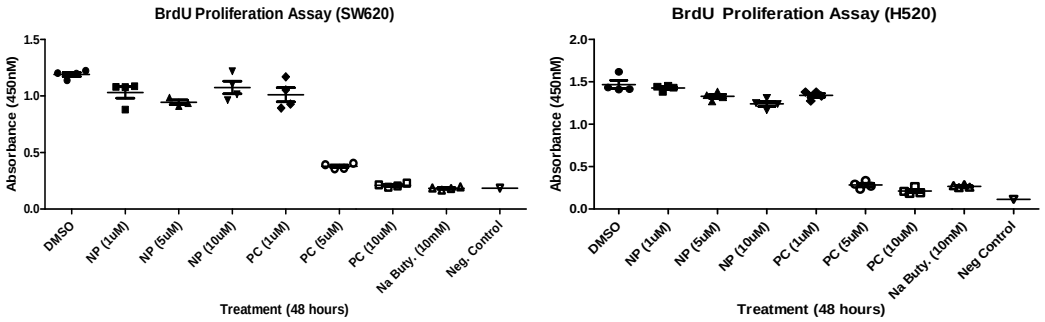

Figure 1.6.1.3: BrdU Cell Proliferation Assay results with **1.7** (NP) and **1.29** (PC). Na Butyrate is a positive control for inhibition of cell proliferation.

Collectively, these data informed us of two important points: 1) the pharmacology of the more electron deficient (+)-7-bromotrypargine (**1.7**) is distinct from **1.5** and **1.6** and warranted further biological evaluation as it lacked toxicity, and 2) unnatural analog **1.29** possesses an intriguing pharmacological profile warranting the synthesis and characterization of additional unnatural analogs of **1.7**.

1.6.2 GPCR, Ion Channel, and Transporter Screens

(+)-7-Bromotrypargine (**1.7**) was then evaluated in an external panel[26] of 68 GPCRs, ion channels and transporters in radioligand binding assays in an attempt to identify discrete molecular targets with therapeutic relevance, a strategy that has been highly successful[6,7]. In this instance, **1.7** was found to have a very clean pharmacological profile, affording significant percent inhibition of radioligand binding at only three targets: H_3 (74% at 10 μM), the Dopamine Transporter, DAT (81% at 10 μM) and the norepinephrine transporter, NET (82% at 10 μM). Interestingly, these are all targets for important pathologies of the central nervous system (CNS), and **1.7** did prove to possess activity at the H_3 receptor as envisioned. Indeed, **1.7** is now the fifth marine natural product with significant activity at H_3, a target of interest for Alzheimer's disease, schizophrenia, ADHD and other indications[8,9,10]. Functional dose-response curves were

generated for the three targets in both binding (K_i) and functional (IC_{50}) assays[26], proving that **1.7** both bound to, and inhibited, the three targets with modest potencies (Table 1.6.2.1).

Table 1.6.2.1: Pharmacological profile of **1.7**, radioligand binding and functional assay results.

Target	% Inhibition (@10 uM)	K_i (uM)	IC_{50} (uM)
H_3	74	1.8	3.6
DAT	81	3.0	3.8
NET	82	1.9	1.9

1.7 Unnatural Analog Development

In order to optimize the H_3 receptor and dual NET/DAT activity, we would need to have reliable chemistry to prepare unnatural analogs of **1.7** (Figure 1.7.1) in short order, while also removing functionality, such as the guanidine, that would limit brain penetration.

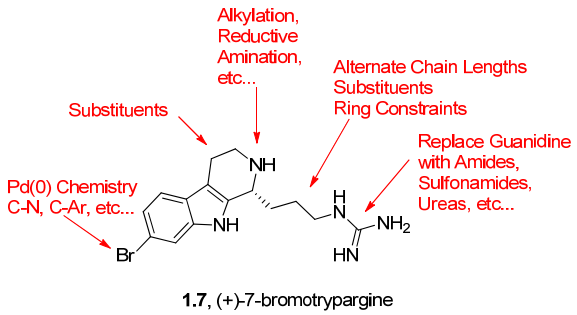

Figure 1.7.1: Potential sites about **1.7** for differentiation in unnatural analog development.

Thus, we piloted a number of 'classical' reactions (reductive amination, acylation, sulfonylation, Suzuki coupling, etc.) that are mainstays in the pharmaceutical industry en route to unnatural analogs of **1.7** (Scheme 1.7.1). Prior to removal of the phthalamide moiety, the secondary amine **1.19** underwent a reductive amination reaction to provide tertiary amine **1.30** in

88% yield. Removal of the phthalmide moiety liberated primary amine **1.31** that was smoothly acylated **1.32**, sulfonylated **1.33** or guanidated **1.34** to afford unnatural analogs of **1.7** in excellent isolated yields (>85%).

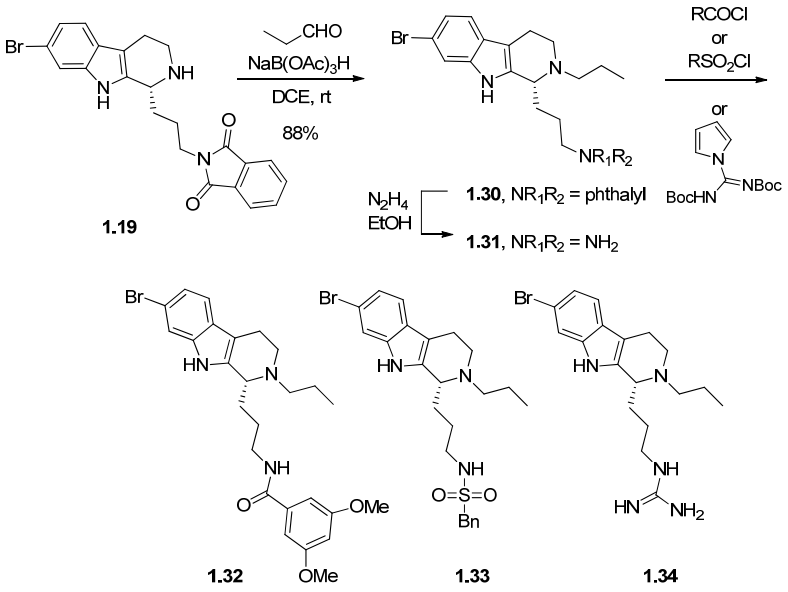

Scheme 1.7.1: Synthesis of unnatural analogs of **1.7**

1.8 Conclusion

In summary, we completed the first total synthesis of (+)-7-bromotrypargine (**1.7**) in nine steps (8 steps longest linear sequence) in 40% overall yield from commercial materials. In the course of this work, we found that the Brønsted-acid catalyzed, enantioselective Protio-Pictet-Spengler reaction works well for electron-rich substrates, but fails for electron-deficient cores, and thus, was ineffective in accessing **1.7**. Biological evaluation of **1.7** and an advanced intermediate **1.29** proved very exciting, as **1.7** displayed divergent pharmacology from related β-carbolines **1.5** and **1.6**. Additionally, we found that **1.29** was extremely cytotoxic in multiple non-transformed and colon cancer cell lines. Receptor profiling efforts identified **1.7** as a moderately potent, dual DAT/NET inhibitor, and only the second known compound and chemotype, to display such a pharmalogical profile devoid of SERT activity. This finding was in addition to the

anticipated activity as an H_3 antagonist, based on the H_3 pharmacophore model. The intriguing pharmacological profile then led us to explore chemistry to access unnatural analogs.

EXPERIMENTAL METHODS

Synthesis:

All reagents were purchased from Sigma-Aldrich Corp., Matrix Scientific, Fisher Scientific, and Strem Corp., and were used without purification. Analytical thin-layer chromatography (TLC) was performed on 250 μm silica gel plates from Sorbent Technologies. Visualization was accomplished via UV light, and/or the use of ninhydrin, 2,4-dinitrophenylhydrazine, and potassium permanganate solutions followed by application of heat. Chromatography was performed using Silica Gel 60 (230-400 mesh) from Sorbent Technologies or Silica RediSep Rf flash columns on a CombiFlash Rf automated flash chromatography system. All ^{1}H and ^{13}C NMR spectra were recorded on Bruker AV-400 (400 MHz), DRX-500 (500 MHz) and AV-600 (600 MHz) instruments. Chemical shifts are reported in ppm relative to residual solvent peaks as an internal standard set to δ 7.26 and δ 77.16 ($CDCl_3$), δ 3.31 and δ 49.00 (CD_3OD), and δ 2.50 and δ 39.52 (DMSO). Data are reported as follows: chemical shift, multiplicity (s = singlet, d = doublet, t = triplet, q = quartet, p = pentet br = broad, dd=doublet of doublets, dq=doublet of quartets, td = triplet of doublets, pd = pentet of doublets, m = multiplet), coupling constant (Hz), integration. Low resolution mass spectra (LCMS) were obtained on an Agilent 1200 LCMS with electrospray ionization. High resolution mass spectra (HRMS) were recorded on a Waters Qtof-API-US plus Acquity system with ES as the ion source. Analytical high pressure liquid chromatography (HPLC) was performed on an Agilent 1200 analytical LCMS with UV detection at 214 nm and 254 nm along with ELSD detection. Chiral separations were performed on a Thar Investigator II supercritical fluid chromatograph (SFC) utilizing Chiralcel® OD, OD-Cl, OJ, and Chiralpak® IA columns. Optical rotations were acquired on a Jasco P-2000 polarimeter at 23°C and 589nm. The specific rotations were calculated according to the equation $[\alpha]_D^{23} = (\alpha / l \times c)$ where *l* is the path length in decimeters and *c* is the concentration in g/100mL.

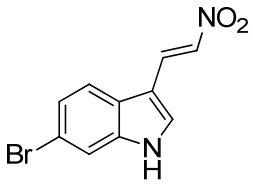

6-bromo-3-(2-nitrovinyl)-1H-indole (1.10).

1-(Dimethylamino)-2-nitroethylene (1.6 g, 13.72 mmol) was dissolved in 20 mL trifluoroacetic acid and stirred 5 min. 6-Bromoindole **(1.9)** (3.23 g, 16.47 mmol) was dissolved in 15 mL dichloromethane and added to the stirring solution. The mixture was stirred for 15 minutes at room temperature and monitored for loss of starting indole by thin layer chromatography. After 15 minutes, the reaction was transferred to a 1 L separatory funnel, rinsing with DCM, and quenched with 200 mL water. The aqueous phase was extracted three times with DCM and the combined organic phase was dried over $MgSO_4$, filtered, and concentrated onto 10 g silica. The product was purified on silica (EtOAc/hexanes 1:2), yielded 3.61 g (98%) **1.10** as a yellow solid. ^{1}H NMR (600.1 MHz, d_6-DMSO) δ (ppm): 8.39 (d, J = 13.5 Hz, 1H) 8.25 (s, 1H), 8.02 (d, J = 13.5 Hz, 1H), 7.95 (d, J = 8.51 Hz, 1H), 7.71 (d, J = 1.75 Hz, 1H), 7.35 (dd, J = 1.85, 8.51 Hz, 1H); ^{13}C NMR (150 MHz, d_6-DMSO) δ (ppm): 138.9, 137.1, 134.4, 132.3, 124.9, 124.1, 122.6, 116.3, 115.8, 108.6; HRMS (TOF, ES+) $C_{10}H_8N_2O_2Br$ $[M+H]^+$ m/z 266.9769, measured 266.9769.

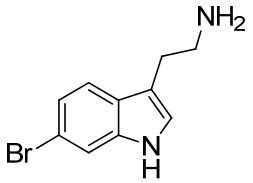

6-bromotryptamine (1.8).

A 250 mL schlenk flask equipped with a stir bar and septa was flame dried under vacuum. $LiAlH_4$ (2.03 g, 53.69 mmol) was added, the flask then was sealed and vacuum purged three

times, refilling with argon. Tetrahyrdofuran (89 mL) was added and the solution was stirred 5 minutes at room temperature before being cooled to -78°C for 10 minutes. 6-bromo-3-(2-nitrovinyl)-1H-indole **1.10** (2.39 g, 8.94 mmol) was dissolved in 89 mL THF and added dropwise via syringe to the stirred solution. The reaction was allowed to warm to room temperature overnight. The reaction was monitored by thin layer chromatography over 24 hours. After 24 hours, the flask was placed in an ice bath and cooled for 5 minutes before the careful addition of 2 mL water, followed by 2 mL 15% aq. NaOH, followed by 6 mL water. The flask was stirred for 30 minutes and a small amount of $MgSO_4$ was added. The mixture was then filtered through a glass frit, washing the formed solid with dichloromethane. The resulting brown solution was then concentrated to afford a crude brown oil. The product was purified on silica (80:18:2 $CHCl_3$:MeOH:NH_4OH), yielded 1.63 g (76%) **1.8** as a brown solid. ^{1}H NMR (600.1 MHz, CD_3OD) δ (ppm): 7.56 (d, *J* = 1.65 Hz, 1 H), 7.51 (d, *J* = 8.51 Hz, 1H), 7.21 (s, 1H), 7.18 (d, *J* = 7.51 Hz, 1H) 3.24 (t, *J* = 7.63 Hz, 2H) 3.12 (t, *J* = 7.63 Hz, 2H); ^{13}C NMR (150 MHz, CD_3OD) δ (ppm): 137.5, 126.2, 122.9, 121.2, 119.2, 114.3, 113.6, 112.4, 41.5, 27.8; HRMS (TOF, ES+) $C_{10}H_{12}N_2Br$ $[M+H]^+$ m/z 239.0184, measured 239.0182.

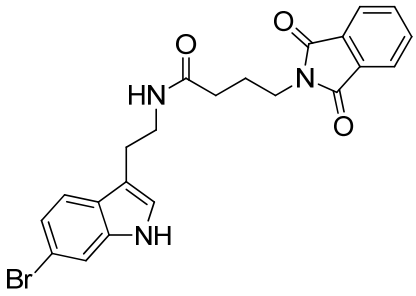

N-(2-(6-bromo-1H-indol-3-yl)ethyl)-4-(1,3-dioxoisoindolin-2-yl)butanamide (1.24).

6-Bromotryptamine **(1.8)** (1.0 g, 4.18 mmol), 4-(1,3-dioxoisoindolin-2-yl)butanoic acid **(1.23)** (1.17 g, 5.01 mmol) EDC (1.60 g, 8.36 mmol), and HOBT (1.12 g, 8.36 mmol) were dissolved in 30 mL 9:1 DCM:DIEA solution. The mixture was stirred 12 hours. Analysis by LCMS showed product conversion. The contents of the flask were transferred to a 500 mL separatory funnel,

150 mL water was added and the solution was extracted 3 times with DCM. The combined organic phase was dried over $MgSO_4$ and concentrated under reduced pressure. The product was purified on silica (DCM → 2% MeOH in DCM) and isolated **1.24** as a yellow solid 1.61 g (85%). ^{1}H NMR (600.1 MHz, $CDCl_3$) δ (ppm): 8.09 (s, 1H), 7.78 (dq, *J* = 8.45, 57.8 Hz, 4H), 7.52 (d, *J* = 1.65 Hz, 1H), 7.48 (d, *J* = 8.45 Hz, 1H), 7.22 (dd, *J* = 1.65, 8.45 Hz, 1H) 7.07 (d, *J* = 2.25 Hz, 1H), 5.93 (s, 1H), 3.69 (t, *J* = 6.36 Hz, 2H), 3.59 (q, *J* = 6.79, 6.10 Hz, 2H), 2.97 (t, *J* = 6.91 Hz, 2H), 2.17 (t, *J* = 7.13 Hz, 2H), 2.01 (p, *J* = 6.91 Hz, 2H), 1.58 (s, 1H); ^{13}C NMR (150 MHz, $_{CD3OD}$) δ (ppm): 171.7, 168.5, 137.0, 134.0, 131.9, 126.3, 123.2, 122.7, 122.5, 120.0, 115.7, 114.0, 113.3, 39.6, 37.1, 33.8, 25.1, 24.8; HRMS (TOF, ES+) $C_{22}H_{21}N_3O_3Br$ $[M+H]^+$ m/z 454.0766, measured 454.0764.

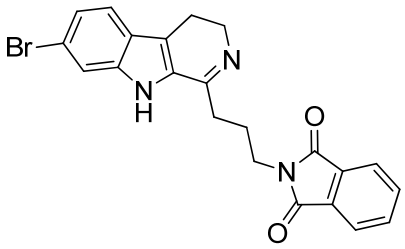

2-(3-(7-bromo-4,9-dihydro-3H-pyrido[3,4-b]indol-1-yl)propyl)isoindoline-1,3-dione (1.28).

N-(2-(6-bromo-1H-indol-3-yl)ethyl)-4-(1,3-dioxoisoindolin-2-yl)butanamide **(1.24)** (1.23 g, 2.71 mmol) was placed in a 250 round bottom flask. Acetonitrile (25 mL) was added, followed by $POCl_3$ (2.08 g, 1.67 mmol). The flask was then brought to reflux for 1 hour. Starting material loss and product conversion were monitored by TLC and LCMS. After 1 hour, the flask was removed from the heating bath and the excess $POCl_3$ was evaporated under reduced pressure. The flask contents were then transferred to a 500 mL separatory funnel, washing with DCM, 100 mL water was added and the solution was extracted three times with DCM. The combined organic phased was concentrated and purified on silica (30:1 $CHCl_3$:MeOH) to afford 1.043 g (88%) **1.28**. ^{1}H NMR (600.1 MHz, $_{CD3OD}$) δ (ppm): 7.73 (s, 4H), 7.66 (d, *J* = 1.49 Hz, 1H), 7.54

(d, J = 8.74 Hz, 1H), 7.27 (dd, J = 1.51 Hz, 8.74, 1H), 3.94 (t, J = 8.97 Hz, 2H), 3.83 (t, J = 6.49 Hz, 2H), 3.15 (t, J = 9.08 Hz, 2H), 3.12 (t, J = 8.93 Hz, 1H), 2.28 (p, J = 7.03 Hz, 2H); ^{13}C NMR (150 MHz, CD_3OD) δ (ppm): 169.5, 168.2, 141.8, 134.0, 131.6, 125.8, 135.1, 125.0, 122.9, 122.85, 122.81, 122.6, 115.5, 42.2, 36.5, 29.9, 25.5, 18.2; HRMS (TOF, ES+) $C_{22}H19N_3O_2Br$ $[M+H]^+$ m/z 436.0661, measured 436.0663.

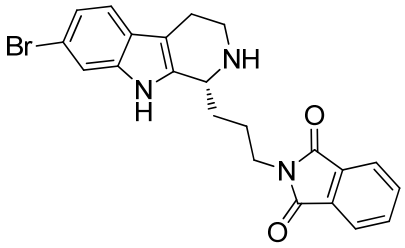

(R)-2-(3-(7-bromo-2,3,4,9-tetrahydro-1H-pyrido[3,4-b]indol-1-yl)propyl)isoindoline-1,3-dione (1.19).

A 100 mL round bottom flask was charged with **1.28** (893 mg, 2.046 mmol) and **1.21** (118.4 mg, 0.204 mmol) and DMF (7.8 mL) was added. The flask was cooled to 0°C and a solution of premixed 5:2 formic acid:triethylamine (1.75 mL) was added. The flask was sealed, stirred, and allowed to warm overnight. Reaction progress was monitored by LCMS. After 12 hours, the flask contents were transferred to a 250 mL separatory funnel, washing with DCM. Water (50 mL) was added and the solution was extracted 3 times with DCM. The combined organic phase was dried over $MgSO_4$ and concentrated. The product was purified on silica (30:1 $CHCl_3$:MeOH), yielded 717.4 mg **1.19** as a golden-brown solid. $[\alpha]_D^{23}$ 35.5° (c = 1.0, MeOH); ^{1}H NMR (600.1 MHz, CD_3OD) δ (ppm): 7.85 (m, 4H), 7.49 (d, J = 1.56 Hz, 1H), 7.38 (d, J = 8.50 Hz, 1H), 7.17 (dd, J =1.56, 8.50 Hz, 1H), 4.75 (m, 1H), 3.84 (t, J = 6.51 Hz, 2H), 3.73 (m, 1H) 3.44 (m, 1H), 3.04 (m, 2H), 2.30 (m, 1H), 1.96 (m, 3H); ^{13}C NMR (150 MHz, CD_3OD) δ (ppm): 168.4, 137.5, 134.0, 131.8, 129.3, 124.8, 122.7, 122.3, 119.1, 115.4, 113.7, 106.2, 52.8, 41.3,

36.6, 29.0, 23.9, 17.8; HRMS (TOF, ES+) $C_{22}H_{21}N_3O_2Br$ $[M+H]^+$ m/z 438.0817, measured 438.0814.

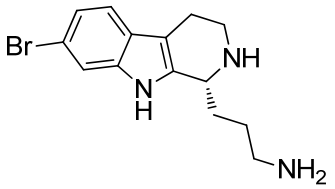

(R)-3-(7-bromo-2,3,4,9-tetrahydro-1H-pyrido[3,4-b]indol-1-yl)propan-1-amine (1.29).

A 100 mL round bottom flask was charged with **1.19** (514 mg, 1.17 mmol). EtOH was added (10 mL), followed by hydrazine hydrate (368 uL, 11.72 mmol). The flask was brought to reflux for 45 minutes, monitoring by LCMS. After 45 minutes, the flask was cooled and the contents were concentrated to remove ethanol. The product was purified on silica (80:18:2 $CHCl_3$:MeOH:NH_4OH), yielded 317.3 mg (88%) **1.29** as a brown solid. $[\alpha]_D^{23}$ 28.5° (*c* = 2.0, MeOH); ^{1}H NMR (600.1 MHz, CD_3OD) δ (ppm): 7.56 (d, *J* = 1.58 Hz, 1H), 7.39 (d, *J* = 8.43 Hz, 1H), 7.17 (dd, *J* = 1.58, 8.43 Hz, 1H), 4.77 (q, *J* = 4.41 Hz, 1H), 3.75 (m, 1H), 3.49 (m, 1H), 3.07 (m, 4H), 2.34 (m, 1H), 2.11 (m, 1H), 1.97 (m, 2H); ^{13}C NMR (150 MHz, CD_3OD) δ (ppm): 161.1, 160.9, 137.6, 129.1, 124.9, 122.4, 119.2, 115.4, 113.9, 106.5, 52.5, 41.2, 38.7, 28.6, 22.8, 17.8; HRMS (TOF, ES+) $C_{14}H_{19}N_3Br$ $[M+H]^+$ m/z 308.0862, measured 308.0759.

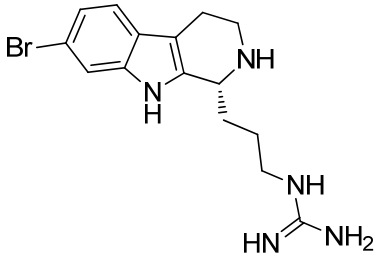

(+)-7-Bromotrypargine (1.7).

A 50 mL round bottom flask was charged with **1.29** (231 mg, 0.749 mmol) and DCM (3 mL). N,N'-Bis(Boc)-1H-pyrazole-1-carboxamidine (255.8 mg, 0.824 mmol) and triethylamine (156

uL, 1.12 mmol) were then added. The flask was stirred 3 hours and monitored by TLC and LCMS. After three hours, 5 mL trifluoroacetic acid were added and the reaction was stirred 4 hours. Reaction progress was monitored by LCMS. After 4 hours, the reaction was concentrated and the product was purified by revere phase high performance liquid chromatography using acetonitrile and 0.1% TFA/water (gradient: 10:90 to 90:10), yielded 225 mg (86% over two steps) **1.7** as a glassy yellow solid. $[\alpha]_D^{23}$ 40.0° (*c* = 1.0, MeOH); ^{1}H NMR (600.1 MHz, d_6-DMSO) δ (ppm): 11.3 (s, 1H), 9.49 (s, 1H), 9.00 (s, 1H), 7.73 (br s, 1H), 7.56 (d, *J* = 1.68 Hz, 1H), 7.46 (d, *J* = 8.50 Hz, 1H), 7.20 (br s, 2H), 7.18 (br s, 2H), 7.18 (dd, *J* = 1.68, 8.50 Hz, 1H), 4.69 (s, 1H), 3.58 (m, 1H), 3.34 (m, 1H), 3.18 (m, 2H), 2.93 (t, *J* = 5.5 Hz, 2H), 2.11 (m, 1H), 1.90 (m, 1H), 1.69 (m, 1H); ^{13}C NMR (150 MHz, d_6-DMSO) δ (ppm): 157.2, 137.5, 131.4, 125.2, 122.4, 120.3, 118.5, 114.9, 114.3, 106.6, 52.2, 40.9, 40.7, 28.9, 24.7, 18.4; HRMS (TOF, ES+) $C_{15}H_{21}N_5Br$ $[M+H]^+$ m/z 350.0980, measured 350.0982.

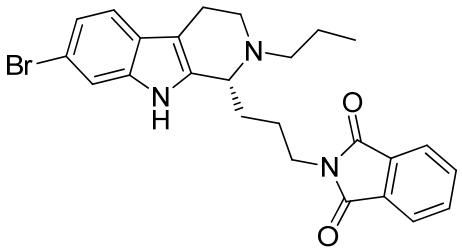

(R)-2-(3-(7-bromo-2-propyl-2,3,4,9-tetrahydro-1H-pyrido[3,4-b]indol-1-yl)propyl)isoindoline-1,3-dione (1.30).

A 50 mL round bottom flask was charged with **1.19** (173 mg, 0.395 mmol), propionaldehyde (45.8 mg, 0.789 mmol), and dichloroethane (3 mL). The solution was stirred 30 minutes before the addition of $NaBH(OAc)_3$ (125.4 mg, 0.592 mmol). The mixture was stirred 2 hours, monitoring by TLC and LCMS. After two hours, the reaction was quenched with the addition of 5 mL water, 2 mL 1N HCl. The reaction mixture was then transferred to a separatory funnel and extracted 3 times with DCM. The combined organic phase was dried over $MgSO_4$ before being

concentrated under reduced pressure. The brown solid was then purified on silica (1:3→1:2 EtOAc:hexanes), yielded 132 mg (70%) **1.30** as a golden brown solid. ^{1}H NMR (500.1 MHz, CD_3OD) δ (ppm): 7.79 (m, 4H), 7.50 (s, 1H), 7.38 (d, *J* = 8.25 Hz, 1H), 7.16 (dd, *J* = 1.47, 8.44 Hz, 1H), 4.71 (m, 1H), 3.78 (t, *J* = 6.44 Hz, 3H) 3.64 (m, 1H), 3.20 (m, 2H), 3.08 (m, 2H), 2.18 (m, 2H), 1.96 (m, 2H), 1.86 (m, 2H), 0.99 (m, 3H); ^{13}C NMR (125 MHz, CD_3OD) δ (ppm): 168.4, 137.6, 133.9, 131.7, 127.9, 124.5, 133.6, 122.4, 119.2, 115.6, 115.5, 113.8, 59.5, 54.0, 45.0, 36.5, 30.1, 24.3, 17.8, 15.3, 9.6; HRMS (TOF, ES+) $C_{25}H_{27}N_3O_2Br$ $[M+H]^+$ m/z 480.1287, measured 480.1287.

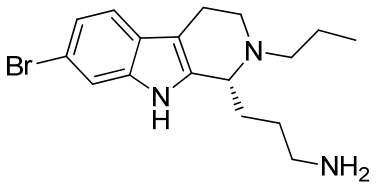

(R)-3-(7-bromo-2-propyl-2,3,4,9-tetrahydro-1H-pyrido[3,4-b]indol-1-yl)propan-1-amine (1.31).

A 100 mL round bottom flask was charged with **1.30** (120 mg, 0.249 mmol). EtOH (2 mL) was added, followed by hydrazine hydrate (78.4 uL, 2.49 mmol). The flask was brought to reflux for 45 minutes, monitoring by LCMS. After 45 minutes, the flask was cooled and the contents were concentrated to remove ethanol. The product was purified on silica (80:18:2 $CHCl_3$:MeOH:NH_4OH), yielded **1.31** 76.7 mg (88%) as a brown solid. ^{1}H NMR (500.1 MHz, CD_3OD) δ (ppm): 7.42 (d, *J* = 1.50 Hz, 1H), 7.30 (d, *J* = 8.49 Hz, 1H), 7.07 (dd, *J* = 1.50, 8.49 Hz, 1H), 4.71 (m, 1H), 3.72 (t, *J* = 5.5 Hz, 1H), 2.87 (m, 1H), 2.77 (m, 2H), 2.60 (m, 2H), 1.95 (m, 2H), 1.63 (m, 3H), 1.29 (m, 2H), 0.95 (m, 3H); ^{13}C NMR (125 MHz, CD_3OD) δ (ppm): 137.1, 135.3, 125.8, 121.2, 118.4, 113.6, 113.1, 107.0, 57.2, 54.7, 45.00, 40.37, 30.3, 26.9, 20.1, 17.7, 10.7; HRMS (TOF, ES+) $C_{17}H_{25}N_3Br$ $[M+H]^+$ m/z 350.1232, measured 350.1235.

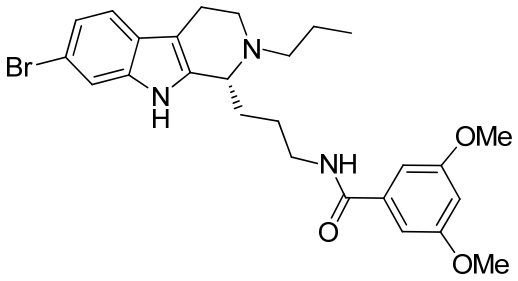

(R)-N-(3-(7-bromo-2-propyl-2,3,4,9-tetrahydro-1H-pyrido[3,4-b]indol-1-yl)propyl)-3,5-dimethoxybenzamide (1.32).

A 10 mL round bottom flask was charged with **1.31** (20 mg, 0.057 mmol), 3,5-dimethoxybenzoylchloride (11.45 mg, 0.057 mmol), triethylamine (20 uL) and DCM (2 mL). The flask was stirred for 3 hours, monitoring by LCMS. After 3 hours, water (3 mL) and DCM (2 mL) were added and the biphasic solution was stirred vigorously before being passed through an Isolute phase separator. The resulting organic layer was then concentrated and purified by revere phase high performance liquid chromatography using acetonitrile and 0.1% TFA/water (gradient: 10:90 to 90:10). Isolated 26 mg (86%) **1.32** as a brown solid. ^{1}H NMR (500.1 MHz, CD_3OD) δ (ppm): 7.54 (d, J = 1.24 Hz, 1H), 7.40 (d, J = 8.50 Hz, 1H), 7.17 (dd, J = 1.24, 8.50 Hz, 1H), 6.97 (d, J = 1.65 Hz, 2H), 6.64 (t, J = 2.15 Hz, 1H), 4.72 (m, 1H), 3.80 (s, 6H), 3.65 (m, 1H), 3.48 (m, 2H), 3.20 (t, J = 8.01 Hz, 2H), 3.08 (m, 2H), 2.18 (m, 2H), 1.88 (p, J = 7.24, 4H), 1.00 (m, 3H); ^{13}C NMR (125 MHz, CD_3OD) δ (ppm): 168.7, 160.9, 137.7, 135.8, 128.2, 124.5, 122.4, 119.2, 115.5, 113.9, 104.7, 103.0, 59.7, 54.5, 54.0, 45.0, 38.9, 38.6, 30.0, 25.4, 17.8, 15.4, 9.6; HRMS (TOF, ES+) $C_{26}H_{33}N_3O_3Br$ $[M+H]^+$ m/z 514.1705, measured 514.1708.

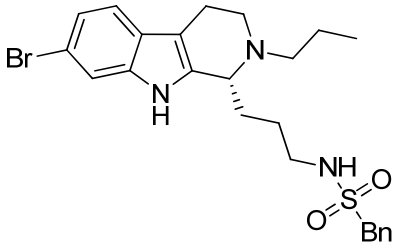

(R)-N-(3-(7-bromo-2-propyl-2,3,4,9-tetrahydro-1H-pyrido[3,4-b]indol-1-yl)propyl)-1-phenylmethanesulfonamide (1.33).

A 10 mL round bottom flask was charged with **1.31** (20 mg, 0.057 mmol), benzylmethanesulfonylchloride (10.86 mg, 0.057 mmol), triethylamine (20 uL) and DCM (2 mL). The flask was stirred for 3 hours, monitoring by LCMS. After 3 hours, water (3 mL) and DCM (2 mL) were added and the biphasic solution was stirred vigorously before being passed through an Isolute phase separator. The resulting organic layer was then concentrated and purified by revere phase high performance liquid chromatography using acetonitrile and 0.1% TFA/water (gradient: 10:90 to 90:10). Isolated 25 mg (85%) **1.33** as a brown solid. ^{1}H NMR (500.1 MHz, CD_3OD) δ (ppm): 7.54 (d, J = 1.45 Hz, 1H), 7.37 (m, 6H), 7.18 (dd, J = 1.45 Hz, 8.40, 1H), 4.65 (m, 1H), 4.30 (m, 2H), 3.76 (m, 1H), 3.63 (m, 1H), 3.17 (t, J = 7.84 Hz, 2H), 3.07 (m, 2H), 3.03 (t, J = 6.19 Hz, 2H), 2.15 (m, 2H), 1.86 (m, 2H), 1.74 (m, 2H), 0.99 (m, 3H); ^{13}C NMR (125 MHz, CD_3OD) δ (ppm): 161.2, 160.9, 137.6, 130.4, 129.7, 128.1, 128.0, 124.5, 122.4, 119.3, 117.7, 115.5, 113.9, 104.8, 59.5, 57.6, 54.0, 45.2, 42.1, 29.7, 26.2, 17.7, 15.5, 9.7; HRMS (TOF, ES+) $C_{24}H3_1N_3O_2Br$ $[M+H]^+$ m/z 504.1320, measured 504.1320.

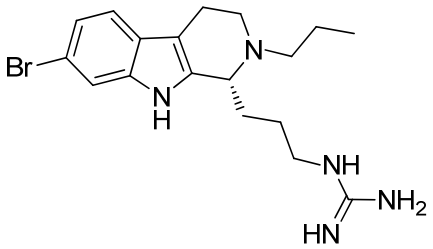

(R)-1-(3-(7-bromo-2-propyl-2,3,4,9-tetrahydro-1H-pyrido[3,4-b]indol-1-yl)propyl)guanidine (1.34).

A 10 mL round bottom flask was charged with **1.31** (20 mg, 0.057 mmol), N,N'-Bis(Boc)-1H-pyrazole-1-carboxamidine (17.69 mg, 0.057 mmol), triethylamine (20 uL) and DCM (2 mL). The flask was stirred for 3 hours, monitoring by LCMS. After 3 hours, water (3 mL) and DCM (2 mL) were added and the biphasic solution was stirred vigorously before being passed through an Isolute phase separator. The resulting organic layer was then concentrated and purified by revere phase high performance liquid chromatography using acetonitrile and 0.1% TFA/water (gradient: 10:90 to 90:10) to afford 20 mg (89%) **1.34** as a glassy brown solid. ^{1}H NMR (600.1 MHz, CD_3OD) δ (ppm): 7.55 (d, J = 1.50 Hz, 1H), 7.43 (d, J = 8.47 Hz, 1H), 7.20 (dd, J = 1.50, 8.47 Hz, 1H), 4.70 (m, 1H), 3.81 (m, 1H), 3.66 (m, 1H), 3.26 (dt, J = 2.33, 7.12 Hz, 2H), 3.23 (m, 2H), 3.11 (m, 2H), 2.22 (m, 2H), 1.87 (m, 4H), 1.04 (m, 3H); ^{13}C NMR (150 MHz, CD_3OD) δ (ppm): 157.2, 137.7, 128.1, 124.6, 122.5, 119.3, 115.7, 113.9, 104.9, 59.6, 54.1, 45.1, 38.9, 34.4, 30.0, 24.8, 19.6, 18.2, 17.8, 15.4, 9.70; HRMS (TOF, ES+) $C_{18}H_{27}N_5Br$ $[M+H]^+$ m/z 504.1320, measured 504.1320.

Table 1.8.1: NMR Shift Correlation Tables for **1.7**.

Natural (+)-7-Bromotrypargine		
^{1}H δ ppm (DMSO)	Integration	J
1.69	m, 2H	
1.92	m, 1H	
2.13	m, 1H	
2.93	m, 2H	
3.19	m, 2H	
3.34	m, 1H	
3.57	dt, 1H	12.0, 4.8
4.69	br m, 1H	
7.1	br s, 2H	
7.1	br s, 2H	
7.16	dd, 1H	1.8, 8.4
7.44	d, 1H	8.4
7.54	d, 1H	1.8
7.81	t, 1H	5.4
9.09	br s, 1H	
9.62	br s, 1H	
11.34	s, 1H	

Synthetic (+)-7-Bromotrypargine		
^{1}H δ ppm (DMSO)	Integration	J
1.69	m, 2H	
1.90	m, 1H	
2.11	m, 1H	
2.93	t, 2H	5.5
3.18	m, 2H	
3.34	m, 1H	
3.58	m, 1H	
4.69	br s, 1H	
7.18	br s, 2H	
7.22	br s, 2H	
7.18	dd, 1H	1.68, 8.5
7.45	d, 1H	8.5
7.55	d, 1H	1.68
7.73	s, 1H	
8.98	br s, 1H	
9.48	br s, 1H	
11.32	s, 1H	

Natural (+)-7-Bromotrypargine	Synthetic (+)-7-Bromotrypargine
^{13}C δ ppm (DMSO)	^{13}C δ ppm (DMSO)
18.6	18.4
23.9	24.7
28.0	28.9
40.3	40.7
40.3	40.9
52.1	52.2
106.5	106.6
114.0	114.9
114.7	116.5
119.1	120.3
122.2	122.4
125.0	125.2
131.0	131.4
137.3	137.5
157.2	157.2

Chiral SFC Traces:

(+)-1.19

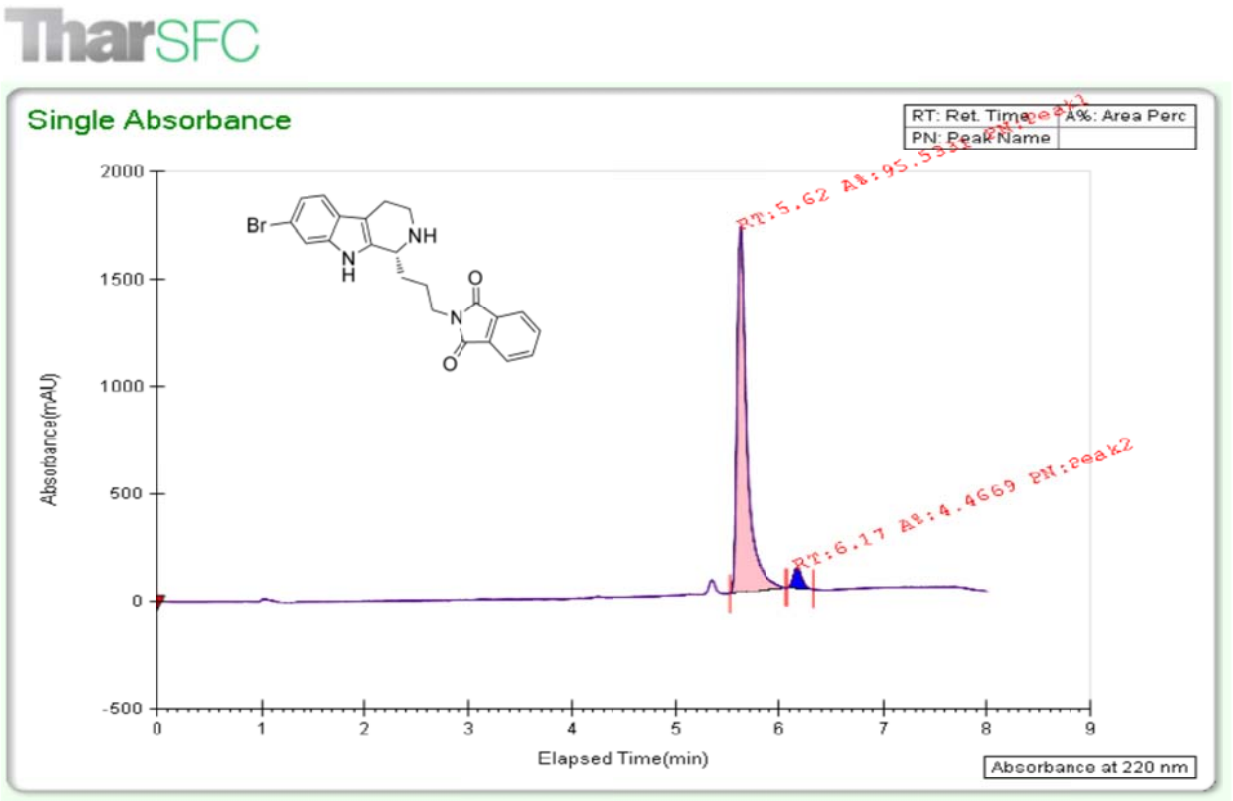

General Info		**Report Date**	3/31/2011
Log Author		**Method Name**	Chiral_screen.met
Log Date	3/31/2011 3:52:43 PM	**Notes**	
Report By	current_User		

Injection Info			
Inj Vol	5	**Temp**	40
Solvent	MeOH 0.1% DEA	**Flow**	3.5
Column	Lux Cellulose-3 (OJ)	**% Modifier**	15
Sample	JTB-5 (R)	**Pressure**	99
Well location	P1: 3B		

Peak Info

Peak No	% Area	Area	RT (min)	Height (mV)	K'
1	95.5331	11286.4354	5.62	1699.7981	0.0059
2	4.4669	527.7272	6.17	95.0801	0.0065
Total:	100	11814.1626			

(±)-1.19

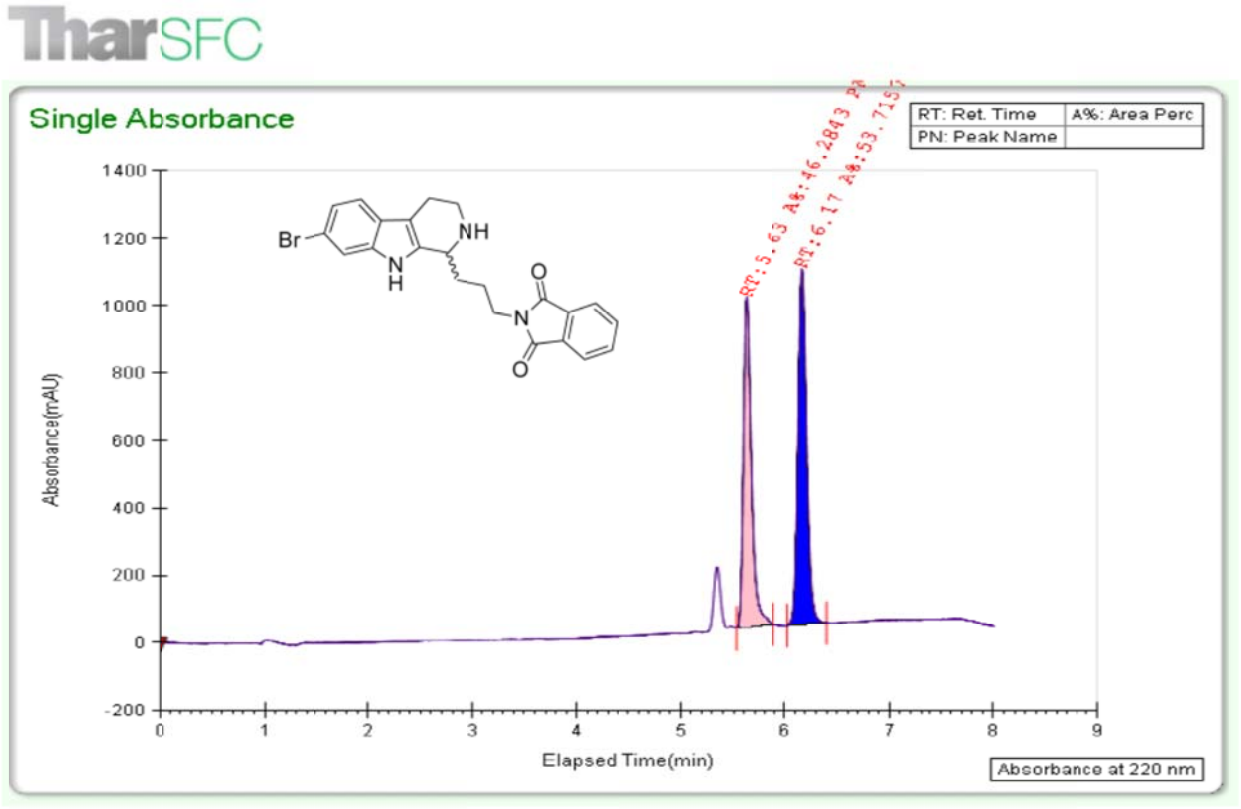

General Info			
Log Author		**Report Date**	3/31/2011
Log Date	3/31/2011 3:13:33 PM	**Method Name**	Chiral_screen.met
Report By	current_User	**Notes**	

Injection Info			
Inj Vol	10	**Temp**	40.2
Solvent	MeOH 0.1% DEA	**Flow**	3.5
Column	Lux Cellulose-3 (OJ)	**% Modifier**	15
Sample	JTB-8-B racemic	**Pressure**	100
Well location	P1: 3A		

Peak Info

Peak No	% Area	Area	RT (min)	Height (mV)	K'
1	46.2843	5144.5554	5.63	978.3584	0.0062
2	53.7157	5970.5658	6.17	1055.0879	0.0067
Total:	100	11115.1212			

Cell Culture and HCT116 Viability Assay:

HCT116 cells were grown at 37°C in a humidified incubator with 5% CO_2 in DMEM + 10% FBS. Cells were plated in growth medium at 8000 cells per well (100 µl) in 96 well plates and allowed to attach for 24 hrs. No cells were plated in the first column. Fresh DMEM + 10% FBS + penicillin/streptomycin (100 µl) containing the final concentrations of DMSO or **1.7** or **1.29** or podophyllotoxin dilutions in DMSO (DMSO concentration maintained at 0.1%) was replaced in each well. After 48 hours of cell growth with respective treatments, WST-1 Cell Proliferation Reagent (Roche, 11644807001) was added (10 µl) to each well for 45-60 min at 37°C. The plates were read (Molecular Devices) at 450 nm for the formazan product and at 690 nm as a reference. Background absorbance (medium only plus WST-1, first column) was averaged and subtracted from all values. Six replicates were used in the calculations per treatment concentration in duplicate experiments. Data was plotted as a percentage of metabolism of WST-1 in the DMSO-treated cells. A colorectal adenocarcinoma cell line, SW620, and a squamous cell lung carcinoma cell line, H520, were obtained from the American Type Culture Collection (Manassas, VA) and maintained in a humidified atmosphere of 5% CO_2 in air at 37 °C. The cells were routinely cultured in RPMI 1640 supplemented with 10% fetal bovine serum (Atlanta Biologicals, GA) and 100 µg/mL penicillin-streptomycin.

Proliferation Analysis:

SW620 and H520 cells (2.5 x 10^4/100 µL) were seeded in 96-well microtiter plates prior to treatment. Cells were treated with 10 µM concentration of synthesized compound in triplicate for 48 hours in RPMI 1640 supplemented medium and 100 µg/mL penicillin-streptomycin. The CycLex® Cellular BrdU ELISA Kit from MBL International (Woburn, MA) was used to measure proliferation. The RPMI media was removed and replaced with 100 µL of 1x BrdU label mix in RPMI media for 2 hours at 37 °C in 5% CO_2 in the air. The BrdU label mix was removed and 200

μL of the Fix/Denature solution was added and incubated for 30 minutes at room temperature. The plate was drained, incubated with 50 μL of primary antibody for 1 hour at room temperature, rinsed with wash buffer, and incubated with 50 μL of secondary antibody. The wells were rinsed with wash buffer followed by a single rinse with PBS and drained. Fifty microliters of substrate solution was added and incubated for 6 minutes followed immediately by 50 μL of Stop solution. The change in proliferation was quantified by measuring the absorbance of the dye solution at 450 nm on a microtiter plate reader.

Radioligand Binding and Functional assays. All biological assays were conducted at Ricerca Pharma according to published protocols.

CHAPTER II

TOTAL SYNTHESIS AND BIOLOGICAL EVALUATION OF PHIDIANIDINES A & B

2.1 Introduction

In the previous chapter, we described the synthesis and evaluation of (+)-7-bromotrypargine (**1.7**), and were excited to find that in addition to H_3 activity (K_i = 1.84 μM, IC_{50} = 3.6 μM), predicted based on the H_3 pharmacophore model, **1.7** also proved to inhibit the dopamine transporter (DAT) and the norepinephrine transporter (NET), with IC_{50} values of 1.8 and 3.0 μM, respectively, without inhibiting the closely related serotonin transporter (SERT)[27]. This unique pharmacological profile for a marine alkaloid prompted our lab to synthesize and evaluate other marine alkaloids to assess their potential as leads for CNS indications.

In 2011, Gavagnin, Guo and co-workers reported on the isolation and characterization of two novel indole alkaloids, phidianidines A (**2.1**) and B (**2.2**) from the from the opisthobranch mollusk *Phidiana militaris*.

Figure 2.1.1: The opisthobranch mollusk *Phidiana militaris*, from which **2.1** and **2.2** were isolated[28].

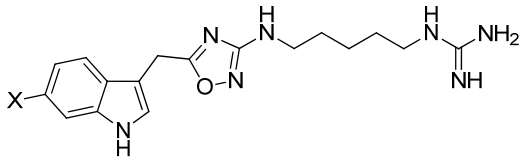

2.1, X = Br (phidianidine A)
2.2, X = H (phidianidine B)

Figure 2.1.2: Structures of phidianidines A(**2.1**) and B(**2.2**).

Compounds **2.1** and **2.2** represent the first natural products identified to contain a 1,2,4-oxadiazole heterocycle (Figure 2.1.2)[29]. These two structures share similar topology with **1.7** and conform to the H_3 pharmacophore model[11]; therefore, we initiated a synthesis campaign towards both **2.1** and **2.2** to provide sufficient material for pharmacological study.

2.2 Retrosynthetic Analysis of Phidianidines A & B

Our retrosynthesis followed the biogenetic pathway proposed by Gavagnin, Guo and co-workers[29]. By disconnecting across the oxadiazole ring, the molecule can be separated into respective "western" and "eastern" sections, enabling a convergent synthesis. The core of **2.1** and **2.2** could be joined by a key coupling between indole acetic acids **2.3** and **2.4** and an appropriately oxidized, alkyl *bis*-guanidine **2.5** (Figure 2.2.1), the latter of which being derived from 1,5-diaminopentane **2.6**.

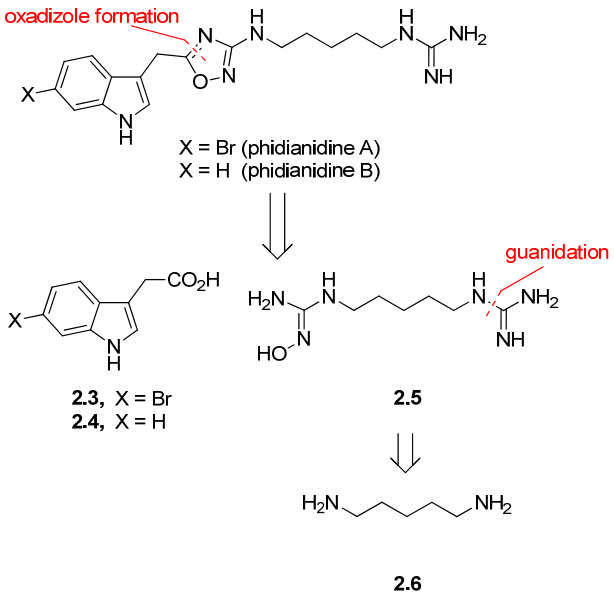

Figure 2.2.1: Retrosynthetic analysis of phidianidines A and B.

2.3 Eastern Section Synthesis

Synthesis of the eastern section began with a mono-carboxybenzyl (CBz) protection of **2.6** to furnish amine **2.7**. This protecting group was selected in order to add a chromophore to the structure in order to ease detection by LCMS and TLC. Cyanation with cyanogen bromide proceeded smoothly, yielding amino nitrile **2.8**. The eastern section was completed with hydroxyguanidine formation using hydroxylamine hydrochloride under basic conditions at room temperature.

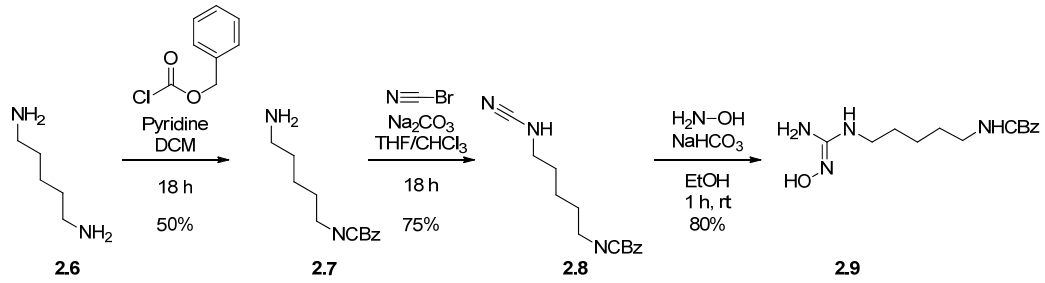

Scheme 2.3.1: First synthesis of eastern section.

However, when we attempted to deprotect the carboxybenzyl group, we found the functionality to be extremely intractable toward all attempted hydrogenation conditions. We modified reaction temperature, solvent, and palladium source, however, no deprotected product was observed. As a result, we returned to the eastern synthesis and replaced the carboxybenzyl group with a *tert*-butyl carbamate (Boc) group.

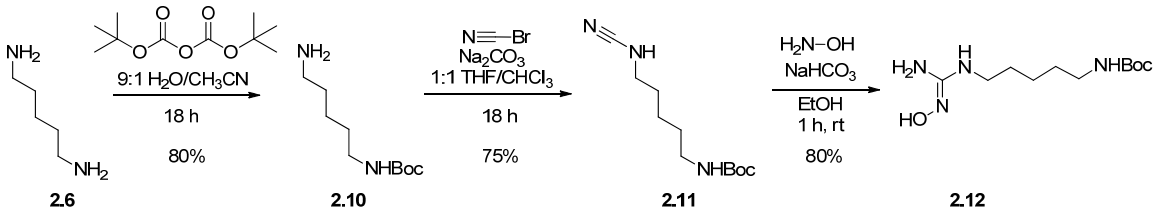

2.6 **2.10** **2.11** **2.12**

Scheme 2.3.2: Second synthesis of eastern section.

2.4 Western Section Synthesis

Synthesis of the western section required significantly more experimentation due to the fact that indole-3-acetic acids remain surprisingly difficult to assemble, despite their relative structural simplicity. Indole-3-acetic acid is an essential plant auxin and has been the subject of significant investigation regarding its plant growth regulating properties[30]. Commercially, indole-3-acetic acid is generated at high temperatures and pressures in a stainless steel rocking autoclave; indole and glycolic acid are heated with aqueous potassium hydroxide to a temperature of 250^{o} C for 18 hours[31]. Subsequent acidification of the potassium salt yields the desired material in reportedly high yields. As a result, the undecorated indole-3-acetic acid required for the synthesis of **2.2** is commercially available; however 6-bromoindole-3-acetic acid (**2.3**) is not, making its synthesis an essential intermediate en route to **2.1**. Due to a lack of access to a stainless steel rocking autoclave, we were prompted to explore alternate routes toward this intermediate.

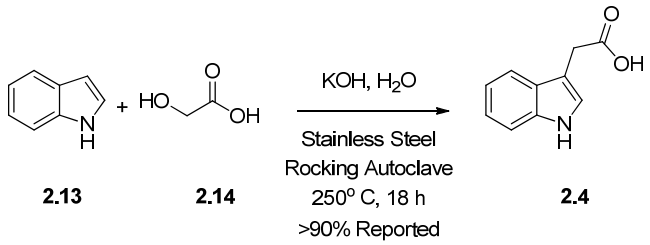

Scheme 2.4.1: Industrial scale synthesis route toward indole-3-acetic acid.

2.4.1 Proposed Routes Toward 6-Bromoindole-3-Acetic Acid

Alternate published routes toward indole-3-acetic acid include preparation by Fischer indole synthesis, hydrolysis of indoleacetonitrile, reaction of indole with ethyl diazoacetate followed by hydrolysis, and ultraviolet irradiation of tryptophan[31]. Of these routes, Fisher indole synthesis was the least optimal. As Scheme 2.4.1.1 shows, reaction of 3-bromophenylhyrdrazine **2.15** with 3-oxopropanoic acid **2.16**, or a protected congener thereof, would yield two inseparable regioisomers of brominated indole-3-acetic acid.

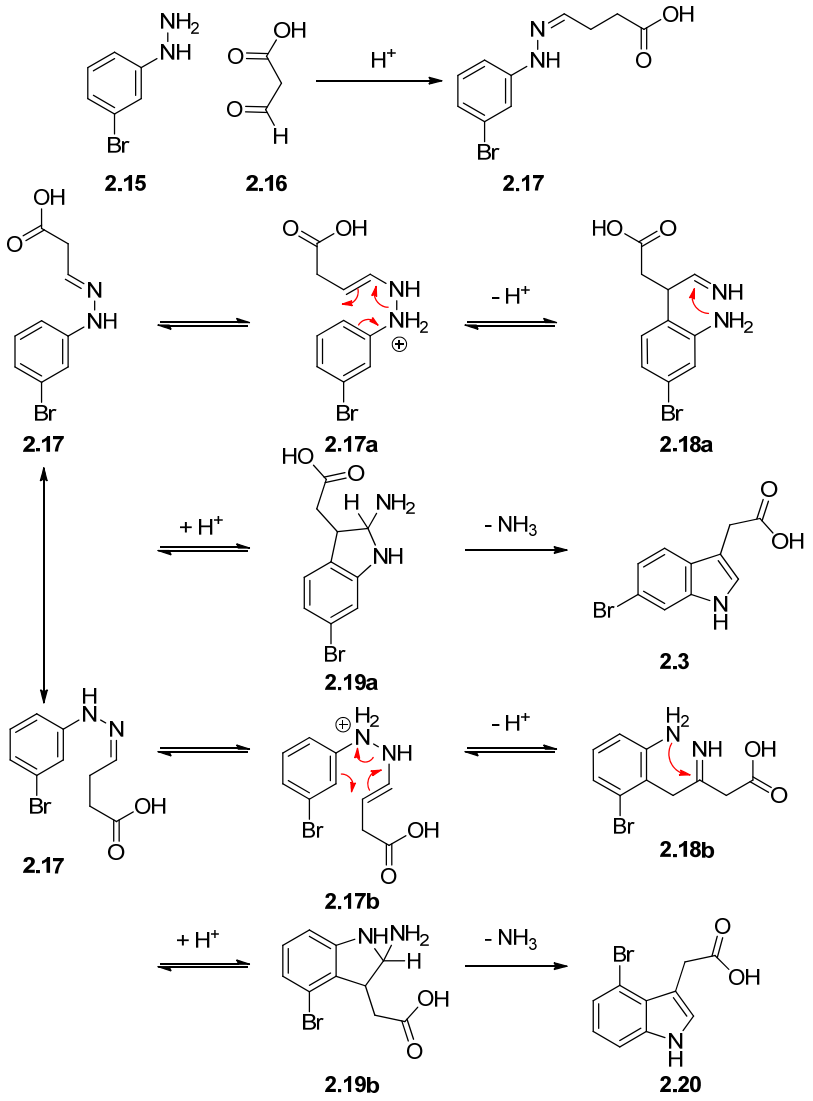

Scheme 2.4.1.1: Fisher indole synthesis of indole-3-acetic acid.

As opening the indole ring would invite issues of regioisomerism, we opted to begin our synthesis of **2.3** with the brominated indole ring intact. Returning to the previously published routes toward **2.3**, the synthesis of 6-bromoindole-3-acetonitrile features the same problems as **2.3**, and ultraviolet irradiation of tryptophan would furnish *des*-bromo material. Thus, our focus centered on routes toward this intermediate that would involve alkylation or acylation of 6-bromoindole at the C3-position.

2.4.2 Acylation Route

For our first route toward **2.3**, we envisioned a Friedel-Crafts acylation of the indole ring, full reduction to the terminal alcohol and subsequent reoxidation to the carboxylic acid oxidation state. Friedel-Crafts acylation of 6-bromoindole at the C3-position with oxalyl chloride in diethyl ether, followed by methanol quench produced the corresponding keto-ester. Exhaustive reduction of the keto-ester with refluxing lithium aluminum hydride furnished the desired tryptanol (**2.23**) in good yield over three steps[32]. From the alcohol, we attempted a number of different oxidation reactions: Swern, Ley[33,34], IBX[35], Oxone[36], Dess-Martin periodinane[37], and chromium reagents including pyridinium chlorochromate and pyridinuim dichromate[38]. All of these attempted reactions resulted in either unaffected starting material or total decomposition.

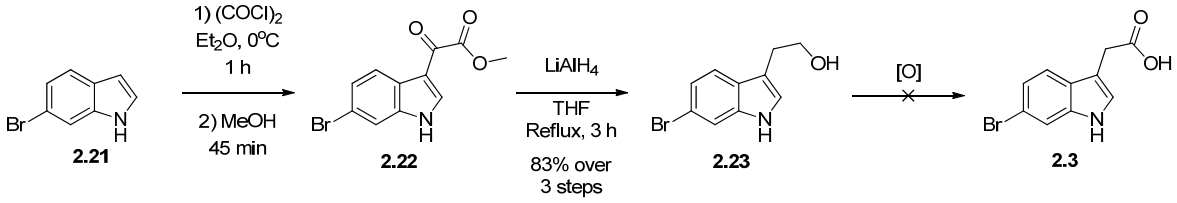

Scheme 2.4.2.1: Attempted acylation route toward **2.3**

2.4.3 Olefin Cleavage Route

Because oxidation upward from the alcohol oxidation state primarily lead to decomposition of starting material, we decided that our next route should convert an alternate functionality directly to the aldehyde or carboxylic acid oxidation states. To that end, we considered the cleavage of a terminal olefin. Kimura and coworkers recently reported on a technique to selectively allylate the C-3 position of indoles with allyl alcohol, triethylborane and a palladium(0) source[39]. We employed palladium tetrakis triphenylphosphine and smoothly allylated **2.21**, furnishing allyl indole **2.24A**. However, we again met with decomposition when

we attempted to cleave the terminal olefin. Ozonolysis, ruthenium trichloride/sodium periodate[40], and osmium tetroxide[41] were all employed under various reaction parameters, however, in each case, the starting material was found to have decomposed during the course of the reaction. Because the indole ring is electron excessive, we considered the possibility that these harsh reagents might be opening the ring across the C-2 to C-3 bond. In order to test this hypothesis, we introduced an electron withdrawing protecting group in the form of a tosylate on the indole nitrogen of **2.24** (**2.23B**)[42] and attempted the range of different cleavage conditions again. Unfortunately, this modification did not prompt these reactions to yield the desired product.

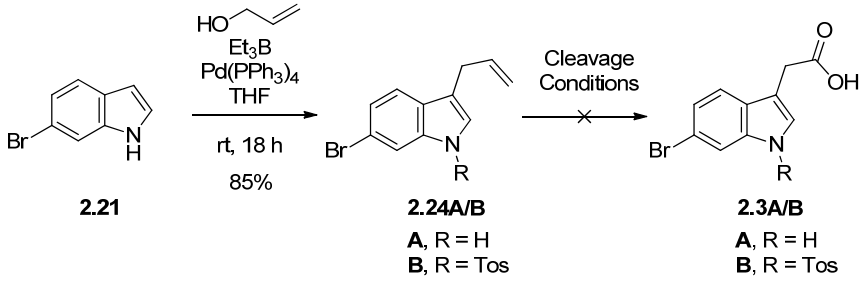

Scheme 2.4.3.1: Attempted olefin cleavage route

2.4.4 Direct Alkylation Route

After encountering the series of issues surrounding oxidation state manipulation and functional group interconversion, we decided to move forward by attempting to install the desired functionality in its correct oxidation state. Yadav and coworkers recently published a procedure for a copper triflate or indium tribromide mediated direct alkylation of indoles and pyrroles with ethyl diazoacetate[43]. When we attempted these reactions, indium tribromide failed to catalyze the reaction entirely, however, copper(II) triflate successfully catalyzed the alkylation of the indole ring with ethyl diazoacetate. Frustratingly, despite variations in stoichiometric ratios of starting materials, catalyst loading, solvent, reaction temperature and reaction concentration, the

alkylation produced an inseparable mixture of *mono-(***2.26***)* and *bis*-(**2.27**) alkylated products at the C-3 and C-4 positions of the indole ring (Scheme 2.4.4.1).

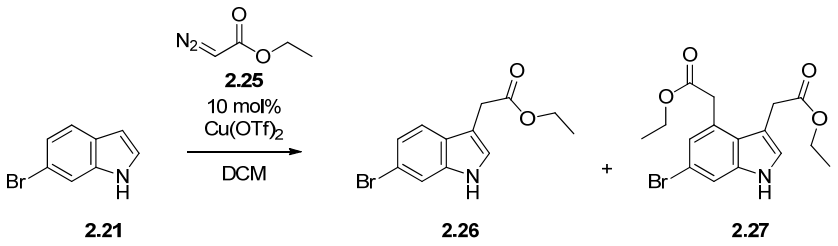

Scheme 2.4.4.1: Attempted alkylation of **2.21** with copper(II) triflate and ethyl diazoacetate.

2.4.5 Chemoselective Reduction Route

Because the Friedel-Crafts C-3 acylation reaction proceeded smoothly and produced the desired oxidation state at the terminal carbon when quenched with an oxygen source such as methanol, we decided to return to this previous route. Rather than performing a total reduction, we decided to focus on a chemoselective reduction of the ketone over the terminal ester/acid functionality. Examples of such chemoselective reductions include a dithiane condensation followed by hydrogenation and the Wolff-Kishner reduction.

2.4.5.1 Dithiane Condensation/Reduction Route

Our first attempted chemoselective reduction began with an acid-mediated dithiane condensation of previously synthesized keto-ester **2.22** with dithioethane, forming dithiane **2.23**. With this material in hand, we attempted a range of different Raney-nickel hydrogenation conditions[44] on the bench top and in the H-cube reactor but were unsuccessful in desulfurizing **2.28** (Scheme 2.4.5.1), as starting material was retrieved from the reaction in each case.

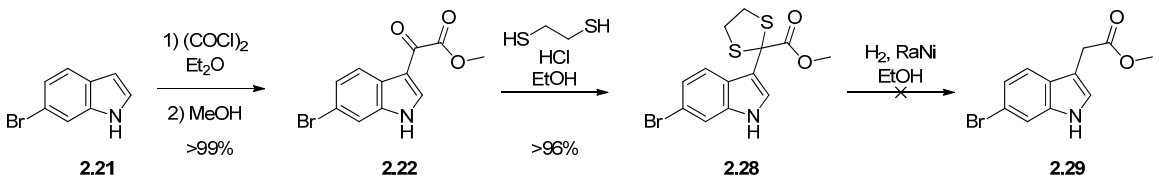

Scheme 2.4.5.1: Attempted dithiane condensation/reduction route.

2.4.5.2 Wolff-Kishner Reduction Route

As an alternative to the unsuccessful dithiane reduction, we attempted standard Wolff-Kishner reduction of **2.22**, but quickly encountered literature precedent showing that, while α-keto-esters fail, α-keto-acids can be efficiently reduced by modifying base from potassium hydroxide to sodium methoxide and solvent from ethylene glycol to 2-ethoxyethanol[45]. By affecting these modifications and heating in the microwave reactor, we were able to successfully synthesize **2.3** in approximately 90% yield over three steps.

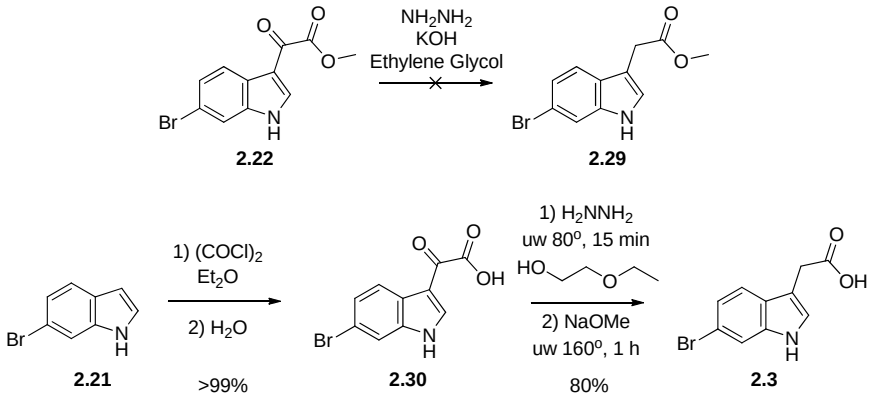

Scheme 2.4.5.2: Synthesis of 6-bromoindole-3-acetic acid[45].

2.5 Coupling, Cyclization and Final Steps

With both the western and eastern sections in hand, we continued forward with the synthesis of **2.1** and **2.2**. Using commercially available **2.4**, we experimented with conditions to couple the two sections together, dehydrate/cyclize the oxadiazole ring, and remove the Boc

protecting group in one pot. Our initial conditions (Scheme 2.5.1) involved a HATU mediated coupling of the two sections in DMF for roughly 30 minutes, heating the reaction to 100° C for 1 hour in order to close the oxadiazole ring, and acidic cleavage of the Boc group.

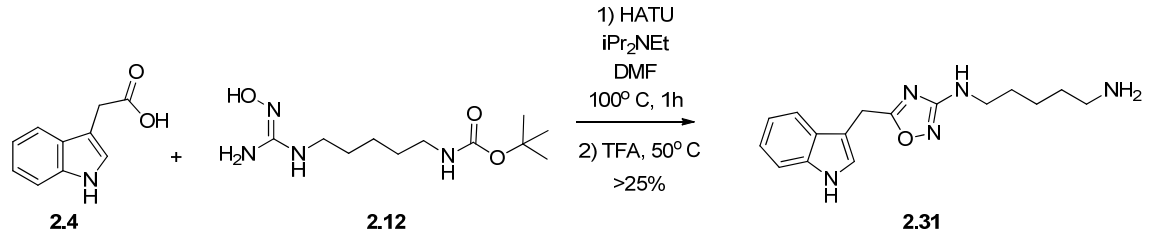

Scheme 2.5.1: Initial conditions for coupling, cyclization, and Boc group removal.

While we were gratified to find that the reaction proceeded, the product yield of 25% was unacceptably low. In an effort to increase the yield, we performed a solvent screen and found that by substituting a co-solvent system of DCM/DCE for DMF, the product yield increased to 45% over two steps from **2.4** and **2.12**. Contrastingly, when we employed **2.3** under the same reaction, we found the yield to be significantly higher (74% over two steps, Scheme 2.5.2). This difference in yield can be attributed to the relatively poor solubility of **2.4** in DCM, whereas **2.3** is readily soluble in the same solvent. Despite the solubility issue, the 45% yield was viewed as acceptable enough to complete the synthesis.

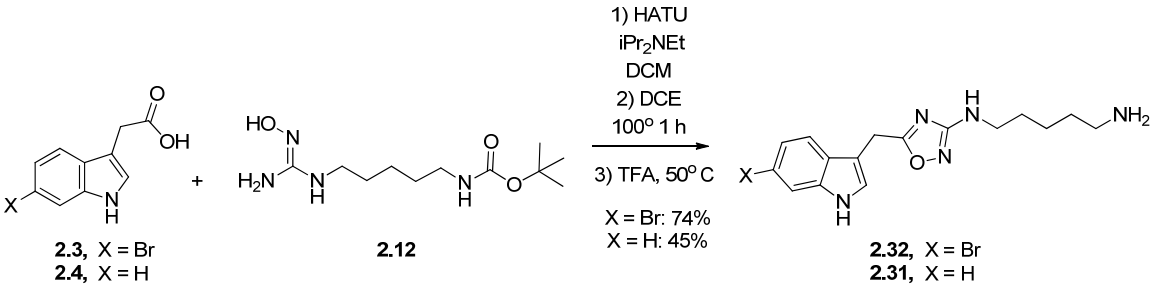

Scheme 2.5.2: Optimized conditions for coupling, cyclization, and Boc group removal.

The final steps of the synthesis involved guanidation of the primary amine with *N,N'-Bis*(Boc)-1*H*-pyrazole-1-carboxamidine and trifluoroacetic acid mediated cleavage of the *bis*-Boc protecting groups (Scheme 2.5.3) to yield the TFA salts of **2.1** and **2.2** in six steps and 40% and 21% overall yields, respectively.

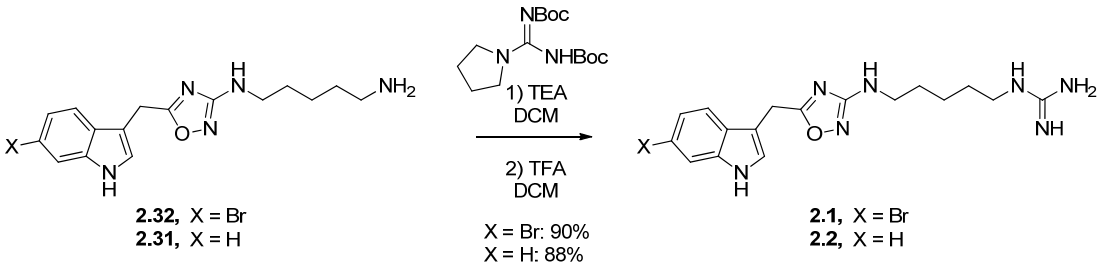

Scheme 2.5.3: Final steps in the synthesis of **2.1** and **2.2**

As we were writing our manuscript, a Letter[46] appeared from Snider describing the synthesis of **2.1** and **2.2**, starting from a 1,5-diazidopentane and a similar approach, requiring 8 steps and 19% overall yields. In their work, **2.1** and **2.2** were evaluated in the National Cancer Institute 60 cell line panel and showed only 5-30% inhibition of cell growth[46]. Our synthetic **2.1** and **2.2** were in complete agreement with natural **2.1** and **2.2**[29], as well as the data reported by Snider[46]; moreover, the expedited route and high yields in our synthesis was amenable to unnatural analog development.

2.6 Cytotoxicity Screening

As **2.1** and **2.2** display a range of cytotoxicity across tumor and non-transformed cell lines[29,46], we first evaluated the cytotoxicity of **2.1** and **2.2** in Human Embryonic Kidney (HEK293) cells after both 24 and 48 hours in a WST-1 cell proliferation assay[47]. At concentrations of 10 μM, neither **2.1** nor **2.2** displayed any toxicity, relative to DMSO control at 24 and 48 hour time points in HEK293 cells (Figure 2.6.1). Thus, we advanced **2.1** and **2.2** into

large panel screens to evaluate their potential as H_3 ligands as well as other CNS targets of therapeutic relevance.

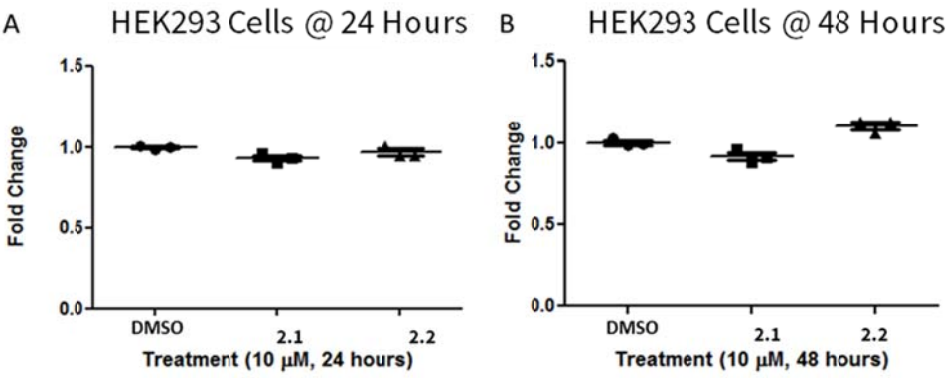

Figure 2.6.1: Cytotoxicity assays in HEK293 cells using a WST-1 cell proliferation assay. A) 25K cells plated at 24 hours when treated with 10 μM **2.1** and **2.2** and DMSO. B) 25K cells plated at 48 hours when treated with 10 μM **2.1** and **2.2** and DMSO. Each point is a single biological replicate (N=3) with 4 technical replicates per biological replicate.

2.7 GPCR, Ion Channel, and Transporter Screens

Following the completion of the total synthesis, phidianidines A (**2.1**) and B (**2.2**) were then evaluated in an external panel of 68 GPCRs, ion channels and transporters in radioligand binding assays[26] in an attempt to identify discrete CNS targets with therapeutic relevance, a strategy that has been highly successful. Interestingly, both **2.1** and **2.2** displayed only very weak activity at H_3 (25% inhibition at 10 μM and 33% inhibition at 10 μM, respectively). This was a surprising result, as **2.1** and **2.2** aligned well with the H_3 pharmacophore model. Similar to **1.**7, both **2.1** and **2.2** showed significant DAT activity (101% inhibition at 10 μM and 96% inhibition at 10 μM, respectively), but both possessed weak NET activity (52-68% inhibition at 10 μM) and no activity at SERT (Table 2.7.1)[27,48]. An even more exciting finding was the profile at the three opioid receptors[49,50]. Phidianidine A (**2.1**) displayed 103% inhibition of the μ-opioid receptor (μOR), but no activity (-5% at 10 μM) at the δ- and κ-opioid receptors; importantly,

phidianidine B (**2.2**) showed a similar profile. The μOR is a Class A GPCR that has been shown to be the OR subtype responsible for the analgesia of clinical opioids[49,50,51,52], and has been implicated in a number of other CNS pathologies[54]. In order to discern preliminary SAR, we also evaluated the amine precursor **2.32** en route to **2.1** in the same panel assay. In this instance, **2.32** not only displayed potent DAT and NET activity (98% and 86% inhibition at 10 μM, respectively), but also selective μOR activity (88% at 10 μM for μOR, 2% at 10 μM for δ- and κOR), suggesting the guanidine moiety of **2.1** is not essential for the pharmacological profiles.

Table 2.7.1: Pharmacological profiles of **2.1**, **2.2,** and precursor amine **2.32**.

Compound	H_3	DAT	NET	SERT	Opiate-μ	Opiate-δ	Opiate-κ
	(% inhibition@ 10 μM)[a]						
2.1	25	101	68	22	103	-5	3
2.2	33	96	45	16	87	-6	5
2.32	23	98	86	21	88	-2	7

[a]% displacement of radioligand at human receptors at a compound concentration of 10 μM. H_3, [^{3}H]-*N*-a-methylhistadine; DAT, [^{125}I]RTI-55; NET, [^{125}I]RTI-55; SERT, [^{3}H] Paroxetine; Opiate-μ, [^{3}H] Diprenorphine; Opiate-δ, [^{3}H] naltrindole; Opiate-κ, [^{3}H] Diprenorphine.

We then followed up the single point radioligand binding assays[26], with full concentration response curves (CRCs) for **2.1**, **2.2** and **2.32**, and determined quantitative K_i values and IC_{50} values for DAT inhibition (Table 2.7.2)[53]. In parallel, we ran the standard GTPγS functional assay, measuring an increase in bound [^{35}S]GTPγS relative to DAMGO response[54], to determine if **2.1**, **2.2** and **2.32** were functional agonists of the μ-opioid receptor. We found that **2.1** and **2.2** were potent ligands for both DAT (K_i values of 310 nM and 680 nM, respectively) and μOR (K_i values of 230 nM and 340 nM, respectively). The amine precursor was weaker, but still displayed submicromolar K_i values for both DAT and μOR (K_i values of 690 nM and 800 nM, respectively). All three compounds also displayed potent inhibition of DAT, with IC_{50} values

ranging from 390 nM to 870 nM. In the GTPγS functional assay,[50,53] **2.32** was inactive, but both **2.1** and **2.2** displayed weak, partial agonism (12-17% increase in bound [^{35}S]GTPγS at 10 μM, relative to DAMGO response) of the μ-opioid receptor. While these represent very weak agonist responses, we were excited to identify a fundamentally new chemotype with high selectivity for binding to the μ-opioid receptor, and an attractive lead for chemical optimization.

Table 2.7.2: Quantitative pharmacological profile of **2.1, 2.2,** and amine precursor **2.32.**

Cmpd	DAT		Opiate-μ	
	K_i (nM)	IC_{50} (nM)	K_i (nM)	EC_{50}[a]
2.1	310	390	230	17%
2.2	680	860	340	12%
2.32	690	870	800	6%

2.8 Unnatural Analog Development

In order to optimize and develop SAR around the selective μOR activity, we required reliable, rapid chemistry to prepare unnatural analogs of **2.1** and **2.2** (Figure 2.8.1). While the phidianidine scaffold features several functional group "handles" that enable access to different chemical modifications, the data concerning **2.32** suggests that the guanidine moiety is not required for μOR activity, therefore key analogs would replace the guanidine functionality with other moieties that might enhance CNS exposure. Thus, we piloted a number of typical, high yielding reactions (acylation, sulfonylation and urea formation) with **2.32** en route to unnatural analogs of **2.1** and **2.2**.

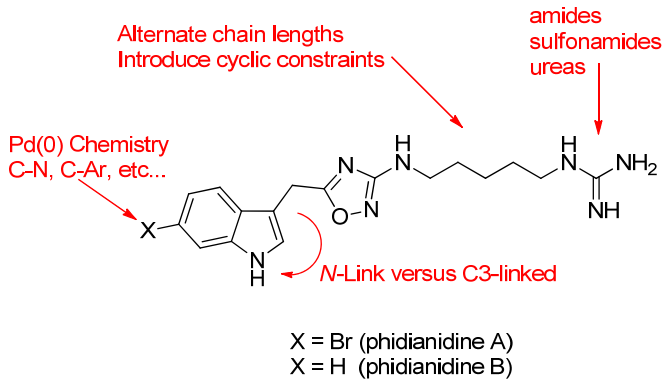

Figure 2.8.1: Potential sites for analog development around **2.1**.

The first round of analogs were based on simple capping of the primary amine of **2.32** to afford amides (**2.33** and **2.34**) sulfonamide (**2.35** and **2.36**) and ureas (**2.37** and **2.38**) in place of the guanidine moiety of **2.1** (Figure 2.8.2).

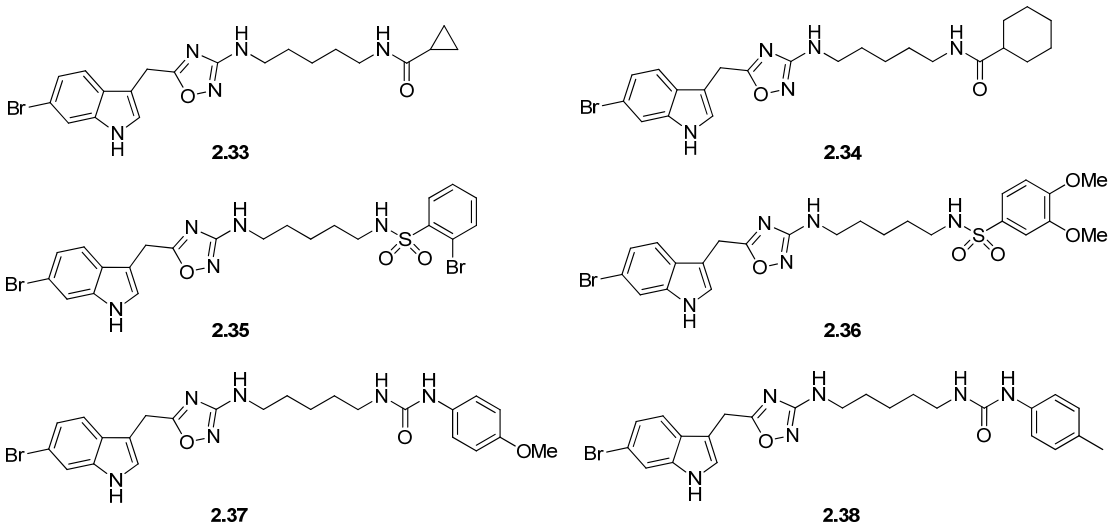

Figure 2.8.2: Library of unnatural analogs of **2.1** and **2.2** with alternative moieties replacing the guanidine.

In an effort to add additional structural diversity, we developed chemistry to access *N*-linked congeners of **2.1** and **2.2** (Scheme 2.8.1). Here, indoles **2.21** and **2.21A** were alkylated under microwave-assisted Finkelstein conditions, and following ester hydrolysis provided *N*-linked acetic acids **2.39** and **2.40** in 76% isolated yields. A HATU-mediated amide coupling with

2.12, subsequent thermal dehydration and Boc deprotection delivered the *N*-linked analogs **2.39** and **2.40** of **2.1** and **2.2** in 45% yield over three steps. Guanidation and acidic Boc group removal rendered N-linked unnatural analogs **2.41** and **2.42**. Thus, the first unnatural analogs of **2.1** and **2.2** have been synthesized in short order, with significant structural diversity.

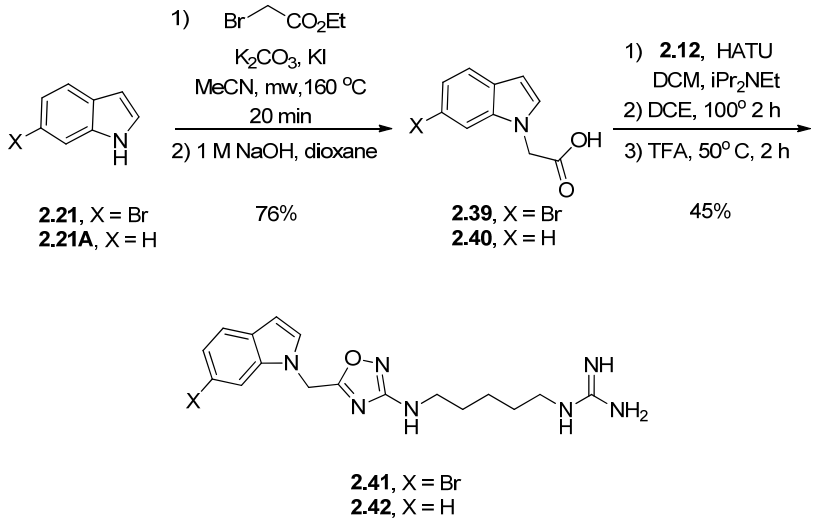

Scheme 2.8.1: Synthesis of *N*-linked Unnatural Analogs **2.41** and **2.42** of **2.1** and **2.2**.

2.9 Conclusion

In conclusion, we completed the total synthesis of phidianidines A (**2.1**) and B (**2.2**), the first 1,2,4-oxadiazole-containing alkaloid, from the marine opisthobranch mollusk *Phidiana militaris* in six steps in 40% and 21% overall yields, respectively, from commercial materials. We explored multiple synthetic strategies toward the synthesis of 6-bromoindole-3-acetic acid (**2.3**). Biological evaluation of **2.1** and **2.2** (including advanced intermediate **2.32**) proved them devoid of cytotoxicity at high doses over 48 hours in HEK293 cells. Importantly, receptor profiling efforts identified **2.1** and **2.2** as potent ligands for, and inhibitors of, DAT, with little or no activity at the highly homologous NET and SERT. Even more exciting was the finding that **2.1** and **2.2** were potent ligands for the μ-opioid receptor, with no activity at the δ- or κ-opioid receptors, and both displayed weak μ-opioid partial agonist activity. These data, and those

generated with dispyrin **1.4** and (+)-7-bromotrypargine **1.7**, argue well for the continued synthesis and profiling of marine natural products as new sources of potent and selective ligands for CNS targets of therapeutic relevance. Moreover, the intriguing pharmacological profile of **2.1** and **2.2** led us to then explore chemistry to access unnatural analogs, and we prepared eight structurally and topologically diverse congeners.

EXPERIMENTAL METHODS

Synthesis:

All reagents were purchased from Sigma-Aldrich Corp., Matrix Scientific, Fisher Scientific, and Ark Pharm Inc., and were used without purification. Analytical thin-layer chromatography (TLC) was performed on 250 μm silica gel plates from Sorbent Technologies. Visualization was accomplished via UV light, and/or the use of ninhydrin, I_2, 2,4-dinitrophenylhydrazine, and potassium permanganate solutions followed by application of heat. Chromatography was performed using Silica Gel 60 (230-400 mesh) from Sorbent Technologies or Silica RediSep Rf flash columns on a CombiFlash Rf automated flash chromatography system. All ^{1}H and ^{13}C NMR spectra were recorded on Bruker AV-400 (400 MHz), DRX-500 (500 MHz) and AV-600 (600 MHz) instruments. Chemical shifts are reported in ppm relative to residual solvent peaks as an internal standard set to δ 7.26 and δ 77.16 ($CDCl_3$), δ 3.31 and δ 49.00 (CD_3OD), and δ 2.50 and δ 39.52 (d_6-DMSO). Data are reported as follows: chemical shift, multiplicity (s = singlet, d = doublet, t = triplet, q = quartet, p = pentet br = broad, dd=doublet of doublets, dq=doublet of quartets, td = triplet of doublets, pd = pentet of doublets, m = multiplet), coupling constant (Hz), integration. Low resolution mass spectra (LCMS) were obtained on an Agilent 1200 LCMS with electrospray ionization. High resolution mass spectra (HRMS) were recorded on a Waters Qtof-API-US plus Acquity system with ES as the ion source. Analytical high pressure liquid chromatography (HPLC) was performed on an Agilent 1200 analytical LCMS with UV detection at 214 nm and 254 nm along with ELSD detection.

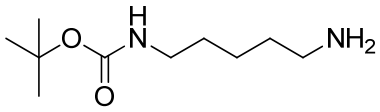

Tert-butyl (5-aminopentyl)carbamate (2.10).

Di-tert-butyl dicarbonate (2.8 mL, 12.23 mmol) in 50 mL of 9:1 dioxane/water was added to a solution of 1,5-diaminopentane **2.6** (5 g, 48.93 mmol) in 50 mL of 9:1 dioxane/water over a period of 3 hours. The solution was stirred at room temperature overnight and concentrated and the residue was taken up in 50 mL of water. The precipitated N,N'-di-Boc-1,5-diaminopentane was removed by filtration through a fritted glass funnel, and the filtrate was extracted with DCM (50 mLx4). The combined organic extracts were washed by water (20 mLx2), then dried by magnesium sulfate. The dried organics were concentrated under reduced pressure, yielding **(2.10)** 2.14 g (22% by 1,5-diaminopentane, 80% by di-tert-butyl dicarbonate) as a colorless oil that solidified upon drying. ^{1}H NMR (400 MHz, $CDCl_3$, δ (ppm)): 4.68 (s, 1H) 3.05 (s, 2H), 2.63 (q, J = 7.40 Hz, 2H), 1.38 (m, 15H), 1.28 (m, 2H), 1.13 (s, 1H); ^{13}C NMR (150 MHz, d_6-DMSO, δ (ppm)): 155.9, 79.8, 41.9, 40.3, 33.3, 29.8, 28.3, 23.9; HRMS (TOF, ES+) $C_{10}H_{22}N_2O_2$ $[M+H]^+$ m/z 203.1760, measured 203.1758.

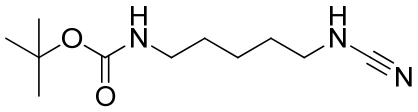

Tert-butyl (5-cyanamidopentyl)carbamate (2.11).

Tert-butyl (5-aminopentyl)carbamate **2.10** (1.52 g, 7.51 mmol) was dissolved in 20 mL THF and sodium carbonate (2.38 g, 22.5 mmol) was added. The resulting suspension was cooled to 0^{o}C. Cyanogen bromide (3.15 g, 30.05 mmol) was added as a solution in 20 mL chloroform via addition funnel over the course of 30 minutes. The solution was stirred 12 hours and monitored by thin layer chromatography. Upon completion, the solution was transferred to a separatory

funnel and extracted 3X with 25 mL DCM. The combined organic layers were dried over magnesium sulfate, filtered and concentrated under reduced pressure to yield a colorless oil. The product was purified on silica (1:1 ethyl acetate:hexanes), yielded 1.32 g (75%) of **2.11** as a colorless solid. ^{1}H NMR (400.1 MHz, CD_3OD, δ (ppm)): 4.67 (s, 1 H), 4.58 (t, J = 5.10 Hz, 1H), 3.04 (m, 4H), 1.59 (m, 2H) 1.47 (m, 2H) 1.40 (m, 12H); ^{13}C NMR (150 MHz, CD_3OD, δ (ppm)): 156.2, 116.7, 79.2, 45.8, 40.0, 29.5, 29.0, 28.6, 23.1 HRMS (TOF, ES+) $C_{11}H_{21}N_3O_2$ $[M+H]^+$ m/z 228.1712, measured 228.1710.

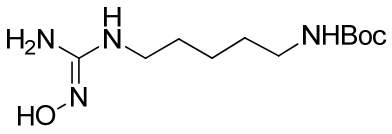

Tert-butyl (5-(2-hydroxyguanidino)pentyl)carbamate (2.12).

Tert-butyl (5-cyanamidopentyl)carbamate **2.11** (657 mg, 2.89 mmol) was dissolved in absolute ethanol. Sodium bicarbonate (485 mg, 5.78 mmol) and hydroxylamine HCl (221 mg, 3.18 mmol) were added and the reaction was stirred at 25^{o}C for 4 hours. Product formation was monitored by thin layer chromatography (80:18:2 $CHCl_3$:MeOH:NH_4OH) visualized with I_2 stain. Upon consumption of starting material, the reaction mixture was concentrated and purified on silica ($CHCl_3$ to 80:18:2 $CHCl_3$:MeOH:NH_4OH) and isolated **2.12** as a colorless solid 641 mg (85%). ^{1}H NMR (400.1 MHz, $CDCl_3$) δ (ppm)): 5.75 (br m, 3H) 5.17 (S, 1H) 2.99 (m, 4H), 1.36 (m, 13H), 1.27 (m, 2H); ^{13}C NMR (150 MHz, $CDCl_3$) δ (ppm)):156.5, 156.1, 78.9, 57.7, 49.9, 41.9, 41.2, 40.3, 29.5, 29.1, 28.3, 23.9, 18.1; HRMS (TOF, ES+) $C_{11}H_{24}N_4O_3$ $[M+H]^+$ m/z 261.1927, measured 261.1926.

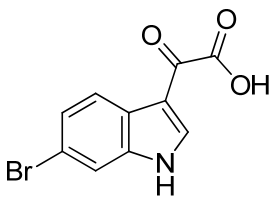

2-(6-bromo-1H-indol-3-yl)-2-oxoacetic acid (2.30).

6-Bromoindole **2.21** (1 g, 5.1 mmol) was dissolved in 20 mL diethyl ether. Oxalyl chloride (890 uL, 10.2 mmol) was added and the reaction was stirred 45 minutes at 25°C. H_2O (500 uL, 25.5 mmol) was added, followed by 50 mL diethyl ether. The reaction was stirred 30 minutes and filtered via buchner funnel. The solid was washed with diethyl ether and dried under high vacuum. Obtained 1.37 g (99.9%) **2.30** as a yellow solid. ^{1}H NMR (400.1 MHz, d_6-DMSO, δ (ppm)): 8.47 (d, *J* = 3.25, 1H), 8.12 (d, *J* = 8.50, 1H), 7.75 (d, *J* = 1.50, 1H), 7.42 (dd, *J* =1.50, 8.50, 1H); ^{13}C NMR (150 MHz, d_6-DMSO, δ (ppm)):181.1, 165.3, 139.1, 137.9, 125.9, 125.0, 123.1, 116.5, 115.7, 112.6; HRMS (TOF, ES+) $C_{10}H_6BrNO_3$ $[M+H]^+$ m/z 267.9609, measured [M ^{79}Br+H], [M ^{81}Br+H] 267.9610, 269.9600.

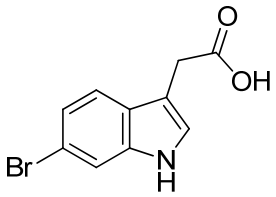

2-(6-bromo-1H-indol-3-yl)acetic acid (2.3).

A microwave vial equipped with stir bar was charged with **2.30** (914 mg, 3.41 mmol) and dissolved in 17 mL 2-ethoxyethanol. Hydrazine hydrate (829 uL, 17.05 mmol) was added and the vial was sealed and heated in a microwave reactor at 80°C for 15 minutes. The vial was then unsealed and solid NaOMe (1.84 g, 34.1 mmol) was added. The vial was again sealed and heated in the microwave at 160°C for 1 hour. The vial contents were transferred to a 250 mL separatory

funnel, acidified with 1N HCl (25 mL) and partitioned between ethyl acetate and H_2O. The aqueous phase was extracted 3X and the combined organic phase was dried over magnesium sulfate. The product was purified on silica (1:1 EtOAc+1%AcOH:Hex), yielded 717 mg (80%) of **2.3** as a beige solid. ^{1}H NMR (400.1 MHz, CD_3OD, δ (ppm)): 7.51 (s, 1H), 7.45 (d, J = 8.5 Hz, 1H), 7.16 (s, 1H), 7.13 (dd, J =1.56, 8.50 Hz, 1H), 3.72 (s, 1H); ^{13}C NMR (150 MHz, CD_3OD, δ (ppm)): 174.7, 137.3, 126.1, 124.1, 121.5, 119.5, 114.3, 113.6, 107.8, 30.3; HRMS (TOF, ES+) $C_{10}H_8BrNO_2$ $[M+H]^+$ m/z 253.9817, measured [M ^{79}Br+H], [M ^{81}Br+H] 253.9815, 255.9792.

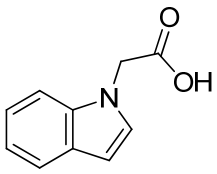

2-(1*H*-indol-1-yl)acetic acid (2.40).

A microwave vial equipped with stir bar was charged with indole **2.21A** (1.0 g, 5.70 mmol) and dissolved in 15 mL acetonitrile. 2-Bromoethylacetate (11.41 mmol), K_2CO_3 (11.41 mmol), and KI (50 mg, cat) were added and the vial was sealed and heated in a microwave reactor at 160^{o}C for 20 minutes. The mixture was transferred to a 250 mL separatory funnel and partitioned between ethyl acetate and H_2O. The aqueous phase was extracted 3x with 25 mL ethyl acetate and the combined organic phase was dried over magnesium sulfate and concentrated under reduced pressure. The crude product was dissolved in dioxane (10 mL) and treated with 1M NaOH (10 mL). The reaction was stirred at 25^{o}C for 3 hours and again transferred to a separatory funnel. The mixture was acidified with 2N HCl (20 mL) and extracted 3x with 25 mL ethyl acetate. The combined organic phase was dried over magnesium sulfate and concentrated under reduced pressure. The product was purified on silica (1:1 EtOAc+1%AcOH:Hex), yielded 987 mg (76% over two steps) **2.40** as a beige solid. ^{1}H NMR (400.1 MHz, d_6-DMSO, δ (ppm)): 7.55 (d, J = 7.80 Hz, 1H), 7.38 (d, J = 8.0Hz, 1H), 7.33 (d, J = 3.25 Hz, 1H), 7.12 (t, J =7.56 Hz, 1H),

7.029 (t, *J* = 7.56 Hz, 1H), 6.44 (d, *J* = 3.25 Hz, 1H) 5.00 (s, 2H); ^{13}C NMR (150 MHz, CD_3OD, δ (ppm)): 170.8, 136.7, 130.0, 128.4, 121.5, 120.6, 119.4, 110.1, 101.3, 47.4; HRMS (TOF, ES+) $C_{10}H_8BrNO_2$ $[M+H]^+$ m/z 176.0712, measured 176.0712.

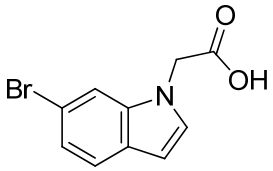

2-(6-bromo-1H-indol-1-yl)acetic acid (2.39).

The procedure for **2.40** was followed, utilizing 6-Bromoindole as starting material. ^{1}H NMR (400.1 MHz, d_6-DMSO, δ (ppm)): 7.70 (s, 1H), 7.51 (d, *J* = 8.5 Hz, 1H), 7.36 (d, *J* = 3.25 Hz, 1H), 7.17 (dd, *J* =1.56, 8.50 Hz, 1H), 6.84 (d, *J* = 3.25 Hz, 1H), 5.05 (s, 2H); ^{13}C NMR (150 MHz, d_6-DMSO, δ (ppm)): 170.7, 137.7, 131.1, 127.5, 122.45, 114.5, 113.2, 101.7, 47.5; HRMS (TOF, ES+) $C_{10}H_8BrNO_2$ $[M+H]^+$ m/z 253.9817, measured [M ^{79}Br+H], [M ^{81}Br+H] 253.9815, 255.9792.

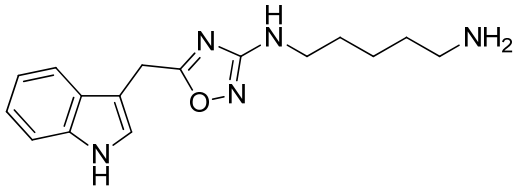

(5-((1H-indol-3-yl)methyl)-1,2,4-oxadiazol-3-yl)pentane-1,5-diamine (2.31).

A flask was charged with **2.4** (105 mg, 0.599 mmol), HATU (227.7 mg, 0.599 mmol), DIEA (174 uL, 0.658 mmol) and DCM (2 mL). The solution was stirred for 30 minutes and transferring via pipette, was added dropwise to a stirred solution of **2.12** (171 mg, 0.658 mmol) in DCM (2 mL). The reaction was stirred 1 hour and concentrated under reduced pressure. The crude mixture was dissolved in DCE (5 mL). The flask was fitted with a reflux condenser and the reaction was heated to 100^{o}C for 1 hour. The reaction mixture was cooled and a 1:1 solution of DCM:TFA (5

mL) was added. The flask was heated to 50°C for 3 hours, monitoring reaction progress by LCMS. The mixture was then transferred to a separatory funnel and partitioned between water and DCM. The mixture was extracted 3x with 25 mL DCM and the combined organic phase was dried over magnesium sulfate and concentrated under reduced pressure. The product was purified by reverse phase HPLC using acetonitrile and 0.1% TFA/water (gradient: 10:90 to 90:10), obtained 78 mg (45%) of **2.31** as a brown glassy solid. ^{1}H NMR (400.1 MHz, CD_3OD, δ (ppm)): 7.53 (d, *J* = 8.25 Hz, 1H), 7.36 (d, *J* = 8.25 Hz, 1H), 7.21 (s, 1H), 7.11 (t, *J* = 7.50 Hz, 1H), 7.01 (t, *J* = 7.50, 1H), 4.22 (s, 2H), 3.16 (t, *J* = 7.0, 2H), 2.89 (m, 2H), 1.65 (m, 4H), 1.44 (m, 2H); ^{13}C NMR (150 MHz, CD_3OD, δ (ppm)): 177.7, 168.6, 126.6, 123.2, 121.2, 118.6, 117.7, 110.9, 106.6, 42.1, 39.1, 28.1, 26.6, 23.1, 22.5; HRMS (TOF, ES+) $C_{16}H_{21}N_5O$ $[M+H]^+$ m/z 300.1824, measured 300.1823.

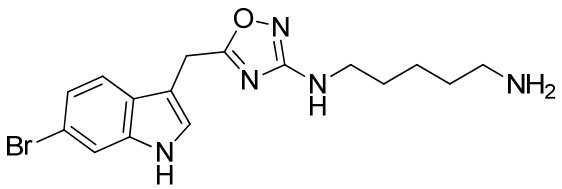

5-((6-bromo-1H-indol-3-yl)methyl)-1,2,4-oxadiazol-3-yl)pentane-1,5-diamine (2.32).

A flask was charged with **2.3** (105 mg, 0.599 mmol), HATU (227.7 mg, 0.599 mmol), DIEA (174 uL, 0.658 mmol) and DCM (2 mL). The solution was stirred for 30 minutes and transferring via pipette, was added dropwise to a stirred solution of **2.12** (171 mg, 0.658 mmol) in DCM (2 mL). The reaction was stirred 1 hour and concentrated under reduced pressure. The crude mixture was dissolved in DCE (5 mL). The flask was fitted with a reflux condenser and the reaction was heated to 100°C for 1 hour. The reaction mixture was cooled and a 1:1 solution of DCM:TFA (5 mL) was added. The flask was heated to 50°C for 3 hours, monitoring reaction progress by LCMS. The mixture was then transferred to a separatory funnel and partitioned between water and DCM. The mixture was extracted 3x with 25 mL DCM and the combined organic phase was

dried over magnesium sulfate and concentrated under reduced pressure. The product was purified by reverse phase HPLC using acetonitrile and 0.1% TFA/water (gradient: 10:90 to 90:10), obtained 119 mg (74%) of **2.32** as a brown glassy solid. ^{1}H NMR (400.1 MHz, CD_3OD, δ (ppm)): 7.51 (s, 1H), 7.44 (d, *J* = 8.50 Hz, 1H), 7.22 (s, 1H), 7.12 (d, *J* = 8.50 Hz, 1H), 4.18 (s, 2H), 3.16 (t, *J* = 7.0 Hz, 2H), 2.88 (t, *J* = 7.50 Hz, 2H), 1.66 (m, 4H), 1.42 (m, 2H); ^{13}C NMR (150 MHz, d_6-DMSO, δ (ppm)):176.7, 168.5, 137.0, 125.7, 125.2, 121.4, 120.1, 114.2, 113.9, 107.2, 45.2, 42.1, 27.9, 26.5, 23.2, 22.5; HRMS (TOF, ES+) $C_{16}H_{20}BrN_5O$ $[M+H]^+$ m/z 378.0929, measured [M ^{79}Br+H], [M ^{81}Br+H] 378.0926, 380.0911.

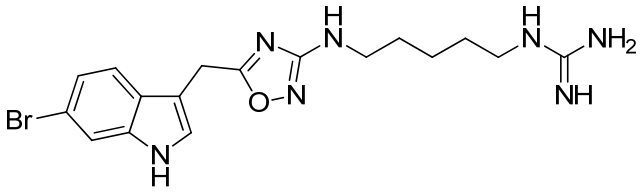

Phidianidine A (2.1).

A 50 mL round bottom flask was charged with **2.32** (20 mg, 0.0528 mmol), DIEA (20 uL), N,N'-Bis(Boc)-1*H*-pyrazole-1-carboxamidine (17.69 mg, 0.058 mmol), and DCM (5 mL). The reaction was stirred 30 minutes, monitoring progress by LCMS. After completion, a 1:1 solution of DCM:TFA (5 mL) was added and the reaction was stirred 8 hours. The mixture was then transferred to a separatory funnel, washed with water and extracted 3 times with DCM. The combined organic phase was dried over magnesium sulfate before being concentrated under reduced pressure. The brown solid was then purified by reverse phase HPLC using acetonitrile and 0.1% TFA/water (gradient: 10:90 to 90:10), obtained 20 mg (90%) of **2.1** as a glassy golden brown solid. ^{1}H NMR (600 MHz, d_6-DMSO, δ (ppm)): 11.18 (s, 1H), 7.56 (d, *J* = 1.80 Hz, 1H), 7.47 (d, *J* = 8.50 Hz, 1H), 7.34 (d, *J* = 2.50, 1H), 7.13 (dd, *J* = 8.50, 1.78, 1H), 6.72 (t, *J* = 5.85 Hz, 1H), 4.2 (s, 2H), 3.00 (dq, *J* = 33.1, 7.0 Hz, 4H) 1.46 (m, 4H), 1.27 (m, 2H); ^{13}C NMR (150 MHz, d_6-DMSO, δ (ppm)): 177.1, 168.9, 157.1, 137.4, 126.1, 125.7, 122.0, 120.6, 114.5, 114.4,

107.8, 42.6, 41.0, 28.54, 28.53, 23.8, 22.9; HRMS (TOF, ES+) $C_{17}H_{22}BrN_7O$ $[M+H]^+$ m/z 420.1147, measured [M ^{79}Br+H], [M ^{81}Br+H] 420.1148, 422.1132.

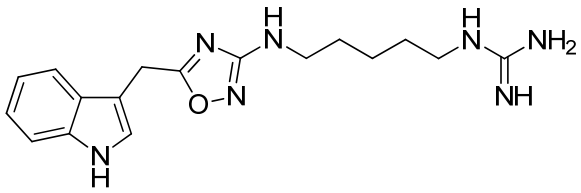

Phidianidine B (2.2).

A 50 mL round bottom flask was charged with **2.31** (20 mg, 0.0668 mmol), DIEA (20 uL), N,N'-Bis(Boc)-1*H*-pyrazole-1-carboxamidine (23.0 mg, 0.073 mmol), and DCM (5 mL). The reaction was stirred 30 minutes, monitoring progress by LCMS. After completion, a 1:1 solution of DCM:TFA (5 mL) was added and the reaction was stirred 8 hours. The mixture was then transferred to a separatory funnel, washed with water and extracted 3 times with DCM. The combined organic phase was dried over magnesium sulfate before being concentrated under reduced pressure. The brown solid was then purified by reverse phase HPLC using acetonitrile and 0.1% TFA/water (gradient: 10:90 to 90:10), obtained 20 mg (78%) **2.2** as a glassy brown solid. ^{1}H NMR (400 MHz, d_6-DMSO, δ (ppm)): 11.0, 7.51 (d, J = 7.85 Hz, 1H), 7.37 (d, J = 8.10 Hz, 1H) 7.31 (d, J = 2.45 Hz, 1H), 7.08-6.99 (dt, J = 58.2, 8.0 Hz, 2H), 6.71 (br t, J = 5.30 Hz, 1H), 4.19 (s, 2H), 3.07-3.00 (m, 4H), 1.50-1.43 (m, 4H), 1.29-1.27 (m, 2H); ^{13}C NMR (100 MHz, d_6-DMSO, δ (ppm)):177.3, 168.9, 157.1, 136.5, 127.2, 124.5, 121.6, 119.0, 118.7, 111.9, 107.3, 42.7, 41.0, 28.57, 28.55, 23.8, 23.1; HRMS (TOF, ES+) $C_{17}H_{23}N_7O$ $[M+H]^+$ m/z 342.2042, measured 342.2041.

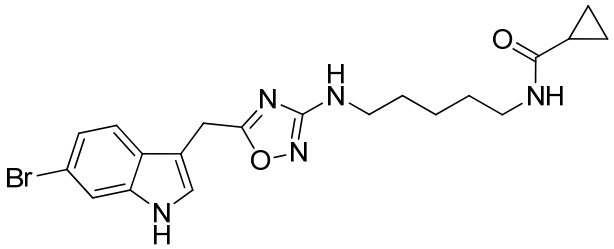

N-(5-((5-((6-bromo-1H-indol-3-yl)methyl)-1,2,4-oxadiazol-3-yl)amino)pentyl)cyclopropanecarboxamide (2.33).

A 10 mL round bottom flask was charged with **2.32** (10 mg, 0.026 mmol), cyclopropanecarbonyl chloride (5 uL, 0.053 mmol), triethylamine (10 uL) and DCM (2 mL). The flask was stirred for 3 hours, monitoring by LCMS. After 3 hours, water (3 mL) and DCM (2 mL) were added and the biphasic solution was stirred vigorously before being passed through an Isolute phase separator. The resulting organic layer was then concentrated and purified by reverse phase HPLC using acetonitrile and 0.1% TFA/water (gradient: 10:90 to 90:10). Isolated 10 mg (85%) of **2.33** as an off white solid. ^{1}H NMR (600.1 MHz, CD_3OD, δ (ppm)): 7.51 (d, J = 1.70, 1H), 7.45 (d, J = 8.50 Hz, 1H), 7.22 (s, 1H), 7.126 (dd, J = 8.50, 1.70, 1H), 4.19 (s, 2H), 3.13 (dt, J = 17.83, 7.13 Hz, 4H), 1.58 (m, 2H), 1.50 (m, 3H), 1.36 (m, 2H), 0.080 (m, 2H), 0.693 (m, 2H) ; ^{13}C NMR (150 MHz, CD_3OD, δ (ppm)): 177.4, 174.9, 168.6, 137.4, 125.7, 124.2, 121.7, 119.3, 114.7, 113.8, 107.2, 42.4, 38.9, 28.7, 28.3, 23.7, 22.4, 13.3, 5.6; HRMS (TOF, ES+) $C_{20}H_{24}BrN_5O_2$ $[M+H]^+$ m/z 446.1192, measured [M ^{79}Br+H], [M ^{81}Br+H] 446.1196, 448.1181.

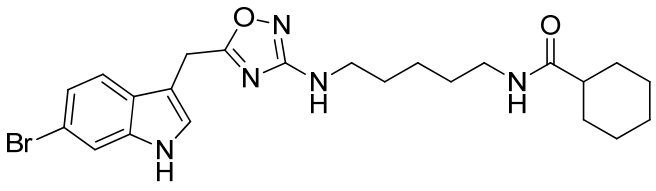

N-(5-((5-((6-bromo-1H-indol-3-yl)methyl)-1,2,4-oxadiazol-3-yl)amino)pentyl)cyclohexanecarboxamide (2.34).

A 10 mL round bottom flask was charged with **2.32** (10 mg, 0.026 mmol), cyclohexanecarbonylchloride (5 uL mg, 0.057 mmol), triethylamine (10 uL) and DCM (2 mL). The flask was stirred for 3 hours, monitoring by LCMS. After 3 hours, water (3 mL) and DCM (2 mL) were added and the biphasic solution was stirred vigorously before being passed through an Isolute phase separator. The resulting organic layer was then concentrated and purified by reverse phase HPLC using acetonitrile and 0.1% TFA/water (gradient: 10:90 to 90:10). Isolated 9 mg (70%) of **2.34** as an off white solid. ^{1}H NMR 600.1 MHz, CD_3OD, δ (ppm)):7.54 (d, *J* = 1.70 Hz, 1H), 7.48 (d, *J* = 8.50 Hz, 1H), 7.25 (s, 1H), 7.157 (dd, *J* = 8.50, 1.70, 1H), 4.21 (s, 2H), 3.15 (m, 4H), 2.14 (m, 2H), 1.79 (m, 4H), 1.69 (m, 1H), 1.61 (dp, *J* = 56.7, 7.33, 4H), 1.46-1.21 (m, 8H); ^{13}C NMR (150 MHz, CD_3OD, δ (ppm)) 177.7, 177.4, 168.6, 137.4, 125.7, 124.2, 121.7, 119.3, 114.7, 113.8, 107.2, 45.1, 45.1, 42.4, 38.7, 38.5, 29.3, 28.6, 28.3, 25.4, 25.3, 23.6, 22.4; HRMS (TOF, ES+) $C_{23}H_{30}BrN_5O_2$ $[M+H]^+$ m/z 488.1661, measured [M ^{79}Br+H], [M ^{81}Br+H] 488.1664, 490.1648.

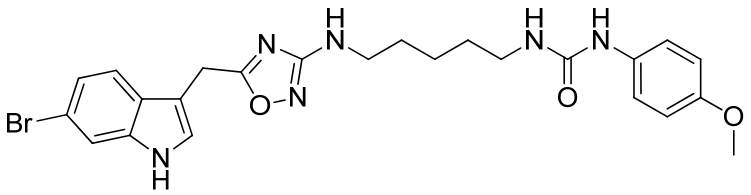

1-(5-((5-((6-bromo-1H-indol-3-yl)methyl)-1,2,4-oxadiazol-3-yl)amino)pentyl)-3-(4-methoxyphenyl)urea (2.37).

A 10 mL round bottom flask was charged with **2.32** (10 mg, 0.026 mmol), 4-methoxyphenylisocyanate (5 uL, 0.057 mmol), triethylamine (10 uL) and DCM (2 mL). The flask was stirred for 3 hours, monitoring by LCMS. After 3 hours, water (3 mL) and DCM (2 mL) were added and the biphasic solution was stirred vigorously before being passed through an Isolute phase separator. The resulting organic layer was then concentrated and purified by

reverse phase HPLC using acetonitrile and 0.1% TFA/water (gradient: 10:90 to 90:10). Isolated 10 mg (73%) of **2.37** as a brown solid. ^{1}H NMR (600.1 MHz, d_6-DMSO, δ (ppm)): 11.16 (s, 1H), 8.17 (s, 1H), 7.50 (d, *J* = 1.70 Hz, 1H), 7.47 (d, *J* = 8.50 Hz, 1H), 7.35 (d, *J* = 2.50 Hz, 1H), 7.27 (dd, *J* = 8.90, 0.87 Hz, 2H), 7.14 (dd, 8.50, 1.85 Hz, 1H), 6.78 (m, 3H), 4.20 (s, 2H), 3.68 (s, 3H), 3.01 (m, 4H),1.50 (m, 2H), 1.40 (m, 2H), 1.27 (m, 2H); ^{13}C NMR (150 MHz, d_6-DMSO, δ (ppm)): 177.1, 168.9, 168.9, 155.8, 155.7, 154.2, 137.4, 134.1, 134.0, 126.2, 125.7, 123.5, 122.0, 120.6, 119.7, 119.6, 114.5, 114.4, 114.2, 107.8, 55.5, 42.8, 42.7, 29.9, 28.7, 24.1, 22.9, ; HRMS (TOF, ES+) $C_{24}H_{27}BrN_6O_3$ $[M+H]^+$ m/z 527.1406, measured [M ^{79}Br+H], [M ^{81}Br+H] 527.1405,529.1391.

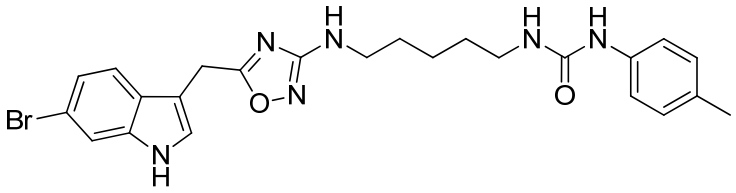

1-(5-((5-((6-bromo-1H-indol-3-yl)methyl)-1,2,4-oxadiazol-3-yl)amino)pentyl)-3-(p-tolyl)urea (2.38).

A 10 mL round bottom flask was charged with **2.32** (10 mg, 0.026 mmol), p-Tolylisocyanate (5 uL, 0.057 mmol), triethylamine (10 uL) and DCM (2 mL). The flask was stirred for 3 hours, monitoring by LCMS. After 3 hours, water (3 mL) and DCM (2 mL) were added and the biphasic solution was stirred vigorously before being passed through an Isolute phase separator. The resulting organic layer was then concentrated and purified by reverse phase HPLC using acetonitrile and 0.1% TFA/water (gradient: 10:90 to 90:10). Isolated 8 mg (60%) of **2.38** as a brown solid. ^{1}H NMR (600.1 MHz, d_6-DMSO, δ (ppm)): 11.16 (s, 1H), 8.17 (s, 1H), 7.50 (d, *J* = 1.70 Hz, 1H), 7.47 (d, *J* = 8.50 Hz, 1H), 7.35 (d, *J* = 2.50 Hz, 1H), 7.27 (dd, *J* = 8.90, 0.87 Hz, 2H), 7.14 (dd, 8.50, 1.85 Hz, 1H), 6.78 (m, 3H), 4.20 (s, 2H), 3.01 (m, 4H), 2.68 (s, 3H), 1.50 (m, 2H), 1.40 (m, 2H), 1.27 (m, 2H); ^{13}C NMR (150 MHz, d_6-DMSO, δ (ppm)): 177.1, 168.9, 168.9,

155.8, 155.7, 154.2, 137.4, 134.1, 134.0, 126.2, 125.7, 1235, 122.0, 120.6, 119.7, 119.6, 114.5, 114.4, 114.2, 107.8, 45.5, 42.8, 42.7, 29.9, 28.7, 24.1, 22.9, HRMS (TOF, ES+) $C_{24}H_{27}BrN_6O_2$ $[M+H]^+$ m/z 510.1441, measured [M ^{79}Br+H], [M ^{81}Br+H] 510.1445, 512.1458.

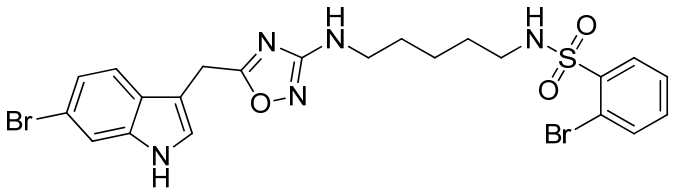

2-bromo-N-(5-((5-((6-bromo-1H-indol-3-yl)methyl)-1,2,4-oxadiazol-3-yl)amino)pentyl)benzenesulfonamide (2.35).

A 10 mL round bottom flask was charged with **2.32** (10 mg, 0.026 mmol), 2-bromophenylsulfonylchloride (10 mg, 0.057 mmol), triethylamine (10 uL) and DCM (2 mL). The flask was stirred for 3 hours, monitoring by LCMS. After 3 hours, water (3 mL) and DCM (2 mL) were added and the biphasic solution was stirred vigorously before being passed through an Isolute phase separator. The resulting organic layer was then concentrated and purified by reverse phase HPLC using acetonitrile and 0.1% TFA/water (gradient: 10:90 to 90:10). Isolated 9 mg (58%) of **2.35** as an off white glassy solid. ^{1}H NMR (600.1 MHz, CD_3OD, δ (ppm)): 8.08 (dd, 7.83, *J* = 1.70 Hz, 1H, 7.75 (dd, *J* = 7.83, 1.15 Hz, 1H), 7.54 (d, *J* = 1.70 Hz, 1H), 7.49 (td, *J* = 7.50, 1.50), 7.48 (d, *J* = 8.50 Hz, 1H), 7.42 (dt, *J* = 7.75, 1.75 Hz, 1H), 7.26 (s, 1H), 7.16 (dd, 8.50, 1.75), 4.60 (s, 2H), 4.22 (s, 2H), 3.06-2.90 (dt, *J* = 92.7, 7.0 Hz, 4H), 1.49-1.42 (m, 4H), 1.31 (m, 2H); ^{13}C NMR (150 MHz, CD_3OD, δ (ppm)): 177.5, 168.5, 139.6, 137.4, 135.0, 133.3, 130.8, 127.4, 125.7, 124.3, 121.8, 119.4, 114.7, 113.8, 107.2, 42.3, 28.7, 28.1, 23.3, 22.4; HRMS (TOF, ES+) $C_{22}H_{23}Br_2N_5O_3S$ $[M+H]^+$ m/z 595.9967, measured 595.9966.

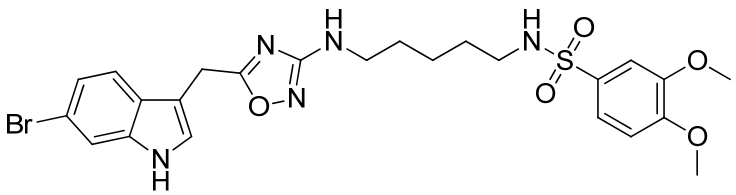

N-(5-((5-((6-bromo-1H-indol-3-yl)methyl)-1,2,4-oxadiazol-3-yl)amino)pentyl)-3,4-dimethoxybenzenesulfonamide (2.36).

A 10 mL round bottom flask was charged with **2.32** (10 mg, 0.026 mmol), 3,4-dimethoxyphenylsulfonylchloride (10 mg, 0.057 mmol), triethylamine (10 uL) and DCM (2 mL). The flask was stirred for 3 hours, monitoring by LCMS. After 3 hours, water (3 mL) and DCM (2 mL) were added and the biphasic solution was stirred vigorously before being passed through an Isolute phase separator. The resulting organic layer was then concentrated and purified by reverse phase HPLC using acetonitrile and 0.1% TFA/water (gradient: 10:90 to 90:10). Isolated 10 mg (66%) **2.36** as an off white glassy solid. ^{1}H NMR (600.1 MHz, CD_3OD, δ (ppm)): 7.54 (s, 1H), 7.47 (d, *J* = 8.50 Hz, 1H), 7.45 (dd, *J* =8.50, 2.20 Hz, 1H), 7.36 (d, *J* = 2.20 Hz, 1H), 7.25 (s, 1H), 7.15 (dd, *J* = 8.50, 1.70 Hz, 1H), 7.05 (d, *J* = 8.50 Hz, 1H), 4.22 (s, 2H), 3.88 (d, *J* = 5.35 Hz, 6H), 3.09 (t, *J* = 7.0 Hz, 4H), 2.88 (t, *J* = 7.0 Hz, 4H), 1.54-1.44 (m, 4H), 1.33 (m, 2H); ^{13}C NMR (150 MHz, CD_3OD, δ (ppm)): 177.5, 168.5, 152.5, 149.1, 137.4, 1319, 125.7, 124.2, 121.8, 120.5, 119.3, 114.7, 113.8, 110.5, 109.4, 107.2, 55.19, 55.14, 42.4, 42.3, 28.6, 28.1, 23.4, 22.4; HRMS (TOF, ES+) $C_{24}H_{28}BrN_5O_5S$ $[M+H]^+$ m/z 578.1073, measured [M ^{79}Br+H], [M ^{81}Br+H] 578.1074, 580.1061.

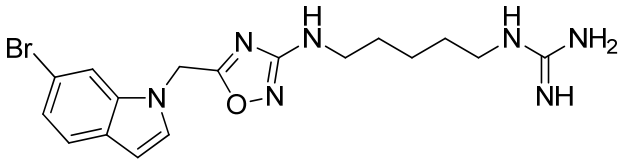

1-(5-((5-((6-bromo-1H-indol-1-yl)methyl)-1,2,4-oxadiazol-3-yl)amino)pentyl)guanidine (2.41).

A flask was charged with **2.40** (100 mg, 0.393 mmol), HATU (150 mg, 0.393 mmol), DIEA (70 uL, 0.393 mmol) and DCM (2 mL). The solution was stirred for 30 minutes and transferring via pipette, added dropwise to a stirred solution of **2.12** (112 mg, 0.432 mmol) in DCM (2 mL). The reaction was stirred 1 hour and concentrated under reduced pressure. The crude mixture was dissolved in DCE (5 mL). The flask was fitted with a reflux condenser and the reaction was heated to 100^{o}C for 1 hour. The reaction mixture was cooled and a 1:1 solution of DCM:TFA (5 mL) was added. The flask was heated to 50^{o}C for 3 hours, monitoring reaction progress by LCMS. The mixture was then transferred to a separatory funnel and partitioned between water and DCM. The mixture was extracted 3x with 25 mL DCM and the combined organic phase was dried over magnesium sulfate and concentrated under reduced pressure. The crude mixture was dissolved in DCM and N,N'-Bis(Boc)-1*H*-pyrazole-1-carboxamidine (134 mg, 0.432 mmol) was added. The reaction was stirred 1 hour and a 1:1 solution of DCM:TFA (10 mL) was added. The reaction was heated to 80^{o}C for 3 hours. The mixture was then transferred to a separatory funnel and partitioned between water and DCM. The mixture was extracted 3x with 25 mL DCM and the combined organic phase was dried over magnesium sulfate and concentrated under reduced pressure. The product was purified by reverse phase HPLC using acetonitrile and 0.1% TFA/water (gradient: 10:90 to 90:10), obtained 112 mg (67%) **2.41** as a bright red glassy solid. ^{1}H NMR (600.1 MHz, CD_3OD, δ (ppm)): 7.58 (s, 1H), 7.43 (d, J = 8.5 Hz, 1H), 7.25 (d, J = 3.25 Hz, 1H), 7.14 (dd, J = 8.50, 1.56 Hz, 1H), 6.49 (d, J = 3.25 Hz, 1H), 5.46 (s, 2H), 3.10 (m, 4H), 1.55 (m, 6H), 1.35 (m, 2H); ^{13}C NMR (150 MHz, CD_3OD, δ (ppm)):157.9, 167.0, 135.8, 124.1,

122.6, 120.2, 117.7, 113.1, 112.2, 105.6, 40.5, 37.5, 26.5, 25.1, 21.6, 20.8; HRMS (TOF, ES+) $C_{17}H_{22}BrN_7O$ $[M+H]^+$ m/z 420.1147, measured [M ^{79}Br+H], [M ^{81}Br+H] 420.1148, 422.1126.

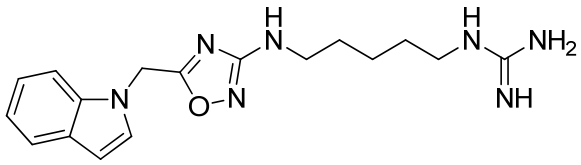

1-(5-((5-((1H-indol-1-yl)methyl)-1,2,4-oxadiazol-3-yl)amino)pentyl)guanidine (2.42).

A flask was charged with **2.41** (100 mg, 0.292 mmol), HATU (111 mg, 0.292 mmol), DIEA (101 uL, 0.584mmol) and DCM (2 mL). The solution as stirred for 30 minutes and transferring via pipette, added dropwise to a stirred solution of **2.12** (112 mg, 0.432 mmol) in DCM (2 mL). The reaction was stirred 1 hour and concentrated under reduced pressure. The crude mixture was dissolved in DCE (5 mL). The flask was fitted with a reflux condenser and the reaction was heated to 100^{o}C for 1 hour. The reaction mixture was cooled and a 1:1 solution of DCM:TFA (5 mL) was added. The flask was heated to 50^{o}C for 3 hours, monitoring reaction progress by LCMS. The mixture was then transferred to a separatory funnel and partitioned between water and DCM. The mixture was extracted 3x with 25 mL DCM and the combined organic phase was dried over magnesium sulfate and concentrated under reduced pressure. The crude mixture was dissolved in DCM and N,N'-Bis(Boc)-1*H*-pyrazole-1-carboxamidine (100 mg, 0.321 mmol) was added. The reaction was stirred 1 hour and a 1:1 solution of DCM:TFA (10 mL) was added. The reaction was heated to 80^{o}C for 3 hours. The mixture was then transferred to a separatory funnel and partitioned between water and DCM. The mixture was extracted 3x with 25 mL DCM and the combined organic phase was dried over magnesium sulfate and concentrated under reduced pressure. The product was purified by reverse phase HPLC using acetonitrile and 0.1% TFA/water (gradient: 10:90 to 90:10), obtained 32 mg (32%) **2.42** as a beige glassy solid. ^{1}H NMR (600.1 MHz, CD_3OD, δ (ppm)): 7.61 (d, J = 7.80 Hz, 1H), 7.44 (d, J = 8.0Hz, 1H), 7.36 (d, J = 3.25 Hz, 1H), 7.22 (t, J =7.56 Hz, 1H), 7.11 (t, J = 7.56 Hz, 1H), 6.55 (d, J = 3.25 Hz, 1H)

5.58 (s, 2H); 3.14 (m, 4H), 1.59 (m, 4H), 1.40 (m, 2H); ^{13}C NMR (150 MHz, CD_3OD, δ (ppm)):174.1, 168.8, 157.1, 157.0, 436.3, 128.9, 128.6, 121.7, 120.7, 119.7, 109.4, 102.1, 42.4, 41.2, 40.9, 28.2, 28.1, 23.5; HRMS (TOF, ES+) $C_{17}H_{23}N_7O$ $[M+H]^+$ m/z 342.2042, measured 342.2042.

Table 2.9.1: NMR Shift Correlation Tables for **2.1** and **2.2**.

1H

Natural PA-A **2.1**	Synthetic PA-A **2.1**	Natural PA-B **2.2**	Synthetic PA-B **2.2**
11.15	11.18	11.00	11.0
7.35	7.34	7.31	7.31
7.53	7.47	7.50	7.51
7.13	7.13	6.99	6.99
7.56	7.56	7.09	7.08
4.2	4.20	7.36	7.37
6.72	6.72	4.20	4.19
2.99	3.00	6.71	6.71
1.36-1.56	1.40-1.52	3.00	3.01
1.28	1.27	1.36-1.56	1.42-1.52
1.36-1.56	1.40-1.52	1.28	1.28
3.02	3.00	1.36-1.56	1.42-1.52
7.41	7.40	3.05	3.01
		7.43	7.49

13C

Natural PA-A **2.1**	Synthetic PA-A **2.1**	Natural PA-B **2.2**	Synthetic PA-B **2.2**
125.0	125.7	125.3	124.50
106.8	107.8	103.9	107.30
125.2	126.1	126.7	127.20
120.0	120.6	117.3	118.70
121.3	122.0	117.6	121.60
113.5	114.4	120.2	119.00
114.1	114.5	111.5	111.90
137.0	137.4	136.1	136.50
22.5	22.9	22.7	23.10
168.5	168.9	168.5	168.90
176.7	177.1	176.9	177.30
40.5	41	40.7	41.00
28.1	28.5	28.1	28.57
23.4	23.8	23.4	23.80
28.1	28.54	28.1	28.55
41.9	42.6	42.3	42.70
156.6	157.1	156.6	157.10

Tables formatted to match Phidianidines A & B isolation NMR data tables by Carbone et al.

Cell proliferation/cytotoxicity assay:

Cytotoxicity assays were performed in HEK293 cells using a WST-1 cell proliferation assay kit at both 24 and 48 hour time points. 25,000 cells were plated in a 96-well plate in 100 mL of culture medium with either DMSO, **2.1** (10 μM) or **2.2** (10 μM). Cells were then cultured for either 24 or 48 hours in a CO_2 incubator at 37 ^oC. Then, 10 mL of WST-1 mixture added to each well, mixed on orbital shaker and cells incubated for another 2 hours at 37 ^oC. The absorbance of each sample was then measured at 450 nm.

Radioligand Binding and Functional assays:

All biological assays were conducted at Ricerca Pharma according to published protocols and each assay employed established control compounds[27,54].

Functional μOR assay (GTPγS)[27,54]:

Human recombinant μ-opioid receptors stably expressed in CHO-K1 cells were used. Compounds **2.1**, **2.2** and **2.32** were preincubated with the membranes (0.016 mg/ml‡) and 3 mM GDP in modified HEPES pH 7.4 buffer for 20 minutes at 25°C and SPA beads were then added for another 60 minutes at 30°C. The reaction was initiated by 0.3 nM [^{35}S]GTPγS for an additional 30 minute incubation period. Test compound-induced increase of [^{35}S]GTPγS binding by 50 percent or more (50%) relative to the 10 mM DAMGO response indicates possible μOR agonist activity. Compounds are screened at 10, 1, 0.1, 0.01 and 0.001 mM.

CHAPTER III

CHARACTERIZATION OF A NOVEL CLASS OF POSITIVE ALLOSTERIC MODULATORS FOR THE METABOTROPIC GLUTAMATE RECEPTORS SUBTYPE I

3.1 Introduction

The metabotropic glutamate receptors (mGlus) are members of the class C GPCR superfamily and are activated by one of the most important excitatory neurotransmitters used in the nervous system, glutamate. Structurally, the mGlus feature a large extracellular agonist binding domain, a cysteine rich domain, and a seven-transmembrane spanning domain that is believed to be the binding site for most known mGlu allosteric modulators[55].

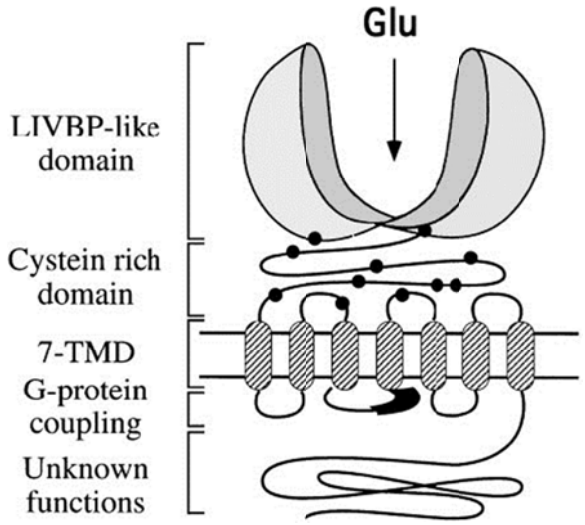

Figure 3.1.1: Schematic representation of an mGlu receptor. The region rich in cysteine residues is indicated with black circles. The segment in the second intracellular loop that is important for G-protein coupling specificity in indicated in black[55].

The eight currently known mGlu receptor subtypes are divided into three groups according to sequence homology, pharmacology, and intracellular signaling mechanism. The group I subfamily contains $mGlu_1$ and $mGlu_5$; group II receptors include $mGlu_2$ and $mGlu_3$ and the group III receptors feature the remaining subtypes: $mGlu_4$, $mGlu_6$, $mGlu_7$, and $mGlu_8$. The group I receptor subtypes are primarily located post-synaptically, where they intracellularly couple to $G_{\alpha q}$ and induce inositol phosphate metabolism through phospholipase C[56]. Activation of $mGlu_1$ causes $G_{\alpha q}$ to dissociate from $G_{\beta\gamma}$ subunits of the G protein heterotrimer. $G_{\alpha q}$ then binds to Phosopholipase C, which causes increased phosphatidylinositol 4,5-bisphosphate (PIP_2) hydrodrolysis to diacyl glycerol (DAG) and inositol 1,4,5-triphosphate (IP_3). While DAG remains bound to the cell membrane, the liberated IP_3 diffuses through the cytosol and binds to IP_3 receptors on the endoplasmic reticulum (ER), causing calcium release from the ER into the cytosol. This increase in intracellular calcium levels causes a range of intracellular responses and changes[57] and can be observed and quantified using calcium sensitive fluorescent dys such as Fluo-4[58] (Figure 3.1.3).

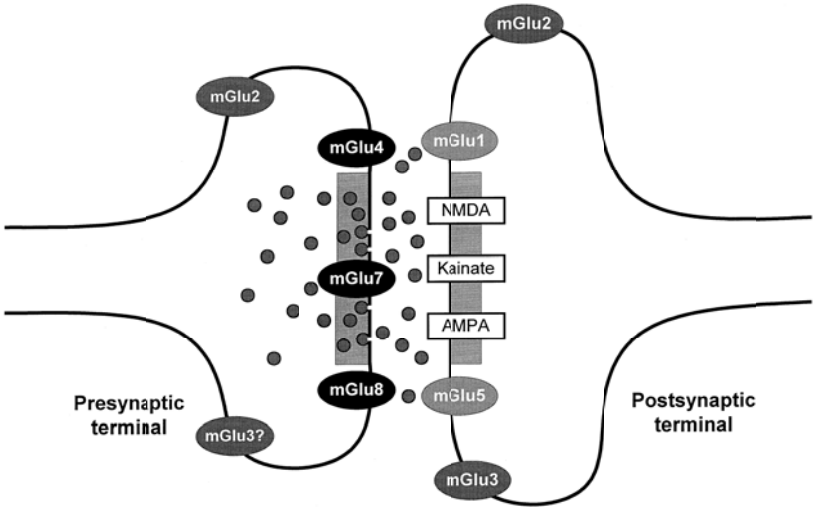

Figure 3.1.2: Synaptic localization of glutamate receptors at a theoretical CNS synapse as shown by immunocytochemical studies[56].

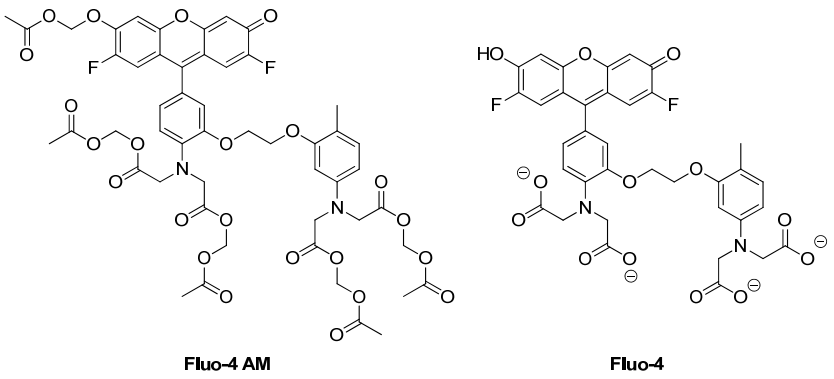

Figure 3.1.3: Chemical structure of non-fluorescent Fluo-4 AM and Fluo-4. The four acetoxymethyl esters on Fluo-4 AM are cleaved inside cells to yield Fluo-4, which fluoresces upon binding to Ca^{2+} ions[58].

While a number of recent publications have highlighted members of the group II and III mGluRs as potential new targets for the treatment of schizophrenia and Parkinsons disease, several new findings have shown a potential link between mutations in the $mGlu_1$ gene cluster and schizophrenia[59,60].

Schizophrenia is a devastating neurological disorder that affects roughly 1% of the population, though its neurobiological cause remains unknown. Current pharmacological studies suggest two potential models: the 'dopamine hypothesis' based on the knowledge that most of the currently available antipsychotic agents function as dopamine antagonists[61] and the 'glutamate hypothesis' which was proposed based on the observation that animals treated with NMDA receptor (*N*-methyl-D-aspartate, an ionotropic glutamate receptor) antagonists demonstrate schizophrenia-like symptoms of psychosis[62,63].

3.2 Background

In order to probe the role of glutamate receptors in schizophrenia and bipolar disorder, Frank and coworkers performed a genetic screen of 10 "hub" genes of 1344 individuals divided into three groups: those with schizophrenia (503), those with bipolar disorder (263), and healthy

controls (538). The "hub" genes investigated are subunits of the ionotropic NMDA and AMPA receptors, as well as the metabotropic glutamate receptor subtype 1 gene cluster (*GRM1*), and the membrane-associated guanylate kinase (MAGUK) primary binding partners *DLG1, DLG2, DLG3,* and *DLG4*, which encode SAP97, PSD93, SAP102, and PSD95, respectively. These genes were selected because ionotropic and metabotropic glutamate receptor function has been shown to be largely dependent upon interactions between complexes formed from various intracellular scaffold proteins, including the MAGUK family[64,65]. In total, 62 different coding variants (non-synonymous single nucleotide polymorphisms; nsSNPs) were identified. Figure 3.2.1 illustrated the results of the screen. Each nsSNP is marked by an asterisk when it was located only in the disease cohort (left column), found at least once in the disease and control cohorts (second from left column), found only in the control cohort (third from left column), or predicted deleterious by sequence conservation analysis (right column).

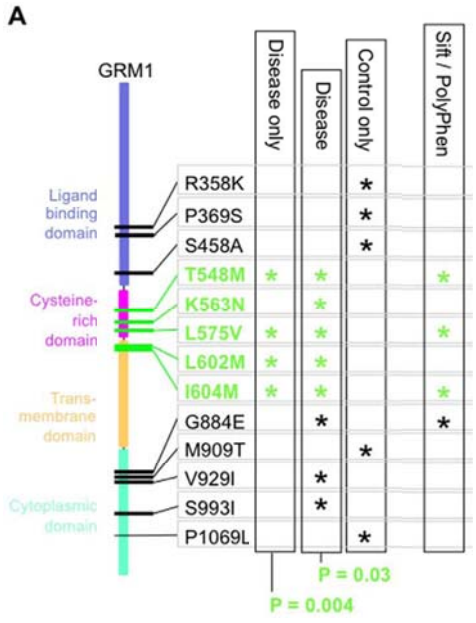

Figure 3.2.1: nsSNP density plot for *GRM1* illustrating the distribution along the length of the protein.

Frank and coworkers expanded on these genetic screening findings by using *in silico* modeling to map the nsSNPs onto available protein models and hypothesizing about their deleterious effects on protein structure and function[59]. This is the first genetic study to directly relate $mGlu_1$ mutations to the pathogenesis of a CNS disorder.

Shortly after the work by Frank and coworkers was published, Ayoub and coworkers produced a similar finding. By screening 1055 individuals (450 schizophrenia patients and 605 healthy controls), Ayoub and coworkers examined the occurrence, inheritance and functional effects of *GRM1* nsSNPs. A total of 47 nucleotide substitution variants were identified, 16 of which were nsSNPs. Half (8/16) of these nsSNPs were classified as benign by bioinformatics programs used for predicting potential functional effects.

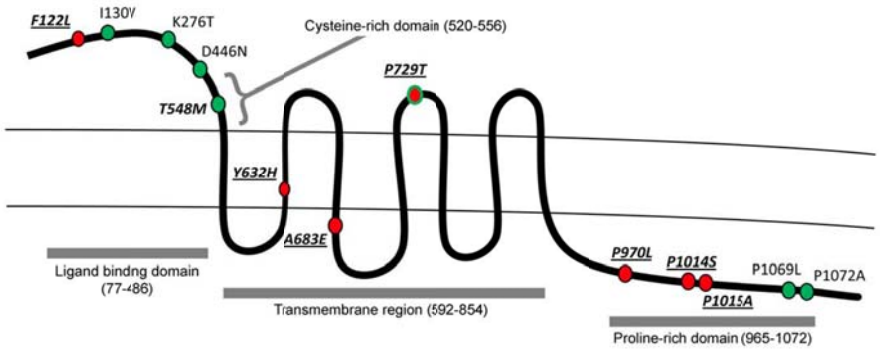

Figure 3.2.2: Non-synonymous coding changes relative to the $mGlu_1$ receptor protein domains (shown as grey bars). Color coding: red circles – case-specific, green circles – control specific, red circles with green outline – detected in cases as well as controls. Mutations that were predicted by bioinformatics programs to have a deleterious effect on protein function are italicized and underlined[60].

Additional information on family history and current status of 1st-degree relatives was collected, and genotyping performed for five potentially deleterious nsSNPs. In addition to the individuals with clinically diagnosed schizophrenia (probands), 4 of the 5 families featured multiple cases of other neuropsychiatric disorders, such as epilepsy, Asperger syndrome, anxiety,

depression and substance abuse (Figure 3.2.3). Importantly, none of the nsSNPs genotyped in family members was a *de novo* mutation, all were inherited. The family history analysis showed that, in addition to the probands, *GRM1* mutations were also present in 1st-degree relatives with other neurological disorders not limited to psychosis, suggesting that this gene may have influence over multiple phenotypic outcomes.

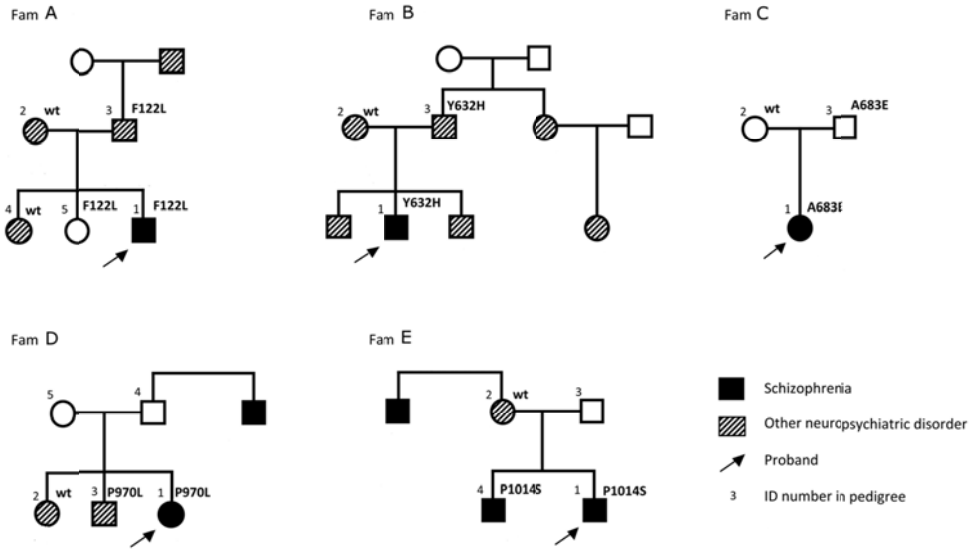

Figure 3.2.3: Structure, neuropsychiatric morbidity and mutation segregation in families of schizophrenia probands with deleterious *GRM1* variants[60].

Ayoub and coworkers analyzed the $mGlu_1$-mediated G protein signaling pathway in COS-7 cells transiently expressing wild-type $mGlu_1$. Additionally, they generated several mutant cell lines, each expressing one of the identified nsSNP mutant $mGlu_1$ proteins. The utilized assay measured inositol phosphate (IP_1) levels in response to treatment with a group I glutamatergic agonist, Quisqualate **3.1**.

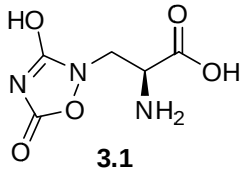

3.1

Figure 3.2.4: Chemical structure of group I glutamatergic agonist Quisqualate.

Comparing wild type and mutant cell lines showed a major divergence in signaling efficacy in four of the seven expressed nsSNP mutant cell lines: F122L, A683E, P970L and P1015A. Because the signaling bias could be due to decreased levels of receptor density on the plasma membrane in the mutant cell lines, Ayoub and coworkers performed an ELISA assay, using an anti-$mGlu_1$ antibody. They found that none of the mutations that affected signaling significantly affected receptor expression at the plasma membrane.

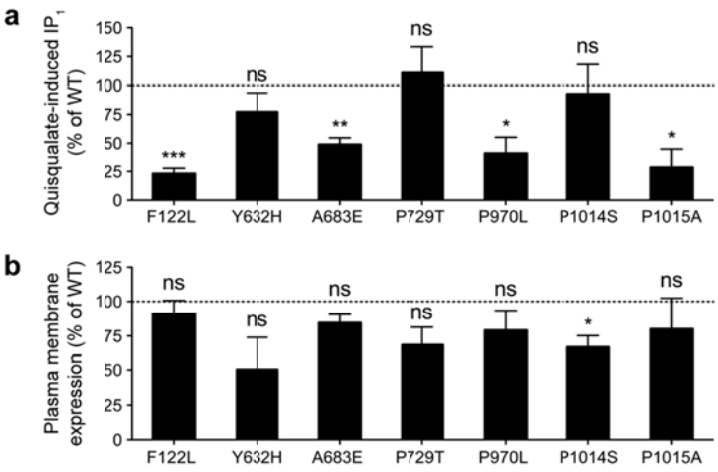

Figure 3.2.5: COS-7 cells transiently expressing either WT $mGlu_1$ or one of seven mutant $mGlu_1$ proteins were assayed for Quisqualate-induced inositol phosphate production using the IP-One assay (a) or plasma membrane expression using ELISA with anti-$mGlu_1$ antibody on intact cells (b). Findings show significantly reduced cell signaling in 4 of 7 mutant cell lines but no significant reduction in receptor density compared to wild type.

Collectively, the work by Frank et al. and Ayoub et al. suggests a possible role of $mGlu_1$ in diverse psychiatric conditions. Decreased $mGlu_1$ mediated signaling due to inefficient mutant

receptor activity could play an essential role in schizophrenia, bipolar disorder, and other CNS pathologies.

3.3 Prior Art - $mGlu_1$ PAMs

A potent and selective $mGlu_1$ positive allosteric modulator would be an ideal tool to restore decreased mutant signaling to wild type levels without constitutively activating the receptor through agonism. A recent literature review[66] notes that all of the currently available subtype selective $mGlu_1$ PAMs were generated at Roche Pharmaceuticals and Vanderbilt (Table 3.3.1). While all of the five compounds are active at the rat $mGlu_1$ isoform, only two compounds show activity at human $mGlu_1$: Ro 67-4853 (**3.3**) and Ro 07-11401 (**3.5**)[67,68].

Table 3.3.1: Prior art - $mGlu_1$ PAMs.

Compound	Structure	Potency/Affinity (EC_{50})	References
3.2	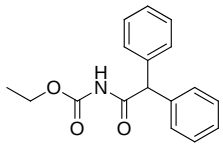	200 nM	Knoflach et al., 2001
3.3	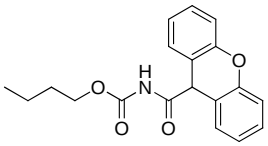	69 nM	Knoflach et al., 2001
3.4	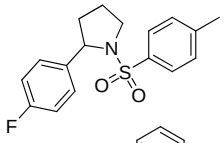	174 nM	Knoflach et al., 2001
3.5	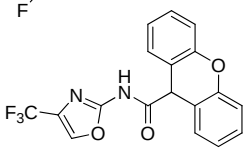	56 nM	Knoflach et al., 2001
3.6	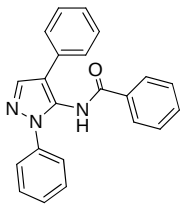	2.4 uM	Hemstapat et al., 2006

Both **3.3** and **3.5** show good potency/efficacy at $mGlu_1$, however, their utility as tool compounds is limited due to poor DMPK profiles. Compound **3.3** features a carbamate moiety which is easily hydrolyzed under aqueous *in vitro* conditions. Additionally, the xanthene moiety which is common to both structures renders them each highly lipophilic and likely to engage in nonspecific binding. Indeed, *in vitro* plasma protein binding analysis of **3.5** by the Daniels laboratory at Vanderbilt shows that only 0.1% of the dosed compound exists as free fraction in rat serum. With so little unbound compound in solution, the chances of drug-target interaction are significantly diminished. Finally, **3.5** was shown to inhibit CYP 2C9 at an IC50 of 600 nM. All of these data combine to show that, while several $mGlu_1$ PAMs have been identified, their utility as tool compounds is highly limited. A potent, selective, and stable $hmGlu_1$ PAM is needed to probe the effects of potentiating the decreased $mGlu_1$ signaling in the schizophrenia mutations described in the Frank and Ayoub genetic studies.

3.4 $hmGlu_1$ PAM First Attempt: VU-71/48 Scaffolds

Due to the lack of suitable selective $mGlu_1$ PAMs, we initiated a synthesis campaign to generate our own ligand by further exploring and optimizing the structure activity relationships of aminopyrazole-based compounds VU-71 (**3.6**) and VU-48 (**3.7**) at $hmGlu_1$ (Figure 3.4.1). These compounds represent the most selective (**3.6**) and potent (**3.7**) $mGlu_1$ potentiators reported in the 2006 *Molecular Pharmacology* article from the Conn laboratory at Vanderbilt[68].

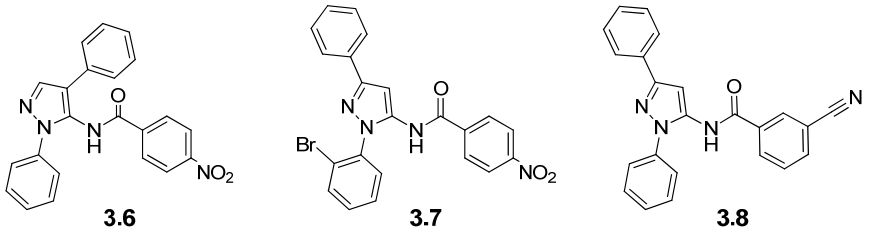

Figure 3.4.1: Structures of VU-71 (**3.6**), VU-48 (**3.7**), and CDPPB (**3.8**).

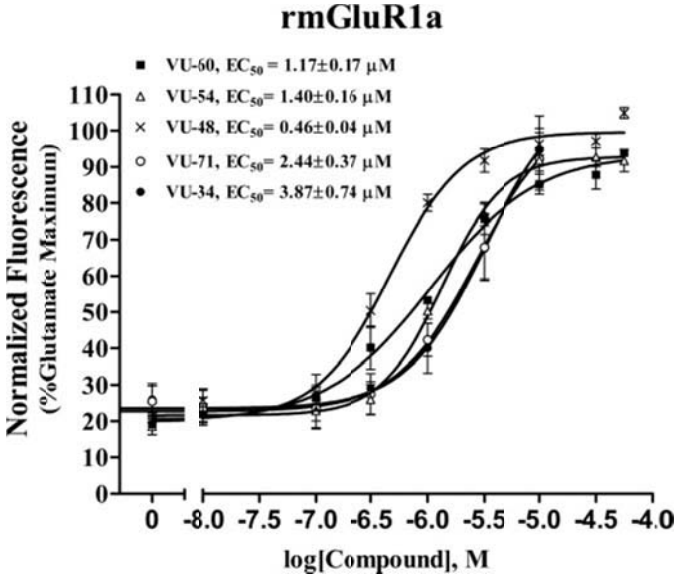

Figure 3.4.2: Concentration response curves (CRCs) showing calculated potencies of several active compounds include VU-71 (**3.6**) and VU-48 (**3.7**) from the 2006 *Molecular Pharmacology* article published by the Conn laboratory at Vanderbilt.

Compounds **3.6** and **3.7** are analogs of CDPPB (**3.8**), the first centrally penetrant, potent, and selective $mGlu_5$ PAM[69]. While CDPPB is selective for $mGlu_5$ over other subtypes, several CDPPB analogs in the same chemical series showed 2.5-fold potentiation of glutamate-induced calcium mobilization in cells expressing $mGlu_1$.

In order to quickly examine the SAR around the aminopyraloze scaffolds of **3.6** and **3.7**, we undertook a matrix based parallel synthesis approach (Scheme 3.4.1). The northern phenyl rings were held constant across each set of libraries; however, variously substituted hydrazines (**3.9**) were employed to sample the southern chemical space (R_1 in Scheme 3.4.1). Phenyl hydrazines with electron withdrawing (2,5-difluorophenyl), electron donating (4-methoxyphenyl), and bulky functional groups (4-Bromo) were employed. Tertbutylhydrazine was also utilized to probe the steric requirements of the southern section of the molecules. The eastern amide (R_2 in Scheme 3.4.1) was subjected to the widest degree of variability in hope of removing the undesirable nitro group. A range of substituted benzoic acids were employed, along with a

number of different heterocycles, including pyradines, pyrazine, pyrimidines, furans, oxazoles, and thiazoles. A total of 75 compounds were synthesized in three libraries.

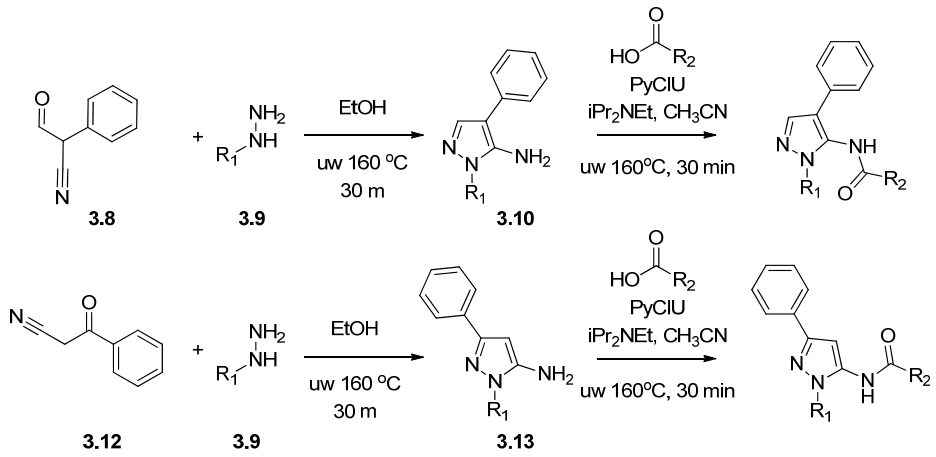

Scheme 3.4.1: Matrix based synthesis of VU-71/VU-48 analogs.

In order to test the newly-synthesized compounds at the human $mGlu_1$, collaborators in the Conn laboratory generated tetracycline-inducible human $mGlu_1$ in TREx293 cells, and also remade rat $mGlu_1$ in the same cell background. As noted above, the 2006 *Mol. Pharm.* publication reported EC_{50} potency values of 2.4 μM and 460 nM for **3.6** and **3.7**, respectively. These values were measured in Ca^{2+} fluorescence assays using BHK cells stably expressing rat $mGlu_1$. Importantly, the compounds were not previously tested at human $mGlu_1$. Thus, each of the newly generated libraries was initially screened in Ca^{2+} fluorescence assays in human $mGlu_1$-TREx293 cells. Unfortunately, no chemical modification of the **3.6**/**3.7** scaffolds engendered $hmGlu_1$ PAM activity (Figure 3.4.3).

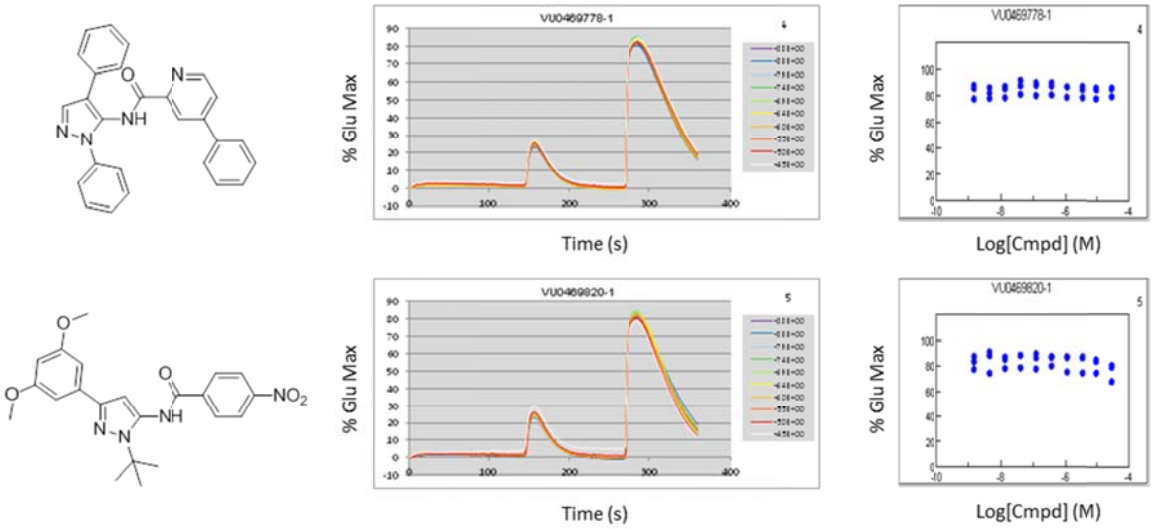

Figure 3.4.3: Structure, waveform graph, and concentration response curve of two representative members of the 75 member **3.6**/**3.7** analog library. The waveform graph demonstrates a triple add protocol where compound is added at 20 seconds, an EC_{20} dose of glutamate agonist is added at 160 seconds, and an EC_{80} dose of glutamate is added at 280 seconds. Neither of the representative compounds was successful in potentiating an EC_{20} or EC_{80} dose of glutamate. Concentration response curves show no increase in EC_{80} maximum glutamate response at compound concentrations up to 30 μM.

With the data in hand showing that all 75 compounds were inactive against the human $mGlu_1$ receptor, the library was rescreened in singlepoint assay format against rat $mGlu_1$-TREx293 cells. The singlepoint screening results of the **3.6**/**3.7** analog libraries are shown below. While several compounds did present moderate activity (Figure 3.4.6), none were able to potentiate an EC_{20} dose of glutamate to the 50% maximum glutamate response of **3.7** or the 80% maximum response of **3.5**.

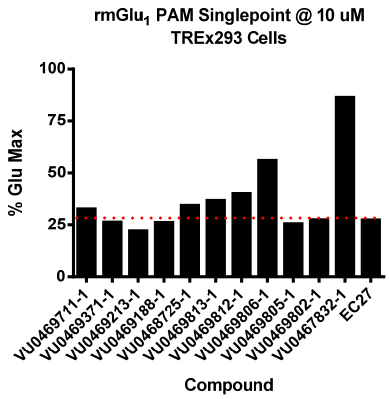

Figure 3.4.4: Singlepoint screen (1 of 3 for **3.6**/**3.7** analog library) at 10 μM compound concentration against $rmGlu_1$. Compounds of note: VU0469806 (**3.7**) and VU0467832 (**3.5**).

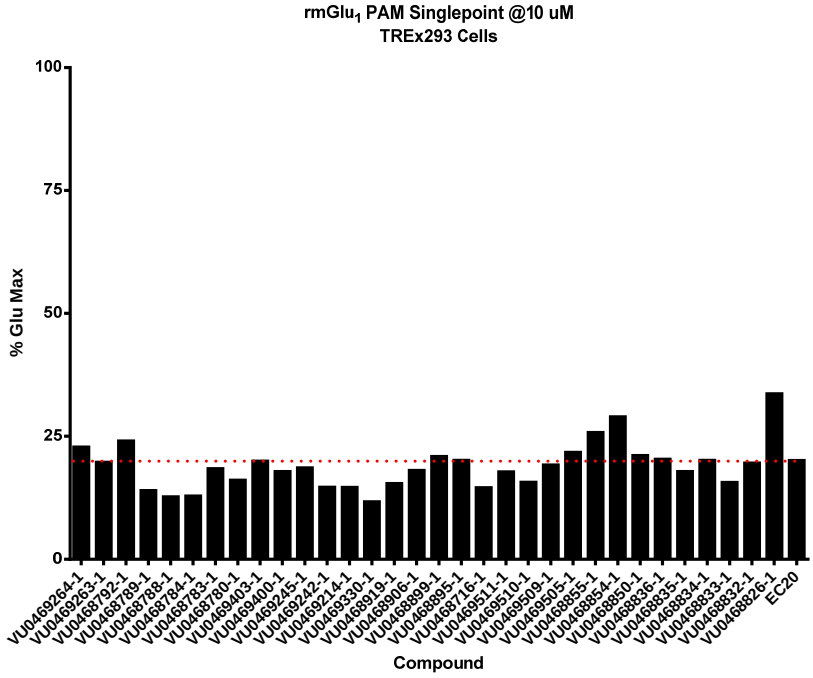

Figure 3.4.5: Singlepoint screen (2 of 3 for **3.6**/**3.7** analog library) at 10 μM compound concentration against $rmGlu_1$.

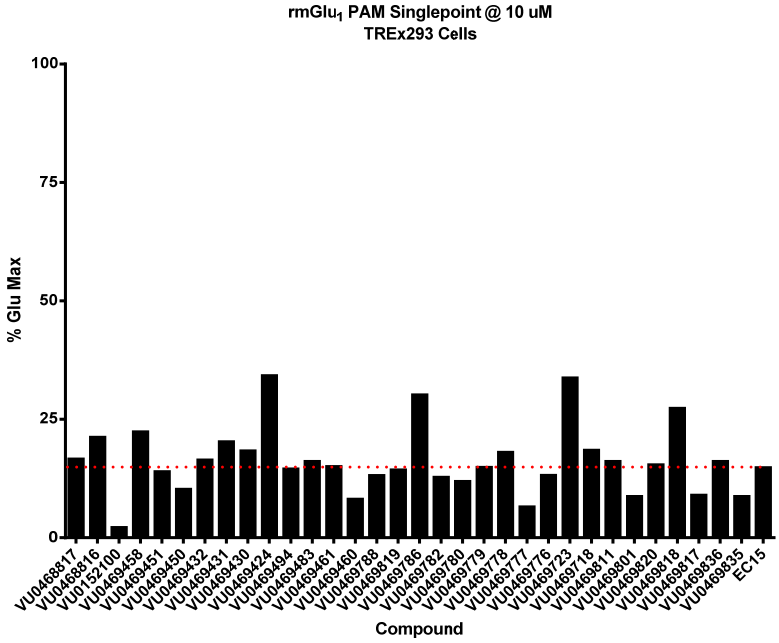

Figure 3.4.6: Singlepoint screen (3 of 3 for **3.6**/**3.7** analog library) at 10 μM compound concentration against $rmGlu_1$.

The relatively poor performance of the **3.6**/**3.7** analog library lead us to revisit the parent compounds. As stated above, the 2006 *Mol. Pharm.* article highlighted EC_{50} potency values of 2.4 μM and 460 nM for **3.6** and **3.7**, respectively, in $rmGlu_1$-BHK cells. When a concentration-response curve was generated for **3.7** in $rmGlu_1$-TREx293 cells, the EC_{50} value was found to be over 2.3 μM (Figure 3.4.7).

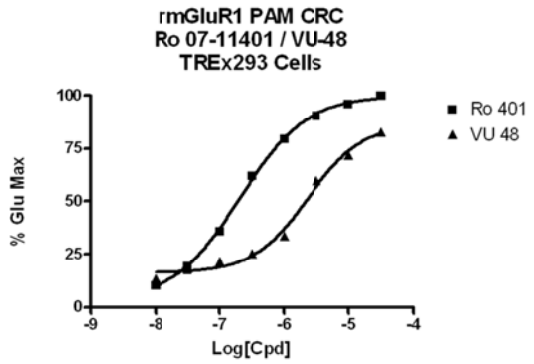

Best-fit values	Ro 401	VU 48
BOTTOM	3.318	16.25
TOP	100.0	86.94
LOGEC50	-6.684	-5.628
HILLSLOPE	0.8548	1.021
EC50	2.070e-007	2.353e-006

Figure 3.4.7: Concentration response curve of VU-48 (**3.7**) and Ro-401 (**3.5**).

The potency difference of **3.7** at $rmGlu_1$ can most easily be explained by different levels of receptor expression in the two cell lines. With this new potency data in hand, it was concluded that the **3.6**/**3.7** scaffolds were suboptimal for the purposes of this project: they showed very modest potency against the rat receptor and no efficacy against the human receptor. As a result, these compounds were not usable in probing the mutant cell line pharmacology and therefore did not warrant further investigation.

3.5 $hmGlu_1$ PAM Second Attempt: $mGlu_4$ PAM Subtype Selectivity Switch

In searching for a new $mGlu_1$ PAM scaffold, a review of the VCNDD historical screening data sets revealed over 90 active $mGlu_1$ PAMs, most of which were discovered through $mGlu_4$ PAM development. A large number of these structures were ruled out due to their role in various drug discovery efforts within the Center, however, a list of 25 available candidates from two distinct chemical series were deemed open for further structural exploration (Figure 3.5.1).

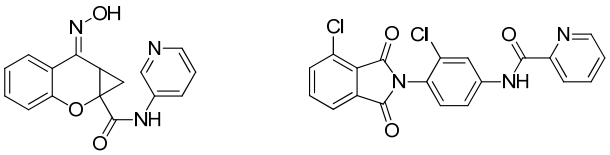

3.14
$hmGlu_1$ EC_{50} = 46 nM
$hmGlu_4$ EC_{50} = 13 nM

3.15
$hmGlu_1$ EC_{50} = 75 nM
$hmGlu_4$ EC_{50} = 61 nM

Figure 3.5.1: Representative members of the two VCNDD $hmGlu_4$ PAM series with good efficacy at $hmGlu_1$.

Of the two structural series, we viewed compound **3.15** as the more desirable lead for library synthesis for several reasons: its potency at $hmGlu_1$ was excellent, the original $mGlu_4$ series was well tolerate in *in vitro* experiments, and finally its $hmGlu_4$ activity was found to be strongly linked to the eastern 2-pyridine moiety. In previous work, removing the 2-pyridine caused $mGlu_4$ potency to decrease dramatically[70]. Contrastingly, **3.14** features an oxime moiety, which is easily hydrolyzed to a highly electrophilic α-cyclopropyl ketone under aqueous conditions. This electrophilic center would be easily attacked by cellular nucleophiles. Additionally, the presence of the cyclopropane ring severely limits the amenability of this scaffold to library synthesis. With these data in mind, we focused our attention on the **3.15** scaffold.

As mentioned previously, the **3.15** scaffold originated from the $hmGlu_4$ PAM development project within the VCNDD. High throughput screening hits **3.16** and **3.17** (Figure 3.5.2) served as lead compounds for multiple rounds of synthesis to arrive at the present structures. These HTS hits represented good starting points for probe development as they were relatively low molecular weight with no undesirable functional groups and were easily assembled from commercially available materials.

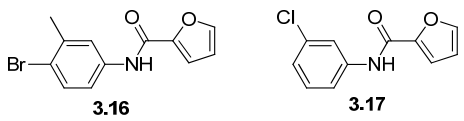

3.16

$hmGlu_4$ = >5 uM
Fold Shift = 4.3
MW = 280
cLogP = 3.45

3.17

$hmGlu_4$ = >5 uM
Fold Shift = 5.0
MW = 222
cLogP = 2.80

Figure 3.5.2: HTS hits that lead to the development of the **3.15** scaffold.

Some initial SAR around the **3.15** scaffold was available at the outset of this new line of investigation into an $hmGlu_1$ PAM. Figure 3.5.3 highlights the data that had been previously generated around the western portion of this scaffold. While functionalizing the phthalamide ring proved to slightly modulate the activity levels at both $hmGlu_1$ and $hmGlu_4$, any attempts at saturating the phthalamide phenyl ring, either partially or fully, caused steep declines in activity levels at both isoforms of the receptor. The planar orientation of the phthalamide phenyl ring was also shown to be critical, as a disconnected phenyl ring that is free to rotate in space resulted in a marked loss of activity, as seen in compound **3.23**.

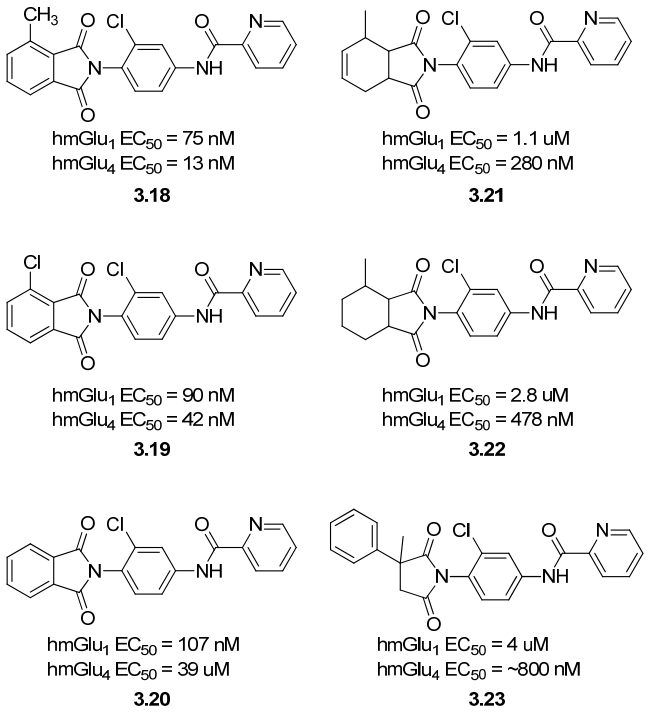

Figure 3.5.3: Initial known SAR around the western section of the **3.15** lead series.

With these data in mind, a second synthesis campaign was undertaken to explore the SAR around the **3.15** chemical scaffold at $hmGlu_1$, starting with the eastern heterocycle. Because **3.15** and **3.20** had highly similar potencies at $hmGlu_1$ and $hmGlu_4$, we decided to begin our work with the unsubstituted phthalamide ring, and return to evaluate the western portion of the scaffold in a later library.

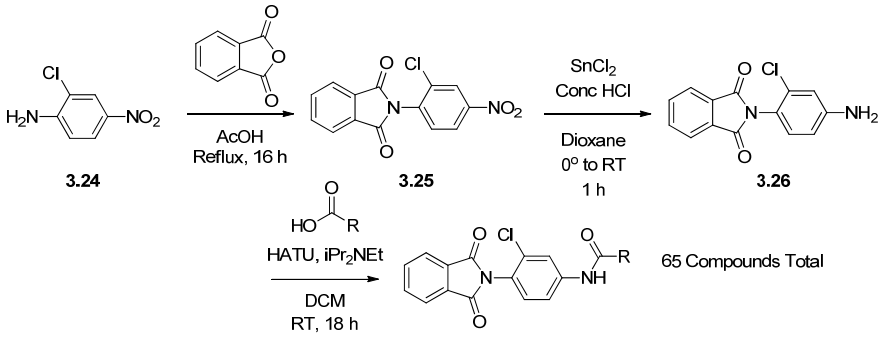

Scheme 3.5.1: Synthetic scheme toward the library of **3.15**-based $hmGlu_1$ PAMs.

Using the chemistry highlighted in Scheme 3.5.1, we synthesized a 65 member library of analogs based on the **3.15** scaffold. Beginning with nitro-analine **3.24**, phthalamide cyclization was affected by refluxing with phthalic anhydride in glacial acetic acid for 18 hours. The nitro group was subsequently reduced to the analine using tin(II) chloride in concentrated hydrochloric acid at 0^{o} C. With gram quantities of **3.26** in hand, the library was generated by employing HATU, diisopropylethylamine, and the corresponding heterocyclic carboxylic acid. A wide range of eastern heterocycles were employed, starting with substituted 2-pyridine containing compounds and diversifying toward 3- and 4-pyridines, pyrimidines, pyrazines, and fused systems in the form of a quinolone (**3.A** in Figure 3.5.4). We experimented with reduced ring size by employing variously substituted pyroles, pyrazoles and triazoles (**3.B** in Figure 3.5.4) and expanded nitrogen containing fused ring systems: indoles, indazoles, etc. (**3.C** in Figure 3.5.4). We also looked beyond nitrogen containing heterocycles by employing variously substituted imidazoles, furans, thiophenes, oxazoles, thiazoles, oxadiazoles, and bezofurans (**3.D** in Figure 3.5.4) and some saturated heterocycles including tetrahydrofurans and tetrahydropyrans.

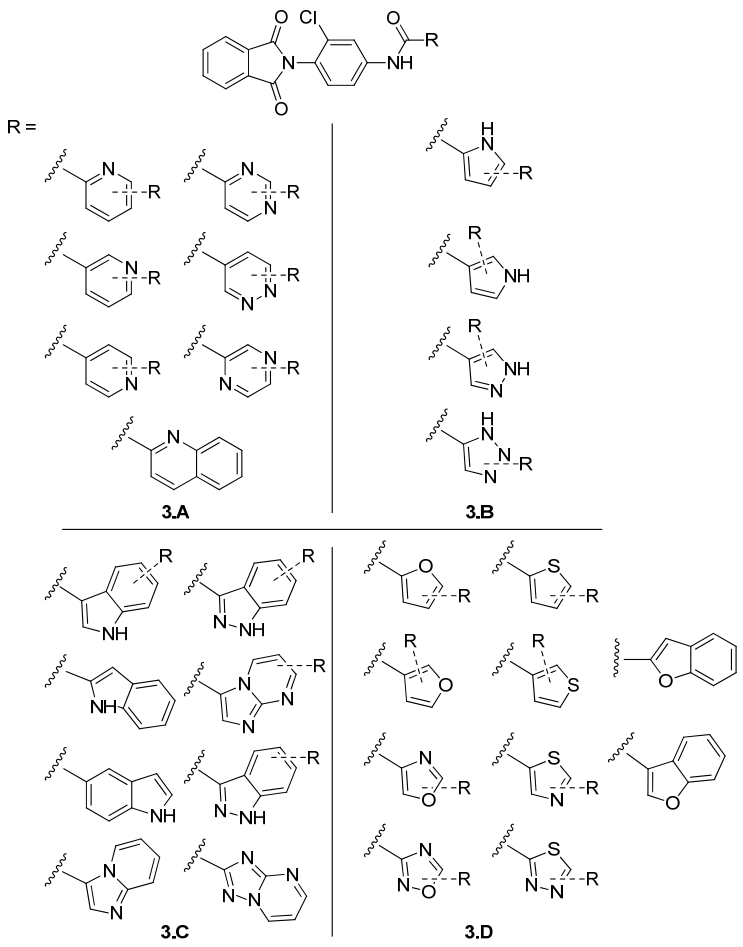

Figure 3.5.4: Eastern heterocycles employed in the 65 member library.

The library was evaluated in Ca^{2+} fluorescence assays at 10 μM singlepoint concentration in order to triage for active PAMs. Figure 3.5.5, Figure 3.5.6, and Figure 3.5.7 show the results of the three singlepoint screens. In each of the screens, an effective concentration (EC_{20}, EC_{22}, and EC_{10}, respectively) is noted on the far right. Any compound that caused the glutamate response to climb above 50% of the maximum was deemed active enough to warrant further investigation.

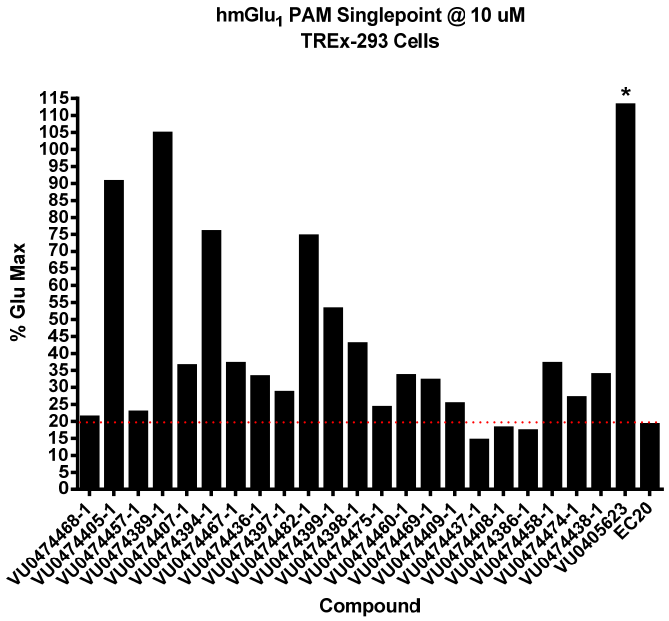

Figure 3.5.5: Singlepoint screen (1 of 3 for **3.15** analog library) at 10 μM compound concentration against $hmGlu_1$. The asterisk denotes VU0405623 (**3.15**), the positive control for this experiment.

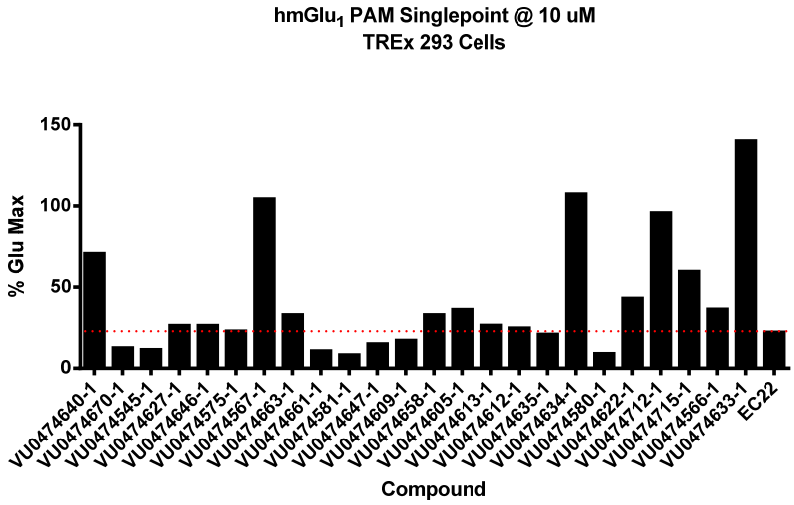

Figure 3.5.6: Singlepoint screen (2 of 3 for **3.15** analog library) at 10 μM compound concentration against $hmGlu_1$.

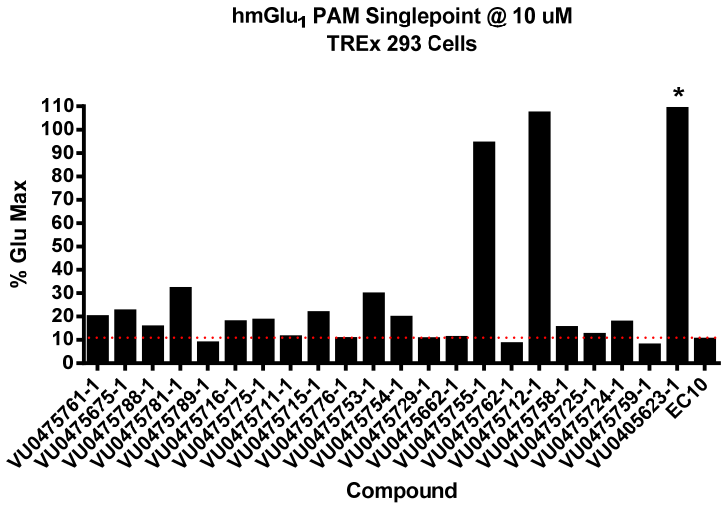

Figure 3.5.7: Singlepoint screen (3 of 3 for **3.15** analog library) at 10 μM compound concentration against $hmGlu_1$. The asterisk denotes VU0405623 (**3.15**), the positive control for this experiment.

As the singlepoint screening data show, a total of 10 compounds successfully potentiated an EC_{20} dose of glutamate above 50% maximum response. We deemed these PAMs active enough to warrant further investigation. In order to determine potencies, concentration response curves were generated in triplicate and experiments were subsequently repeated on three separate dates for each active compound (Figure 3.5.8, Figure 3.5.9).

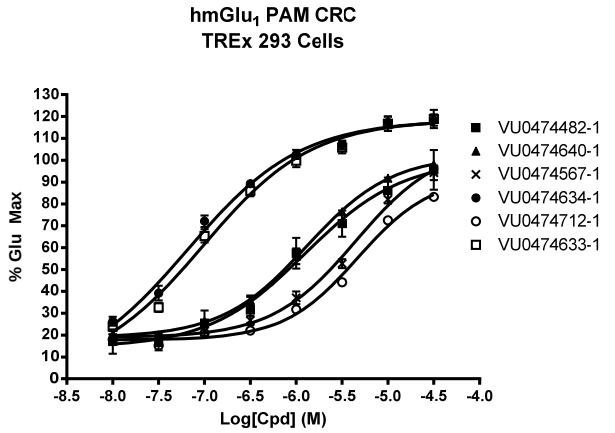

	VU0474482-1	VU0474640-1	VU0474567-1	VU0474634-1	VU0474712-1	VU0474633-1
Best-fit values						
Bottom	14.30	18.91	18.84	-0.3657	17.74	3.180
Top	100.1	102.2	107.3	118.5	92.75	118.6
LogEC50	-5.904	-5.887	-5.349	-7.184	-5.330	-7.014
HillSlope	0.8249	0.9380	0.9534	0.7067	1.080	0.7352
EC50	1.246e-006	1.296e-006	4.475e-006	6.553e-008	4.676e-006	9.688e-008

Figure 3.5.8: Concentration response curves for 6 of the 11 active PAMs. Curve fit data is shown, with EC_{50} values for each compound listed in the final row.

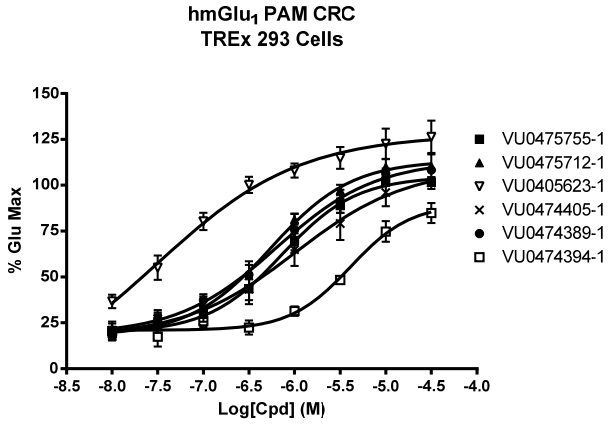

	VU0475755-1	VU0475712-1	VU0405623-1	VU0474405-1	VU0474389-1	VU0474394-1
Best-fit values						
Bottom	19.73	17.98	-12.88	17.40	18.57	20.94
Top	104.7	113.5	127.7	109.4	113.5	89.84
LogEC50	-6.138	-6.262	-7.503	-5.990	-6.196	-5.389
HillSlope	1.069	0.9791	0.5562	0.7139	0.7994	1.313
EC50	7.285e-007	5.473e-007	3.143e-008	1.023e-006	6.373e-007	4.083e-006

Figure 3.5.9: Concentration response curves for 5 of the 11 active PAMs, including VU0405623 (**3.15**) as positive control. Curve fit data is shown, with EC_{50} values for each compound listed in the final row.

At this point, the most active $hmGlu_1$ PAMs were counterscreened against $hmGlu_4$, in order to determine if a successful subtype selectivity switch was made. Table 3.5.1 shows the counterscreening results.

Table 3.5.1: Screening results for 10 active PAMs identified in the 65 member library.

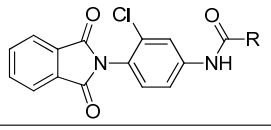

Cmpd	VU Number	R =	$hmGlu_1$ EC_{50}	$hmGlu_4$ EC_{50}
3.19	VU0474405	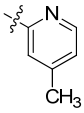	1.02 uM	Inactive
3.20	VU0474389	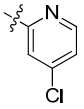	637 nM	Inactive
3.21	VU0474394	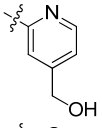	4.08 uM	10 uM
3.22	VU0474634		65 nM	236 nM
3.23	VU0475755		592 nM	370 nM
3.24	VU0474640		1.29 uM	Inactive
3.25	VU0474712	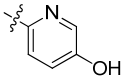	4.67 uM	Inactive
3.26	VU0474567		4.47 uM	120 nM
3.27	VU0474482	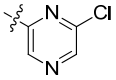	1.24 uM	Inactive
3.28	VU0475712	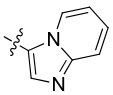	526 nM	4.4 uM

Collectively, these screening results informed us of several key elements of SAR around **3.15**: 1) the 2-position of the eastern heterocycle must be substituted with a strongly

electronegative atom. All attempts at moving the nitrogen to the 3- and 4-positions resulted in a loss of activity. Nitrogen was not the only option; oxygen was tolerated at the 2-position, as **3.22** showed excellent potency at $hmGlu_1$. Additional substituted furans will be employed in further libraries. 2) The steric requirements of the system are somewhat more flexible as compared to the electronic requirements. While more active PAMs were identified with six membered rings than five membered rings, the furan **3.22** proved to be the most potent compound at $hmGlu_1$. 3) As has been observed with other allosteric modulators[71], selectivity for one receptor subtype over another can be engendered by the addition of a single atom. While **3.15** is highly potent at both $hmGlu_1$ and $hmGlu_4$, **3.19**, which differs by the presence of a single methyl group and **3.20**, which differs by a single chlorine atom, are both selective for $hmGlu_1$ with no appreciable activity at $hmGlu_4$. Future libraries will explore the careful substitution of 2-pyridine and 2-furan systems.

3.6 Schizophrenia Mutant Cell Line Studies

While the singlepoint and CRC screening work was being conducted, Hyekyung Plumley in the Conn laboratory generated a collection of stable cell lines expressing the schizophrenia mutants identified in the previously discussed genetic studies. These mutant cell lines were generated in the same tetracycline-inducible TREx293 cell background as wild type (WT) $hmGlu_1$.

When these mutant cell lines were analyzed in fold-shift Ca^{2+} response assays, they showed significantly decreased signaling compared to wild type $hmGlu_1$. These findings are in good agreement with those of Ayoub and coworkers. When both wild type and mutant cells were treated with **3.5** (VU0467832 in the below foldshift results) followed by increasing concentrations of glutamate, they showed a strong leftward curve shift, but no increase in

maximum glutamate response (Figure 3.6.1). This leftward foldshift represents a partial restoration of $mGlu_1$ mediated Ca^{2+} signaling.

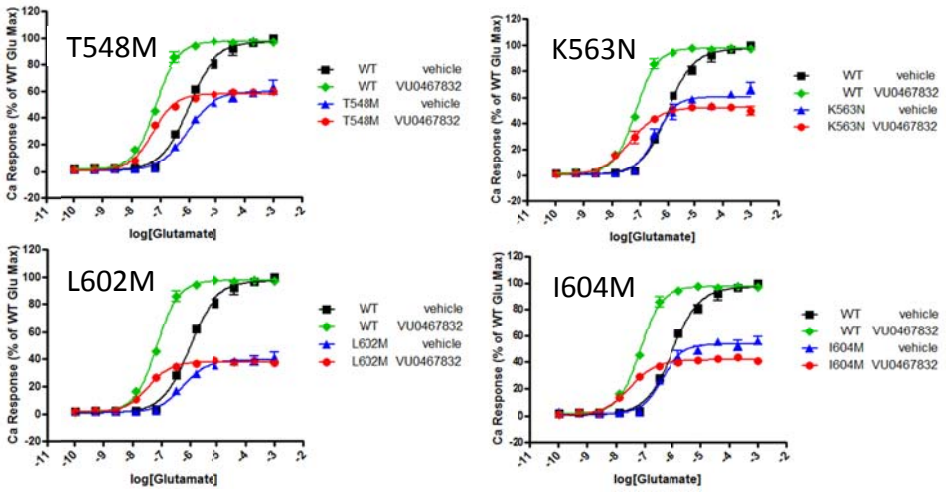

Figure 3.6.1: Foldshift assay of wild type cells treated with vehicle plus glutamate (black line), **3.5** (VU0467832) plus glutamate (green line). Additionally, four representative mutant cell lines are shown. Mutant cells were treated with vehicle plus glutamate (blue line), **3.5** (VU0467832) plus glutamate (red line).

When wild type and certain mutant cells were treated with the parent compound **3.15** followed by increasing concentrations of glutamate, they showed a strong leftward curve shift and an appreciable increase in maximum glutamate response (Figure 3.6.2). This increase in efficacy was not found in every mutant cell line; some mutants showed left shifted curves in the presence of the PAM without resulting in an increased maximum glutamate response. This increase in response represents a partial restoration of $mGlu_1$ mediated Ca^{2+} signaling. While these data are encouraging, more screening with the newly discovered PAMs is needed to further understand this effect.

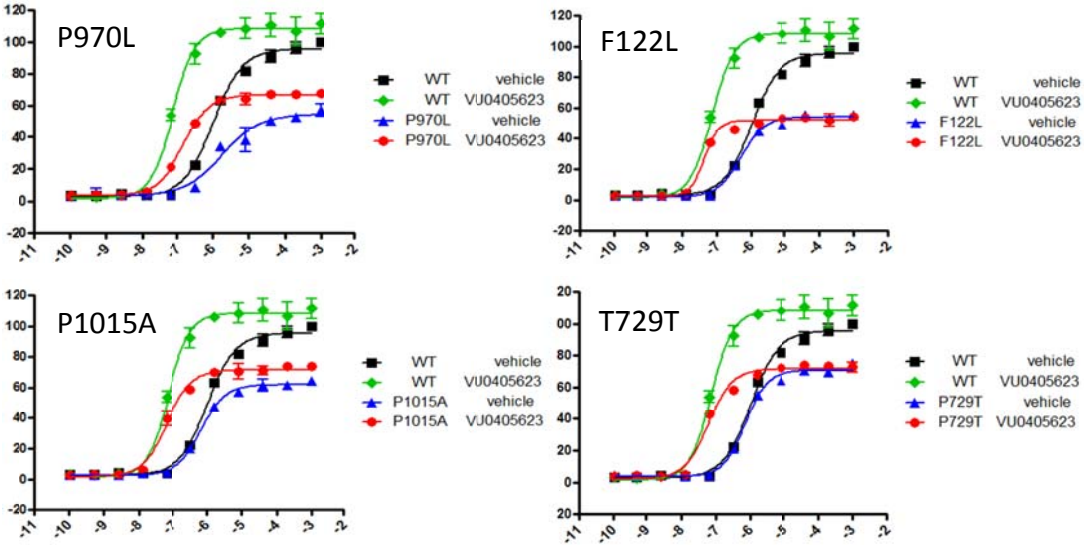

Figure 3.6.2: Foldshift assay of wild type cells treated with vehicle plus glutamate (black line), **3.15** plus glutamate (green line). Additionally, four representative mutant cell lines are shown. Mutant cells were treated with vehicle plus glutamate (blue line), **3.15** plus glutamate (red line).

3.7 Drug Metabolism/Pharmacokinetics Studies

As **3.15** represents the structural core of the library, we evaluated it in the VCNDD Tier 1 drug metabolism/pharmacokinetics studies. Compound **3.5** was studied alongside **3.15** as a standard for comparison. These studies include human and rat hepatic and intrinsic clearance calculations, plasma/protein binding, and cytochrome P450 inhibition analysis.

Clearance is defined as 'the volume of blood cleared of drug per unit time' and thus, the defined units are volume per time with a species mass correction[72]. The hepatic clearance experiment measures the concentration of parent test compound in hepatic microsomal incubation to determine the compound half-life ($t_{1/2}$). The $t_{1/2}$ is first used to calculate intrinsic clearance (Cl_{Int}), which represents the ability of the liver to remove (metabolize) drug in the absence of restrictions imposed on drug delivery to the liver cell by blood flow and protein binding. CL_{Int} can be described as what hepatic clearance would be if blood flow were unlimited and all drug was unbound to protein. As a result, CL_{Int} can feature values many times higher than human

hepatic blood flow[72]. Alternately, the CL_{Hep} value is calculated to predict the rate of *in vivo* clearance by the liver, taking into account hepatic blood flow rates and the efficiency of removal of presented drug. As a result, CL_{Hep} values can never be greater than the rate of host hepatic blood flow. In this instance, CL_{Int} values are used to calculate CL_{Hep} values.

This metabolism experiment was carried out by incubating test compound at 1 μM concentration in either human or rat liver microsomes containing cytochrome P450 (CYP) drug metabolizing enzymes and NADPH, a co-factor required for CYP activity. As the compound was metabolized, its concentration decreases. Concentrations of intact parent were measured over a 45 minute time period by running the assay in parallel and quenching a certain number of wells on the plate (triplicate per timepoint) and analyzing by LCMSMS. When the data is plotted using concentration of parent on Y-axis and time on X-axis, a line with negative slope is generated that provides a rate of metabolism, which is expressed as the half-life ($t_{1/2}$) of the test compound. This calculated $t_{1/2}$ is then inserted into the equations below (Figure 3.7.2, Figure 3.7.1) in order to determine CL_{Int} and CL_{Hep}.

$$CL'_{Int}\ mL/min/kg = 0.693 \times \frac{1}{t_{½\,(min)}} \times \frac{1\ mL}{0.5\ mg\ of\ protein_{mic}} \times \frac{45\ mg\ protein_{mic}}{1\ g\ Liver\ weight} \times \frac{(A) g\ of\ Liver\ weight}{kg\ of\ body\ weight}$$

Where (A) is:
Scale up factors (g liver / kg body weight) among different animal species commonly used:

Human	20*
Beagle Dog	25*
Cynomolgus Monkey	30*
Rat	45*
Mouse	87.5

*Scaling factors were derived from Ref [73].

Figure 3.7.1: Equation used to calculate intrinsic clearance (CL_{int}) based on parent compound half-life ($t_{1/2}$).

$$CL_{HEP}\ mL/min/kg = \frac{Q_H \times CL_{int}}{Q_H + CL_{int}}$$

Where (Q_H) is:
Hepatic blood flow for different animal species commonly used:

Human	21
Beagle Dog	31
Cynomolgus Monkey	44
Rat	70
Mouse	90

Figure 3.7.2: Equation used to calculate hepatic clearance (CL_{Hep}) based on intrinsic clearance CL_{Int}.

Table 3.7.1: VCNDD Tier 1 DMPK study with **3.15** and **3.5**. A * denotes that compounds were unstable in species plasma.

Compound		**3.15**	**3.5**
VU Number		VU0405623	VU0467832
Structure		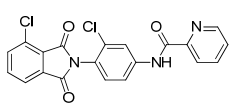	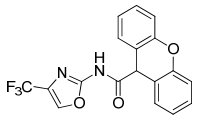
Human CL_{int} (mL/min/kg)		210	262
Human CL_{hep} (mL/min/kg)		19.1	19.4
Rat CL_{int} (mL/min/kg)		166	661
Rat CL_{hep} (mL/min/kg)		49.3	63.3
Human PPB (Fu,p)		*	0.003
Rat PPB (Fu,p)		*	0.014
P450 Inhibition IC_{50} (μM)	**1A2**	>30	13.0
	2C9	4.5	0.6
	2D6	>30	>30
	3A4	>30	>30
	2C19	-	-

Table 3.7.1Both **3.5** and **3.15** featured hepatic clearance rates just under the human hepatic blood flow rate of 20 mL/min/kg (Table 3.7.1). Theoretically, this value indicates that both compounds would be cleared from the body by the liver at a similar rate and would feature relatively short half-lives. The intrinsic clearance rate of **3.15** was slightly lower at 210 mL/min/kg compared to that of **3.5** at 262 mL/min/kg. This indicates that **3.15** is metabolized slightly slower than **3.5** in an unrestricted system. The same experiment carried out in rat liver microsomes revealed that **3.15** was metabolized significantly slower than **3.5**, with CL_{Hep} values of 49.3 and 63.3 mL/min/kg, respectively, compared to rat hepatic blood flow rate of 70 mL/min/kg. Additionally, **3.15** featured a CL_{Int} value of 166 mL/min/kg, compared to the 661 mL/min/kg of **3.5**. Collectively, these clearance data show that the lead compound **3.15** is marginally better from a pharmacokinetics standpoint than the most potent and selective currently $mGlu_1$ PAM. Further clearance studies with a more optimized PAM will build on these initial findings.

Table 3.7.1 also shows that **3.15** is unstable in both rat and human plasma. The most likely sites of metabolism include the western phthalamide and the eastern amide, which could both be hydrolyzed by esterase enzymes in plasma. Similar instability has been found in the Daniels laboratory recently with succinimides, which are close structural relatives to phthalamides. Metabolite identification experiments are currently underway to determine the metabolic liability on this compound. Additional SAR work around the western portion of the molecule is planned to address this concern. As a comparison, 0.3% of compound **3.5** exists unbound in human plasma and 1.4% exists unbound in rat plasma.

The final set of drug metabolism experiments involved cytochrome P450 enzyme inhibition analysis. Of the 4 CYP enzyme subtypes studied, **3.5** and **3.15** were almost entirely inactive at all but one subtype. While **3.5** features an IC_{50} value of 600 nM at CYP 2C9, **3.15** has a greater than 2-fold higher IC_{50} value of 4.5 μM at the same enzyme. These data show that CYP

inhibition would likely not be a major source of concern if the **3.15** scaffold were carried forward into animal models.

Overall, these experiments showed that, while there is an initial question of compound stability, **3.15**, is a strong lead for further optimization toward the development of a potent and selective $mGlu_1$ PAM. In the short term, because the goal of this project is to develop a new tool compound to study mutant receptor cell lines *in vitro*, the high clearance values in human and rat are not immediately detrimental to the chemical series. A similar comment can be made about the CYP inhibition. The plasma/protein binding instability does raise some concerns, though the structural liabilities will be addressed in future libraries of analogs. The CYP inhibition data is highly encouraging and offers an early indication that ancillary pharmacology may not be a major concern in the future for this scaffold, though additional experiments similar to the panel screens run in Chapters I and II will reveal more along these lines. Finally, these drug metabolism/pharmacokinetics studies represent an initial glance into the profile of the **3.15** scaffold. A strong DMPK profile was achieved in this series in $hmGlu_4$ and it remains a goal for the future work at $hmGlu_1$.

3.8 Conclusion

Pedro Garcia, a first year graduate student who recently joined the Lindsley laboratory, has carried this work forward in recent weeks. He has confirmed all of the human $mGlu_1$ screening data by repeating the experiments in the rat $mGlu_1$ cell line and has synthesized an additional focused library of analogs around **3.15** and **3.24**, the most selective $hmGlu_1$ PAM**.** The rat screening data has shown that the active PAMs at the human receptor show similar potencies at the rat isoform. Garcia's most recent library built on the SAR that we determined from the previous 65 member library. The eastern 2-pyridine was methodically probed with halogen and methyl substituents around the 3, 4, and 5 positions of the ring. From this work, a highly potent

PAM (more potent that **3.5** at rmGlu$_1$) has been identified. This new compound is now the most advanced mGlu$_1$ PAM lead. Figure 3.8.1 shows some of the planned libraries that will be generated around the **3.15** scaffold.

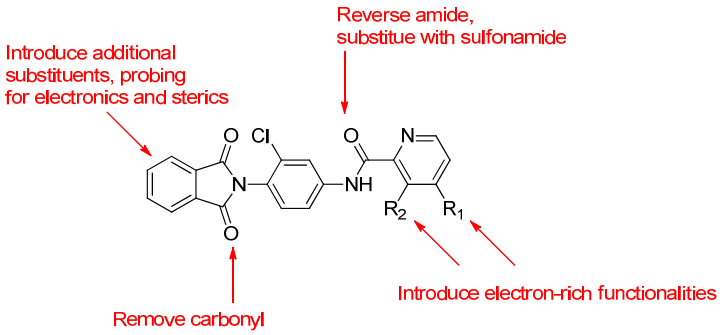

Figure 3.8.1: Potential sites of SAR development around the **3.15** scaffold to be investigated in the future.

Additional experiments have been planned moving forward: concentration response curves for the various mutant cell lines will be generated using the most advance PAM lead compound alongside **3.5** and **3.15** as positive controls. The differences in Ca^{2+} signaling in the mutant and wild type cells could be attributed to receptor reserve issues. In this matter, we will take advantage of the tetracycline-inducible system of our cell lines. The receptor expression level will be controlled by treating cells with varying doses of tetracycline and the Ca^{2+} signaling response will be measured. In addition, saturation binding experiments will be conducted directly to measure the receptor expression level. These experiments will be done in collaboration with the Conn laboratory and the VCNDD.

This work represents the first series of investigations by our laboratory into a centrally penetrant, potent, and selective positive allosteric modulator of human mGlu$_1$. While the VU-71/48 (**3.6**/**3.7**) series ultimately proved unproductive, the **3.15** series has already shown great promise and will continue to be the focus of the project moving forward.

EXPERIMENTAL METHODS

Synthesis:

All reagents were purchased from Sigma-Aldrich Corp., Matrix Scientific, Fisher Scientific, and Ark Pharm Inc., and were used without purification. Analytical thin-layer chromatography (TLC) was performed on 250 μm silica gel plates from Sorbent Technologies. Visualization was accomplished via UV light, and/or the use of ninhydrin, I_2, 2,4-dinitrophenylhydrazine, and potassium permanganate solutions followed by application of heat. Chromatography was performed using Silica Gel 60 (230-400 mesh) from Sorbent Technologies or Silica RediSep Rf flash columns on a CombiFlash Rf automated flash chromatography system. Low resolution mass spectra (LCMS) were obtained on an Agilent 1200 LCMS with electrospray ionization. High resolution mass spectra (HRMS) were recorded on a Waters Qtof-API-US plus Acquity system with ES as the ion source. Analytical high pressure liquid chromatography (HPLC) was performed on an Agilent 1200 analytical LCMS with UV detection at 214 nm and 254 nm along with ELSD detection.

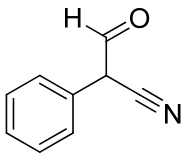

3-oxo-2-phenylpropanenitrile 3.8.

A 500 mL 3 neck schlenk flask was fitted with a stirbar and condenser. The flask was flame dried and vacuum purged with argon 3X. The flask was then charged with 3.82 g (0.166 mmol) sodium and then repurged with argon 3X. EtOH (150 mL) was added and the flask is stirred until the sodium was consumed. Phenyl acetonitrile (15 g, 0.128 mmol) was added and the flask was stirred 5 minutes, followed by ethyl formate (15.44 mL, 0.921 mmol). The reaction was brought

to reflux for 2 hours. Product formation was confirmed by LCMS. The reaction mixture was then cooled and concentrated under reduced pressure. The resulting organics were then partitioned between EtOAc (50 mL) and H_2O (50 mL). The organic phase was then dried over $MgSO_4$, filtered, and concentrated. The product was purified on silica (1:1 EtOAc:Hex), yielding 11.6 g (62%) **3.8**. Product mass confirmed by LCMS.

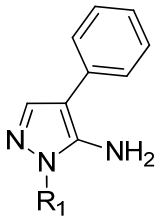

General procedure for synthesis of 4-substituted amino-pyrazoles (3.10).

A large size microwave vial was charged with a stirbar and **3.8** (500 mg, 3.44 mmol) and a corresponding hydrazine (3.44 mmol). EtOH was added (10 mL) and the vial was sealed. The vial was heated in the microwave reactor at 160°C for 30 min. Product formation was judged by LCMS. The resulting aminopyrazole was then passed through a silica plug, washing with EtOAc, and carried forward crude.

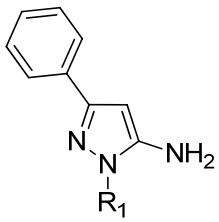

General procedure for synthesis of 3-substituted amino-pyrazoles (3.13).

A large size microwave vial was charged with a stirbar and **3.12** (500 mg, 3.44 mmol) and a corresponding hydrazine (3.44 mmol). EtOH was added (10 mL) and the vial was sealed. The vial was heated in the microwave reactor at 160°C for 30 min. Product formation was judged by

LCMS. The resulting aminopyrazole was then passed through a silica plug, washing with EtOAc, and carried forward without further purification.

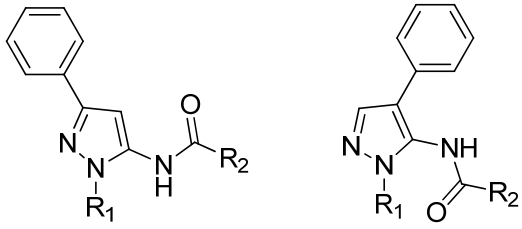

General procedure for synthesis of 75 member library around 3.6/3.7 scaffolds.

A microwave vial was charged with a stirbar, either **3.10** or **3.13** (0.185 mmol), PyClU (0.20 mmol), the corresponding heterocyclic carboxylic acid (0.20 mmol) and 3 mL of a premixed 9:1 solution of CH_3CN: *i*Pr_2NEt. The vial was then sealed and heated in the microwave reactor at 160^o C for 30 minutes. After heating, each sample was analyzed by LCMS to determine product formation. DCM (2 mL) and H_2O (2 mL) were then added to each tube. The tubes were resealed, shaken vigorously, and then the contents were passed through a phase separator (Isolute). The organic phase was then concentrated on drying blocks, before being redissolved in DMSO (1 mL). Products were then purified using reverse phase high performance liquid chromatography, affording sixty five compounds (10-80% total yield) as TFA salts when applicable with >98% purity.

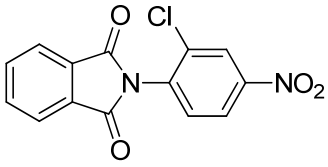

2-(2-chloro-4-nitrophenyl)isoindoline-1,3-dione (3.25).

A 100 mL round bottom flask was charged with a stir bar, 10 g (57.94 mmol) 2-chloro-4-nitroaniline (**3.24**), 12.8 g phthalic anhydride, and 25 mL glacial acetic acid. A reflux condenser

was added and the flask was heated to reflux for 18 hours. The reaction was monitored by TLC. Upon completion, the flask was removed from heat and allowed to cool to room temp. H_2O was added (50 mL) and the flask was stirred for approximately 30 min. After stirring in H_2O, a solid precipitated out of solution. The flask contents were then poured over a Buchner funnel fitted with filter paper. The bright yellow solid precipitate was then washed with 2 L H_2O, yielding the product **3.25** as an off white solid. The product was then subjected to high vacuum for 12 hours until dry. Obtained 12.56 g (71%) **3.25** as an off white solid, product confirmed by LCMS.

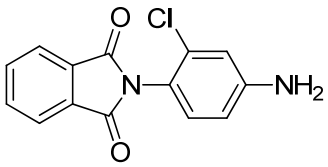

2-(4-amino-2-chlorophenyl)isoindoline-1,3-dione (3.26).

A 250 mL round bottom flask was charged with a stirbar, 2.43 g (8.02 mmol) of **3.25,** and 40 mL dioxane, before being cooled to 0^o C. A separate flask was charged with 7.6 g (40.1 mmol) $SnCl_2$ and 13.4 mL conc. HCl.. The $SnCl_2$ was stirred until completely dissolved and then added dropwise to the cooled flask containing starting material. The reaction was stirred 20-30 minutes, monitoring by TLC for consumption of starting material. Upon completion, the reaction was quenched by raising the pH of the acidic solution with 1 N NaOH to roughly pH 6 (~120-150 mL 1N NaOH). Once the pH was sufficiently elevated, a precipitate formed. The precipitate was filtered off using a fine grain glass fritted funnel, washing with dichloromethane. The resulting organic solution was then concentrated and purified on silica (1:1 EtOAc:Hex), yielding 1.96 g (89%) **3.26** as a light yellow solid, confirmed by LCMS.

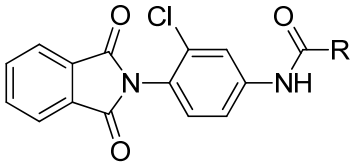

General procedure for hmGlu$_1$ library around 3.15 scaffold.

Each of 65 test tubes (13x100 mm) was fitted with a stir bar, and 20 mg (0.073 mmol) **3.26**. The corresponding heterocyclic carboxylic acid was added (roughly 15-20 mg as the excess reagent) and 40 mg (0.11 mmol) HATU. Approximately 2 mL of a premixed 9:1 DCM:*i*Pr$_2$Net solution was then added. Each test tube was sealed with a plastic stopper and stirred at room temperature for 12 hours. After stirring, each sample was analyzed by LCMS to determine product formation. DCM (1 mL) and H_2O (2 mL) were then added to each tube. The tubes were resealed, shaken vigorously, and then the contents were passed through a phase separator (Isolute). The organic phase was then concentrated on drying blocks, before being re-dissolved in DMSO (1 mL). Products were then purified using reverse phase high performance liquid chromatography, affording sixty five compounds (15-85% total yield) as TFA salts when applicable with >98% purity.

Mutagenensis:

Human mGlu$_1$ WT cDNA was cloned into tetracycline-inducible expression vector, hmGlu$_1$-pcDNA5/TO. All schizophrenic mutant plasmids were generated by site-directed mutagenesis in hmGlu$_1$-pcDNA5/TO using QuickChange II mutagenensis kit (Agilent). All point mutations were confirmed by sequencing. In order to generate stable cell lines, each expression plasmid was transfected into TREx293 cells stably expressing Tet Repressor. Cells were then subject to hygromycin selection for 2 weeks. The resulting hygromycin-resistant cells were examined in Ca^{2+} assay to ensure the function of mGlu$_1$ protein, Gq-coupled Ca^{2+} response.

Ca^{2+} Fluorescence Assays:

For all FDSS screens/assays, cells (10,000 cells/20 μl/well) were plated in blackwalled, clear-bottomed, poly-D-lysine treated, 384 well plates (Greiner Bio-One, Monroe, North Carolina) in Ham's F12 medium supplemented with 10% FBS and 20 mM HEPES. The cells were grown overnight at 37° C in the presence of 5% CO2. The next day, the medium was removed and replaced with 20 μl of 2 μM Fluo-4AM in calcium assay buffer (Hank's Balanced Salt Solution supplemented with 20 mM HEPES and 2.5 mM Probenecid) and the cell plates incubated for 60 minutes at 37 °C. Dye solution was removed and replaced with 20 μl of fresh assay buffer. Test compounds were transferred from a 384-well source plate (10 mM DMSO, 30 μl/well) to 384-well daughter plates using an ECHO acoustic plate reformatter (Labcyte) and then diluted into assay buffer to 20 μM stock concentration (2X). Glutamate (Aldrich) was diluted in a 384-well plate containing submaximal (~EC20, determined empirically) and maximal (10 μM) stock concentrations (5X). Mobilization of intracellular calcium was measured using the Functional Drug Screening System 6000 (FDSS6000, Hamamatsu). Baseline readings were taken and then test compounds (30 μM final, 20 μl/well) were added using the FDSS's integrated pipettor. After 150 seconds of equilibration, glutamate (EC20 and maximal concentrations, 10 μl/well) was added using the FDSS's integrated pipettor. Data were obtained as max-min fluorescent ratios and then normalized to percentage of maximum Glu response and represent mean values obtained from three independent determinations (error bars represent +/- SEM) unless otherwise specified.

For Flexstation screens/assays methods used were in a format similar to those described above using the same reagents. TREx293 cells stably expressing Tet Repressor and $hmGlu_1$ were plated in 100 mL of growth medium $8x10^4$ cells per well in poly-D-lysine coated Costar 96-well black-walled, clear-bottom plates (Fisher). Cells were incubated overnight at 37 °C under 5% CO2.

The next day, medium was removed from the cells, and they were incubated with 50 mL of 2 mM Fluo-4 AM diluted in assay buffer for 1 h at 37 °C. Dye was then removed and replaced with 45 mL of fresh assay buffer. Test compounds were diluted in assay buffer at 2X concentration and glutamate was diluted in assay at a 10X concentration. FLEXstation II (Molecular Devices) automated plate reader was used for assay execution and measurement of calcium flux. After establishing baseline fluorescence, test compounds (45 mL) were added to the cells using the FLEXstation II's integrated pipettor and allowed to equilibrate for 150 seconds before addition of glutamate (10 mL). Data were obtained as max-min fluorescent ratios and then normalized to percentage of maximum Glu response. For test compounds exhibiting intrinsic fluorescence (typically found only at 30 μM final), adjustment of analysis time window for max-min values was sometimes performed in order to obtain more accurate baseline readings. Calculation of potentiation EC_{50} was performed using the curve-fitting software GraphPad Prism (version 4.0c). Data shown represent mean values obtained from at least three independent determinations performed in triplicate or greater (error bars represent +/- SEM) unless otherwise specified.

Drug Metabolism/Pharmacokinetics:

Microsomal Stability:

The metabolic stability of each compound was investigated in human and rat hepatic microsomes (BD Biosciences, San Jose, CA) by using substrate depletion methodology (percentage of parent compound remaining). In separate 96-well plates for each time point, a mixture of 0.1 M potassium phosphate-buffered, pH 7.4, 1 μM test compound, 0.5 mg/ml microsomes, and 1 mM NADPH (t = 3, 7, 15, 25, or 45 min) or buffer (t = 0) were continually incubated at 37°C under ambient oxygenation. At the respective time, each plate's reaction was precipitated by the addition of 2 volumes of ice-cold acetonitrile containing glyburide as an internal standard (50 ng/ml). The plates were centrifuged at 3000 rpm (4°C) for 10 min. The resulting supernatants

were transferred and diluted 1:1 (supernatant/water) into new 96-well plates in preparation for LC/MS/MS analysis. Each compound was assayed in triplicate within the same 96-well plate. The in vitro half-life ($t_{1/2}$, min), intrinsic clearance (CL_{int}, ml/min/kg), and subsequent predicted hepatic clearance (CL_{HEP}, ml/min/kg) was determined by using the following equations t ½ = Ln(2)/k where k represents the slope from linear regression analysis (percentage of test compound remaining) and equations listed in Figure 3.7.1 and Figure 3.7.2.

Plasma Protein Binding:

The protein binding of each compound was determined in human and rat plasma via equilibrium dialysis of mGlu4 PAM using Single-Use RED Plates with inserts (Thermo Fisher Scientific, Waltham, MA). Plasma (220 µl) was added to the 96-well plate containing test compound (5 µl) and mixed thoroughly. Subsequently, 200 µl of the plasma-compound mixture was transferred to the cis chamber (red) of the RED plate, with an accompanying 350 µl of phosphate buffer (25 mM, pH 7.4) in the trans chamber. The RED plate was sealed and incubated for 4 hours at 37° C with shaking. At completion, 50-µl aliquots from each chamber were diluted 1:1 (50 µl) with either plasma (cis) or buffer (trans) and transferred to a new 96-well plate, at which time ice-cold acetonitrile (2 volumes) was added to extract the matrices. The plate was centrifuged (3000 rpm, 10 min) and supernatants were transferred and diluted 1:1 (supernatant/water) into a new 96-well plate, which was then sealed in preparation for LC/MS/MS analysis. Each compound was assayed in triplicate within the same 96-well plate.

CYP450 Inhibition:

A four-in-one, 96-well plate assay for determining IC50 values against human CYP450 1A2, 2C9, 2D6, and 3A4 was developed based on previous reports (Youdim et al., 2008). Human liver microsomes (final concentration of 0.1 mg/ml) and a substrate mixture containing the CYP450 probe substrates phenacetin (10 µM), diclofenac (5 µM), dextromethorphan (5 µM), and

midazolam (2 μM) were added to a potassium phosphate-buffered solution (0.1 M, pH 7.4) and warmed to 37°C. The reaction mixture was divided evenly into the 96-well plate, and various dilutions of each inhibitor/compound of interest (in duplicate) were then added to this reaction mixture such that the final concentration of each compound ranged from 100 nM to 30 μM. This mixture was allowed to preincubate for 15 min while shaken at 37°C. Buffer or NADPH (1 mM) was added, and the reaction mixture was incubated for an additional 8 min at 37°C before quenching with 2 volumes of ice-cold acetonitrile containing 50 ng/ml of carbamazepine as internal standard. The plates were centrifuged at 4000 rpm (4°C) for 10 min, and the supernatant was removed and diluted with water (1:4, v/v) in preparation for LC/MS/MS analysis. The IC50 values for each compound were obtained for the individual CYP450 enzymes by quantitating the inhibition of metabolite formation for each probe: acetaminophen (1A2), 4-hydroxydiclofenac (2C9), dextrorphan tartrate (2D6), and 1-hydroxymidazolam (3A4). Miconazole was included as a positive control broad-spectrum CYP450 inhibitor. For discrete 2C19 inhibition experiments, a similar assay design was used with the following exceptions: the probe substrate was S-mephenytoin (40 μM), the NADPH incubation with the reaction mixture went for 30 min, the supernatant was reconstituted 1:1 with water for analysis, and the metabolite used for quantitation was 4-hydroxymephenytoin.

APPENDIX A1

Spectra Relevant to Chapter I

600 MHz, d_6-DMSO

1.10

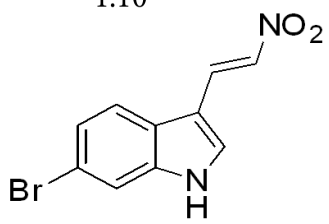

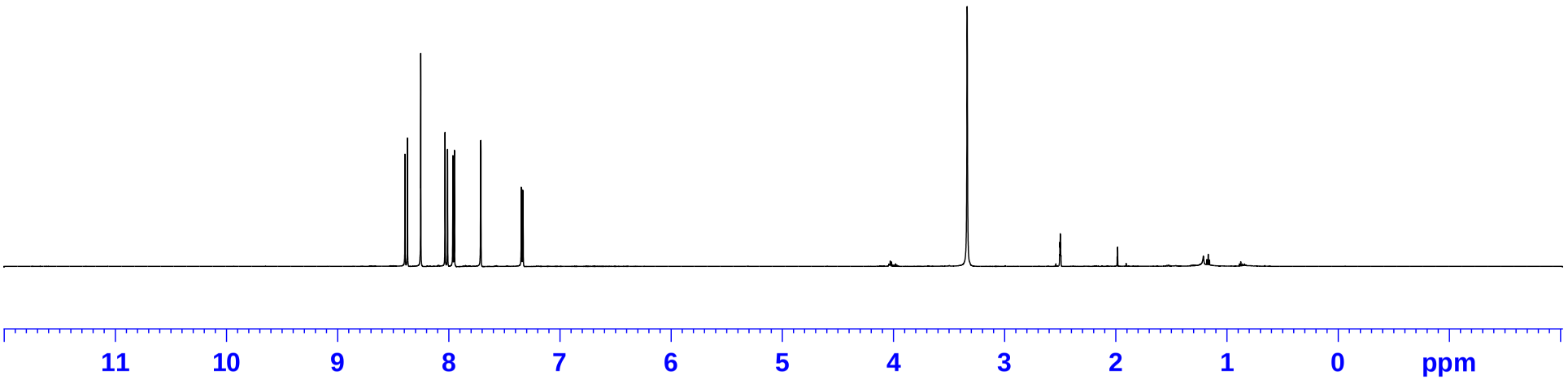

150 MHz, d_6-DMSO

1.10

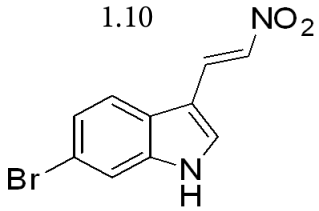

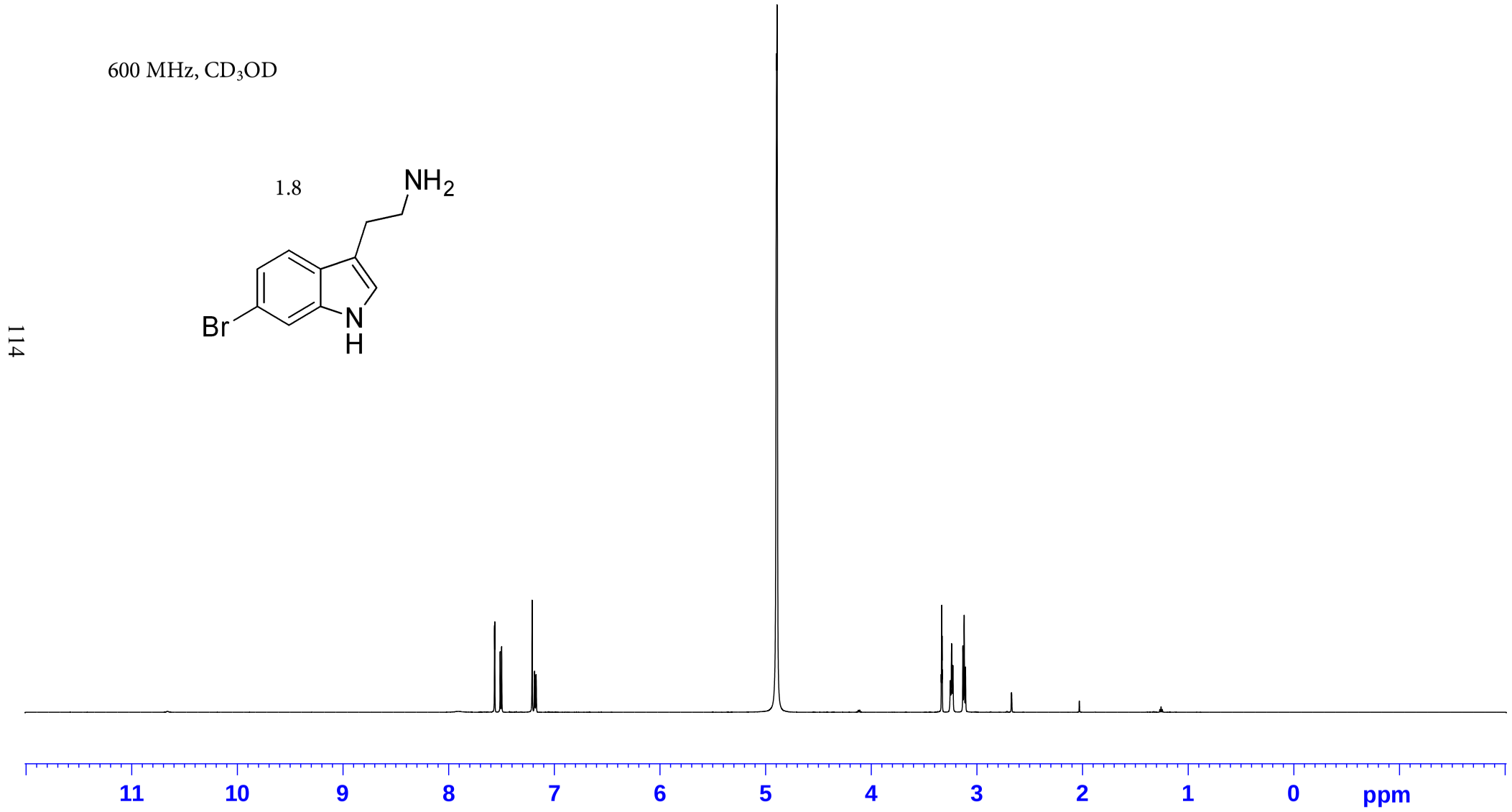
600 MHz, CD3OD
1.8
NH2
Br
N
H
114
11
10
9
8
7
6
5
4
3
2
1
0
ppm

150 MHz, CD_3OD

1.8

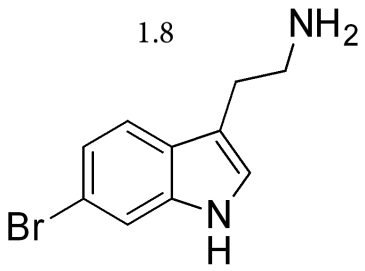

115

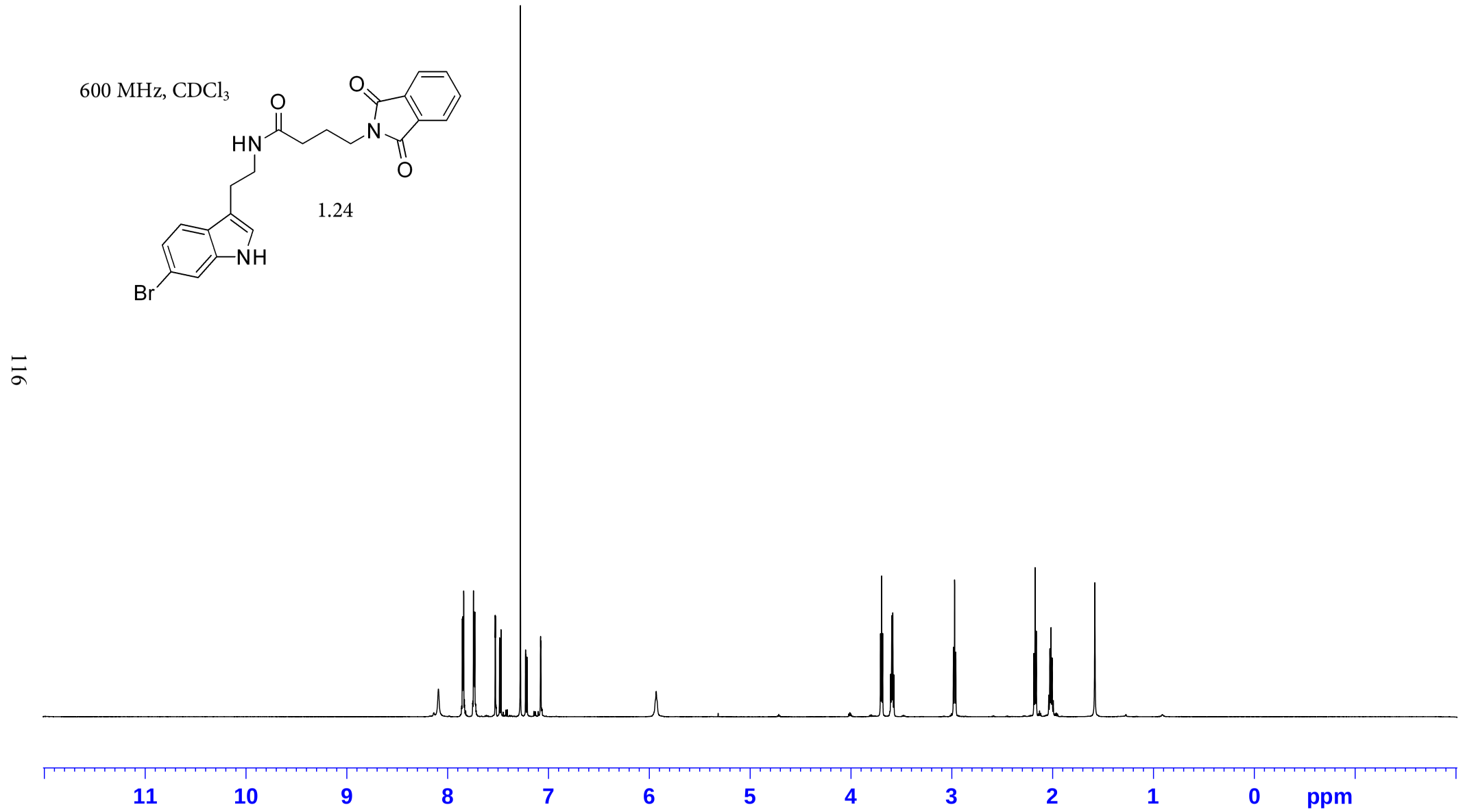
600 MHz, CDCl3
O
HN
O
N
O
1.24
NH
Br
11
10
9
8
7
6
5
4
3
2
1
0
ppm

150 MHz, $CDCl_3$

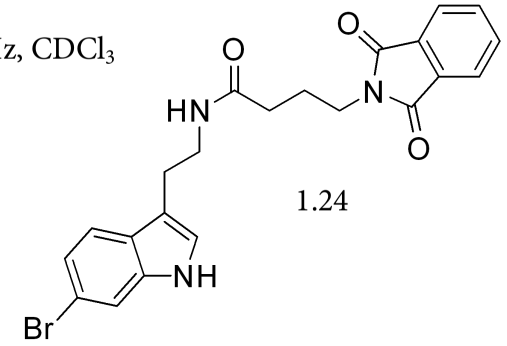

1.24

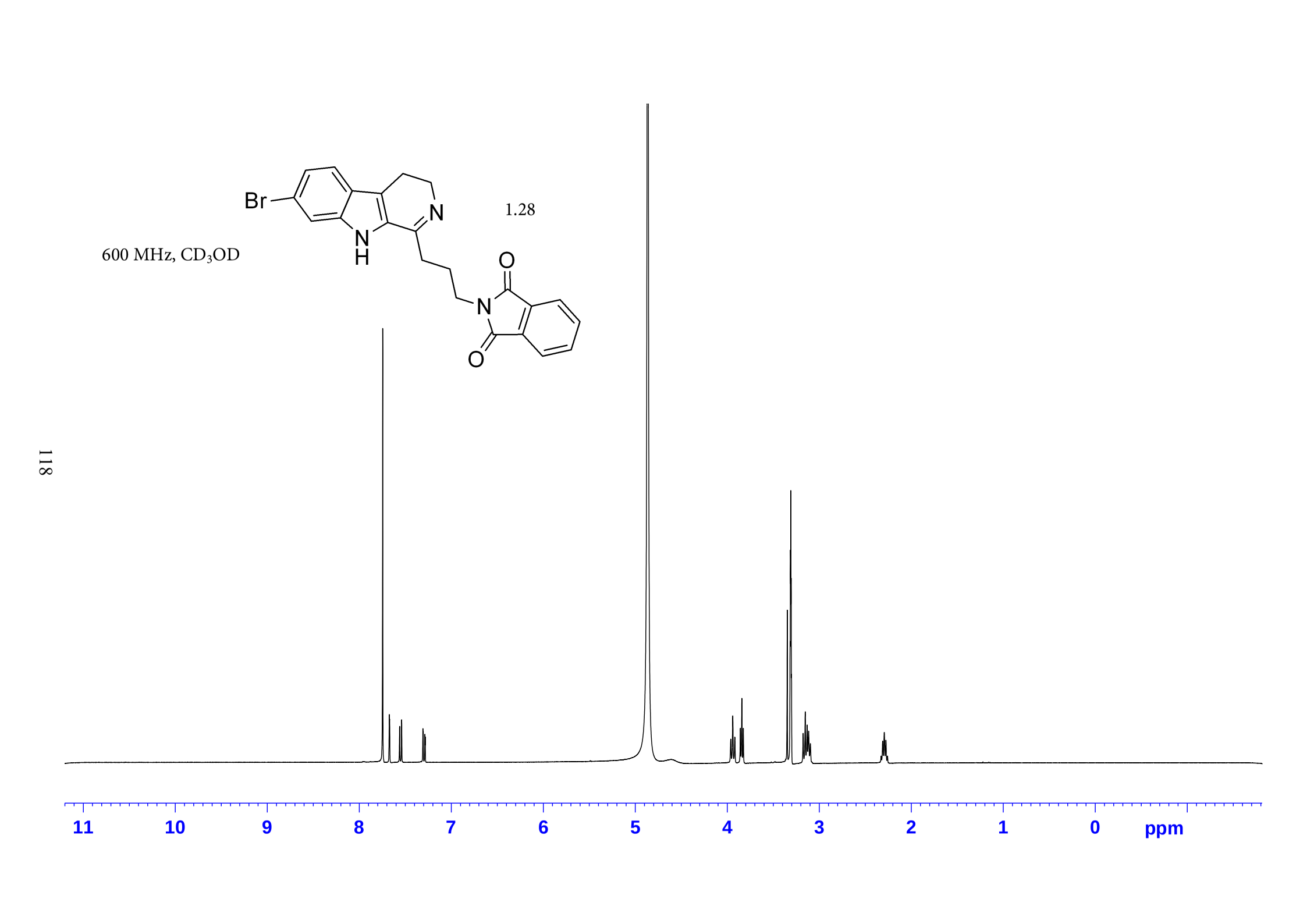
Br
N
H
N
O
N
O
1.28
600 MHz, CD3OD
118
11
10
9
8
7
6
5
4
3
2
1
0
ppm

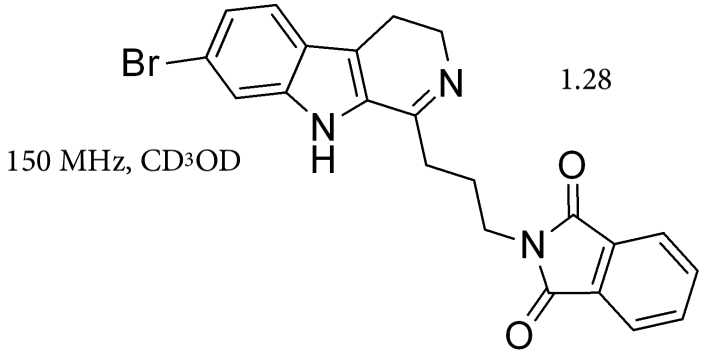

1.28

150 MHz, CD_3OD

119

1.19

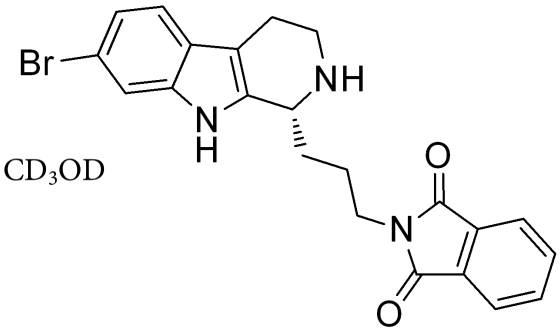

600 MHz, CD_3OD

120

11 10 9 8 7 6 5 4 3 2 1 0 ppm

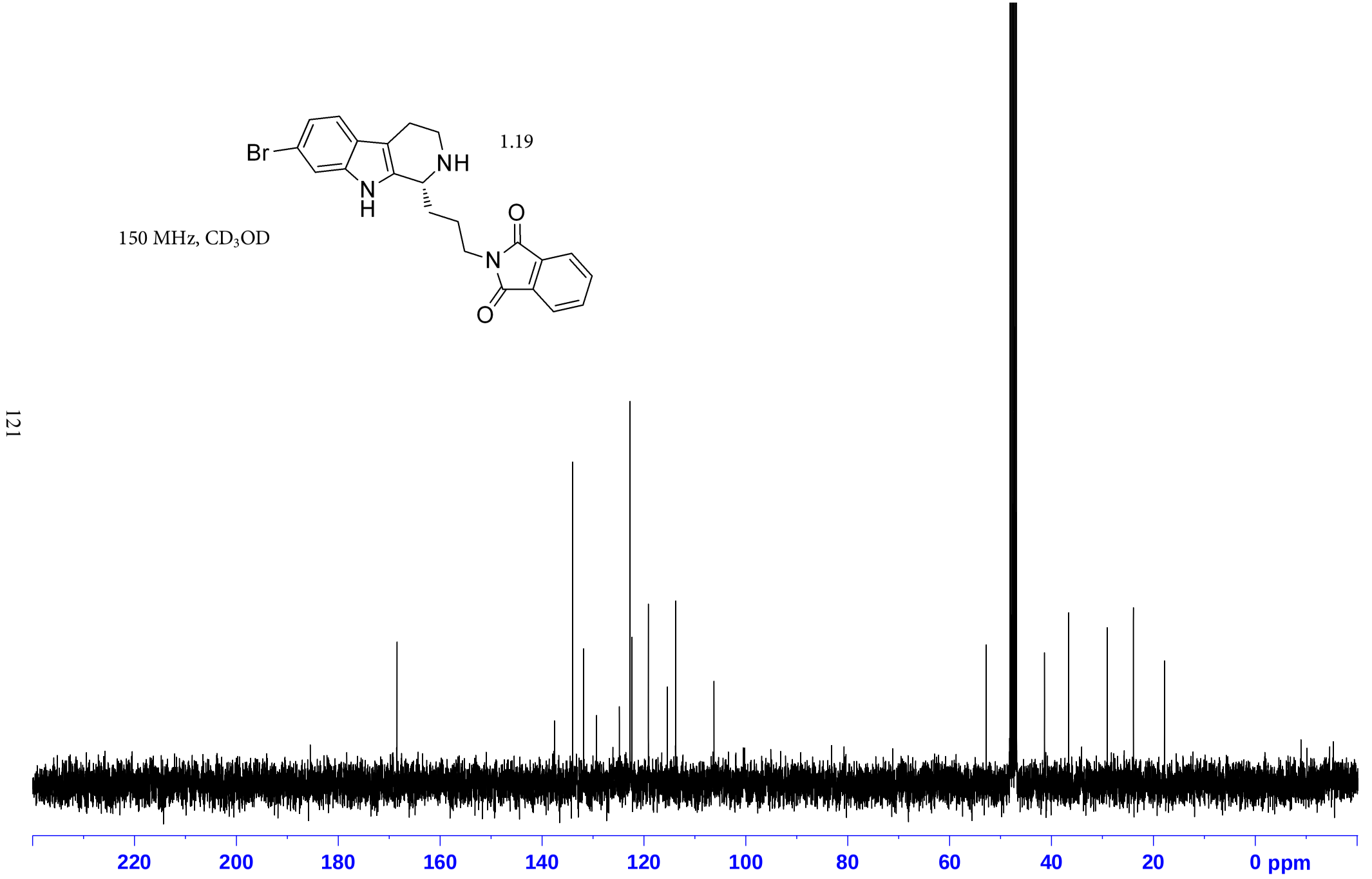
Br
NH
N
H
O
N
O
1.19
150 MHz, CD3OD
121
220
200
180
160
140
120
100
80
60
40
20
0 ppm

1.29

600 MHz, CD_3OD

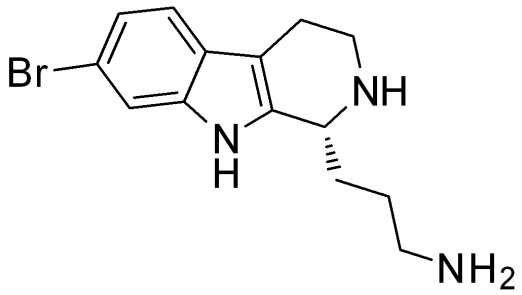

122

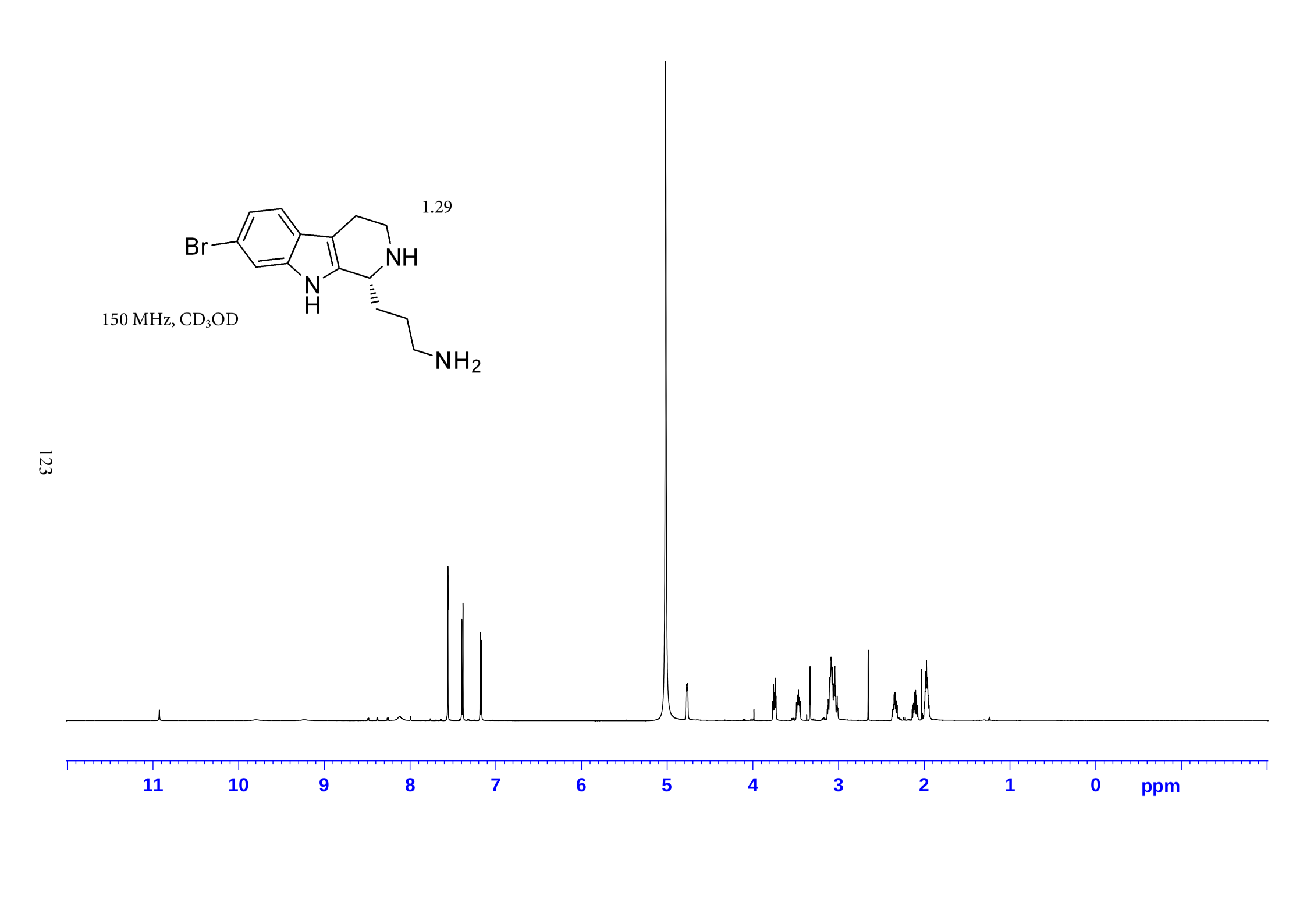
1.29
Br
NH
N
H
NH2
150 MHz, CD3OD
123
11
10
9
8
7
6
5
4
3
2
1
0
ppm

600 MHz, d_6-DMSO

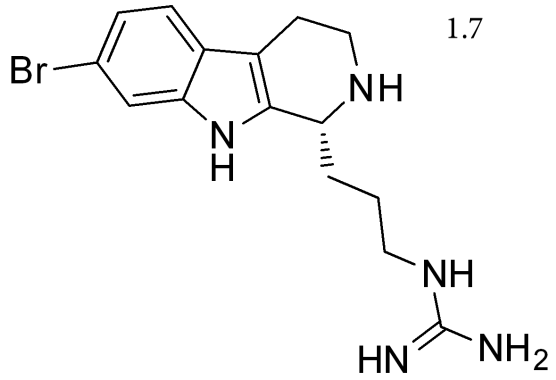

1.7

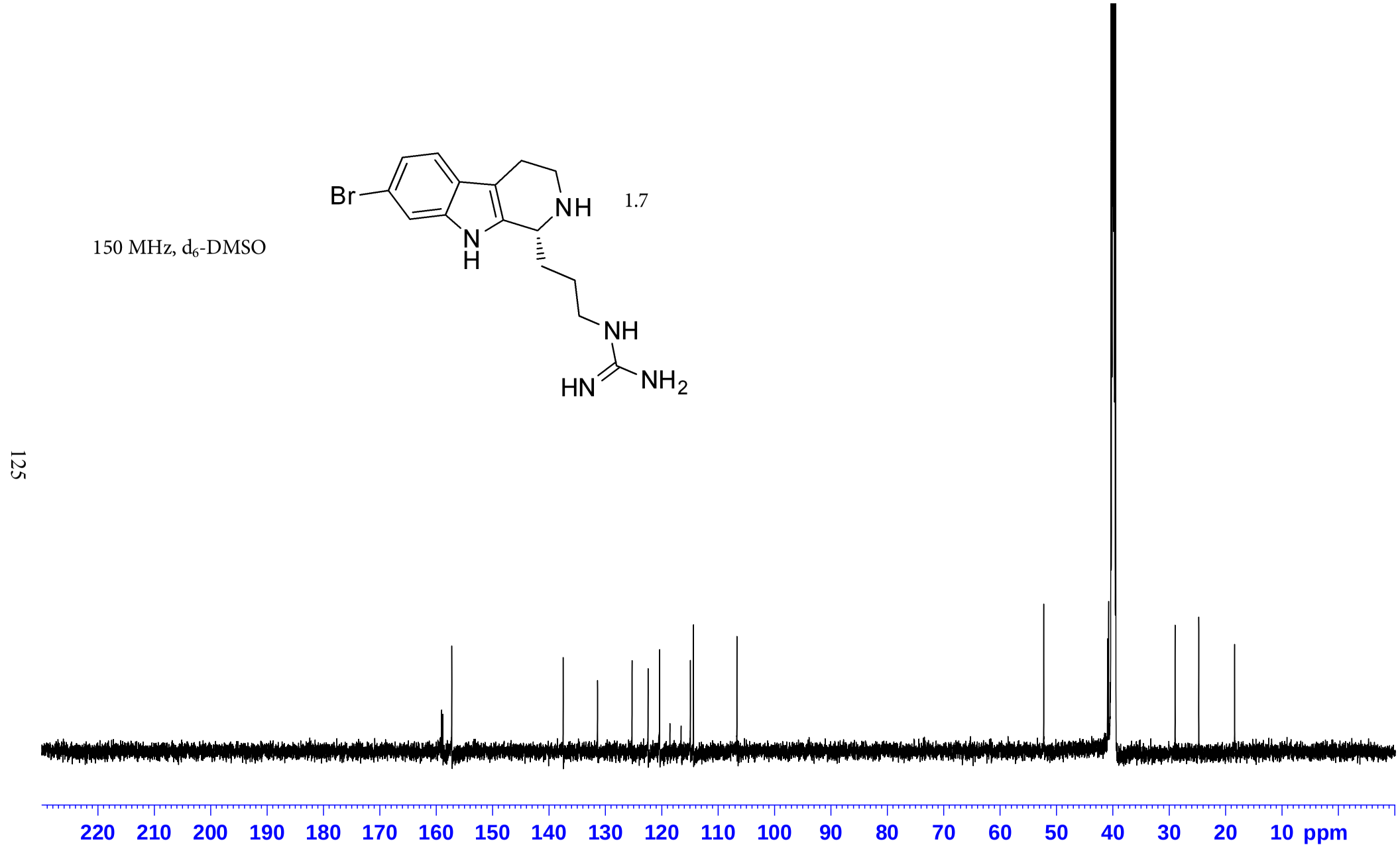
150 MHz, d6-DMSO
Br
NH
N
H
NH
HN
NH2
1.7
125
220 210 200 190 180 170 160 150 140 130 120 110 100 90 80 70 60 50 40 30 20 10 ppm

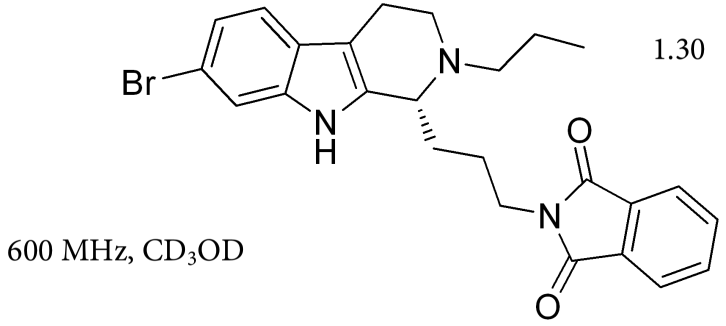

1.30

600 MHz, CD_3OD

126

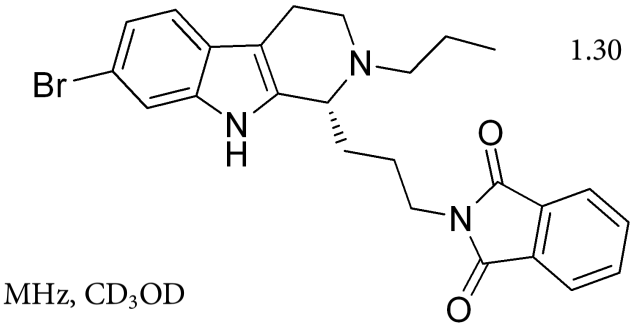

1.30

150 MHz, CD_3OD

127

1.31

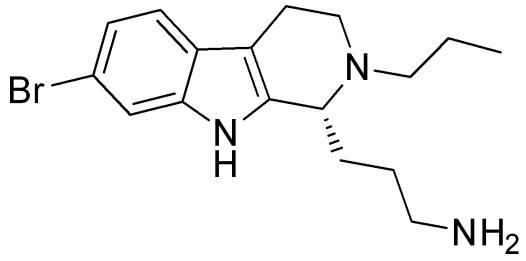

500 MHz, CD_3OD

1.31

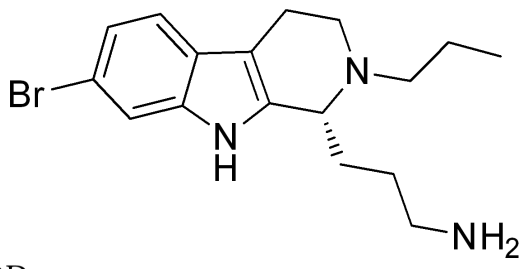

125 MHz, CD_3OD

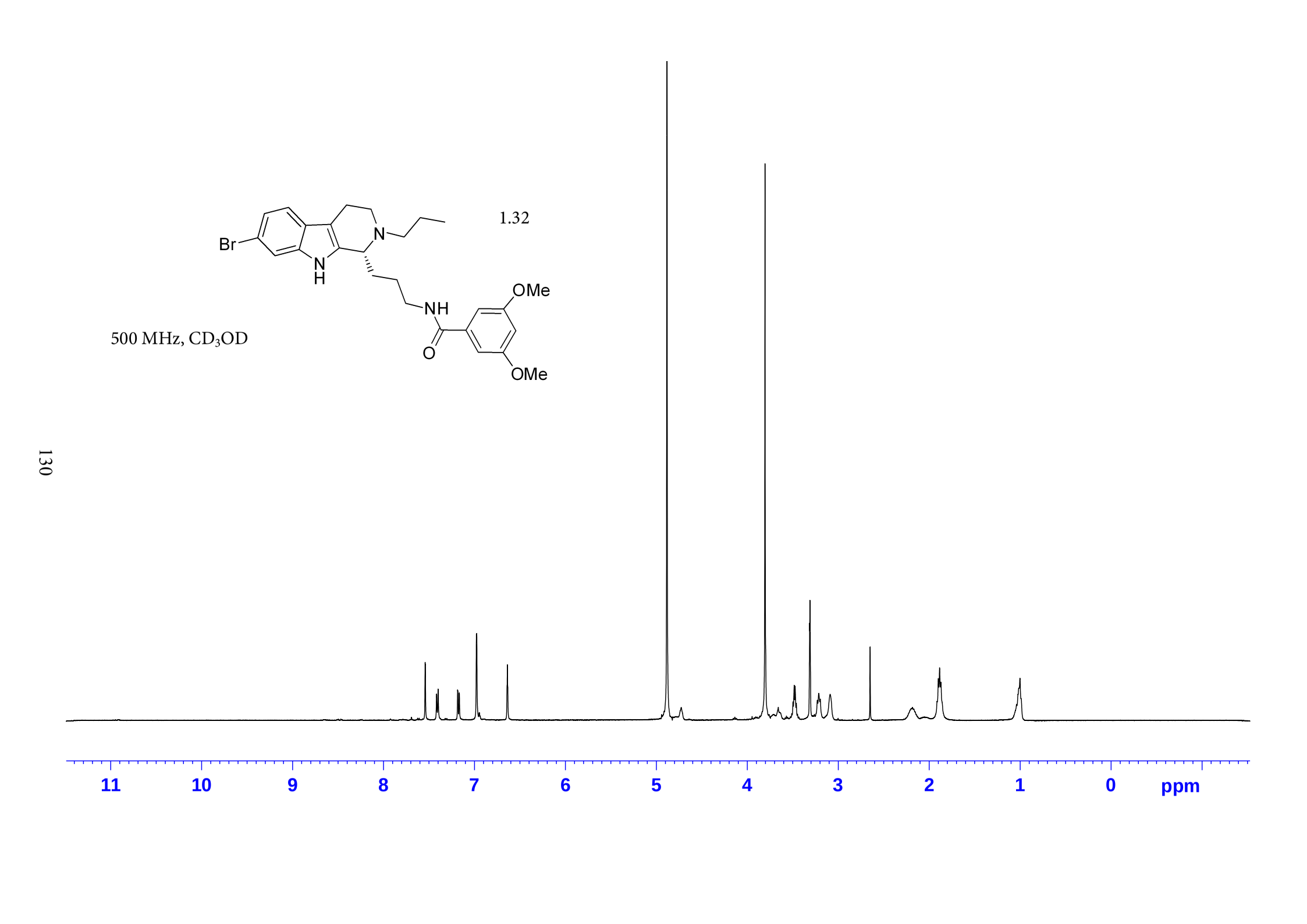
1.32
500 MHz, CD3OD
Br
N
H
N
NH
O
OMe
OMe
130
11
10
9
8
7
6
5
4
3
2
1
0
ppm

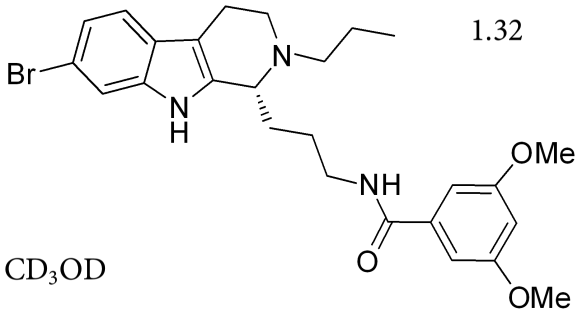

1.32

125 MHz, CD_3OD

1.33

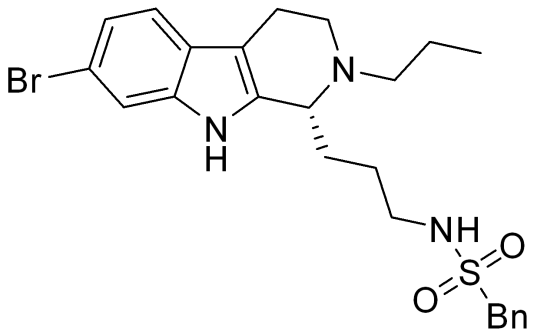

500 MHz, CD_3OD

132

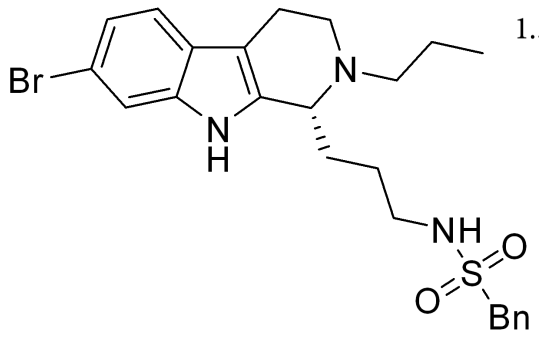

1.33

125 MHz, CD_3OD

1.34

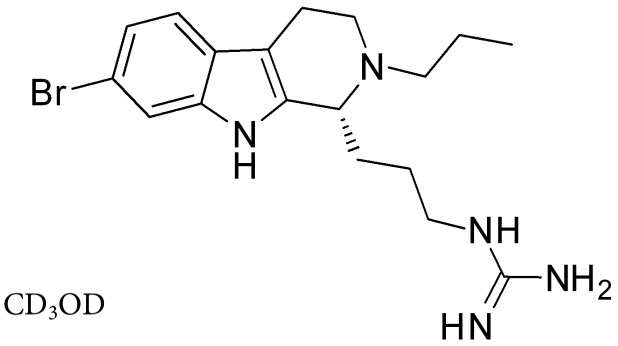

600 MHz, CD_3OD

134

1.34

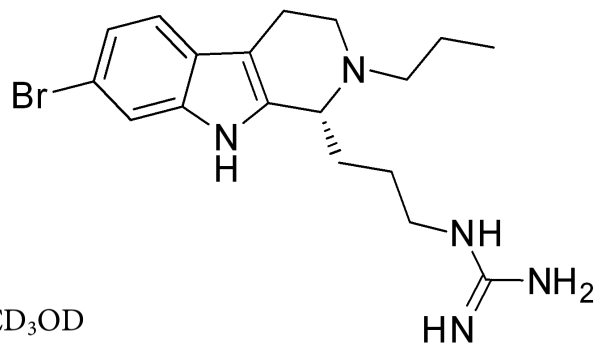

150 MHz, CD_3OD

APPENDIX A2

Spectra Relevant to Chapter II

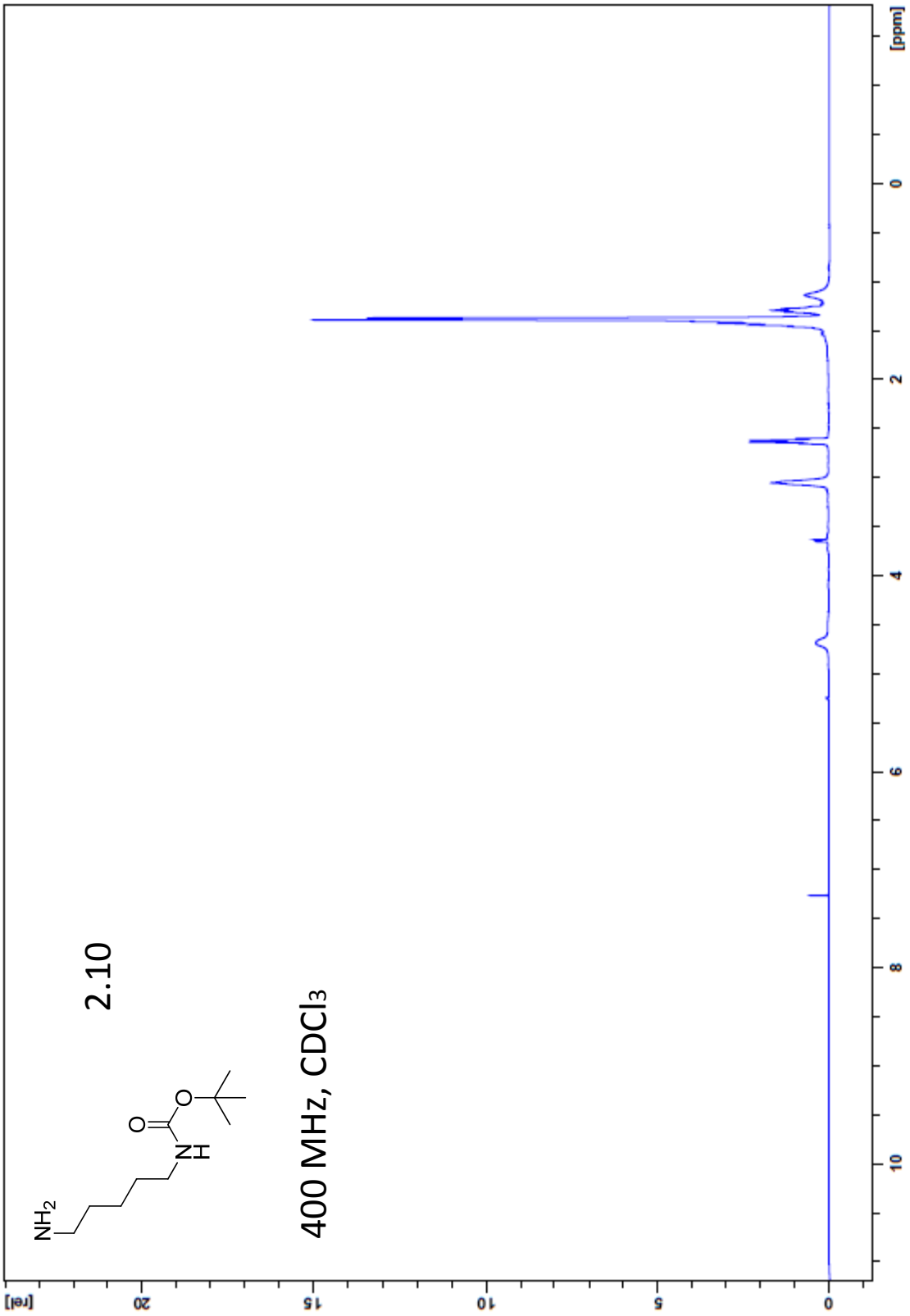
2.10
400 MHz, CDCl3
NH2
O
O
N
H
[rel]
20
15
10
5
0
[ppm]
0
2
4
6
8
10

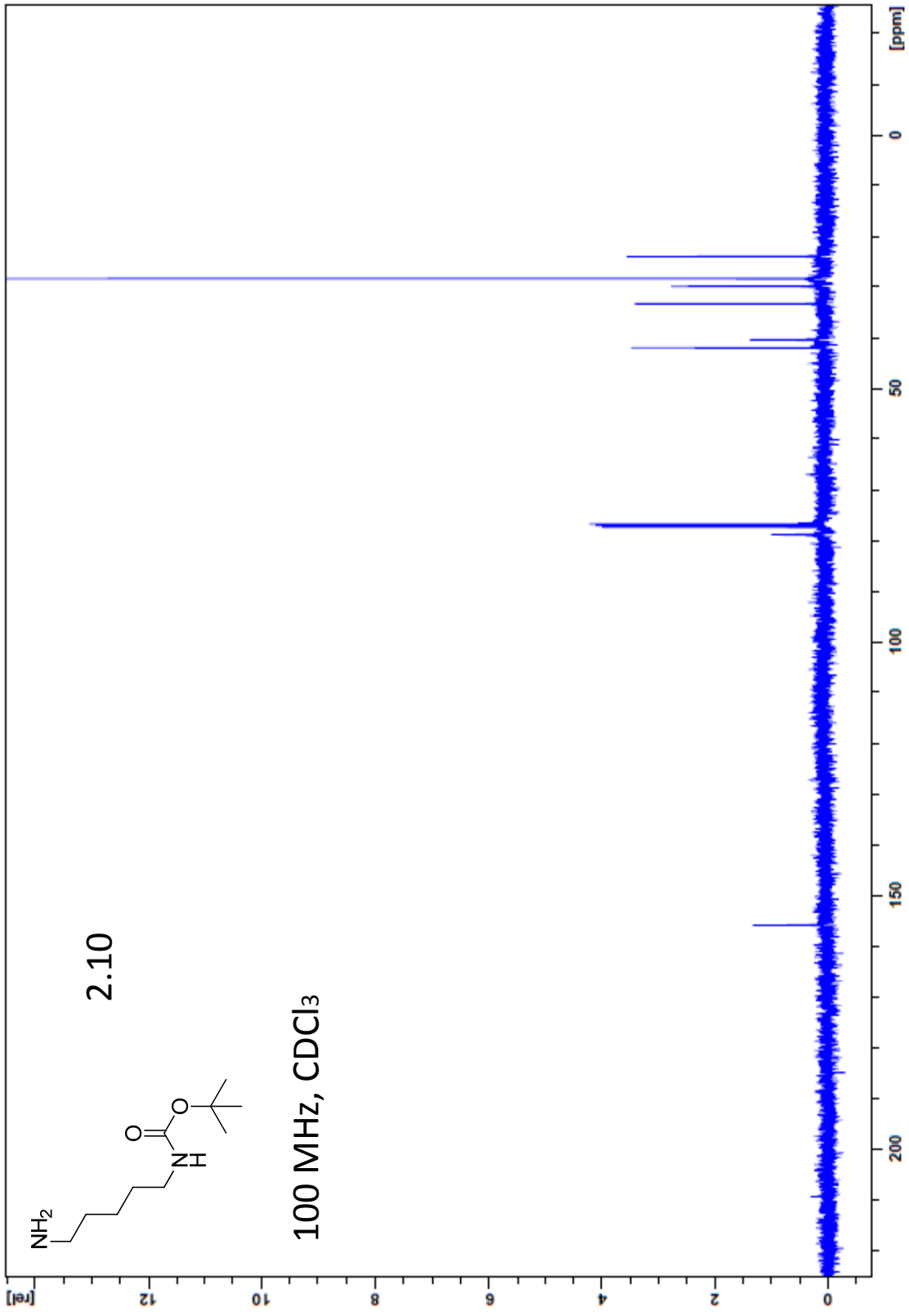
2.10
100 MHz, CDCl3
NH2
O
O
N
H
[rel]
[ppm]
0
2
4
6
8
10
12
50
100
150
200

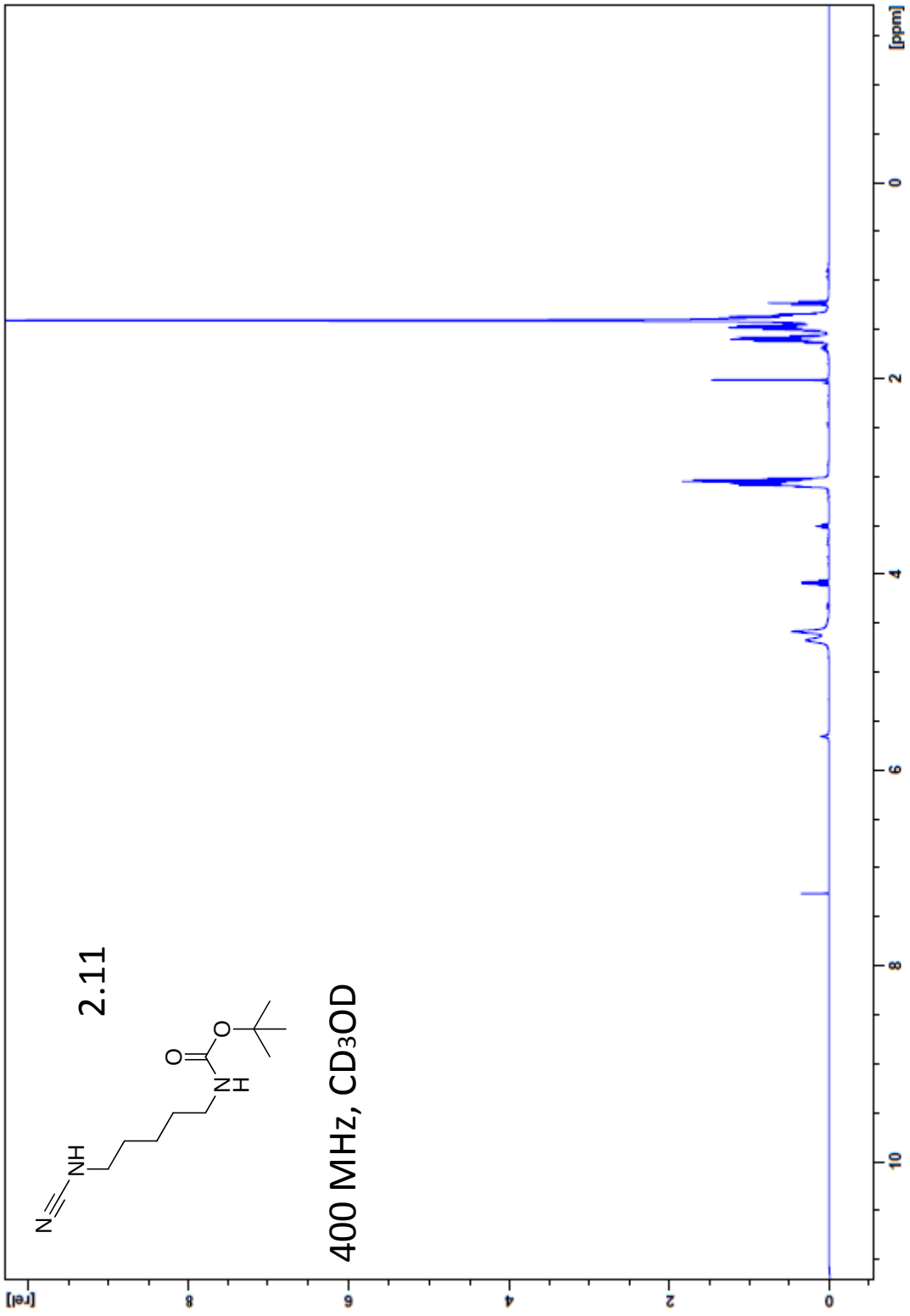
2.11
400 MHz, CD3OD
[rel]
[ppm]

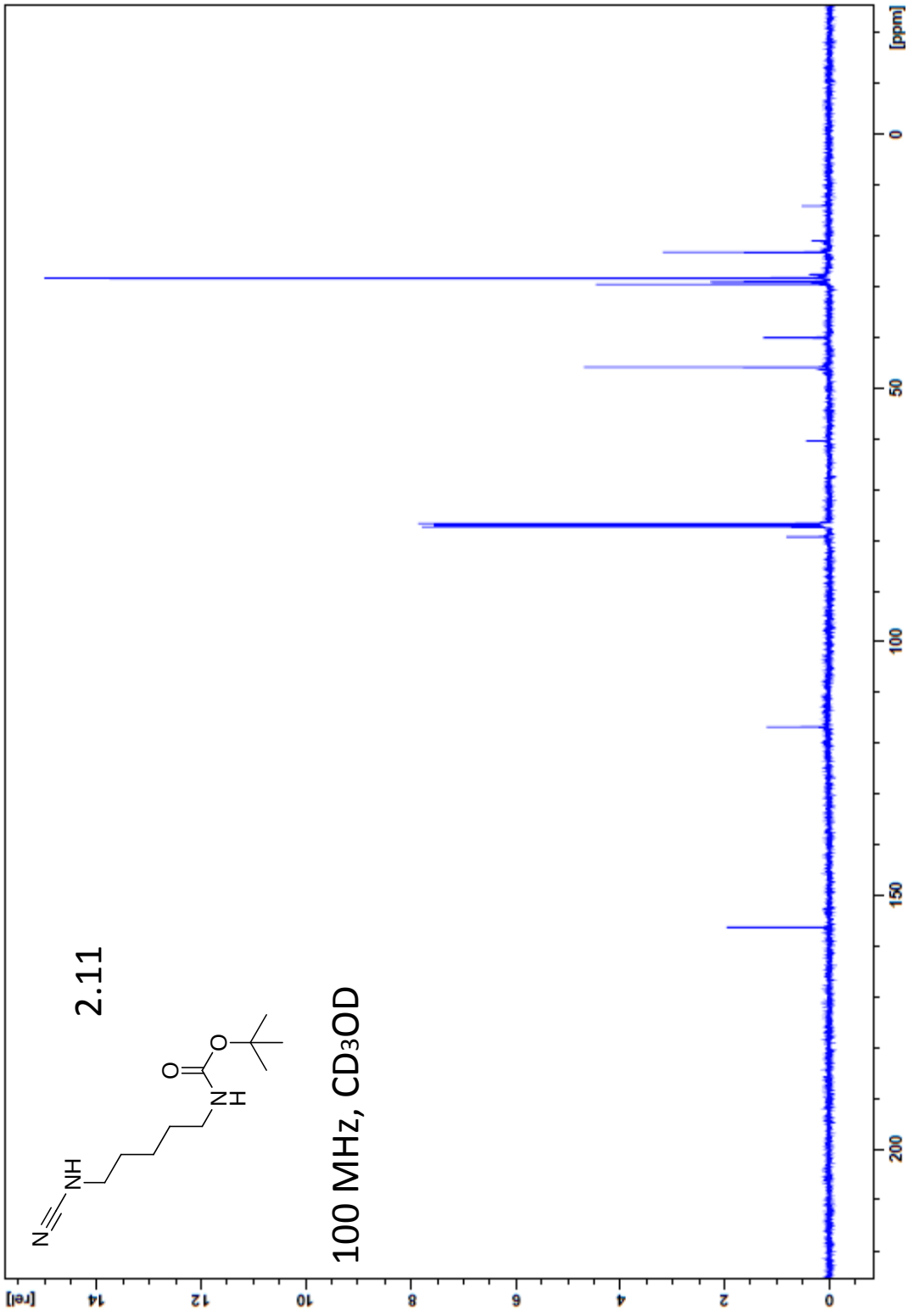
2.11
100 MHz, CD3OD
[rel]
[ppm]

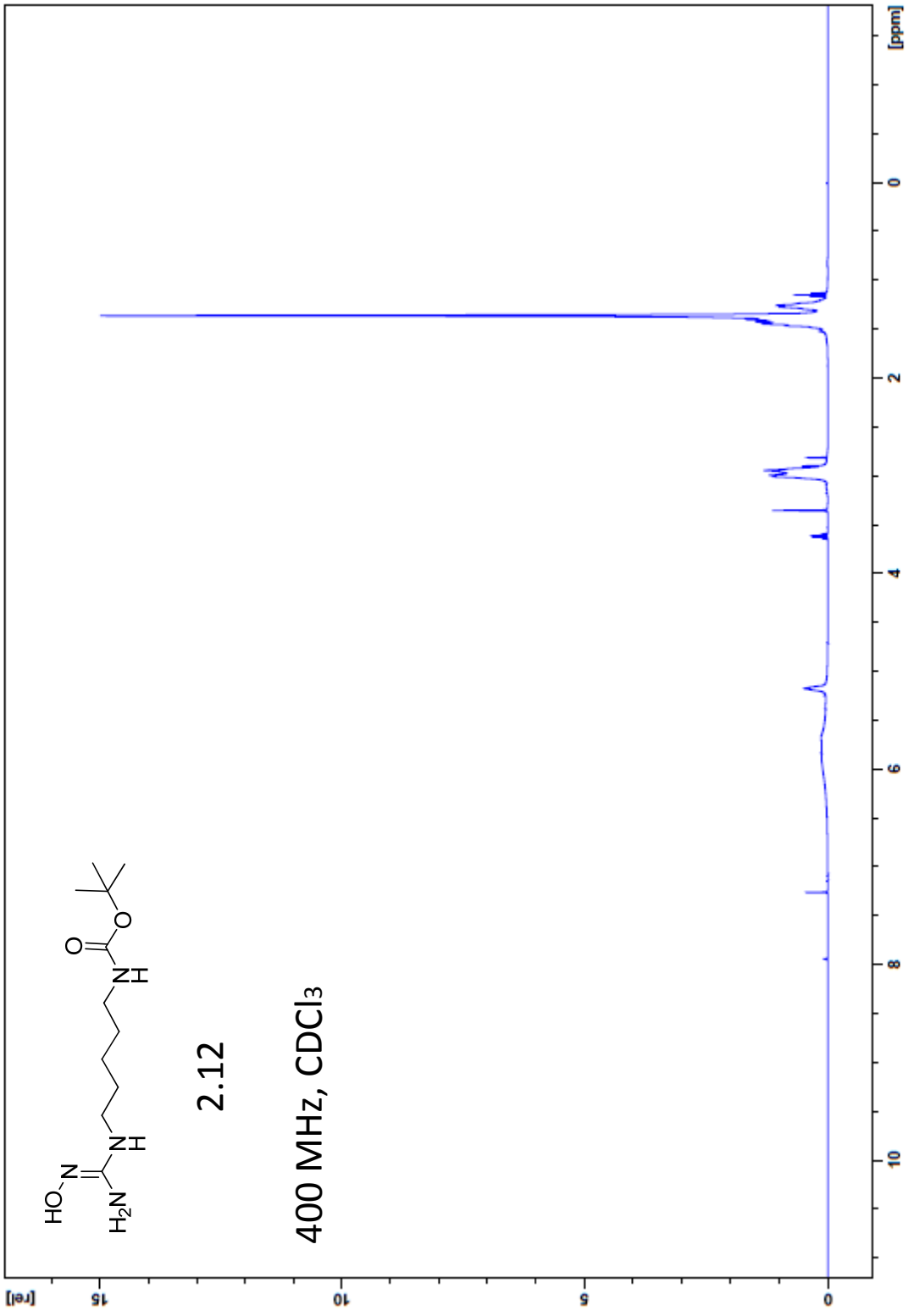
2.12
400 MHz, CDCl3
[rel]
15
10
5
0
[ppm]
0
2
4
6
8
10

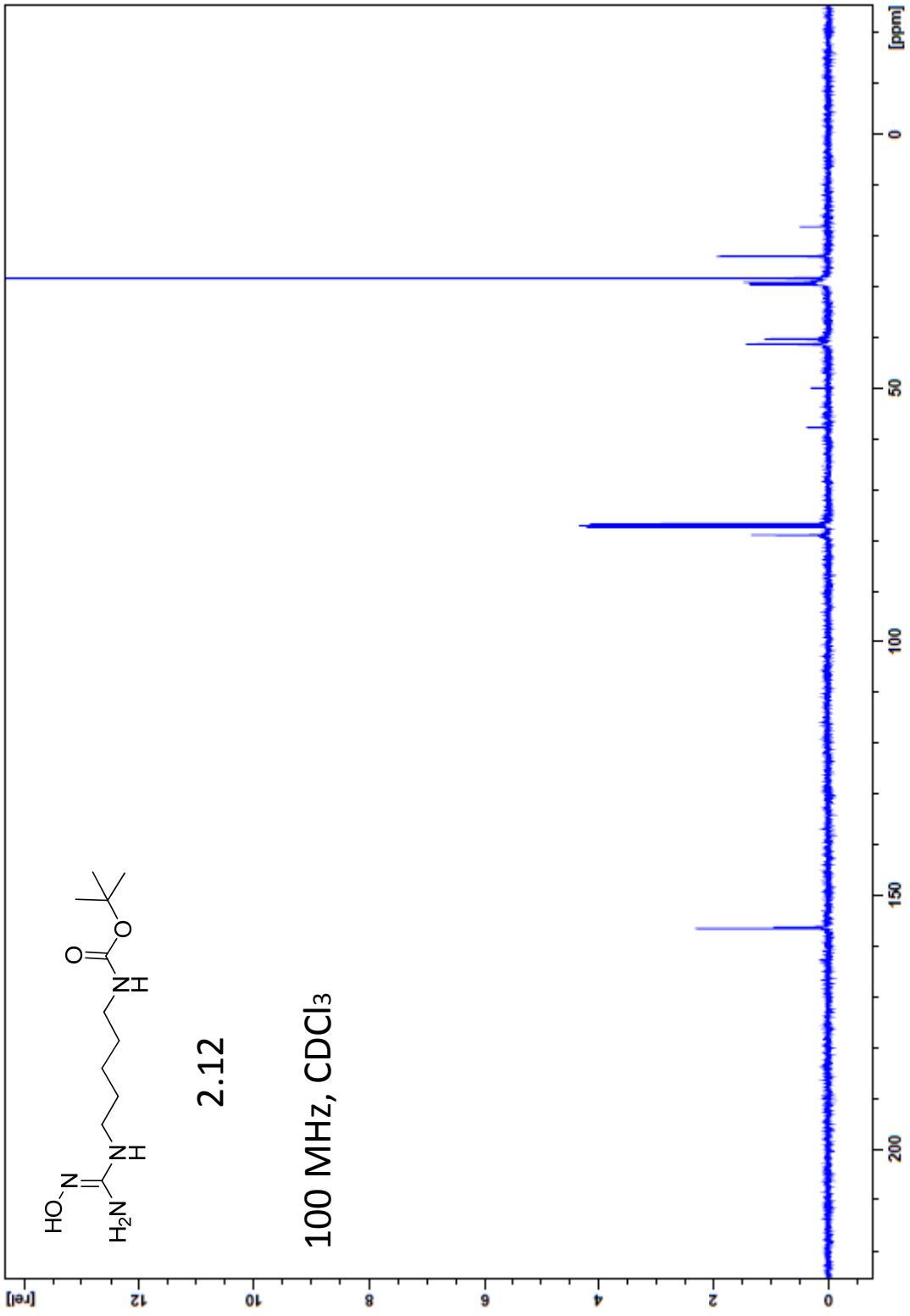
2.12
100 MHz, CDCl3
[rel]
[ppm]

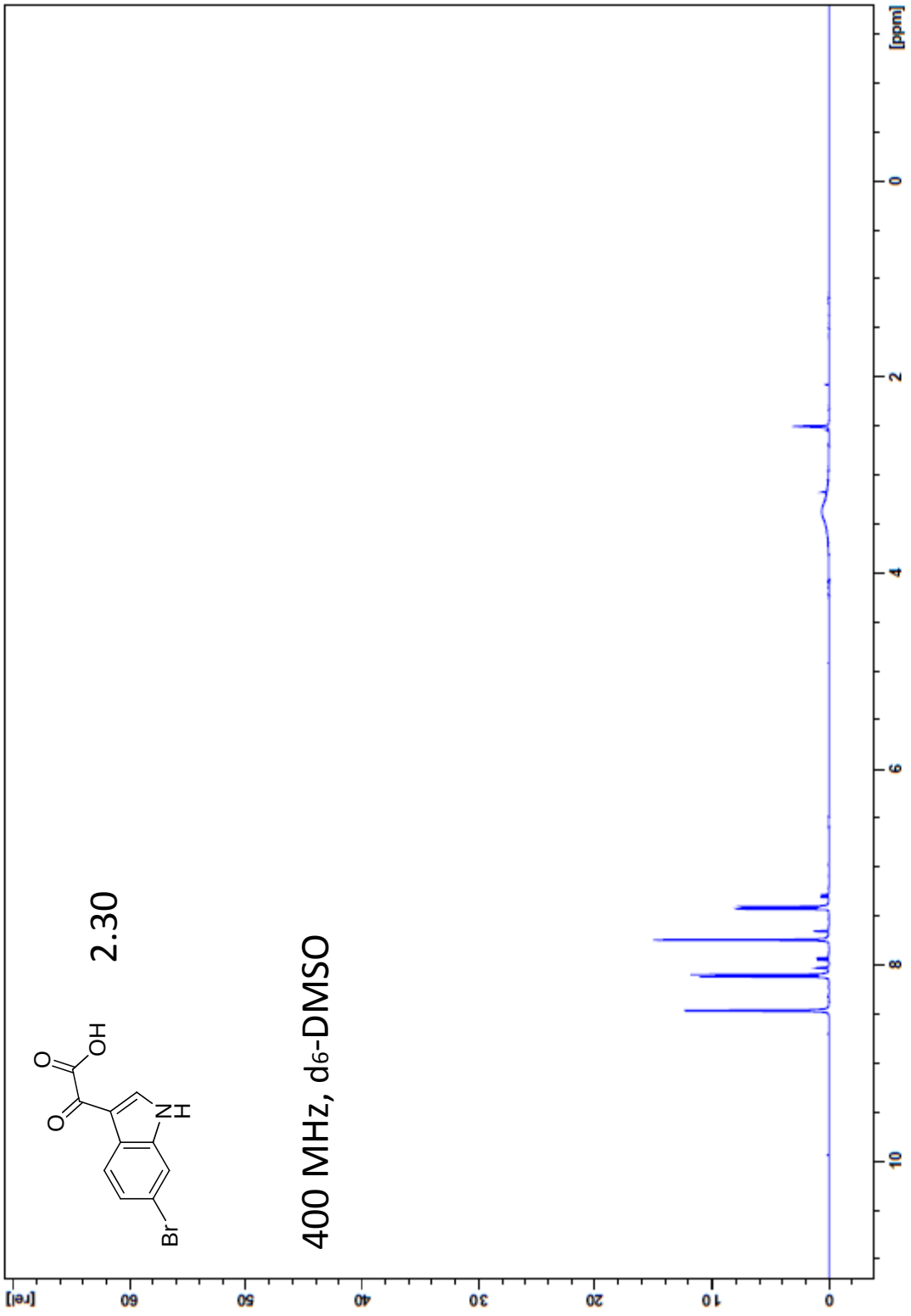
2.30
400 MHz, d6-DMSO
O
OH
O
N
H
Br
[rel]
[ppm]

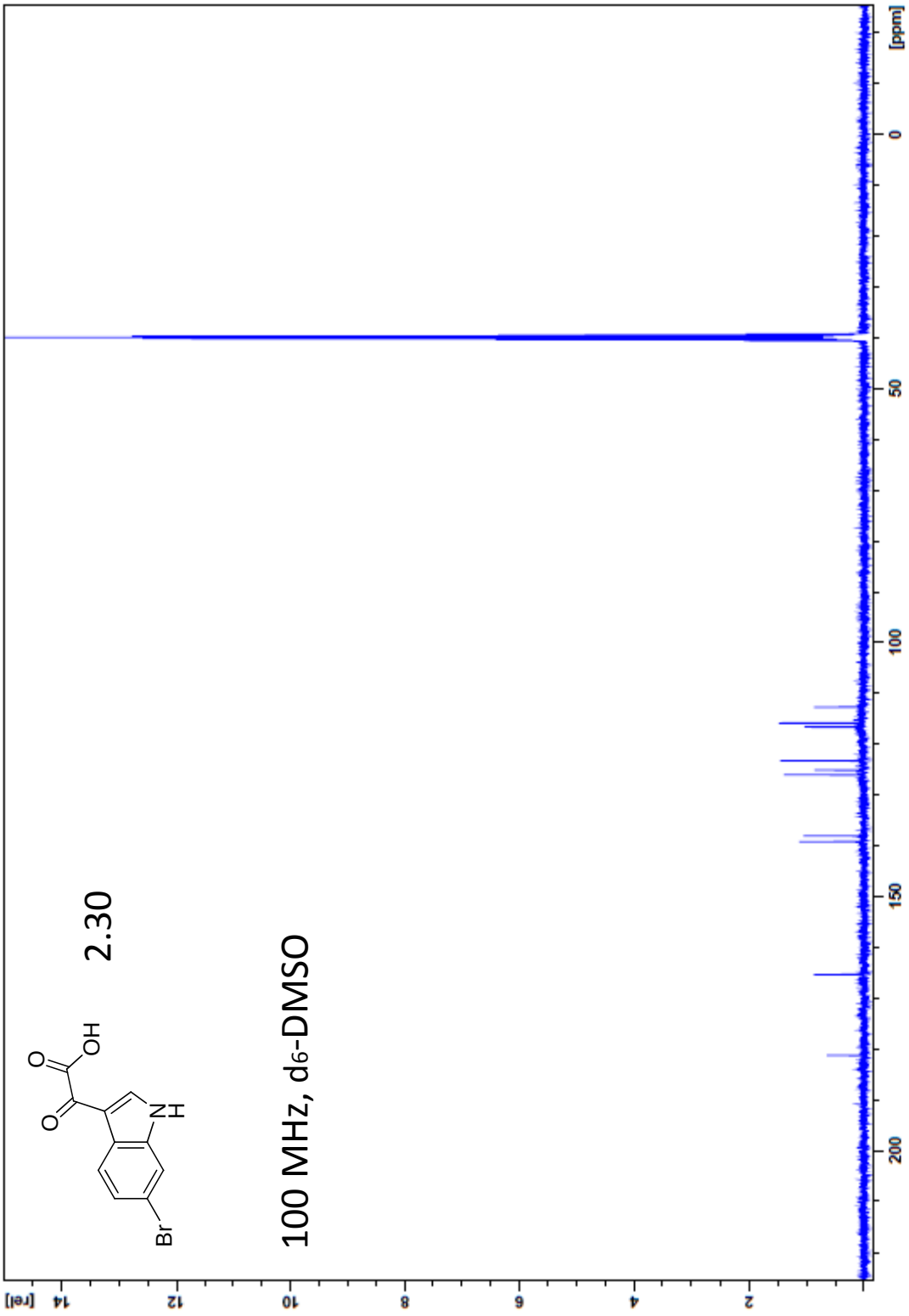
2.30
100 MHz, d6-DMSO
O
OH
O
N
H
Br
[rel]
14
12
10
8
6
4
2
200
150
100
50
0
[ppm]

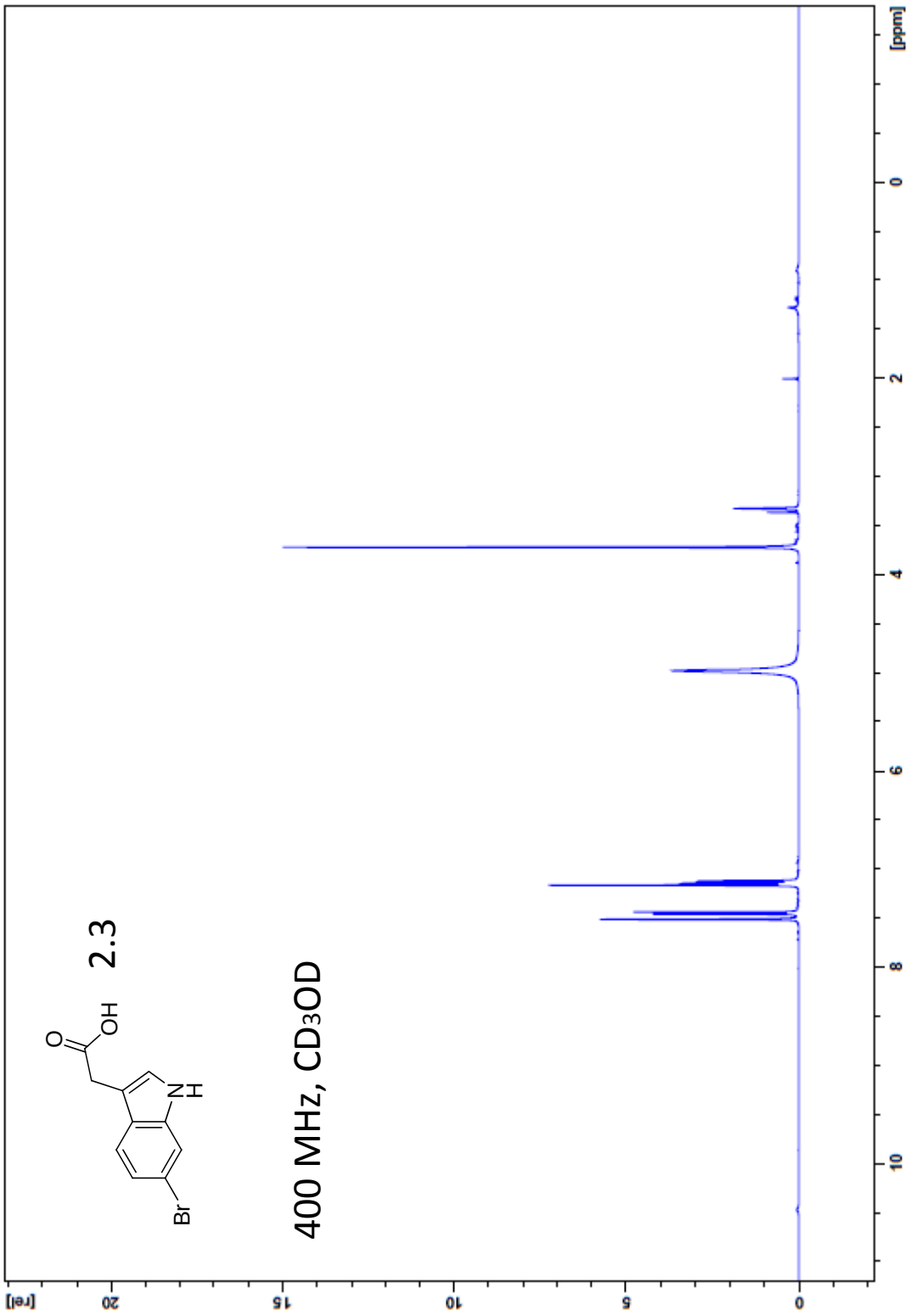
2.3
400 MHz, CD3OD
[rel]
20
15
10
5
0
[ppm]
10
8
6
4
2
0
O
OH
N
H
Br

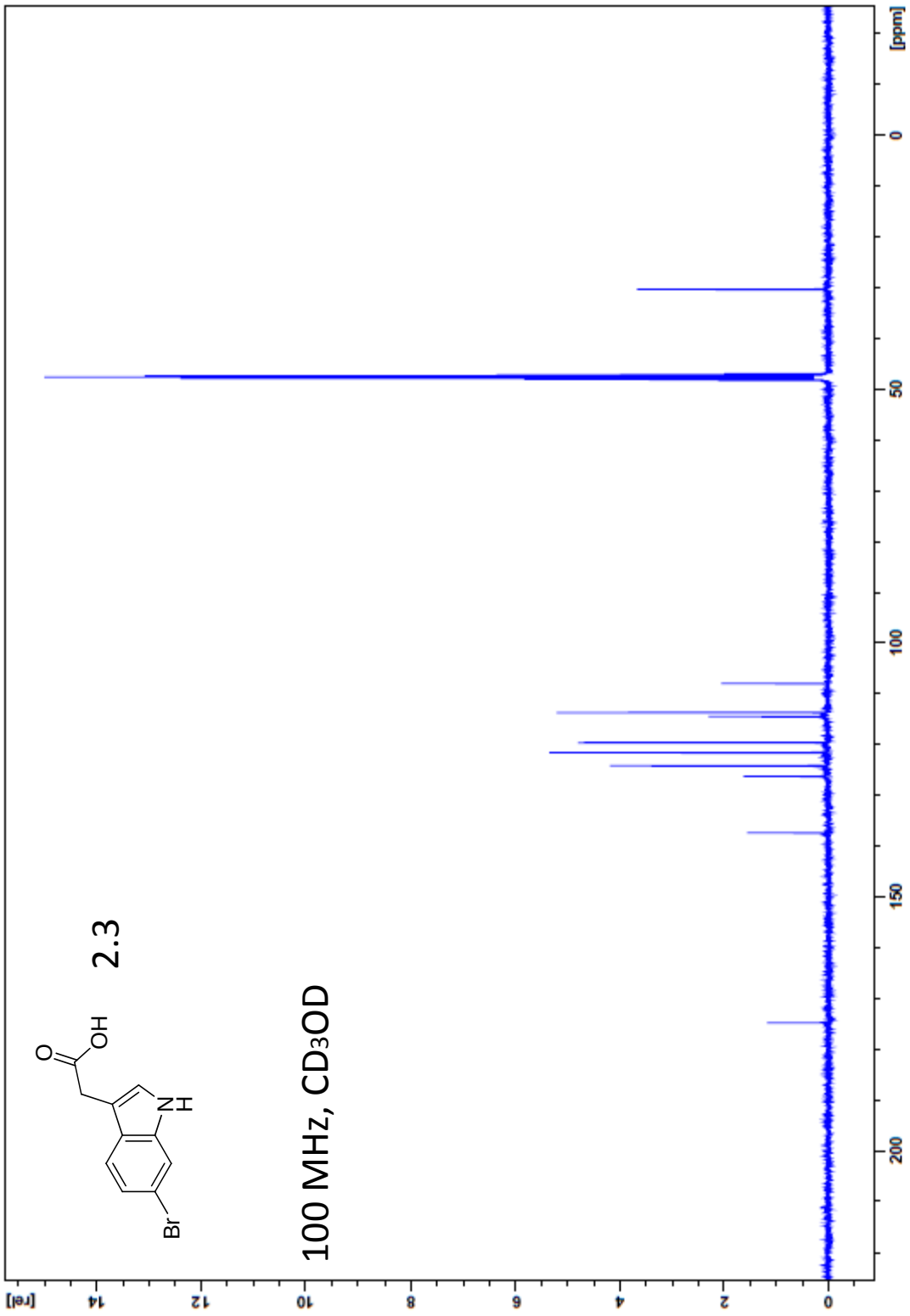
2.3
100 MHz, CD3OD
OH
O
N
H
Br
[rel]
[ppm]

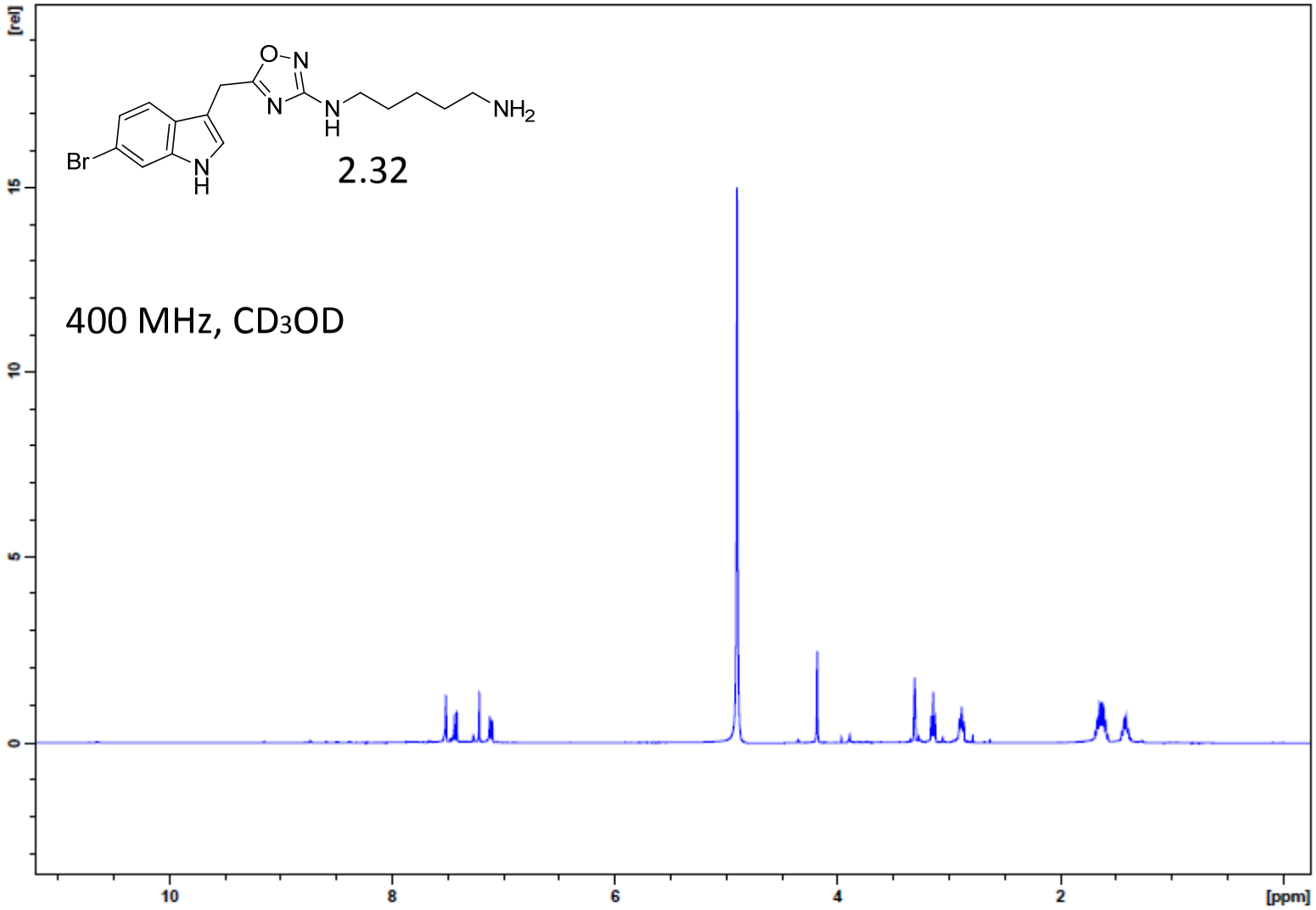
[rel]
15
10
5
0
Br
N
H
O
N
N
N
H
NH2
2.32
400 MHz, CD3OD
10
8
6
4
2
[ppm]

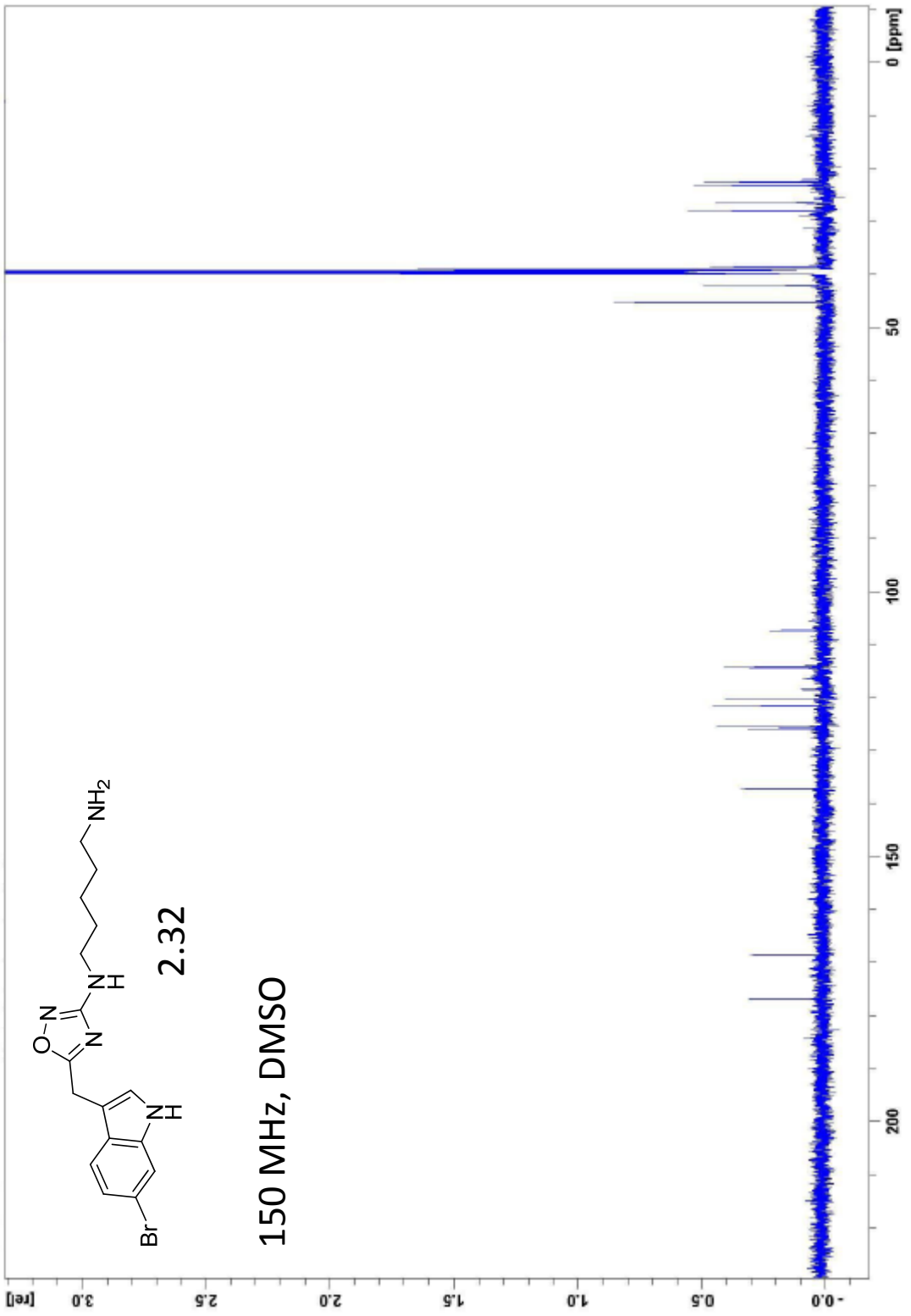
150 MHz, DMSO
2.32
NH2
N
H
O
N
N
N
H
Br
[rel]
3.0
2.5
2.0
1.5
1.0
0.5
-0.0
0 [ppm]
50
100
150
200

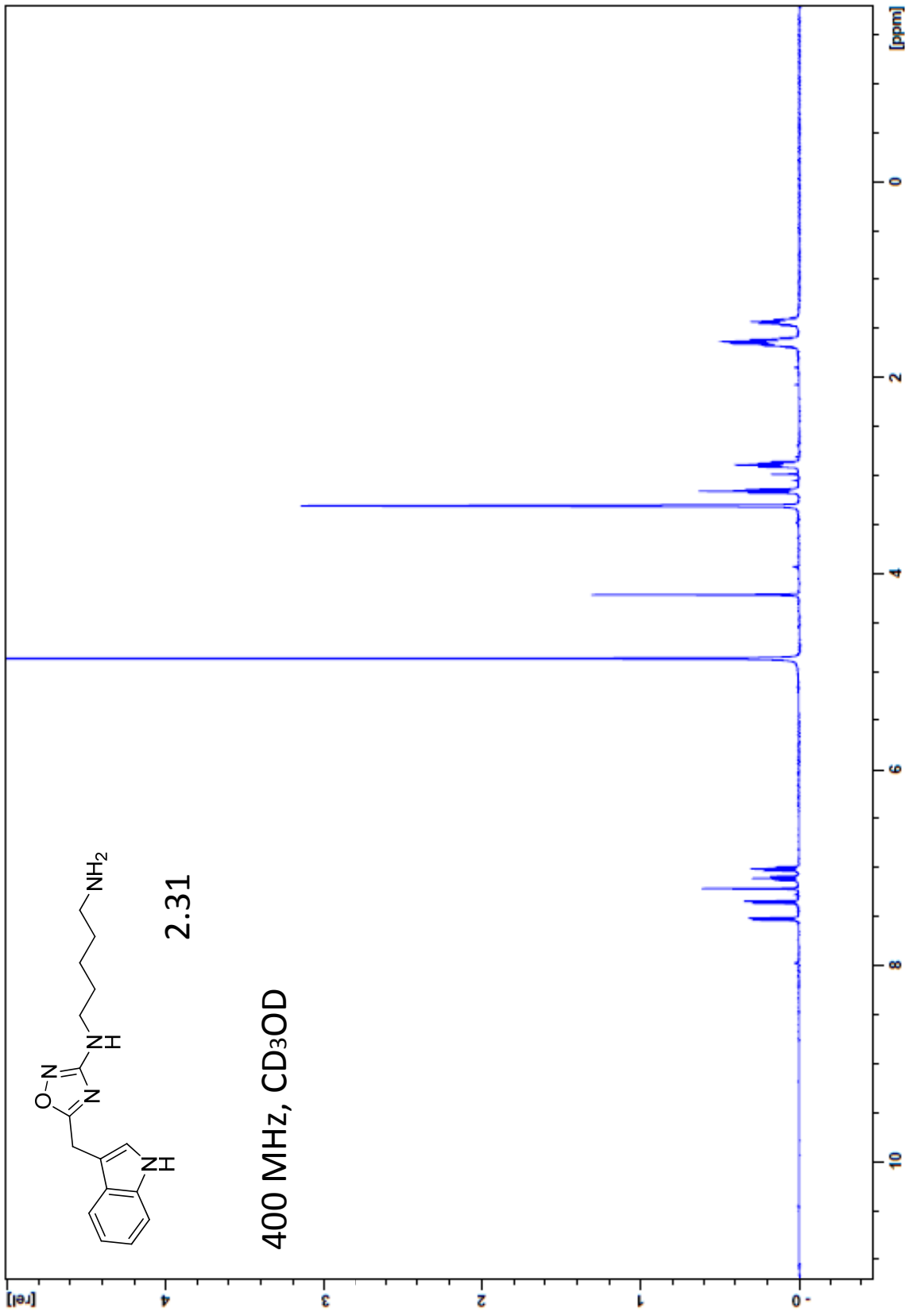
2.31
400 MHz, CD3OD
NH2
N
H
N
O
N
N
H
[rel]
[ppm]

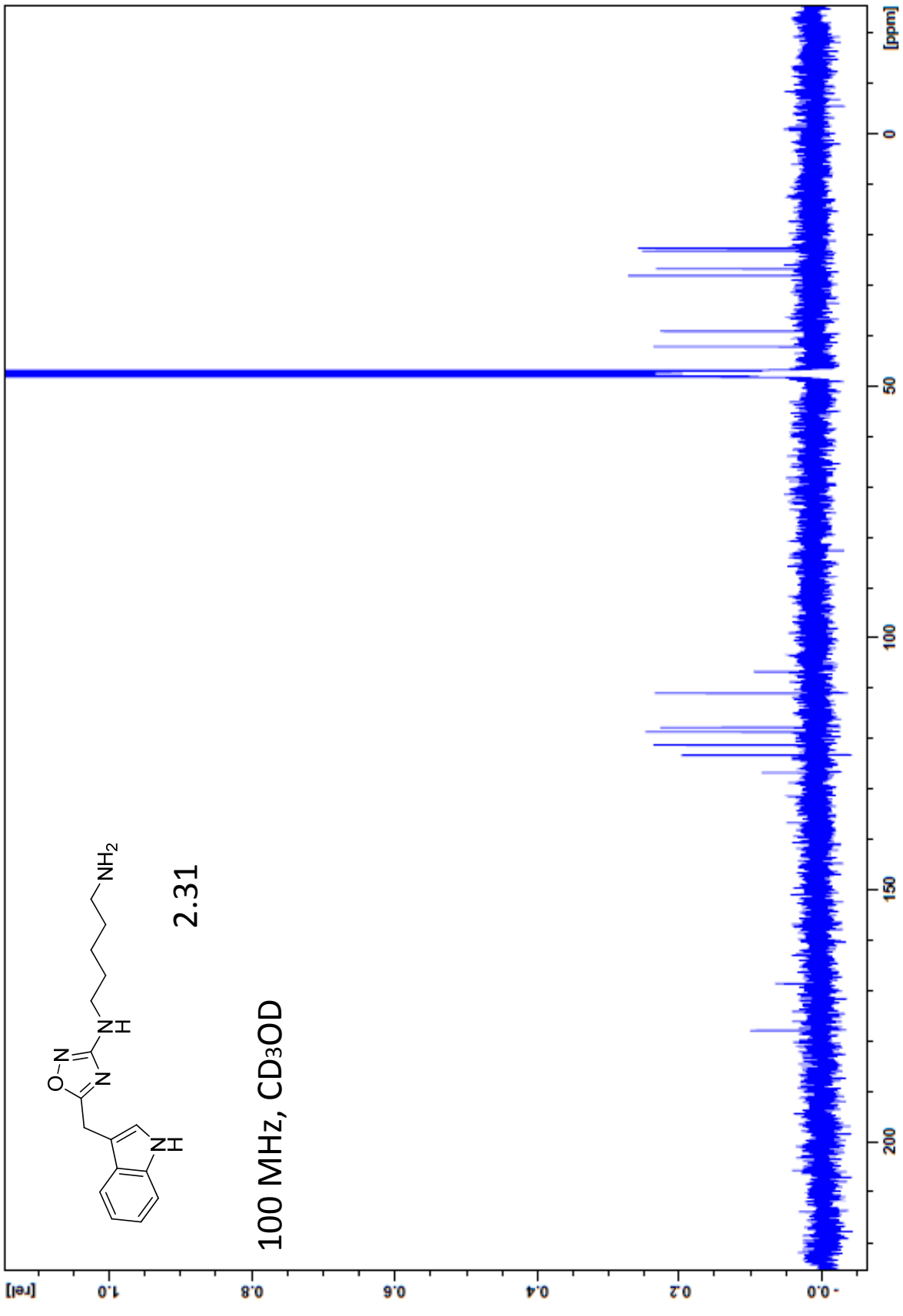
2.31
100 MHz, CD3OD
[rel]
[ppm]

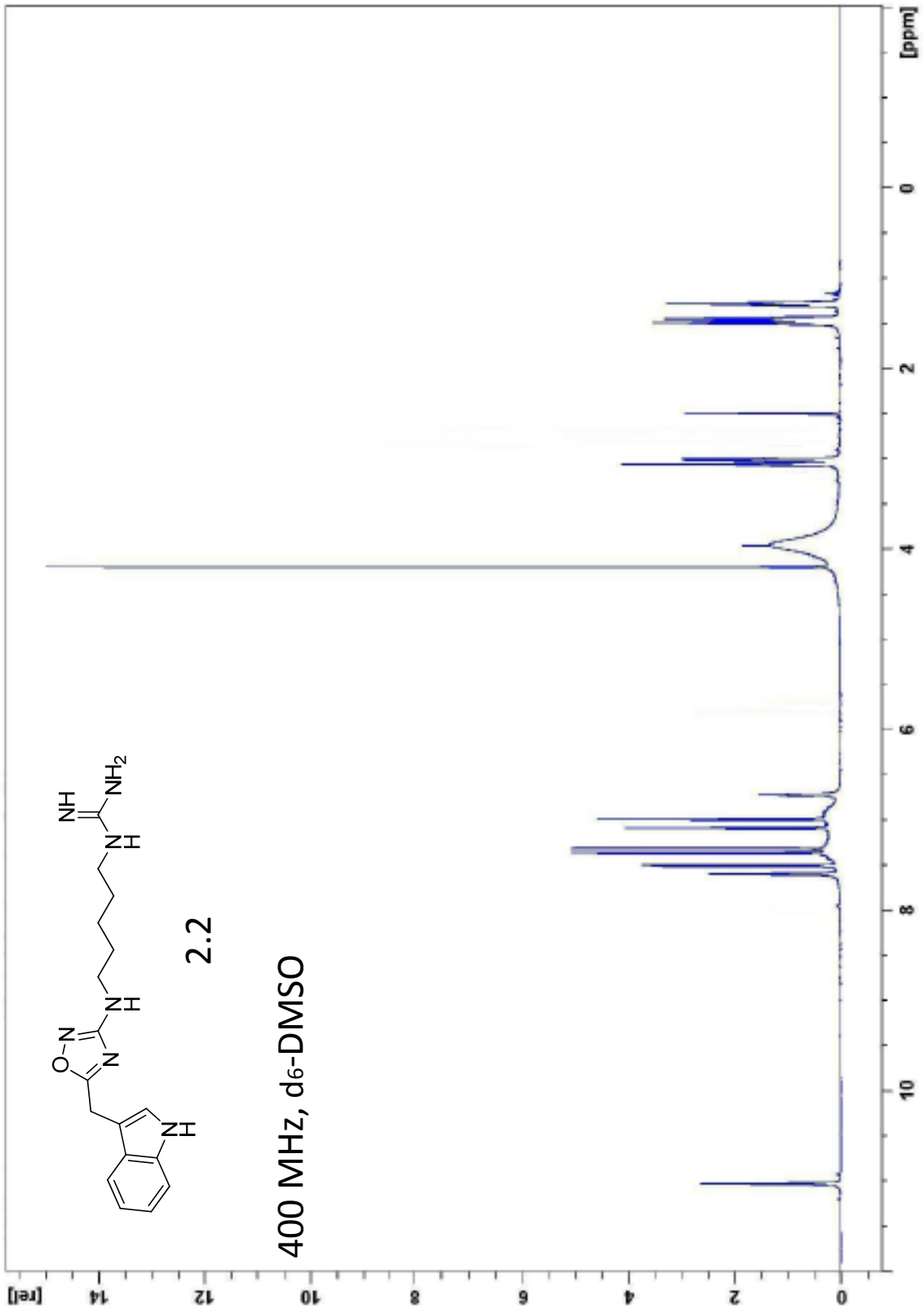
2.2
400 MHz, d6-DMSO
[rel]
[ppm]

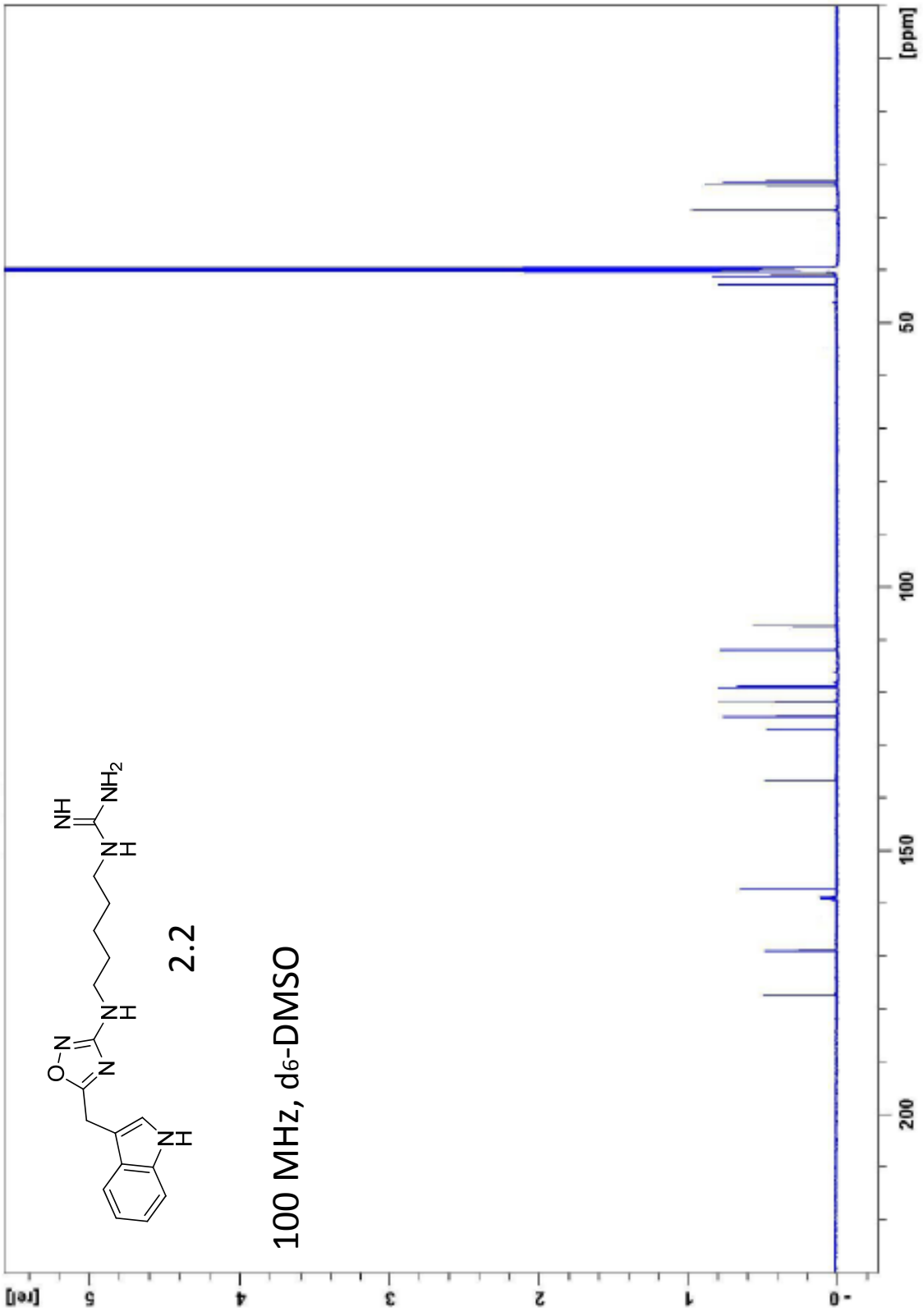
2.2
100 MHz, d6-DMSO
[ppm]
200
150
100
50
0
1
2
3
4
5
[rel]

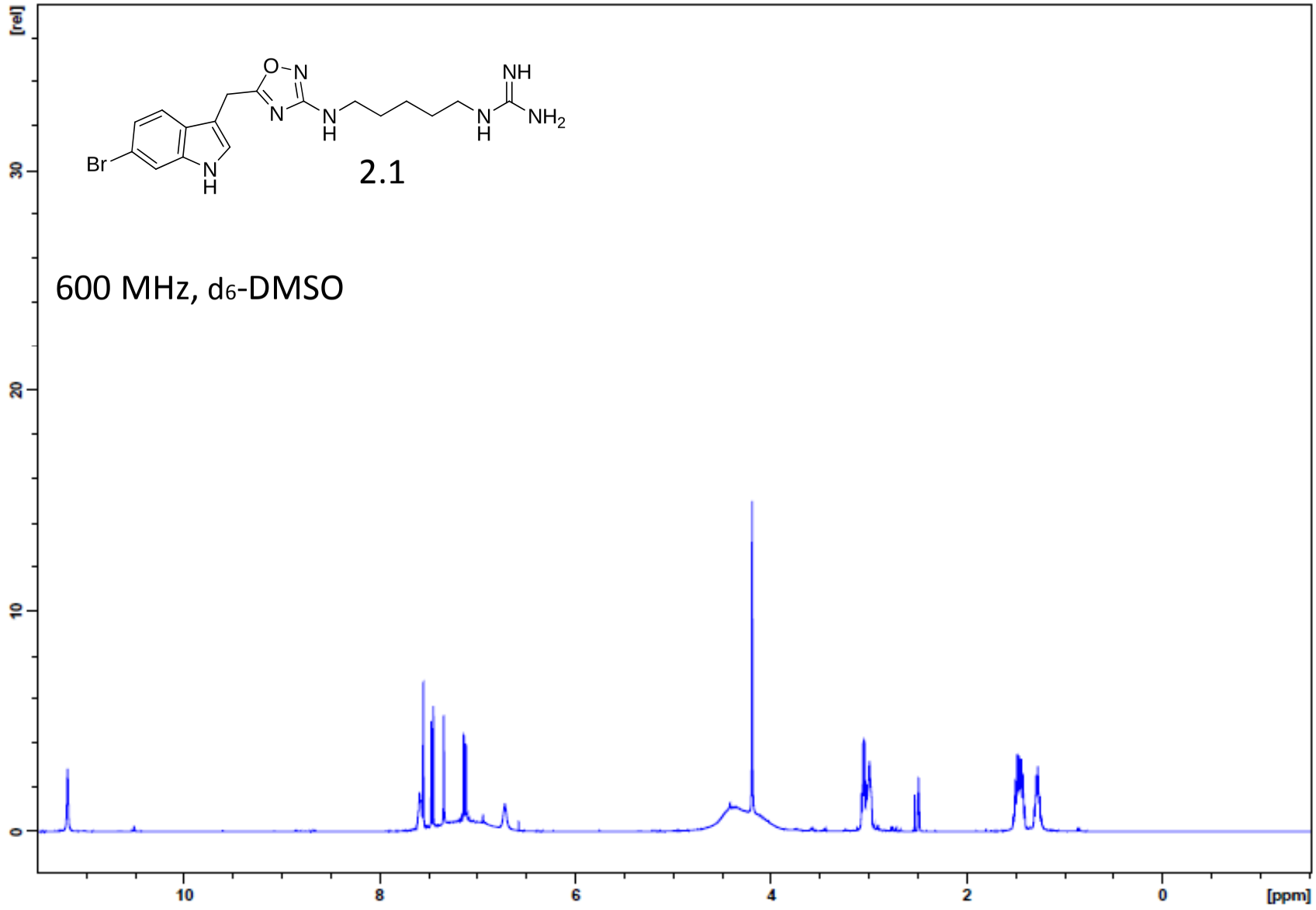
[rel]
30
20
10
0
Br
N
H
O
N
N
N
H
N
H
NH
NH2
2.1
600 MHz, d6-DMSO
10
8
6
4
2
0
[ppm]

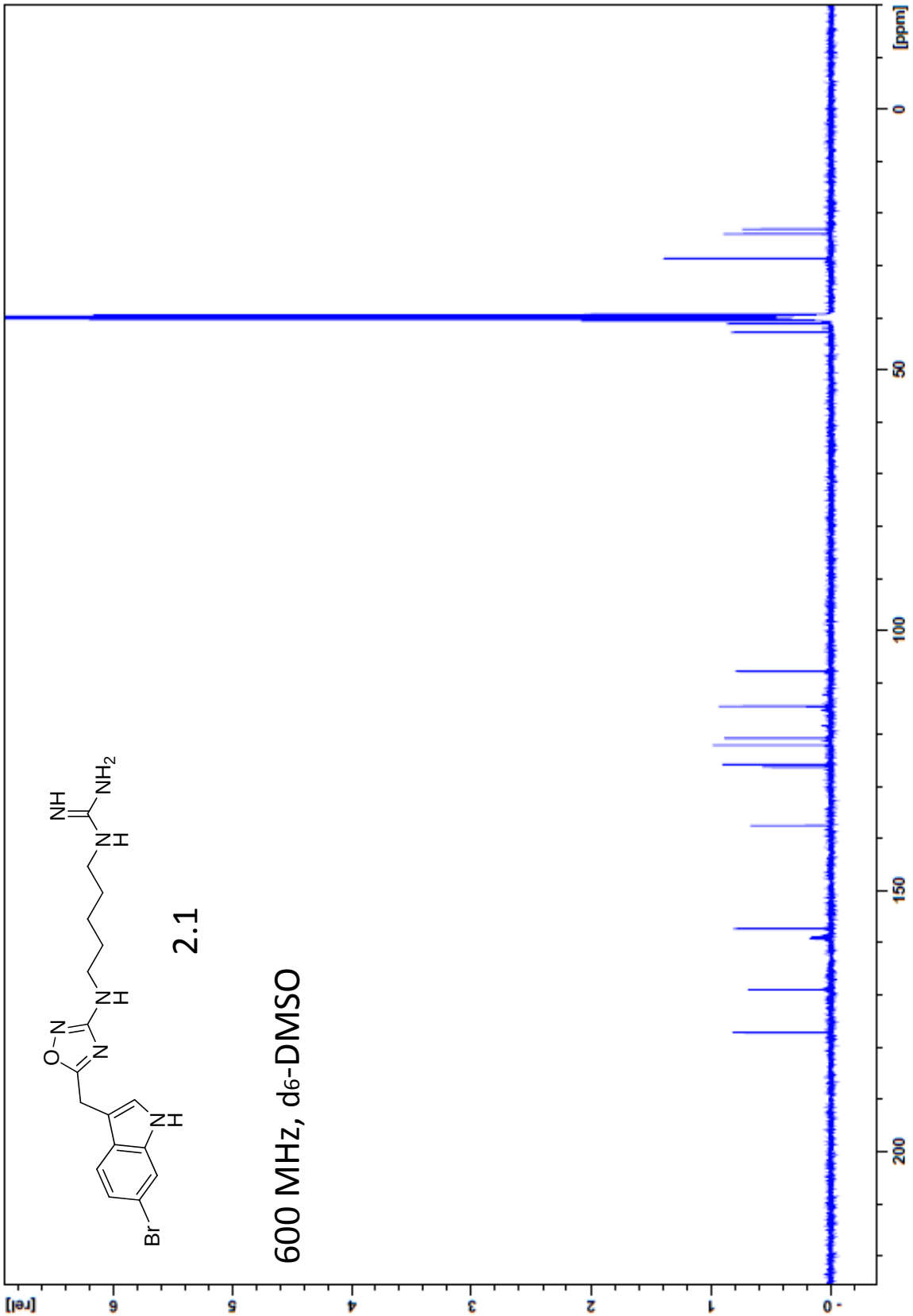
600 MHz, d6-DMSO
2.1
[rel]
[ppm]
0
50
100
150
200
1
2
3
4
5
6
NH
NH2
N
H
O
N
Br

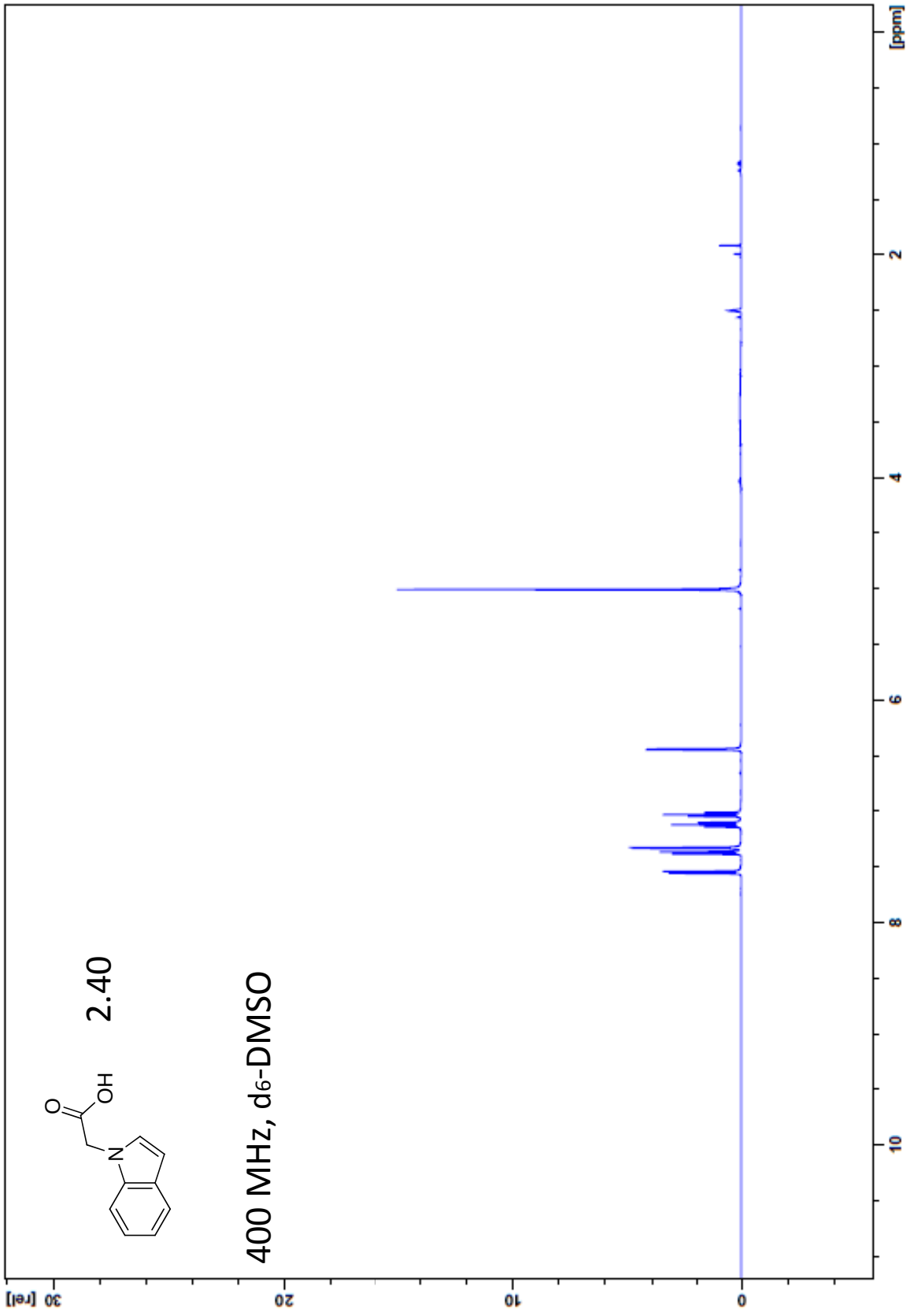
2.40
400 MHz, d6-DMSO
O
OH
N
30 [rel]
20
10
0
10
8
6
4
2
[ppm]

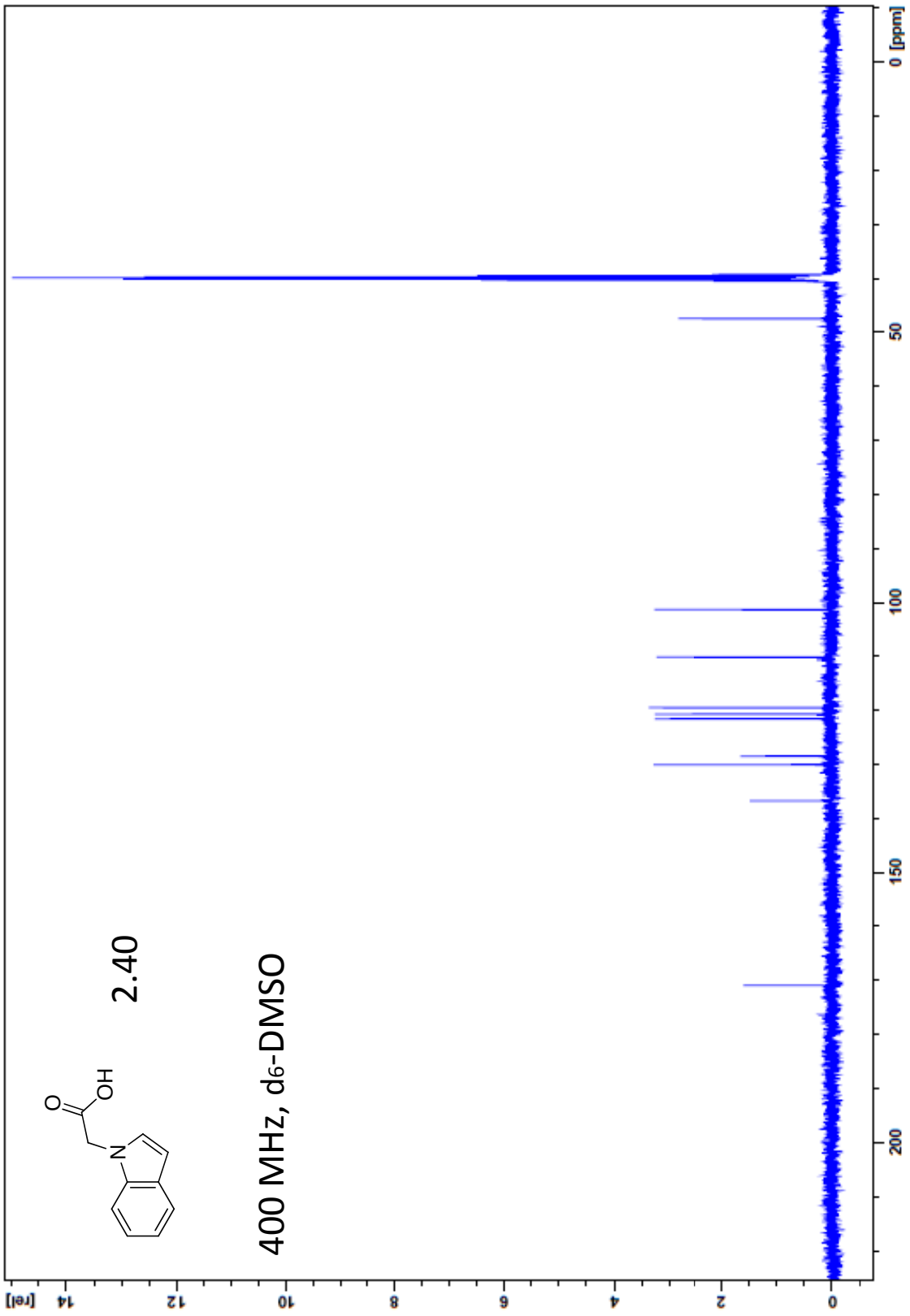
2.40
400 MHz, d6-DMSO
O
OH
N
[rel]
14
12
10
8
6
4
2
0
0 [ppm]
50
100
150
200

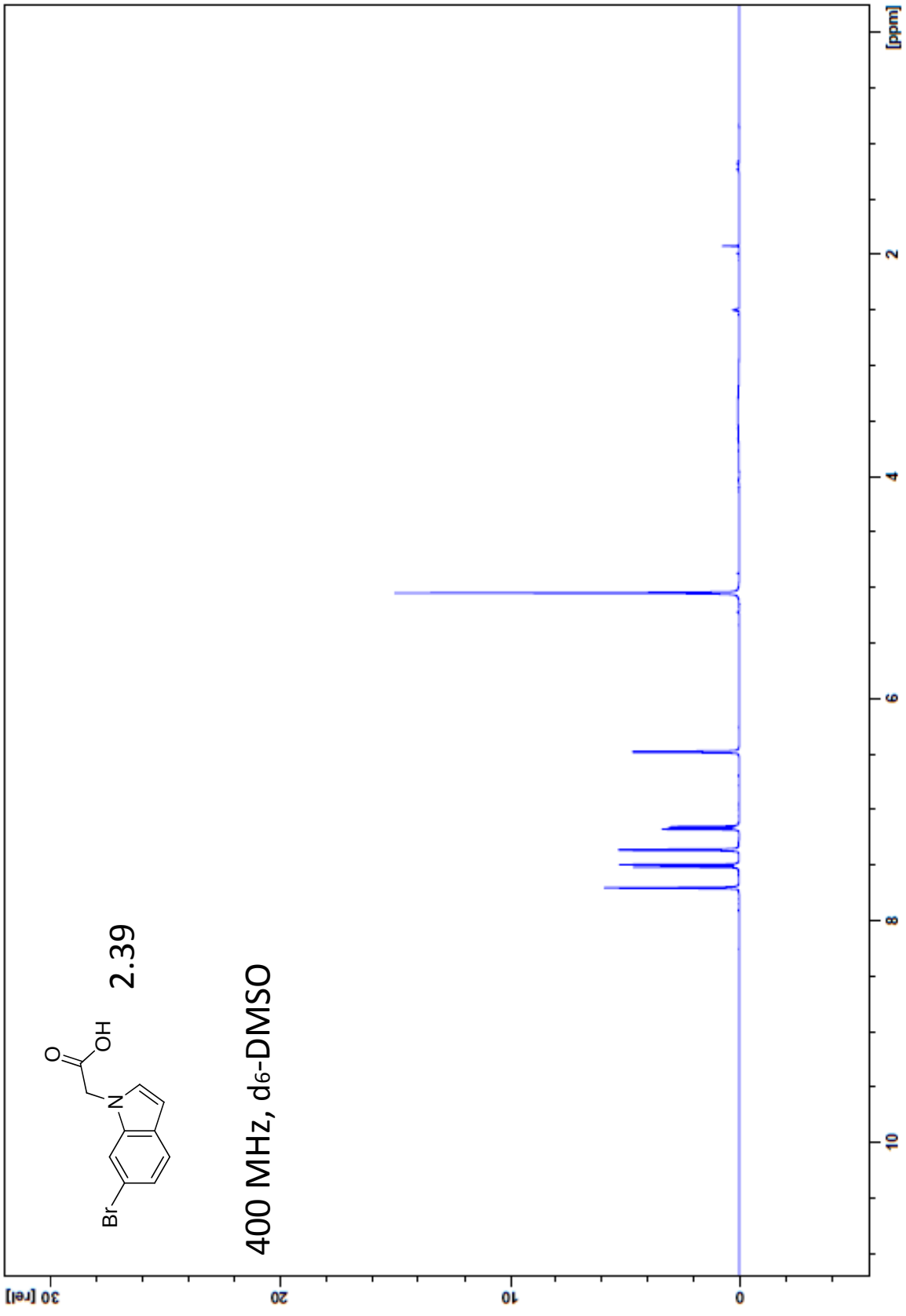
2.39
400 MHz, d6-DMSO
O
OH
N
Br
30 [rel]
20
10
0
10
8
6
4
2
[ppm]

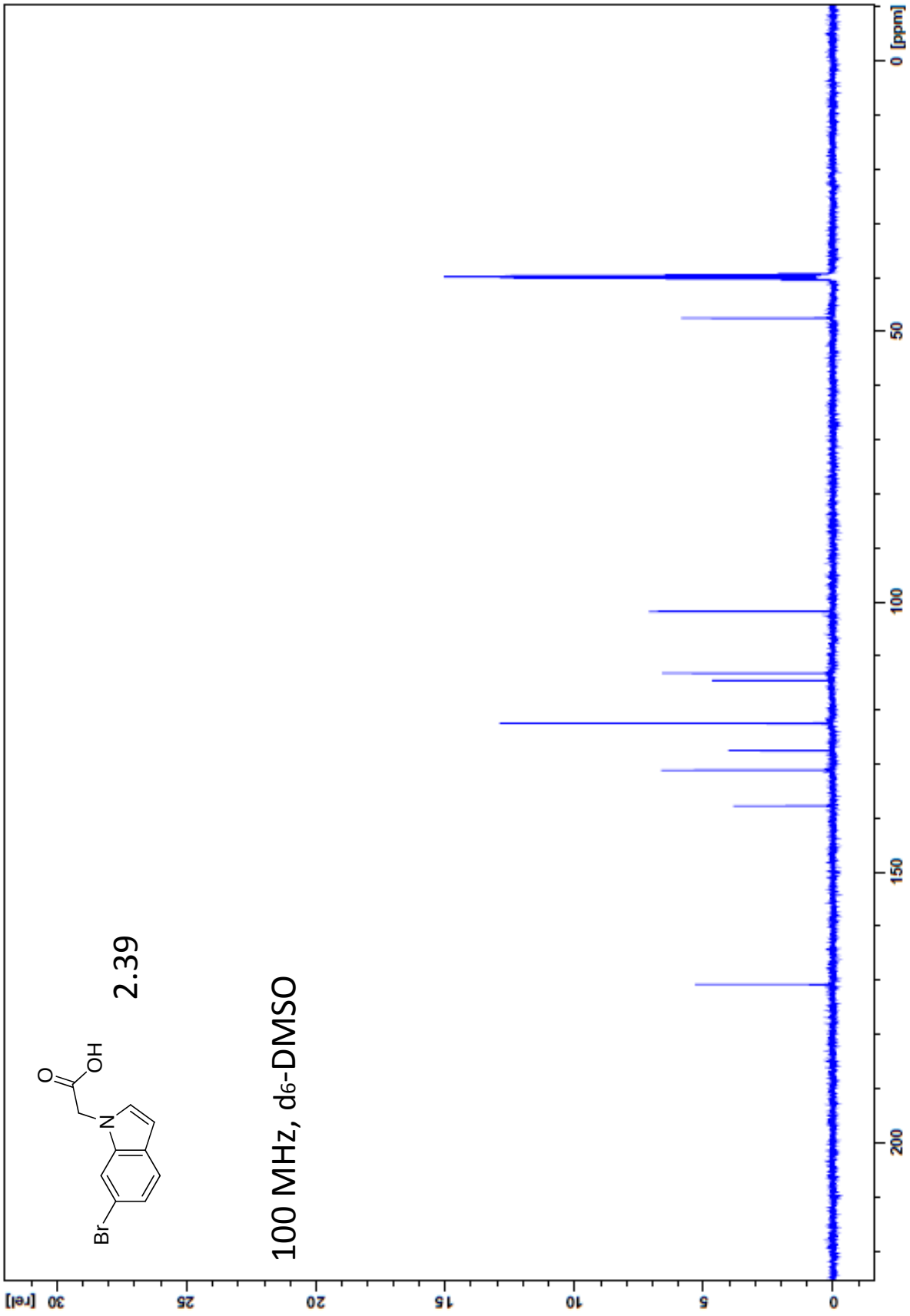
2.39
100 MHz, d6-DMSO
O
OH
N
Br
[rel]
30
25
20
15
10
5
0
200
150
100
50
0 [ppm]

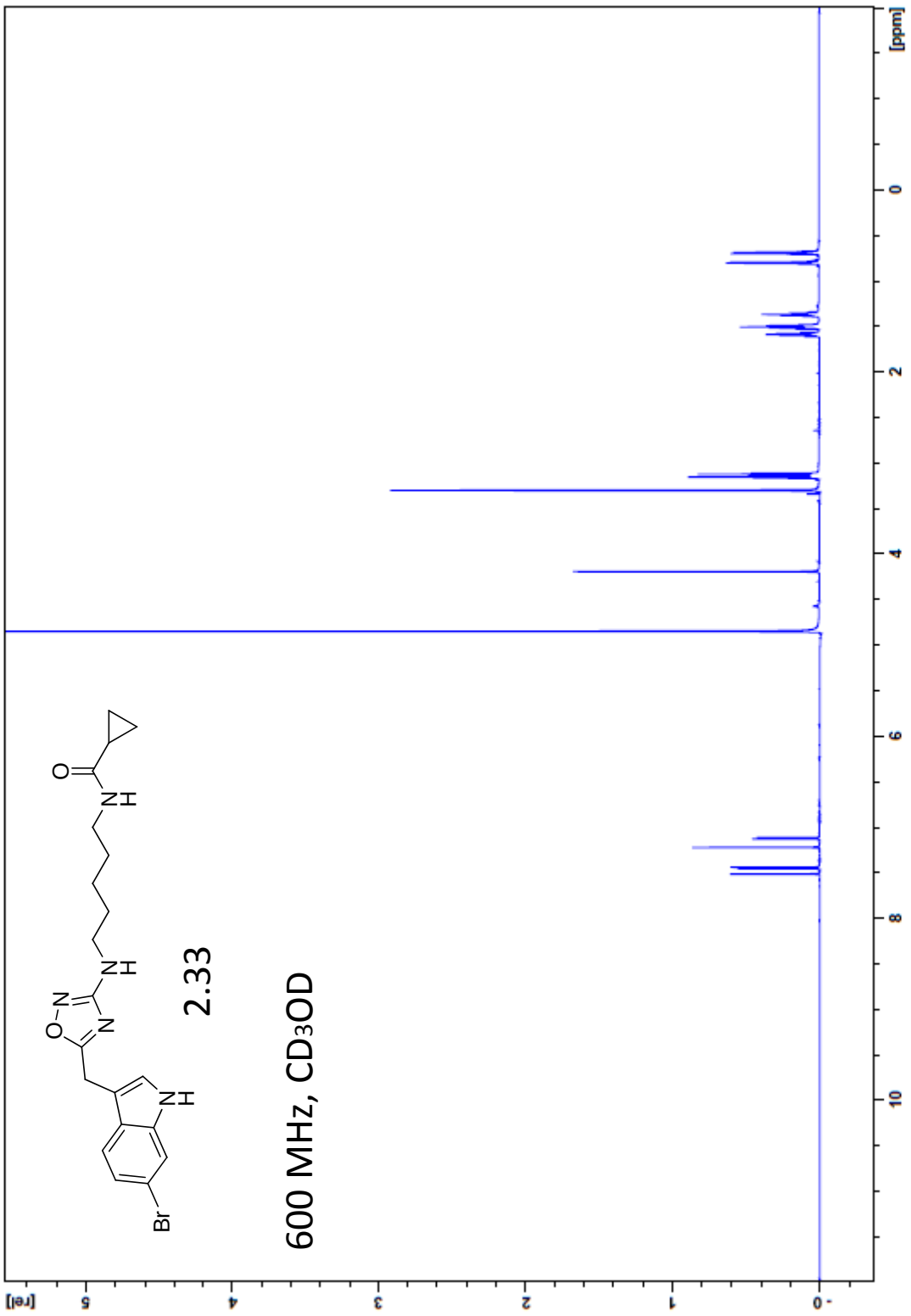
2.33
600 MHz, CD3OD
[rel]
[ppm]

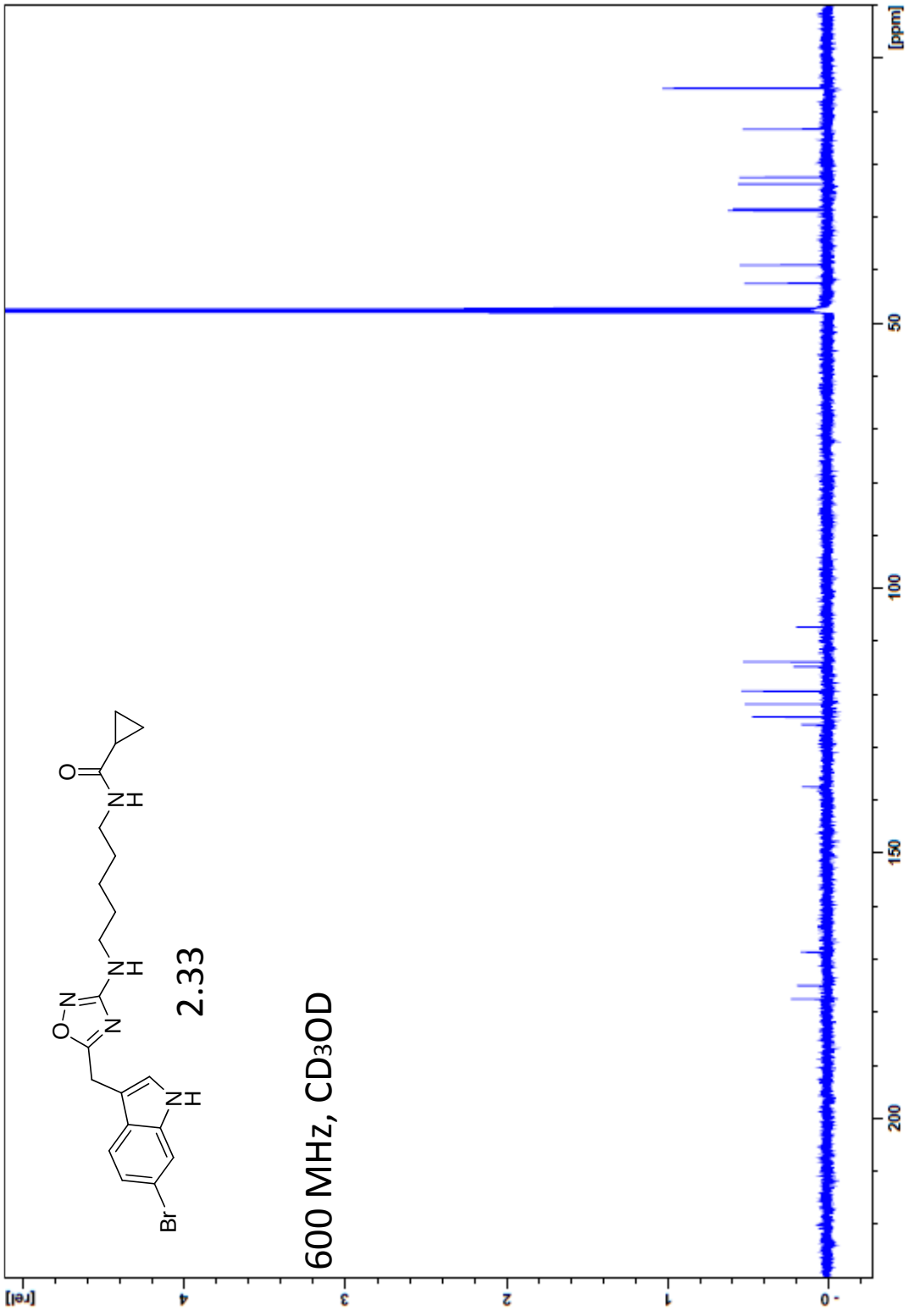
2.33
600 MHz, CD3OD
[rel]
[ppm]
0
1
2
3
4
50
100
150
200
O
N
H
N
H
O
N
N
N
H
Br

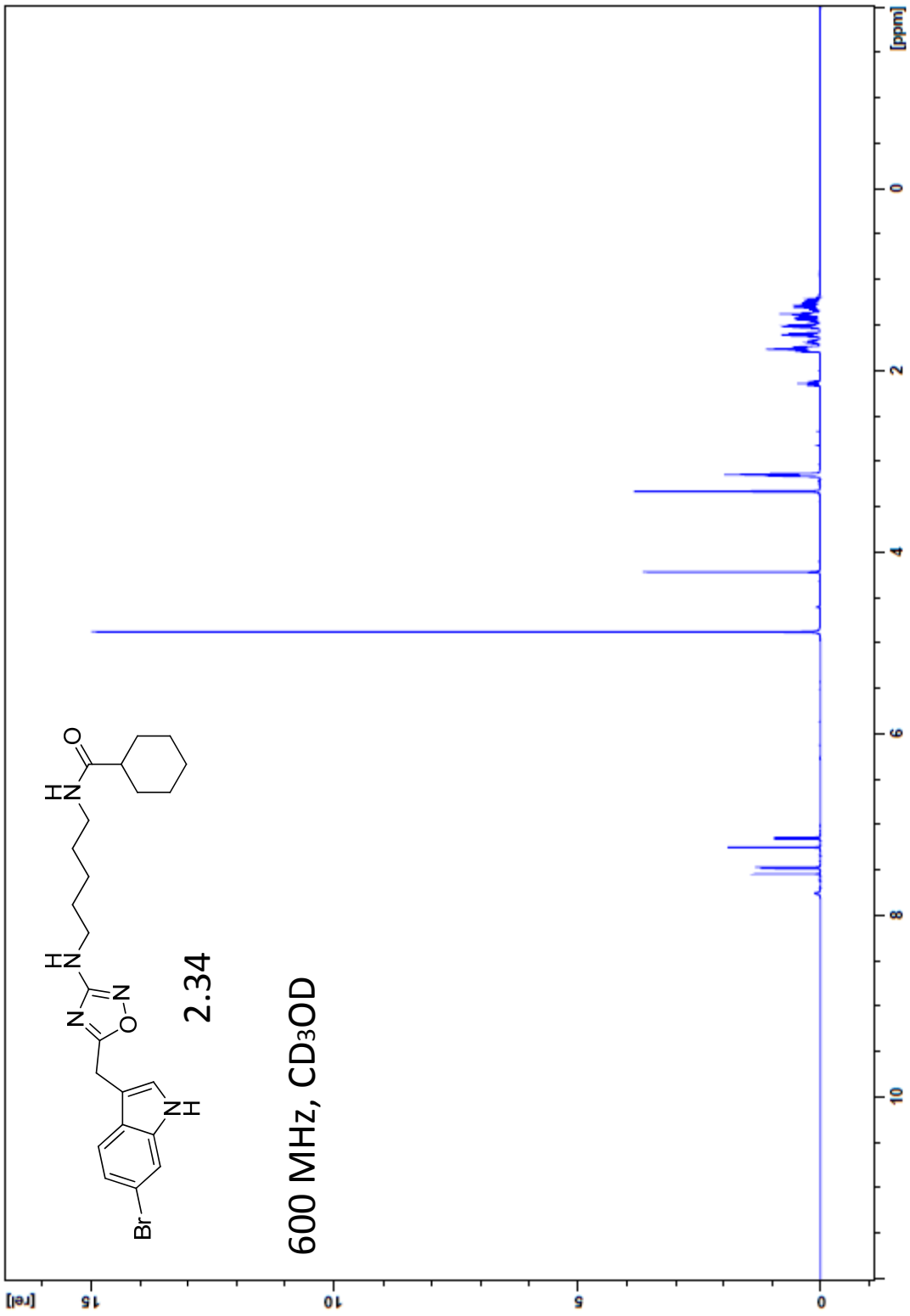
2.34
600 MHz, CD3OD
[rel]
15
10
5
0
[ppm]
10
8
6
4
2
0

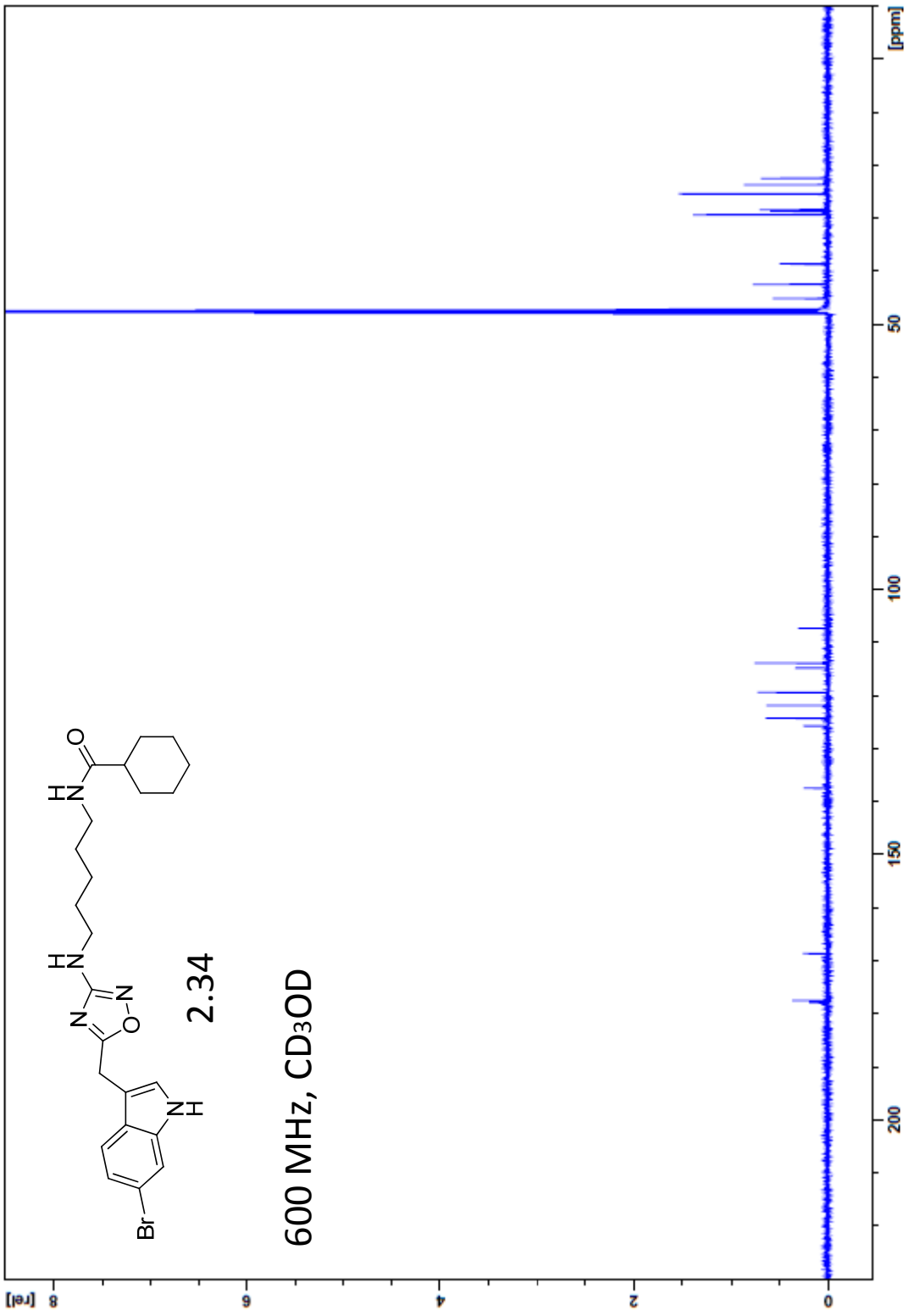
2.34
600 MHz, CD3OD
[ppm]
[rel]

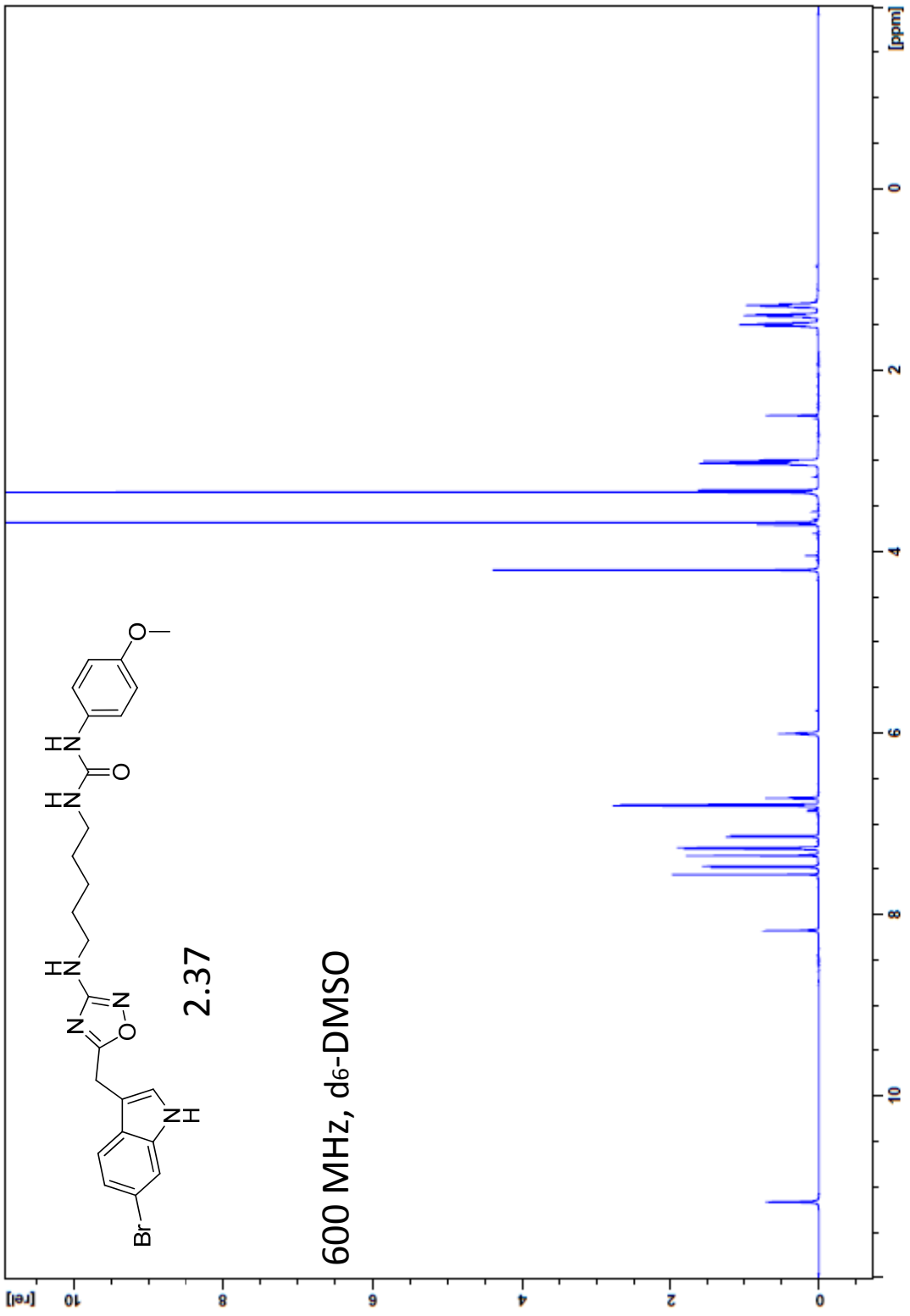
600 MHz, d6-DMSO
2.37
[rel]
[ppm]

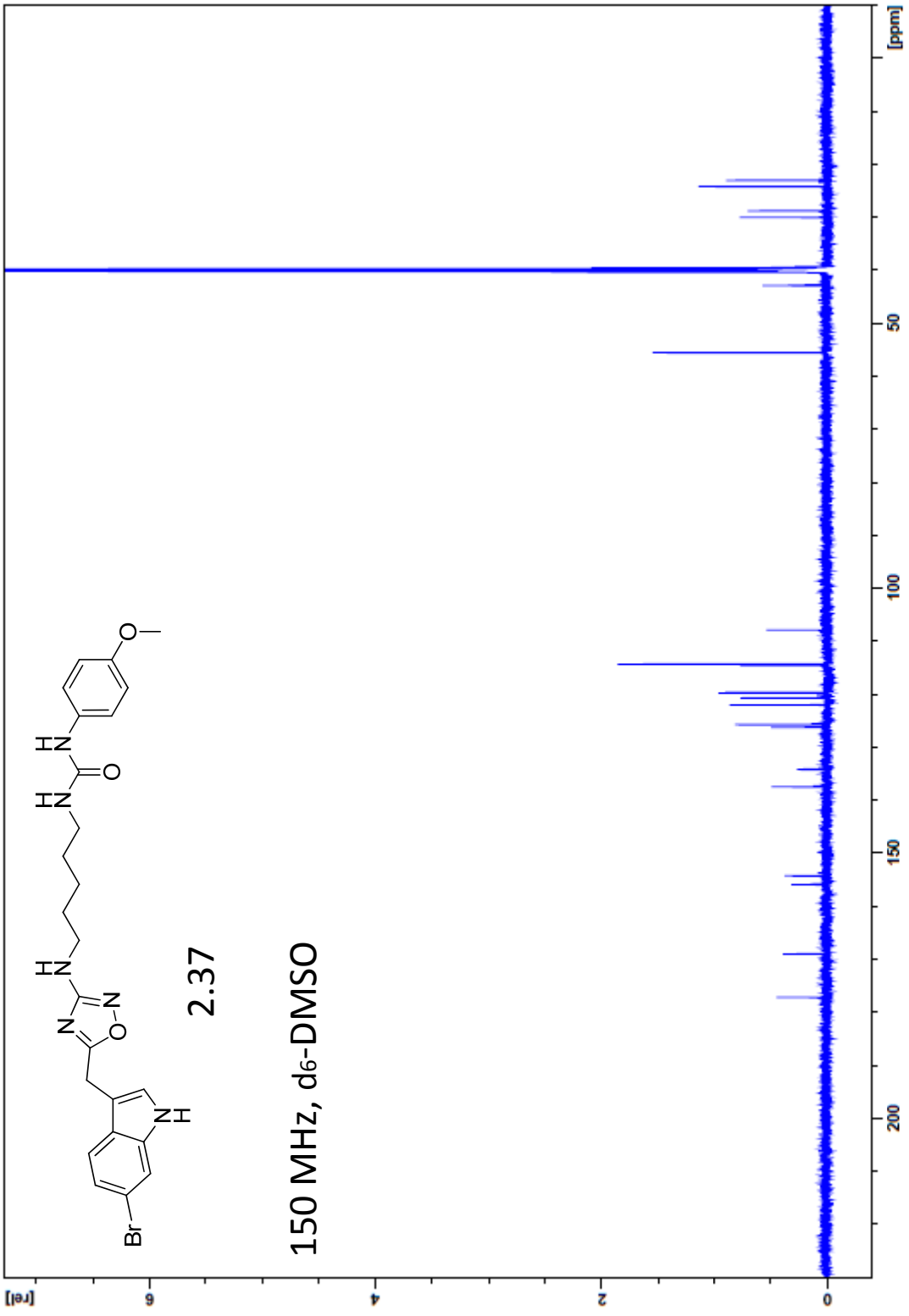
2.37
150 MHz, d6-DMSO
[rel]
[ppm]

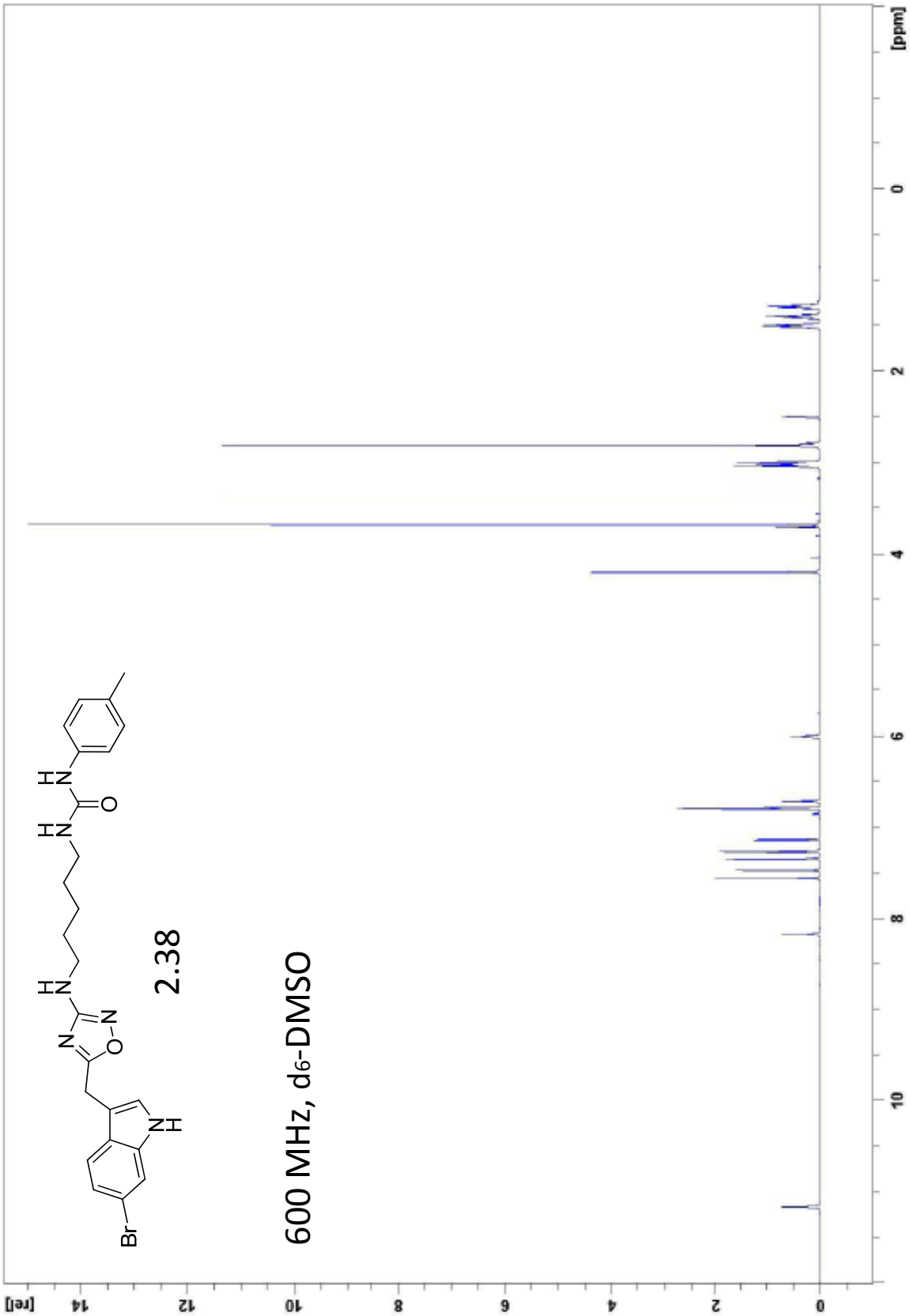
2.38
600 MHz, d6-DMSO
[rel]
[ppm]

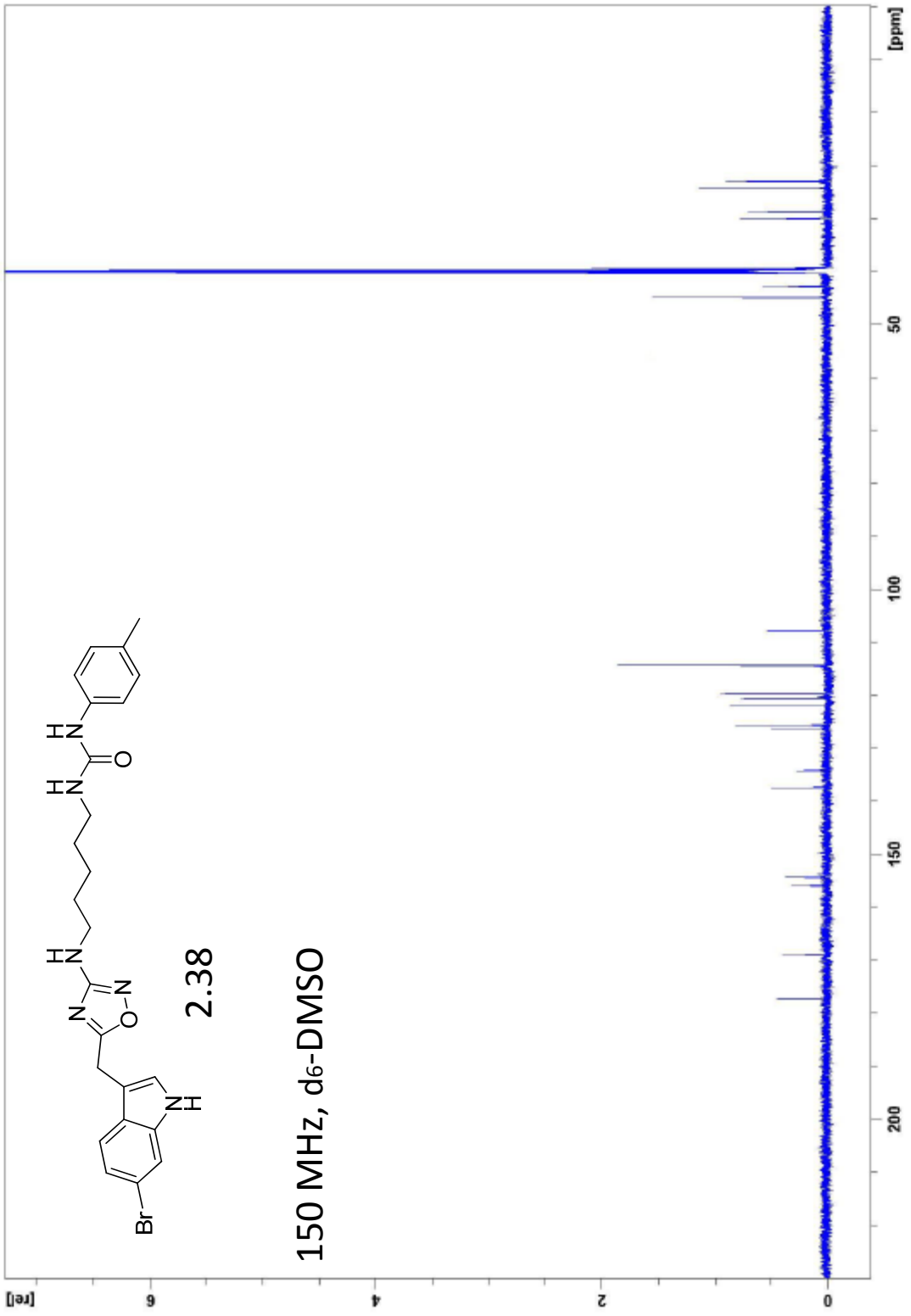
2.38
150 MHz, d6-DMSO
[rel]
[ppm]

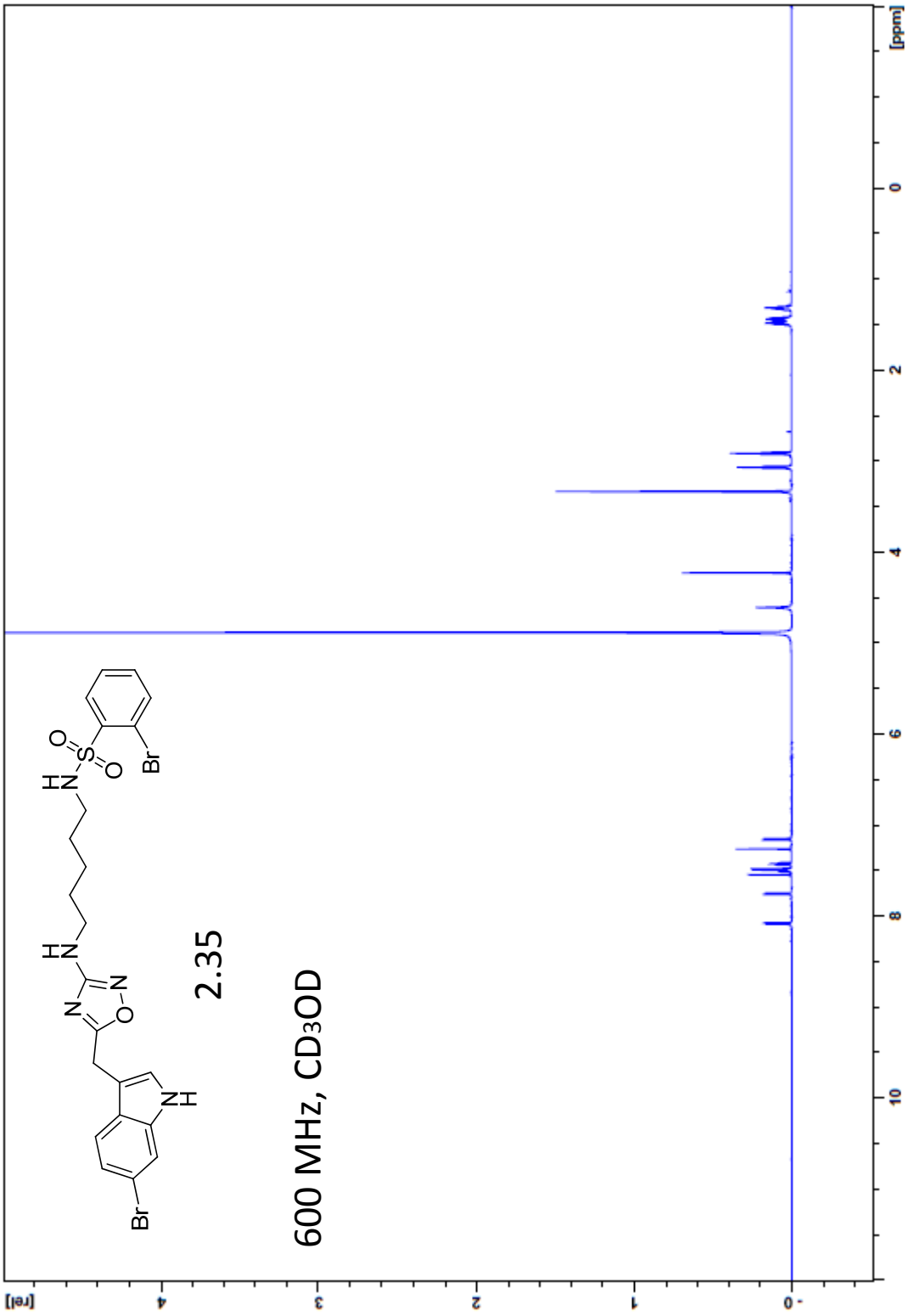
2.35
600 MHz, CD3OD
[rel]
[ppm]

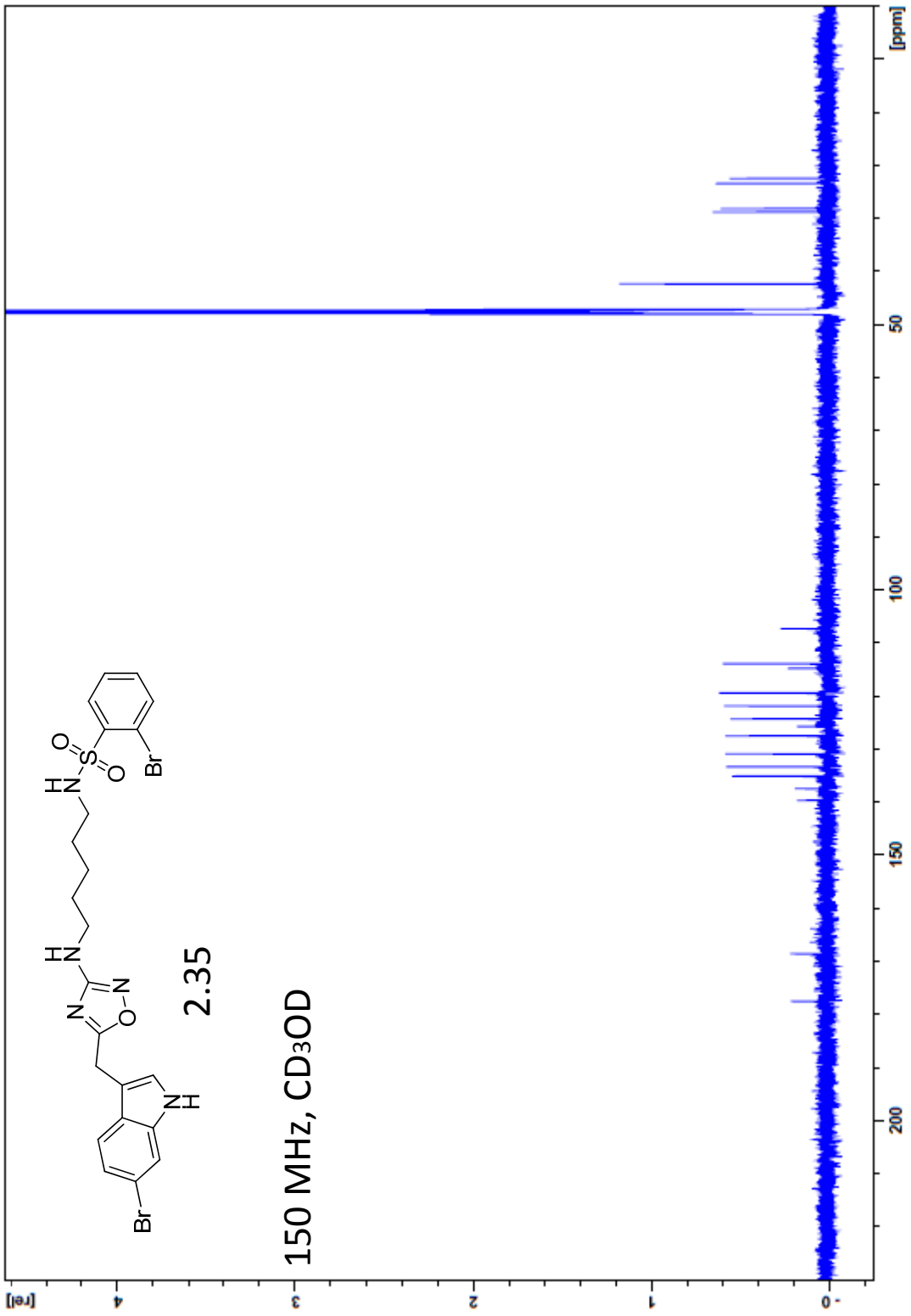
2.35
150 MHz, CD3OD
[rel]
[ppm]

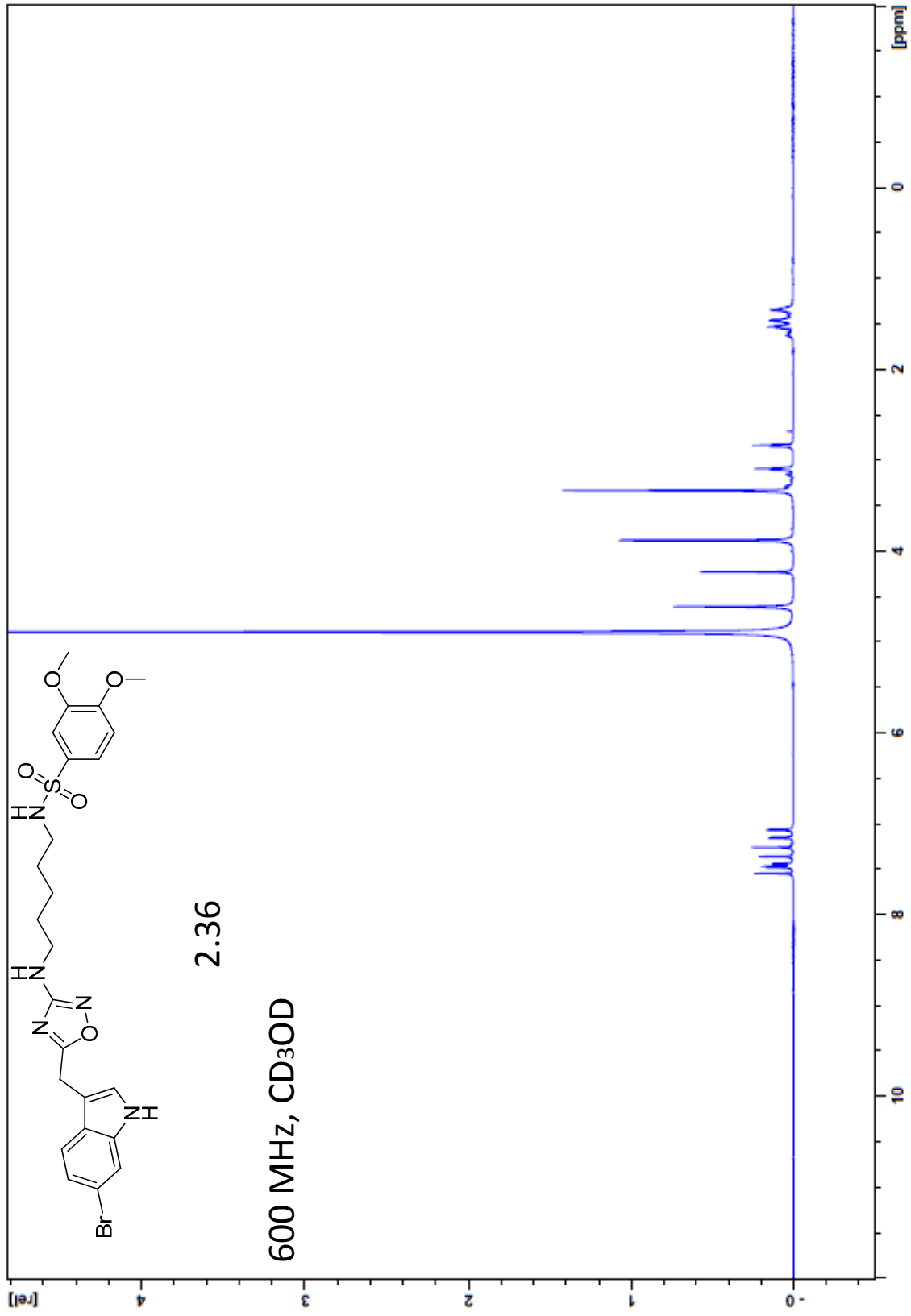
2.36
600 MHz, CD3OD
[rel]
[ppm]

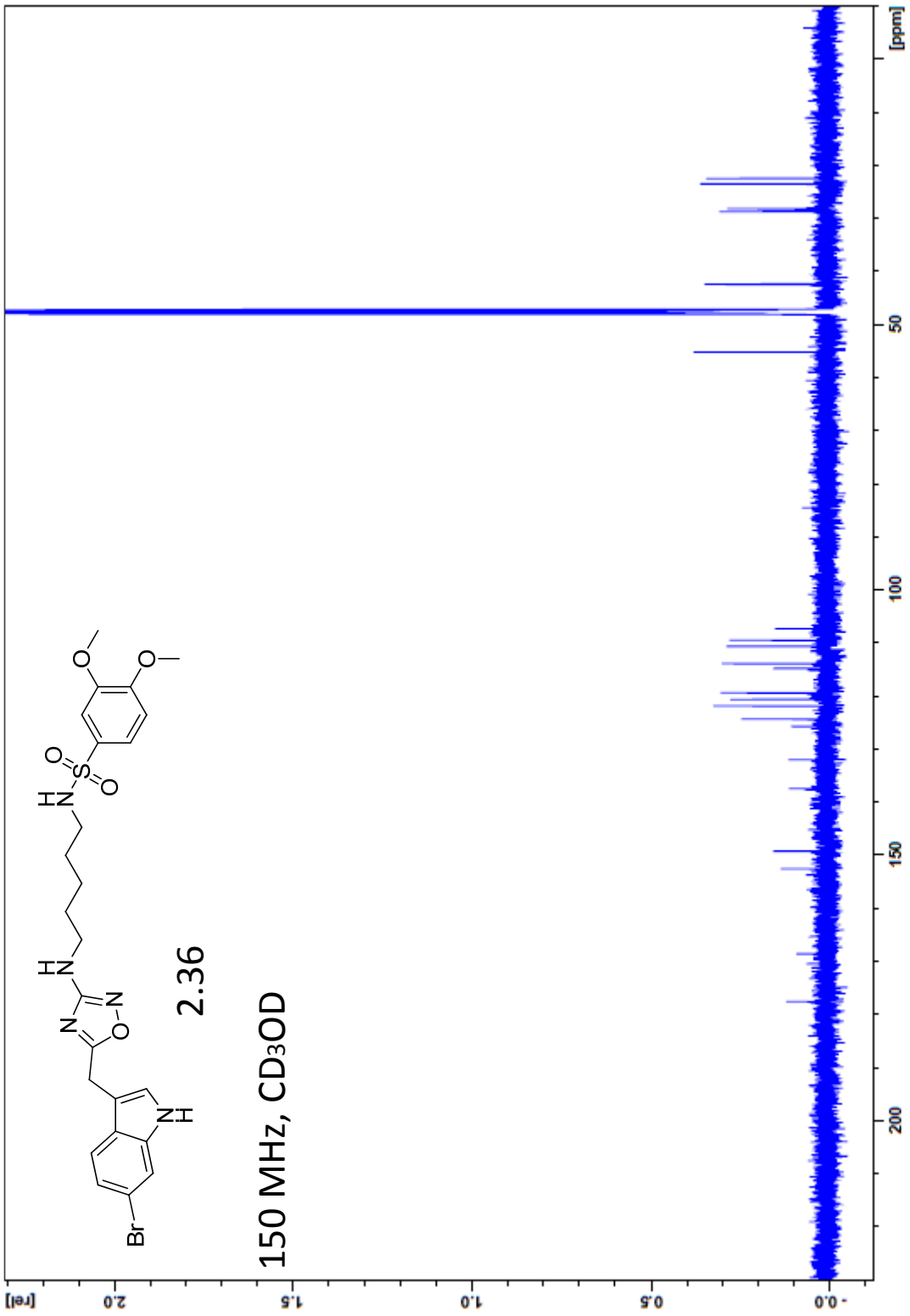
2.36
150 MHz, CD3OD
[rel]
[ppm]

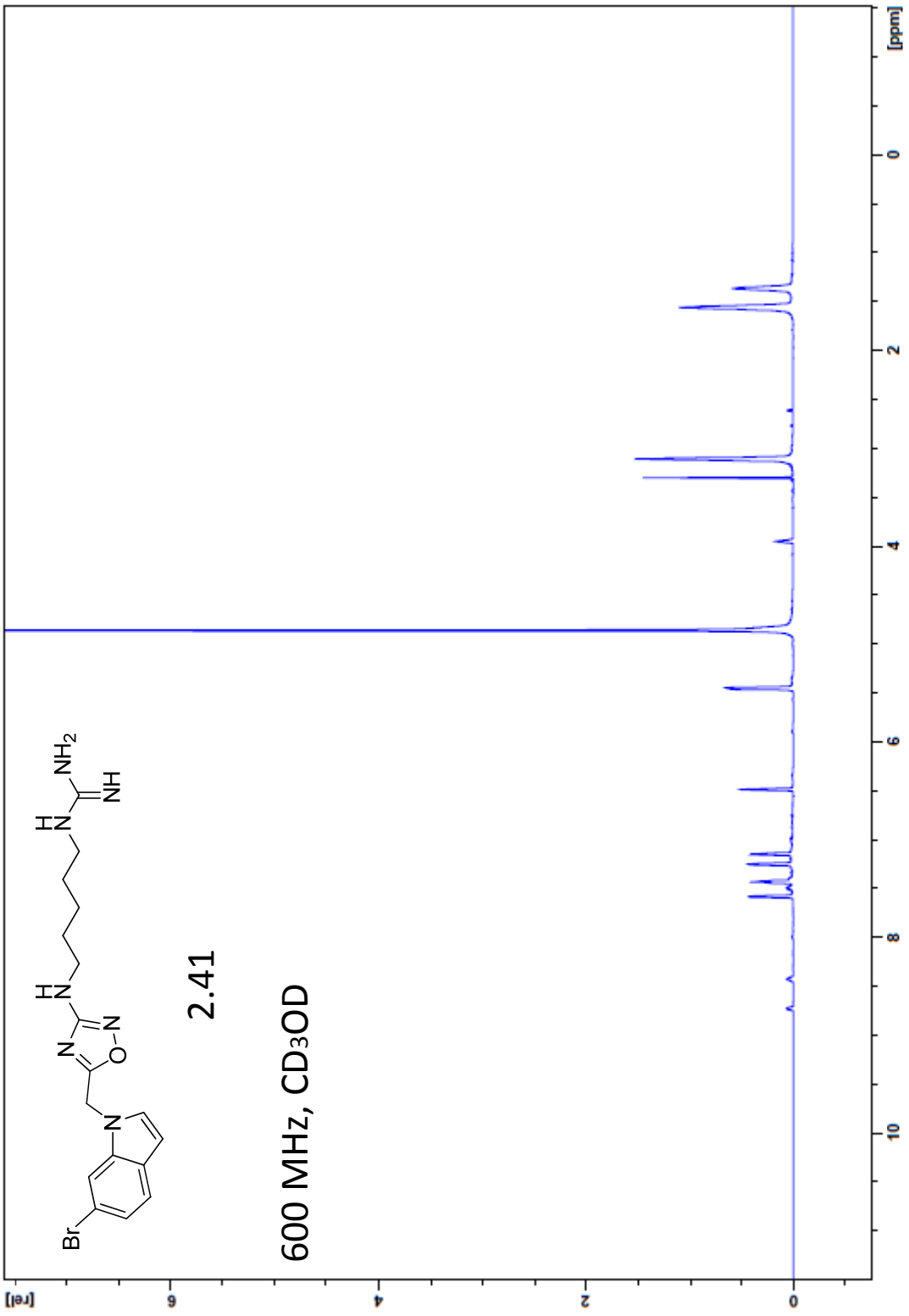
2.41
600 MHz, CD3OD
[rel]
[ppm]

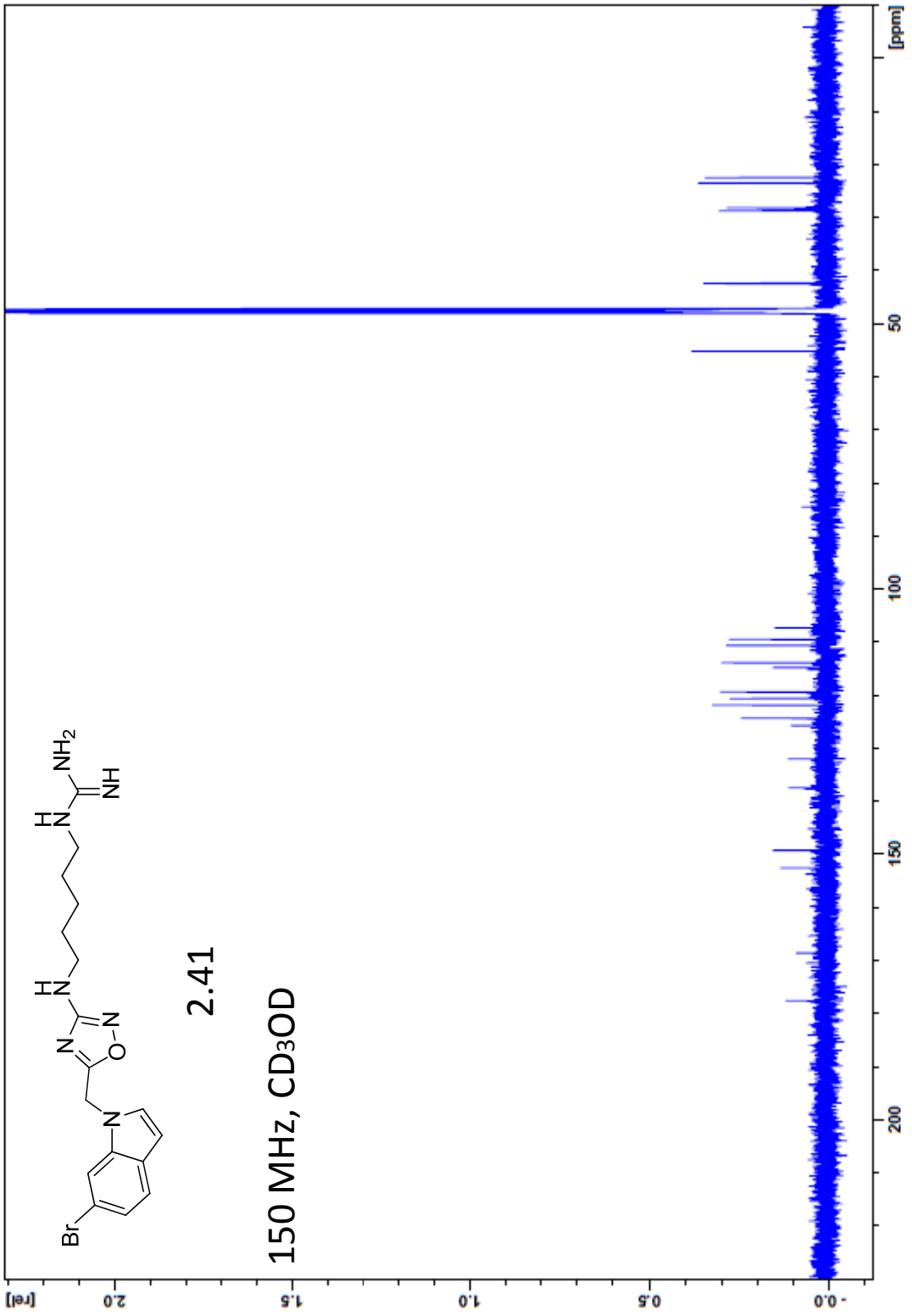
2.41
150 MHz, CD3OD
[rel]
[ppm]

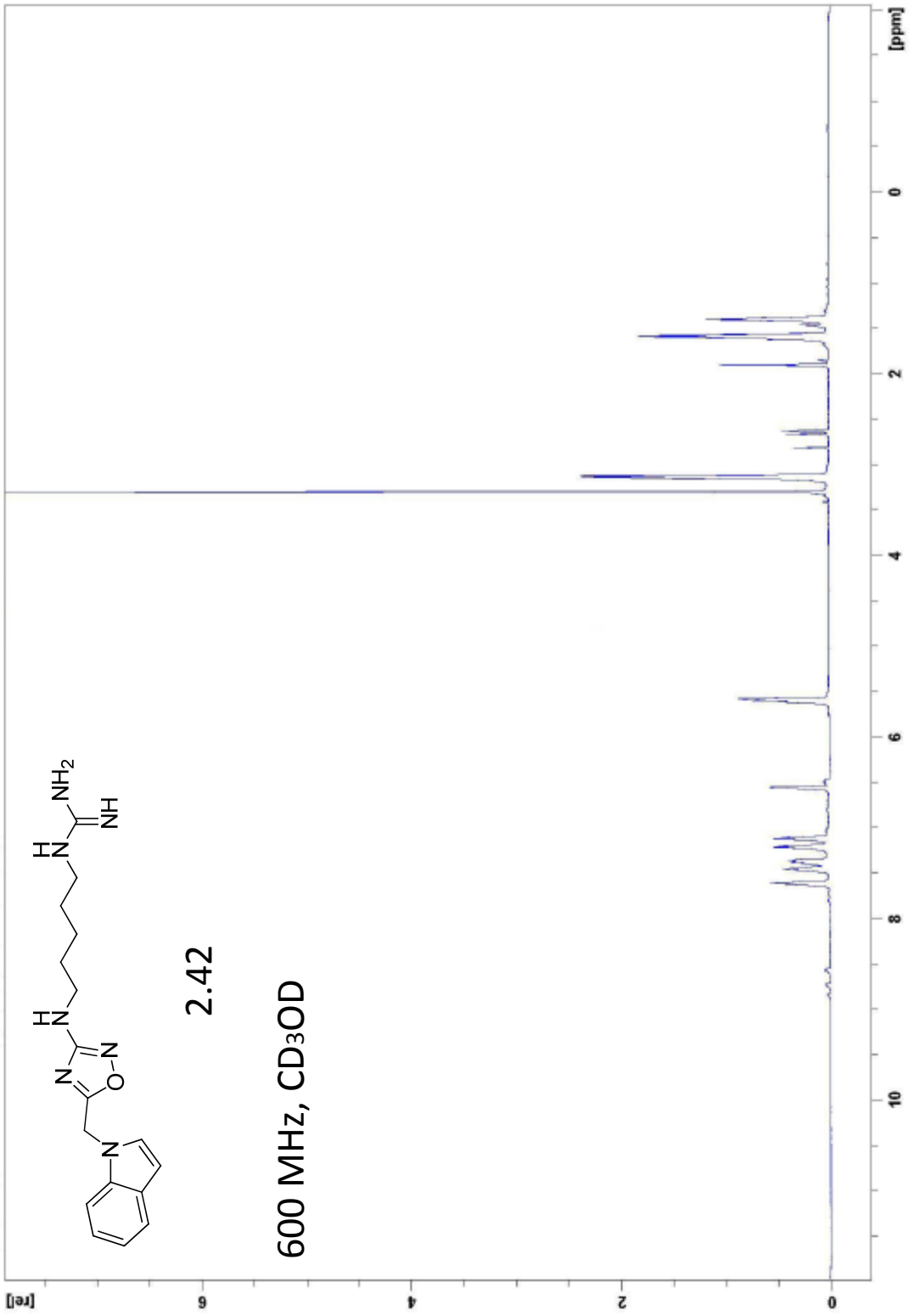
2.42
600 MHz, CD3OD
[rel]
[ppm]

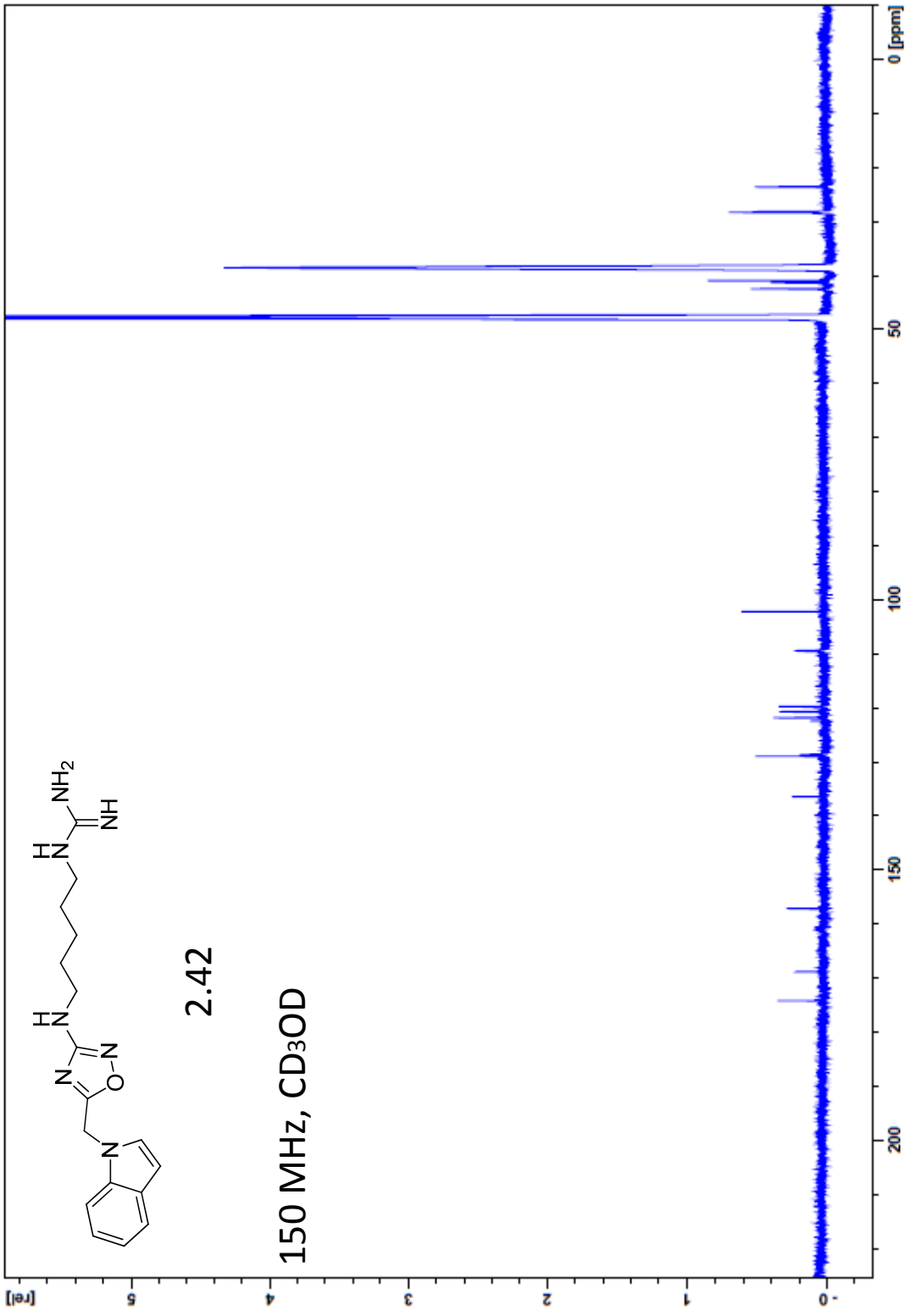
2.42
150 MHz, CD3OD
[rel]
0 [ppm]

REFERENCES

[1] Koehn, F.E., and Carter, G.T.. The evolving role of natural products in drug discovery. *Nat. Rev. Drug Discov.* **2005** *8*, 69-85

[2] Molinski, T.F., Dalisay, D.S., Lieven, S.L., Sauldes, J.P.. Drug development from marine natural products. *Nat. Rev. Drug Discov.* **2009** *8*, 69-85.

[3] Koehn, Frank E. Carter, Guy T.. *Nat. Rev. Drug Discov.* **2005,** *4*, 206-220.

[4] Swanson, D. M.; Wilson, S. J.; Boggs, J. D.; Xiao, W.; Apodaca, R.; Barbier, A. J.; Lovenberg, T. W.; Carruthers, N. I.. Aplysamine-1 and related analogs as histamine H3 receptor antagonists. *Bioorg. Med. Chem. Lett*. **2006** *16*, 897-900.

[5] Mierzwa, R.; King, A.; Conover, M. A.; Tozzi, S.; Puar, M. S.; Patel, M.; Coval, S. J.; Pomponi, S. A. Verongamine, a novel bromotyrosine-derived histamine H3-antagonist from the marine sponge Verongula gigantea. *J. Nat. Prod.* **1994** 57, 175-177.

[6] Zhao, C.; Sun, M.; Bennani, Y. L.; Gopalakrishnan, S. M.; Witte, D. G.; Miller, T. R.; Krueger, K. M.; Browman, K. E.; Thiffault, C.; Wetter, J.; Marsh, K. C.; Hancock, A. A.; Esbenshade, T. A.; Cowart, M. D. The alkaloid conessine and analogues as potent histamine H3 receptor antagonists. *J. Med. Chem.* **2008** 51, 5423-5430.

[7] Kennedy, J.P.; Brogan, J.T.; Lindsley, C.W. Total synthesis and biological evaluation of the marine bromopyrrole alkaloid dispyrin: elucidation of discrete molecular targets with therapeutic potential. *J. Nat. Prod.* **2008** 71, 1783-1788.

[8] Kennedy, J. P.; Conn, P. J.; Lindsley, C. W. A novel class of H3 antagonists derived from the natural product guided synthesis of unnatural analogs of the marine bromopyrrole alkaloid dispyrin. *Bioorg. Med. Chem. Lett.* **2009** 19, 3204-3208.

[9] Leurs, R.; Bakker, R. A.; Timmerman, H.; de Esch, I. J. P. The histamine H3 receptor: from gene cloning to H3 receptor drugs. *Nat. Rev. Drug Discov.* **2005** 4, 107-120.

[10] Hudkins, R. L. Raddatz, R. Recent advances in drug discovery of histamine H3 antagonist. *Ann. Rep. Med. Chem.* **2008** 42, 49-63.

[11] LeBois, E.P.; Jones, C.K.; Lindsley, C.W. The Evolution of Histamine H3 Antagonists/Inverse Agonists' *Curr. Topics in Med. Chem.* **2011,** 11, 648-660.

[12] Cain, M.; Weber, R.W.; Guzman, F.; Cook, J.M.; Barker, S.A.; Rice, K.C.; Crawley, J.N.; Paul, S.M.; Skolnick, P. β-Carbolines: synthesis and neurochemical and pharmacological actions on brain benzodiazepine receptors. *J. Med. Chem.* **1982,** 25, 1081-1091.

[13] Phuong, N. M.; Van Sung, T.; Porzel, A.; Schmidt, J.; Merzweiler, K.; Adam, G. β-Carboline alkaloids from Hedyotis capitellata. *Phytochemistry* **1999,** 52, 1725-1731.

[14] Lindsley, C.W.; Wisnoski, D.D.; Leister, W.H., Wang, Y.; Zhao, Z. A 'one pot' microwave-mediated synthesis of the basic canthine skeleton: expedient access to unnatural β-carboline alkaloids. *Tet. Lett.* **2003,** 44, 4495-4498.

[15] Kennedy, J.P.; Breininger, M.L.; Lindsley, C.W. Total synthesis of Eudistomins Y1-Y6. *Tet. Lett.* **2009,** 50, 7067-7069.

[16] Akizawa, T.; Yamazaki, K.; Yasuhara, T.; Nakajima, T.; Roseghini, M.; Erspamer, G.F.; Erspamer, V. Trypargine, a new tetrahydro-β-carboline of animal origin: isolation and chemical characterization from the skin of the African rhacophorid frog, Kassina senegalensis *Biomed. Res.* **1982,** 3, 232-234.

[17] Cesar, L.M.; Mendes, M.A.; Tormena, C.F.; Marques, M.R.; de Souza, B.M.; Saidemberg, D.M.; Bittencourt, J.C.; Palma, M.S. () Isolation and chemical characterization of PwTx-II: A novel alkaloid toxin from the venom of the spider Parawixia bistriata (Araneidae, Araneae). *Toxicon.* **2005,** 46, 786-796.

[18] Davis, R.A.; Duffy, S.; Avery, V.M.; Camp, D.; Hooper, J.N.A. Quinn, R.J. (+)-7-Bromotrypargine: an antimalarial β-carboline from the Australian marine sponge Ancorina sp. *Tet. Lett.* **2010,** 51, 583-585.

[19] Klausen R.S.; Jacobsen, E.N. Weak Brønsted Acid-Thiourea Co-catalysis: Enantioselective, Catalytic Protio-Pictet-Spengler Reactions. *Org. Lett.* **2009,** 11, 887-890.

[20] Holloway, C.A.; Muratore, M.E.; Storer, R.I.; Dixon, D.J. Direct Enantioselective Brønsted Acid Catalyzed N-Acyliminium Cyclization Cascades of Tryptamines and Ketoacids. *Org. Lett.* **2010,** 12, 4720-4723.

[21] Czarnocki, S.J.; Wojtasiewicz, K.; Jozwiak, A.P.; Maurin, J.K.; Czarnocki, Z.; Drabowicz, J. Enantioselective synthesis of (+)-trypargine and (+)-crispine E. *Tetrahedron* **2008,** 64, 3176-3182.

[22] Uematsu, N.; Fujii, A.; Hashiguchi, S.; Ikariya, T.; Noyori, R., Asymmetric Transfer Hydrogenation of Imines. *JACS* **1996,** *118*, 4916-4917.

[23] Daniels, R.N.; Melancon, B.J.; Wang, E.A.; Crews, B.S.; Marnett, L.M.; Sulikowski, G.A.; Lindsley, C.W. (2009) Progress towards the total synthesis of Lucentamycin A: Total synthesis and biological evaluation of 8-epi-Lucentamycin A *J. Org. Chem.* **2009**, 74, 8852-8855.

[24] Aldrich, L.N.; Stoops, S.L.; Crews, B.C.; Marnett, L.J.; Lindsley, C.W. Total synthesis and biological evaluation of tabjamine K and a library of unnatural analogs. *Bioorg. Med. Chem Lett.* **2010,** 20, 5207-5211.

[25] Stoops, S.L.; Pearson, S.A.; Weaver, C.; Waterson, A.G.; Days, E.; Farmer, C.; Brady, S.; Weaver, C.D.; Beauchamp, R.D.; Lindsley, C.W. Identification and optimization of small molecules that restore E-cadherin expression and reduce invasion in colorectal cells' *ACS Chem. Bio.* **2011,** 6, 452-465.

[26] For information on the Lead Profile Screen, see: www. ricerca.com

[27] Brogan, J. T.; Stoops, S. L.; Crews, B. C.; Marnett, L. J.; Lindsley, C. W., Total Synthesis of (+)-7-Bromotrypargine and Unnatural Analogues: Biological Evaluation Uncovers Activity at CNS Targets of Therapeutic Relevance. *ACS Chem. Neurosci.* **2011**, 2, 633-639.

[28] http://www.marinespecies.org/aphia.php?p=taxdetails&id=404960

[29] Carbone, M., Li, Y., Mollo, E., Castelluccio, F., Di Pascale, A., Cimino, G., Santamaria, R., Guo, Y-W., Gavagnin, M. Stucture and cytotoxicity of phidiadinines A and B. First findings of 1,2,4-oxadiazole system in a marine natural product. *Org. Lett.* **2011,** 13, 2516-2519.

[30] Simon, Sibu; Patrasek, Jan. Why plants need more than one type of auxin. *Plant Science*. **2011**, 180 (3), 454-460.

[31] Johnson, E.; Crosby, D., Indole-3-Acetic Acid. *Org. Synth*. **1964**, *5*, 654.

[32] Fuchs, J. R.; L. Funk, R., Total Synthesis of (±)-Perophoramidine. *JACS*. **2004,** 126 (16), 5068-5069.

[33] Ley, S. V.; Norman, J.; Griffith, W. P.; Marsden, S. P., Tetrapropylammonium Perruthenate, Pr4N+RuO4, TPAP: A Catalystic Oxidant for Organic Synthesis. *Synthesis* July **1994**, 639-665.

[34] Schmidt, A.-K. C.; Stark, C. B. W., TPAP-Catalyzed Direct Oxidation of Primary Alcohols to Carboxylic Acids through Stabilized Aldehyde Hydrates. *Org. Lett.* **2011**, *13* (16), 4164-4167.

[35] Frigerio, M.; Sntagostino, M.; Sputore, S.; Palmisano, G., Oxidation of Alcohols with o-Iodoxybenzoic Acid (IBX) in DMSO: A New Insight into an Old Hypervalent Iodine Reagent. *J. Org. Chem.* **1995**, *60* (7272-7276).

[36] Travis, B.; Borhan, B., Facile Oxidation of Aldehydes to Acids and Esters with Oxone. *Org. Lett.* **2003**, *5* (7), 1031-1034.

[37] Meyer, S.; Schreiber, S. L., Acceleration of the Dess-Martin Oxidation by Water. *J. Org. Chem.* **1994**, *59*, 7549-7552.

[38] Corey, E. J.; Schmidt, G., Useful Procedures for the Oxidation of Alcohols Involving Pyridinium Dichromate in Aprotic Media. *Tet. Lett.* **1979**, *5*, 399-402.

[39] Kimura, M.; Futamata, M.; Mukai, R.; Tamaru, Y., Pd-Catalyzed C3-Selective Allylation of Indoles with Allyl Alcohols Promoted by Triethylborane. *JACS* **2005**, 127, 4592-4593.

[40] Kolomiets, E., Neoglycopeptide dendrimer libraries as a source of lectin binding ligands. *Org. Lett.* **2007**, *9* (8), 1465-1468.

[41] Travis, B.; Narayan, R.; Borhan, B., Osmium Tetroxide-Promoted Catalytic Oxidative Cleavage of Olefins: An Organiometallic Ozonolysis. *JACS.* **2001**, *124*, 3824-3825.

[42] Ottoni, O.; Cruz, R.; Alves, R., Efficient and Simple Methods for the Introduction of the Sulfonyl, Acyl, and Alkyl Protecting Groups on the Nitrogren of Indole and its Derivatives. *Tetrahedron* **1998**, *54*, 13975-13928.

[43] Yadav, J. S.; Reddy, B. V. S.; Satheesh, G., *Tet. Lett.* **2003**, 8331-8334

[44] Melhado, L. L.; Brodsky, J. L., Synthesis of 4-Azidoindole-3-acetic Acid, a Photoprobe Causing Sustained Auxin Activity. *J. Org. Chem.* **1988,** *53*, 3852-3855.

[45] Lozano, O.; Blessley, G.; Martinez del Campo, T.; Thompson, A. L.; Giuffredi, G. T.; Bettati, M.; Walker, M.; Borman, R., Organocatalyzed Enantioselective Fluorocyclizations. *Angew. Chem. Int. Ed.* **2011**, *50*, 8105-8109.

[46] Lin, H-Y., Snider, B.B. Synthesis of phidiadinines A and B. *J. Org. Chem.* **2012,** 77, 4832-4836.

[47] (A) Stoops, S.L., Pearson, S.A., Weaver, C., Waterson, A.G., Days, E., Farmer, C., Brady, S., Weaver, C.D., Beauchamp, R.D., Lindsley, C.W. Identification and optimization of small molecules that restore E-cadherin expression and reduce invasion in colorectal cells. *ACS Chem. Bio.* **2011,** 6, 452-465.
(B) Francoeur, A-M., Assalian, A. Microcat: A novel cell proliferation and cytotoxicity assay based on WST-1. Biochemica **1996,** 3, 19-25.
(C) For information of the WST-1 assay kit employed, see: http://www.caymanchem.com/pdfs/10008883

[48] Howell, L. L., and Kimmel, H. L. Monoamine transporters and psychostimulant addiction. *Biochem. Pharmacol.* **2008,** 75, 196–217.

[49] Raehal, K.M., Schmid, C.L., Groer, C.E., Bohn, L.M. Functional selectivity at the μ-opioid receptor: Implications for understanding opioid analgesia and tolerance. *Pharmacol. Rev.* **2011,** 63, 1001-1019.

[50] Colasanti, A., Rabiner, E.A., Lingford-Hughes, A., Nutt, D.J. Opioids and anxiety. J. *Psychopharmacology* **2012,** 25, 1415-1433.

[51] Melancon, B.J., Hopkins, C.R., Wood, M.R., Emmitte, K.A., Niswender, C.M., Christopoulos, A., Conn, P.J., Lindsley, C.W. Allosteric Modulation of 7 Transmembrane Spanning Receptors: Theory, Practice and Opportunities for CNS Drug Discovery' *J. Med. Chem.* **2012,** 55, 1445-1464.

[52] Kennedy, S.E., Koeppe, R.A., Young, E.A., Zubieta, J.K. Dysregulation of endogenous opioid emotion regulation circuitry in major depression in women. *Arch. Gen Psychiatry* **2006,** 63, 1199-1208.

[53] For information on the Lead Profiling Screen (68 targets in radioligand binding assays), and the GTPγS fucntiopnal assay employed see: www.ricerca.com

[54] Alt, A., Mansour, A., Medzihhradsky, F., Traynor, J.R., Woods, J.H. Stimulation of guanosine -5'-O-(3-[35S]thio)triphosphate binding by endogenous opioids acting at a cloned mu receptor. *J. Pharmacol. Exp. Ther.* **1998,** 286 (1), 282-288.

[55] Conn, P. J.; Pin, J.-P. Pharmacology and functions of metabotropic glutamate receptors. *Annu. Rev. Pharmacol. Toxicol.* **1997**, 37, 205–237.

[56] Cartmell, J.; Schoepp, D. D., Regulation of Neurotransmitter Release by Metabotropic Glutamate Receptors. *J. Neurochem.* **2000**, 75, 889-907.

[57] Alberts B, Lewis J, Raff M, Roberts K, Walter P (**2002**). *Molecular biology of the cell* (4th Edition ed.). New York: Garland Science.

[58] Gee, K.R.; Brown, K.A.; Chen, W-N.U.; Bishop-Stewart, J.; Gray, D.; Johnson, I. Chemical and physiological characterization of fluo-4 Ca^{2+}-indicator dyes. *Cell Calcium.* **2000**, 27 (2), 97-106.

[59] Frank, R. A. W.; McRae, A. F.; Pocklington, A. J.; van de Lagemaat, L. N.; Navarro, P.; Croning, M. D. R.; Komiyama, N. H.; Bradley, S. J.; Challiss, R. A. J.; Armstrong, J. D.; Finn, R. D.; Malloy, M. P.; MacLean, A. W.; Harris, S. E.; Starr, J. M., Clustered Coding Variants in the Glutamate Receptor Complexes of Individuals with Schizophrenia and Bipolar Disorder. *PLoS ONE* **2011,** *6* (4), 1-9.

[60] Ayoub, M. Akli; Angelicheva, D.; Vile, D.; Chandler, D.; Morar, B.; Cavanaugh, J. A.; Visscher, P. M.; Jablensky, A.; Pfleger, K. D. G.; Kalaydjieva, L., Deleterious GRM1 Mutations in Schizophrenia. *PLoS ONE.* **2012**, 7 (3), 1-8.

[61] Snyder S., Dopamine Receptor Excess and Mouse Madness. *Neuron.* **2006**, 49:484–485.

[62] Anis NA, Berry SC, Burton NR, Lodge D The dissociative anaesthetics, ketamine and phencyclidine, selectively reduce excitation of central mammalian neurons by N-methyl-aspartate. *Brit. J. of Pharm.* **1983,** 79: 565–575.

[63] Gunduz-Bruce H., The acute effects of NMDA antagonism: From the rodent to the human brain. *Brain Res. Rev*. **2009**, 60, 279–286.

[64] Sprengel R, Suchanek B, Amico C, Brusa R, Burnashev N, et al. Importance of the intracellular domain of NR2 subunits for NMDA receptor function in vivo. *Cell* **1998**, 92, 279–289.

[65] Fagni L.. Homer as Both a Scaffold and Transduction Molecule. *Science's STKE* **2002,** 8re–8.

[66] Urwyler, S., Allosteric Modulation of Family C G-Protein-Coupled Receptors: from Molecular Insights to Therapeutic Perspectives. *Pharmacological Reviews* **2011**, 63, 59-126.

[67] Knoflach F, Mutel V, Jolidon S, Kew JN, Malherbe P, Vieira E, Wichmann J, and Kemp JA. Positive allosteric modulators of metabotropic glutamate 1 receptor: characterization, mechanism of action, and binding site. *Proc Natl Acad Sci* USA **2001,** 98:13402–13407.

[68] Hemstapat, K.; de Paulis, T.; Chen, Y.; Brady, A. E.; Grover, V. K.; Alagille, D.; Tamagnan, G. D.; Conn, P. J., A Novel Class of Positive Allosteric Modulators of Metabotropic Glutamate Receptor Subtype 1 Interact with a Site Distinct from That of Negative Allosteric Modulators. *Molecular Pharmacology* **2006**, 70, 616-626.

[69] Lindsley, C. W.; Wisnoski, D. D.; Leister, W. H.; O'Brien, J. A.; Lemaire, W.; Williams, D. L.; Burno, M.; Sur, C.; Kinney, G. G.; Pettibone, D. J.; Tiller, P. R.; Smith, S.; Duggan, M. E.; Hartman, G. D.; Conn, P. J.; Huff, J. R., Discovery of Positive Allosteric Modulators for the Metabotropic Glutamate Receptor Subtype 5 from a Series of N-(1,3-Diphenyl-1H- pyrazol-5-yl)benzamides That Potentiate Receptor Function in Vivo. *J. Med. Chem.* **2004**, 47 (24), 5825-5828.

[70] Engers, D. W.; Niswender, C. M.; Weaver, C. D.; Jadhav, S.; Menon, U. N.; Zamorano, R.; Conn, P. J.; Lindsley, C. W.; Hopkins, C. R., Synthesis and Evaluation of a Series of Heterobiarylamides That Are Centrally Penetrant Metabotropic Glutamate Receptor 4 (mGluR4) Positive Allosteric Modulators (PAMs). *J. Med. Chem.* **2009**, 52, 4115-4118.

[71] Wood, M. R.; Hopkins, C. R.; Brogan, J.T.; Conn, P. J.; Lindsley, C. W., "Molecular Switches" on mGluR Allosteric Ligands That Modulate Modes of Pharmacology. *Biochemistry* **2011**, 50, 2403-2410.

[72] Birkett, D., Pharmacokinetics Made Easy. McGraw-Hill: North Ryde, Australia, **2002**.

[73] J H Lin, M Chiba, S K Balani, I W Chen, G Y Kwei, K J Vastag, J A Nishime, Species differences in the pharmacokinetics and metabolism of indinavir, a potent human immunodeficiency virus protease inhibitor. *Drug Metab. Dispos.* **1996**, 24, 1111-1120.